DOE/NV/10461--T44

TRAC *Technology and Resource Assessment Corporation*

3800 Arapahoe Avenue, Suite 225
Boulder, Colorado 80303
(303) 443-3700 FAX No. (303) 443-8626

Annual Report - Nevada

Investigations of Hydro-Tectonic Hazards at the Proposed Yucca Mountain High-Level Nuclear Waste Repository

CONTRACT No. 92/94-.0004

Submitted to the
Nuclear Waste Project Office
State of Nevada

January, 1994

Edited by:
Dr. Donald E. Livingston

db

Investigations of Hydro-Tectonic Hazards at the Proposed Yucca Mountain High-Level Nuclear Waste Repository

Contents

Executive Summary

During this past year we have extended and strengthened the basis of our arguments for epigenetic, metasomatic alteration of the tuffs at Yucca Mountain (see List of Reports for Fiscal Year 1993, appendix to this executive summary). The status of these studies is given in Livingston and Szymanski (this report). We now include stratigraphic, mineralogical and geochronological information along with the geochemical data. The broadened scope of these studies provides a clearer picture of the spatial and temporal distribution of zeolite alteration. The concepts of diagenetic and supergene origins for the alteration at Yucca Mountain, as proposed by numerous DOE scientists, becomes even less tenable as additional data are examined. The remarkable range of the chemical composition of clinoptilolites and their high Ca content, remains as the foundation stone of our arguments for epigenetic metasomatic alteration of the tuffs. The diversity of the chemical composition of the clinoptilolites, which is independent of the stratigraphy and position relative to the present day groundwater table, argues against any origin other than by hypogene solutions which have come from rocks whose chemical compositions were vastly different from that of the original alkali-rich tuff. The chemical diversity of clinoptilolite persist over spatial scales from tens of kilometers to centimeters. Again the larger scale spatial differences of chemistry argues for different sources of altering solutions for different parts of the mountain. The small scale differences in chemistry argue for episodic alteration and for faults, fractures and breccias as conduits for the invasion of some of the altering solutions. The

small spatial scale differences in chemistry indicate that equilibrium among clinoptilolites is not always achieved in the natural setting and suggests that the zeolites may not inhibit radionuclide migration as much as might be expected. K-Ar dating of clinoptilolites suggests that zeolitization may have persisted into the Quaternary in which case zeolitic alteration may necessarily become an expected condition because of regulatory requirements. The amount of calcium which has been introduced into the mountain is to large to be accounted for by diagenetic and supergene processes. This leaves the hypogene hypothesis as the only meaningful origin for the calcium metasomatism. The calcic chemical affinity among the altered tuffs, calcite/silica veins and calcite/silica surficial deposits suggests similar hypogene origins for all.

For the coming year we plan to incorporate more mineralogical and stratigraphic information into the examination of alteration and mineralization at Yucca Mountain. We will examine the distribution of calcite, illite/smectite and silica (Opal-CT) in the tuffs and the chemistry and mineralogy of veins and fracture within the boreholes. These studies will strengthen the linkages between the alteration and mineralization of the tuffs and the surficial calcite/silica deposits discussed by Hill et al. (this report).

The status of our studies of near surface calcite/silica deposits over the past year (see appendix to this executive summary) is given in the section prepared by Hill, et al. (this report). We have included the efforts of a number of scientists of international and national stature as a part of our team. The work is lead by Carol

Hill an independent geologist from Albuquerque, New Mexico and includes Dr. Russell Harmon, an isotope geochemist from Raleigh, North Carolina, formerly of Natural Environment Research Council, in the United Kingdom and Geochemisches Institut der Universität Göttingen, Germany. Analytical data for samples collected at Yucca Mountain have been performed in the laboratories of Professor S. Moorbath, Oxford University, United Kingdom; Prof. Dr. J Hoefs, University of Göttingen, Germany; Professor D, C. Ford, McMaster University, Ontario, Canada; Dr. D. M. H. Alderton, University of London, United Kingdom; and Dr. R. A. Schmitt, Radiation Laboratory, Oregon State University, U.S.A. We have also included on our team Dr. Curtis Monger, a geologist and specialist in arid soils, New Mexico State University, La Cruces, New Mexico. All of these workers have made substantial contributions to our studies and have been included in the list of authors as appropriate.

As a result of our studies we recognize pedogenic calcite soil horizons, hypogene calcite/silica veins, and surficial calcite/silica spring deposits at Yucca Mountain. The true pedogenic deposits can be distinguished from hypogene deposits by a variety of petrographic textural characteristics and the lack of significant amounts of silica in pedogenic deposits. Supergene pedogenic processes in some instances have over-printed hypogene calcite/silica deposits thus causing confusion among some workers. Pedogenic deposits of various stages of development occur widely at Yucca Mountain, as would be expected, but calcite/silica deposits are only found associated with faults. Some calcite/silica deposits give high fluid inclusion temperatures and contain pyrite and chalcopyrite as rare components. Calcite,

silica, sepiolite and sulfides (pyrite and chalcopyrite) are common hypogene minerals. Some trace elements, which are characteristic of hydrothermal deposits, are found enriched in some calcite/silica deposits when compared to their abundance in soils. Isotopic data do not "preclude" a hypogene source for calcite/silica deposits but instead are compatible with such an origin. The consistency of the multitude of characteristics of calcite/silica deposits with the characteristics of known spring and hydrothermal deposits require the recognition of a hypogene origin for calcite/silica deposits at Yucca Mountain.

We plan to continue our studies of calcite/silica deposits by collecting and analyzing carefully selected samples from specific localities to answer critical questions regarding the durations and rates of formation of hypogene and pedogenic deposits in order to clarify distinctions between their characteristics and origins.

During this past year we have extended our analysis of hydrofracture and slug tests at Yucca Mountain (see appendix to this executive summary) to include the extension of fractures by excess head and their intersection with networks of open fractures (J. B. Davies, this report). This model has produced solutions of head decay that match experimental observations at Yucca Mountain. These results show that only flow out to these open conduits can explain the data observed at the highest pressures in the slug tests and imply that the hydrofractures intersect the open conduits through narrow fingers whose interconnect widths are much less than the length of the hydrofracture. An important result of this analysis is that certain

regions of the Yucca Mountain hydrological system are dominated by a network of open conduits along joints and fractures in the tuffs. In the coming year hydrological modeling will consider the effects that changes of the permeability of the tuffs of Yucca Mountain have on the steady state configuration (elevation) of the water table.

During this past year we began the formulations of solutions for fluid flow in an intersecting network of fractures within a deformable and dyanmically changing solid such as the tuffs at Yucca Mountain (C. B. Archambeau, this report). Solutions have been obtained for both steady state and transient conditions and all solutions contain constant parameters which are fixed by boundary and initial conditions. These solutions, or variants of them, should have sufficient generality and flexibility to incorporate fluid flow equations to be developed in further and more complete formulations in the coming year.

THE SPATIAL DISTRIBUTION AND CHEMICAL HETEROGENEITY OF CLINOPTILOLITE AT YUCCA MOUNTAIN, NYE COUNTY, NEVADA: EVIDENCE FOR POLYGENETIC HYPOGENE ALTERATION

Authored by:

D. E. Livingston

and

J. S. Szymanski

TABLE OF CONTENTS

List of Tables

List of Figures

INTRODUCTION

This part of TRAC's Annual Report for 1993 summarizes the findings of previous reports (Livingston, 1992, 1993a and 1993b) on the major element geochemistry of zeolitic alteration of the tuffs at Yucca Mountain and updates the status of work. In this report we examine the spatial distribution of zeolites by stratigraphic units and boreholes and the various types of chemical alteration of clinoptilolite indicated by the data reported in Broxton et al. (1986) and Bish and Chipera (1989). The purpose is to evaluate the extent of the metasomatic alteration and to test the hypogene hypothesis of Szymanski (1989 and 1992). In this regard, it is of prime importance to evaluate whether the metasomatic alteration at Yucca Mountain is due to supergene or hypogene processes. In this report, the term "supergene" denotes alteration and mineralization produced by fluids derived directly from atmospheric precipitation and infiltration through the vadose zone, and the term "hypogene" denotes alteration and mineralization produced by fluids from the phreatic zone regardless of their former location or residence time in the Earth's crust. This report begins with a review of previous work on the genesis of zeolites at the Nevada Test Site.

PREVIOUS WORK

The first to have dealt with the origin of zeolites that occur in the vadose zone of the Nevada Test Site was Hoover (1986). In his paper (p. 275) he stated: "At the

Nevada Test Site, zeolites, cristobalite, quartz, feldspar, and clay minerals were deposited by ground water that leached vitric volcanic rocks in the unsaturated zone..." and, "...Ca and Mg are concentrated in the uppermost part of the zeolitized rocks, K in the middle part and Na in the lowermost part". The zonation Hoover (1986) described is not unlike the large scale vertical zonation of zeolites along the northern and western sides of Yucca Mountain (Broxton et al., 1986, 1987 and Livingston, 1993b). Hoover (1986, p. 276) also noted that zeolites can form by: "(1) hydrothermal alteration, (2) burial metamorphism, (3) reaction of glass and water in a saturated system (below a water table), and (4) leaching and deposition in an unsaturated system (above a water table)". In his description of the hydration of glass, the first step in the formation of zeolites, Hoover commented (p. 282): "Relative changes in calcium and magnesium during hydration are the largest changes of any of the constituents, but the source of the calcium and magnesium to account for the increase is not known" (emphasis added). Without knowing and/or proposing the source of the calcium and magnesium, Hoover dismissed hydrothermal alteration and burial metamorphism with the statement (p. 277): "Temperatures in the zeolitized rocks measured in drill holes are 25° to 65°C, and there is no evidence for higher temperatures during zeolitization. This temperature range is below the presently known stability field of analcime and is very narrow for the zoning. Thus, a hydrothermal or burial metamorphic origin is unlikely". However, Hoover did not consider the possibility that the zeolites really did form at higher than the present ambient temperature. He dismissed zeolite formation below the water table by a spate of "Geologic evidence..." (pgs. 278 and 279). By rejecting

elevated temperature of formation in a water saturated, pheatic, zone, Hoover made the unsubstantiated assumption that the zeolites had formed in the vadose zone at present-day ambient temperature.

Broxton et al. (1986) discussed the distribution of chemical alteration at Yucca Mountain in the context of the diagenetic zones of Vaniman et al. (1984). Broxton et al. (1986, p. 6) stated: "The nonwelded tuffs...were highly susceptible to alteration because of the instability of glass in the presence of groundwater. During diagenesis, glass was replaced primarily by the zeolites, clinoptilolite, heulandite, and mordenite" and "These mineralogical zones are similar to those described by Iijma (1975, 1978, 1980) for burial diagenesis of volcanic ash beds in thick sedimentary sequences" (emphasis added). Broxton et al. (1986) stated that zeolite-rich tuffs are laterally extensive beneath Yucca Mountain in three well defined intervals extending from the base of the Topopah Spring member of the Paintbrush tuff to the top of the Tram member of the Crater Flat tuff.

They recognized four zones of diagenesis (pg. 7):

(1) "Zone I, the shallowest zone, is characterized by tuffs that contain substantial unaltered volcanic glass." Exceptions to this generalization were the calcic zeolites and other alteration minerals in the Paintbrush tuff in borehole USW G-2.

(2) "Zone II is characterized by complete replacement of volcanic glass by

clinoptilolite – mordenite, with minor quartz, potassium feldspar, and smectite."

(3) "Zone III is characterized by the progressive replacement of clinoptilolite and mordenite by analcime, potassium feldspar, quartz, and minor calcite and smectite."

(4) "Zone IV, the deepest diagenetic zone penetrated by drill holes, is characterized by the replacement of analcime by authigenic albite".

Broxton et al. (1987) provide a more extensive discussion of the possible genesis of the several types of chemical alteration while using the concept of diagenetic alteration and including the spatial distribution of alteration phases of Bish and Vaniman (1985). Unfortunately, their analysis of the distribution of both the alteration mineralogy and the chemistry seems to be restricted by their rigorous adherence to the concept of diagenetic alteration. The study of diagenetic zeolites in marine deposits (Iijima; 1975, 1978, 1980) has provided important information with respect to parameters such as temperature and chemical character of fluids necessary for the formation of zeolite minerals. Obviously, evidence for a marine environment is lacking at Yucca Mountain, however, the temperature and chemical information derived from diagenetic environments is useful to the study of the origin of zeolites at Yucca Mountain.

Broxton et al. (1987) did consider a hypogene origin of alteration, but only for the deep and calcic-rich zeolitization in the southeastern part of Yucca Mountain. These authors recognized many of the markedly distinctive chemical anomalies in the vadose zone. They did state that (p. 107): "Alteration of volcanic glass to clinoptilolite-group minerals occurred in an open chemical system, resulting in significant rearrangement of mobile cations in the host tuffs" (emphasis added). An "...open chemical system..." would seem to negate the appropriateness of the concept of diagenetic alteration. Thus, Broxton et al. (1987) missed the most significant implication of the spatial and chemical diversity of the zeolitic alteration: that much, if not all, of the chemical alteration may be the result of intermittent upwelling and lateral incursions of ground water. Many authors do not appear to be aware of the fact that, in the context of the known history of the Yucca Mountain site, the term "diagenetic alteration" is inappropriate and misleading. At this site, the process of diagenetic alteration was completed upon the solidification and compaction of the volcanic glass and upon the completion of vapor phase mineralization and isochemical devitrification of the welded tuffs. Any additional chemical alteration must be regarded as both epigenetic and metasomatic with respect to these processes.

Peterman et al. (1993, p. 1940) adopted the same erroneous assuption about diagenesis as Broxton et al. (1987): "In agreement with earlier studies, zeolitization is shown to have occurred under wholesale open-system conditions. Calcium was increased by up to two to three times the baseline values and strontium up to twenty

times" (emphasis added). These words refer to chemical comparisons between rocks from borehole UE-25 a#1 and b#1 and the relatively unaltered rocks collected from Raven Canyon, in the southern part of Yucca Mountain just north of U.S. Highway 95 (Fig. 17). In addition, these authors stated (p. 1941): "Much of the section of nonwelded to partially welded tuffs in the unsaturated zone, including the rhyolite of Calico Hills and part of the Prow Pass and Bullfrog members of the Crater Flat tuff, was extensively altered to clinoptilolite and mordenite during regional diagenesis" (emphasis added). The fact that both the relatively pristine and the altered sections, studied by these workers, occur in relative close proximity of one another indicates that this alteration is more local in nature that regional. Peterman et al. (1993, p. 1941) go on to state: "However, K-Ar dating of zeolites, which are less retentive for Ar than illite, yields a wide spectrum of ages suggesting that the rock has continued to be susceptible to low-temperature alteration long after the main episode of diagenesis" (pg. 1941). This statement both condemed the validity of K-Ar ages of clinoptilolites without substantiation and acknowledged that at least some of the alteration of the tuffs is epigenetic and post-dates the hydrothermal stages of the activity associated with the formation of the Timber Mountain caldera. However, the obvious question of the genesis of the "low-temperature alteration long after the main episode of diagenesis" is left unanswered. In this regard, Peterman et al. (1993, pg. 1946) added: "Future detailed isotopic studies of these units will hopefully contribute to a better understanding of the ultimate source of Ca and Sr added to the Calico Hills and of the degree of water-rock interaction necessary to accomplish this immense mass transfer". Levy (1991, pg. 481) stated, "Yucca

Mountain researchers recognize a few probable examples of perched-water alteration but tend to favor alteration at or below a SWL" (SWL = static water level). In addition Levy stated (p. 481), "...researchers generally agree that zeolitization required the presence of abundant water over a long period of time..." and "...Because the pyroclastic section originally consisted of alternating intervals of mostly devitrified welded tuffs and vitric non-welded tuffs, the positon of the zeolitic boundary in some places is artificially fixed at an original boundary between devitrified and vitric tuff". In other words the zeolitic alteration is spatially constrained by the primary lithologic charateristics of the tuffs. Her statements indicate that most scientists of the DOE Yucca Mountain Project rigorously adhere to a concept of the formation of zeolites at or below a stable, long term, static water table with only slight attention being given to fault-based incursions of hypogene solutions be they driven by geothermal or other geotectonic forces.

Contrary to the above interpretations, Szymanski (1992, p. 7-32 to 7-34) proposed that the zeolitic alteration of tuffs at Yucca Mountain is the product of two chemically- and temporally-distinct hydrothermal systems. One system is alkaline in character and could be zoned -- potassic at shallower depths and sodic at deeper depths. This system is localized in the northern and western portions of Yucca Mountain and is related to the later stages of development of the Timber Mountain caldera. It was driven by the thermal energy associated with this eruptive center. The hydrothermal activity of this system occurred about 11-9 Ma and was responsible for the argillic alteration at about 10 Ma (Aronson and Bish,1987). It was also responsible for older

zeolitic alteration dated between 11-9 Ma (WoldeGabriel, 1991; WoldeGabriel et al. 1992). The chemical characteristics of the rocks altered by this system are alkali-rich, similar to those of the parent glass.

The alteration aureole of this older system, however, was over-printed by an aureole developed in response to a second, younger, hydrothermal system of much different chemical and thermodynamic character (Szymanski, 1992). This younger system was a fault-based hydrothermal system located to the southeast of Yucca Mountain. This was the system responsible for the alkaline earth variety of zeolitic alteration that is so abundant in the southeast. The likely major conduits of this system were the Stage Coach Road fault and splays related to this fault such as the Paintbrush Canyon fault and the Bow Ridge fault. Upwelling of calcic solutions along faults, through the underlying Precambrian and Paleozoic bedrock and the previously altered alkali-rich tuffs and spread through faults into still permeable overlying unaltered bedded tuffs. The alteration products of this system take on the geochemical characteristics of the various basement rocks. The chemical character of these products reflects, in part, the underlying Paleozoic carbonate rocks and, in part, the Precambrian basement rocks.

According to Szymanski (1992) the large scale shape of this second alteration aureole is that of a giant mushroom. Laterally to the west and northwest, the younger system is responsible for the calcium-rich zeolitization of the Paintbrush Tuff, within and near the base of the unaltered or slightly altered "diagenetic Zone I".

The fault-based system is believed to have continued to operate intermittently through the Pliocene and maybe into the Quaternary. This younger system is the one responsible for the younger K/Ar ages (8-12 Ma) of clinoptilolites reported by WoldeGabriel (1991) and WoldeGabriel et al. (1992), and was thought by Szymanski (1992) to be responsible for the opal-calcite-sepiolite veins and calcretes cross-cutting and overlying unconsolidated deposits of Quaternary age.

SPATIAL AND TEMPORAL DISTRIBUTION OF CLINOPTILOLITE

STRATIGRAPHY

All of the samples discussed in this section of this Annual Report were collected from boreholes at and near Yucca Mountain (Fig. 1). Chemical analyses on clinoptilolite, were reported by Broxton et al. (1986, 1987), K/Ar ages by WoldeGabriel (1990), and WoldeGabriel et al. (1992) and mineralogical analyses were reported by Bish and Chipera (1989). These data are available for each of the stratigraphic units Tpc through Tot (Fig. 2, Table 1). The location of the samples with respect to stratigraphy is shown in Figs. 3, 8, and 10 through 16. The stratigraphy shown in the figures has been modified from Craig and Johnson (1984), Maldonado and Koether (1983), Scott and Castellanos (1984), Spengler et al. (1981), and Peterman et al. (1993). Boreholes indicated by the solid circles in Fig. 1 are those presented in Figs. 2, 3, 4, 5, 7, 8 and 11 through 16. Locations and borehole features are listed in Table 2.

The numbers of samples and their stratigraphic settings are given in Tables 3a - 3c. Although the total number of chemical analyses is very large, it can be seen from these tables that the data set is both sparse and spotty with respect to the number of sampled boreholes and stratigraphic units present at Yucca Mountain. The most completely sampled stratigraphic units are the Topopah Spring Member (Tpt) of the Paintbrush Tuff, the tuff of Calico Hills (Tht), and the Prow Pass Member (Tcp) of the Crater Flat Tuff. Glass is more heavily represented in the younger (upper) units of the stratigraphic section in keeping with the greater alteration of older (lower) units in the section.

Spatial Distribution of Unaltered and Altered Rocks in Boreholes

Prior to a detailed examination of the distribution of the chemical diversity of clinoptilolites at Yucca Mountain, it is important to examine the spatial distribution of unaltered and altered rocks in the subsurface. This can be accomplished by examining the mineralogical data of Bish and Chipera (1989). In order to interpret this data properly, one must keep in mind the physical processes of the formation of ash fall tuffs and ash flow tuffs. These deposits formed by the violent eruption of gaseous silica-rich magma. During these eruptions the molten magma vesiculated to such a degree that the glass was mostly disrupted into finely divided shards only millimeters in size. These dense clouds of hot glass shards and vapor fall to the ground and flow coherently over the surface at very high speeds until they come to rest. Such deposits are known as ash flow tuffs or ignimbrites. If highly dispersed in the atmosphere the shards of glass settle through the air and fall to the ground and

are known as ash fall tuffs. The shards which form into ash fall tuffs lose most of their heat prior to coming to rest on the ground surface and do not compact greatly and these deposits have high porosity. Such deposits at Yucca Mountain include the nonwelded to partialy welded beds of the Crater Flat Tuff, the tuff of Calico Hills and parts of the Pah Canyon Member. Ash flow tuffs, however, due to their high temperatures, great mass of material, and plastic nature, retain most of their heat as they come to rest and so compact into solid masses of glass. Many such eruptions, when deposited in rapid succession, may weld together into one cooling unit called a welded ashflow tuff. The Topopah Spring and Tiva Canyon Members of the Paintbrush Tuff are such welded ash flow deposits. Given sufficient thickness, the interior portions of these welded ash flow tuffs may cool slowly enough for the glass to devitrify into its component minerals. For silica- and alkali-rich tuffs such as those at Yucca Mountain the component minerals are alkali feldspar and the silica polymorphs: quartz, tridymite, and cristobalite. During cooling and divitrification, gasses and water are expelled from the glass along with some of the other more fugitive constituents. These form the so-called vapor phase minerals occuring in cavities, cooling joints, and fractures. Vapor phase minerals are formed of constituents of the original glass. Rainfall may enter the cooling mass of volcanic materal causing fumarolic activity and minor fumarolic deposits. More complex scenarios can be conceived, but the above described scenario is that which is appropriate for arid continental settings such as Yucca Mountain. Yucca Mountain itself is a sequence of interlayered nonwelded to partially welded tuffs and detritified densely welded tuffs.

The densely welded devitrified ash flow tuffs of Yucca Mountain can readily be recognized in Fig. 3 where the sum of glass, quartz, tridymite, cristobalite, and alkali feldspar are close to 100%. Where less than 100%, the tuffs are nonwelded to moderately welded and they are altered to other mineral phases. The devitrified densely welded tuffs of the Tiva Canyon (Tpc), Topopah Spring (Tpt), Prow Pass (Tcp), Bullfrog (Tcb), and the Tram (Tct) members can all be recognized in the borehole logs plotted in Fig. 3.

The distribution of zeolites in the boreholes at Yucca Mountain is shown in Fig. 4. With some important exceptions, the zeolites occur predominantly in the tuff of Calico Hills (Tht) and in three levels within the Crater Flat tuff (Tcp, Tcb, and Tct). Important exceptions to this general distribution are the occurrences in the upper layers of the Topopah Spring Member (Tpt) and in the lower Pah Canyon Member (Tpp) of boreholes USW G-2 and USW G-1. It should be also noted in Fig. 4 that only a very small amount of zeolite is reported for the tuff of Calico Hills in borehole USW GU-3. These features have been pointed out by Broxton et al. (1986, 1987). Also, as previously pointed out by Livingston (1992), clinoptilolite occurs well below the top of the analcime zone (diagenetic zone III, Broxton et al., 1986) in borehole USW G-1 at an elevation near -1,000 to -1,250 feet. Similar occurrences of clinoptilolite far below the top of the analcime zone are found in the lower portions of boreholes UE-25 p#1 and USW G-3. Thus, even though there is an overall vertical zonation of clinoptilolite, mordenite and analcime (from top to bottom), there are important exceptions which suggest at least some of the zeolite occurrences are

spatially unique and require a polygenetic, fracture-based, mode of formation. Note also that the present day ground water table is not systematically related to the occurrences of zeolite.

Temporal Distribution of Alteration

The available geochronological data must be accounted for by any genetic model of zeolilization at Yucca Mountain. Potassium-argon ages have been reported for both clinoptilolite and illite-smectite from Yucca Mountain. These ages are shown in Fig. 5. The solid circles represent the ages for clinoptilolite and the solid diamonds the ages for illite-smectite. The solid curve represents the abundance of clinoptilolite. Additional illite-smectite ages have been reported (Bish and Aronson, 1993), but a copy of that report was not obtained early enough to incorporate the data into Fig. 5. These newer data will be evaluated in future reports.

For borehole USW G-2 (Fig. 5), the illite-smectite ages are taken from Bish (1989) and the clinoptilolite ages from WoldeGabriel (1991) and WoldeGabriel et al. (1992). The two illite-smectite ages (both ages = 11.0 ± 0.6 Ma, for an elevation of -73 and 1223 feet) and the deepest clinoptilolite age (10.6 ± 0.2 Ma, for an elevation of 1906 feet), agree with one another and suggest that clinoptilolite may be as good a geochronometer as illite-smectite even though the potassium-argon age retention properties of clinoptilolite are poorly known at present. It is worth noting that, in borehole USW G-2, the two youngest clinoptilolite ages are 4.6 ± 0.2 Ma (at an

elevation of 2,668 feet) and 4.1 ± 0.1 Ma (at an elevation of 3,407 feet). It does not seem likely that this nearly six million year difference in apparent ages for the clinoptilolites in this one borehole can be due to some intrinsic lack of retentivity for argon in clinoptilolites. It would seem more likely that these minerals either were formed at different times or that they were altered at different times.

For borehole USW G-3, the four clinoptilolite ages are taken from WoldeGabriel (1991) and WoldeGabriel et al. (1992). The two clinoptilolite ages, at an elevation of 1,267 feet, are 10.0 ± 0.2 Ma agreeing nicely with the older clinoptilolite ages in borehole USW G-2. The two upper clinoptilolite ages, from boreholes USW G-3/GU-3, are 3.9 ± 0.1 Ma (at an elevation of 2,843 feet) and 2.5 ± 0.2 Ma (at an elevation of 2,982 feet). These young apparent ages are even younger than the young ages in borehole USW G-2.

WoldeGabriel (1991) and WoldeGabriel et al. (1992) report six K/Ar ages for clinoptilolite from borehole USW G-4. They are: 7.3 ± 0.1 Ma (at an elevation of 2,378 feet); 7.5 ± 0.1 Ma (at an elevation of 2,388 feet) ; 4.4 ± 0.2 Ma (at an elevation of 2,404 feet); 3.9 ± 0.2 Ma (at an elevation of 2,433 feet); 4.6 ± 0.1 Ma (at an elevation of 2,482 feet) ; and 4.2 ± 0.1 Ma (at an elevation of 2,786 feet). These apparent ages span the range of ages of clinoptilolites from boreholes USW G-2 and G-3 / GU-3.

WoldeGabriel (1991) and WoldeGabriel et al. (1992) also reported one K/Ar age

from borehole UE-25 p#1. This age is 8.5± 0.2 Ma (~1,910 feet).

For borehole USW G-1, K/Ar ages are known for both illite-smectite and clinoptilolite. For illite-smectite, Bish (1989) reported one K/Ar age of 10.9 ± 0.6 Ma (at an elevation of -1288 feet) and WoldeGabriel (1991) reported two ages of 15.9 ± Ma and 14.5 ± 0.3 Ma (at an elevation of 408 feet). WoldeGabriel (1991) and WoldeGabriel et al. (1992) also reported eight K/Ar ages for clinoptilolite samples from four levels in borehole USW G-1. The deepest clinoptilolite sample (at an elevation of 1,060 feet) yielded an age of 10.6 ± 0.2 Ma in nice agreement with the older clinoptilolite ages in boreholes USW G-2 and USW GU-3 and the illite-smectite ages of Bish (1989) in borehole USW G-2 and deep in borehole USW G-1. Samples obtained from the three upper levels were treated by the standard mineral separation procedure. These samples yielded K/Ar ages of: 6.9 ± 0.2 Ma (at an elevation of 2,158 feet); 5.4 ± 0.2 Ma (at an elevation of 2,530 feet); and 2.2 ±0.1 and 2.0 ± 0.1 Ma (at an elevation of 2,788 feet). Separate portions of the sample collected from an elevation of 2,530 feet were treated with solutions of sodium chloride and barium chloride and then dated by the K/Ar method (WoldeGabriel, 1991). Forty-eight hours of exchange by 1 N NaCl solution resulted in an increase of apparent age from 5.4 ± 0.2 to 7.0 ± 0.2 Ma and a decrease in K_2O content from 4.91%, for the untreated sample, to 3.55%, for the treated sample. Forty-eight hours of exchange by 1 N BaCl solution resulted in a further increase of the K/Ar age to 7.5 ± 0.2 Ma and a decrease of K_2O to 3.20%; seventy-two hours of exchange by 1 N BaCl solution resulted in still further increase of the K/Ar age to 8.4 ± 0.2 Ma. and

a decrease of K_2O to 3.97%. These results suggest a possibility of zoned clinoptilites with overgrowths of younger material on older. Some of the younger apparent ages of clinoptilolites could be mixed ages of younger and older material. On the other hand, the young zeolites at Yucca Mountain may have lost radiogenic argon but if so, how have the older clinoptilolites, about 10 Ma of age, managed to retain their radiogenic argon?

It is important to note that the clinoptilolite ages are systematically younger with increasing elevation in each borehole. For deeper parts of the section (boreholes USW G-1, G-2, and G-3, Fig. 5), the K/Ar ages of clinoptilolites are equivalent to the younger, ~10Ma, K/Ar ages of montmorillonitic clays (illite-smectite). It may be recalled that the four samples of the deepest clinoptilolites yielded K/Ar ages ranging from 9.5 to about 10.6 Ma. For the epigenetic montmorillonitic clays, the ages are about 11.0 Ma. The close correspondence of the K/Ar ages, from samples representing different epigenetic alteration minerals, is important. It indicates that at least some of the Yucca Mountain clinoptilolites are suitable for K/Ar geochronometric analysis. In the local alteration environment these older clinoptilolites, although they are excellent molecular sieves that are prone to ionic exchange, seem to have adequately retained their potassium and argon. Clinoptilolite - fluid ionic exchanges do not appear to have caused loss of radiogenic argon with the result of the resetting of the K/Ar radiometric clock.

CHEMICAL DATA

PRESENTATION OF DATA

The following two sections present the main data set that is the subject of this report. The data are presented graphically so that the chemical, spatial, and temporal variabilities can be readily examined. As noted in Fig. 1, data for only six of the Yucca Mountain boreholes are considered in this report. These six boreholes were selected on the basis of the large number of samples available and the fact that they represent nearly the full range of chemical variability at Yucca Mountain. The abundance and distributions of unaltered and zeolitic rocks are portrayed in Figs. 3 and 4 and K-Ar ages in Fig. 5. The normalization of chemical data is shown in Fig. 6. The distribution and variability of SiO_2 and Al_2O_3 are examined in Figs. 7 and 8 as cross plots and borehole logs, respectively. After examining the total range of variability of exchangable cation oxides of glass, whole rock, and clinoptilolite in Fig. 9, the chemical variability of clinoptilolite is examined as a function of stratigraphic units in Fig. 10. The distributions of the exchangeable oxides of clinoptilolite are examined in individual boreholes in Figs. 11 through 16. In all of these figures (11 through 16) all of the samples from each borehole are represented by three diagrams. The right-hand diagrams present the mole fraction of the exchangeable cation oxides. The left-hand diagrams present this information in a borehole log format, plotted as a function of the elevation of the sample above mean sea level. The dashed horizontal line with open circles indicates the elevation of the present-day water table. The solid horizontal lines indicate the elevation of the ground

surface (at the top) and the total depth (at the bottom). Other solid horizontal lines are formation boundaries and horizontal dotted lines are member boundaries. The solid curve gives the mole fraction of MgO. The second curve (dashed) is the sum of MgO and CaO, thus, the difference between the two curves indicates the mole fraction of CaO. The third curve (dotted) is the sum of MgO, CaO, and K_2O. The abundance of K_2O is the difference between the second and third curves and the abundance of Na_2O is the difference between the third (dotted) curve and the right-hand edge of the diagram. Different symbols are used to identify stratigraphic setting of the samples.

The two diagrams on the right-hand side of Figs. 11 through 16 are cross plots of the mole fraction of the four exchangeable cation oxides. The left-hand part of the diagram represents the mole fraction of the alkali oxides. The lower left corner represents 100% of CaO and MgO. The diagonal line from 1.0 to 1.0 represents 100% of alkali oxides. The right-hand part of the diagram presents the mole fractions of CaO and MgO. The upper right corner is 100% alkali oxides, and the line from 1.0 to 1.0 represents 100% alkaline earth oxides. The symbols used in these two diagrams are the same as in the diagram on the left-hand side of each figure.

NORMALIZATION OF DATA

For the purposes of reviewing the geochemistry of the zeolitic alteration, the data reported by Broxton et al. (1986) were manually keyed into a data base for graphical presentation (Livingston, 1992, 1993a and 1993b). Critiques of the earliest report (Livingston, 1992) showed that it would be more appropriate to evaluate the data on a volatile-free basis and so this was done in later reports (Livingston, 1993a, 1993b). The results are illustrated in Fig. 6 as SiO_2 vs. Al_2O_3 cross plots for glass, whole rock, and clinoptilolite. The first row of diagrams gives the data as reported in Broxton et al. (1986). The second row of diagrams presents the results normalized to the sum of all metal oxides. By using this technique, there has been a remarkable improvement in the coherence of the data. In addition, Livingston (1993a) noted that, during zeolitic alteration, iron and titanium are excluded from clinoptilolite relative to the parent material, glass. Because of this, the data used in this report have been normalized to the sum of SiO_2, Al_2O_3, MgO, CaO, Na_2O, and K_2O, the six major oxides of zeolites, and then recalculated as molar quantities of oxides. Molar oxide quantities are preferred because the valences of the oxides Al_2O_3, MgO, CaO, Na_2O, and K_2O in alumino-silicate minerals are equal in absolute value, and the amount of the exchangeable cations is limited by the charge deficiency of the framework elements which is determined by the abundance of Al_2O_3. The results of this normalization are shown in the third and fourth rows of diagrams in Fig. 6. The third row shows the results for glass, whole rock, and clinoptilolite in the form of SiO_2 vs. Al_2O_3 cross plots. Little difference is noted from the similar plots of normalized oxides shown in the second row. The utility of using molar oxide

quantities, however, is shown in the lower row of three diagrams of Fig. 6. Here, the molar concentration of Al_2O_3 is plotted against the sum of the molar quantities of MgO, CaO, Na_2O, and K_2O. The glass compositions (microprobe analyses) plot close to the line of equal abundance while the whole rock compositions show considerable scatter as might be expected from the presence of minor and trace minerals included in results of the whole rock X-ray fluorescence analyses. The clinoptilolite compositions (also microprobe analyses) plot parallel to the equal abundance line but slightly and systematically to the left. This could be caused by the omission of trace alkali and alkaline earth elements in the analyses or by volatilization of sodium during microprobe analyses, as discussed by Broxton et al. (1986). These diagrams attest to the very excellent quality of the chemical analyses reported by Broxton et al. (1986), and serve to justify the use of normalized molar values to eliminate variations in the data that would otherwise be present.

Throughout this work and, indeed, in the previous reports of Livingston (1992, 1993a and 1993b) and Broxton et al. (1986 and 1987), the chemical abundances of major elements for glass have been assumed to accurately represent the initial composition of all of the tuffs. In this regard, the seven low silica and high alumina glass compositions shown in the upper left hand diagram of Fig. 6 are of interest. These samples were collected from bedded tuff between the Tiva Canyon and Topopah Spring Members of the Paintbrush Tuff in the upper part of borehole UE-25 a#1 (Table 3a, Fig. 3). Whole rock and clinoptilolite analyses are not available for this stratigraphic unit.

RESULTS

OVERVIEW OF CHEMICAL HETEROGENEITY OF CLINOPTILOLITES

Silica And Alumina

In Fig. 6, the chemical distribution of silica and alumina (shown as cross plots) is seen to be bimodal, or at least strongly skewed toward higher Al_2O_3 and lower SiO_2, for both glass and clinoptilolite. The skewness for clinoptilolite is much greater than for glass. In Fig. 7, the clinoptilolite data are presented in the form of cross plots for the individual boreholes. Fig. 8 shows the Al_2O_3 data in borehole log format. The symbols in these diagrams indicate the host stratigraphic units for the analyzed samples and are the same in Figs. 7 and 8. In Fig. 7, the data are bimodally distributed along a linear trend with negative slope for both boreholes UE-25 a & b #1 and in UE-25 p #1. Although not as clearly expressed, the same trends are present in the cross plots for boreholes USW G-1 and USW G-2. Tight clusters are noted in the cross plots for boreholes USW GU-3 and G-3 and for USW G-4. The high alumina of clinoptilolites in USW G-2 are not nearly as high as those in UE-25 p#1, a#1, and b#1. In Fig. 8, in borehole USW G-2 the highest Al_2O_3 is located at the shallowest level (Tpp) and at the deepest level (Tcp). Samples obtained between Tpp and Tcp are low in Al_2O_3 and the lowest being located in Tcp. The variations of silica and alumina in boreholes USW G-2 and USW G-1 are similar in magnitude to the alumina variation shown for glass in Fig. 6. These smaller variations may reflect original chemical composition of the parent glass. Indeed the upper group of high alumina clinoptilolite in USW G-2 occurs in the same

stratigraphic horizon as the high alumina glass in borehole UE-25 a#1 (Table 3a). The Al_2O_3 composition of clinoptilolites from boreholes USW GU-3, USW G-3, USW G-1, and USW G-4 (Figs. 7 and 8) show no significant variation with depth. The high alumina clinoptilolites shown for boreholes UE-25 a#1, b#1 and UE-25 p#1 are also high in lime (see also Figs. 15 and 16). As discussed below, all high-lime clinoptilolites have been formed by metasomatic alteration. With respect to the silica and alumina data set alone, it can not be determined whether the very high lime and high alumina clinoptilolites owe their high alumina concentrations to initial glass composition or to the chemistry of the altering solutions. Both possibilities must be considered.

Soda, Potash, Lime, And Magnesia

Fig. 9 displays the concentrations of the exchangeable cation oxides of all glass, whole rock, and clinoptilolite analyses at Yucca Mountain as reported in Broxton et al. (1986). As noted in Tables 3a, b and c, these concentrations are based on the results of 112 analyses for glass, 63 for whole rock, and 436 for clinoptilolite. Fig. 9 shows the concentrations as mole fractions of the total oxides of soda, potash, lime, and magnesia, the exchangeable oxides. This makes the axes of the cross plots homogeneous with respect to one another because of valence requirements (see the bottom set of diagrams in Fig. 6) rather than non-homogeneous as would be the case for elemental or cation mole fractions. The space within each diagram is uniform throughout for mole fraction quantities and, therefore, the full extent of possible substitution is readily displayed.

Fig. 9 provides a synoptic view of the degree of cation replacement that has occurred for the whole rock tuffs and the clinoptilolites with respect to the parent material, the glass. For clinoptilolite, nearly all of the field for the alkali metals is occupied; for the alkaline earth elements, the degree of chemical diversity is smaller and only one half of the field is occupied (with one markedly obvious exception with very high MgO). The composition of clinoptilolites, as well as their altered rocks, is quite remarkable when compared to the composition of the parent glass. The chemical diversities support the point that, beyond all reasonable doubt, the tuffs of Yucca Mountain have been strongly metasomatically altered by a variety of solutions from a variety of sources. This open system chemical alteration of the tuffs at Yucca Mountain also has been recognized by Peterman et al. (1993) and Broxton et al. (1986, 1987). Open system chemical alteration is properly considered as epigenetic rather that diagenetic.

Fig. 10 presents the cation chemistry of clinoptilolites from several of the local stratigraphic units. The upper left-hand diagrams are for the Pah Canyon (Tpp) and Topopah Spring (Tpt) members of the Paintbrush tuff. The clinoptilolites in these two units are high in alkaline earth metals. The samples from the tuff of Calico Hills (Tht) range in compositions from close to that of the original glass to lime- and potash-rich. Similarly, samples from the Prow Pass member (Tcp) of the Crater Flat tuff range from compositions close to that of the original glass to lime-rich. Each of the remaining stratigraphic units, however, contains clinoptilolites both enriched in CaO and enriched in alkalis except that those from the flow breccia (Tfb) show

strong enrichments of soda. The chemical composition of clinoptilolites is not a strong function of lithostratigraphy.

CHEMICAL HETEROGENEITY OF CLINOPTILOLITES FROM SIX BOREHOLES

This section discusses the data given by Broxton et al. (1986, App. F). The samples were collected from ten boreholes and one surface location at Yucca Mountain (Fig. 1), only six of these boreholes are discussed in this report.

USW G-2

Borehole USW G-2 is located in the northern part of Yucca Mountain, south of Yucca Wash, and just to the east of the Solitario Canyon fault near the head of Solitario Canyon (Fig. 1). The ground elevation is 5,098.4 feet and the water table elevation is 3,387.8 feet (Table 2). Fifty-four samples of clinoptilolite, from 13 different elevations, were analyzed and the results are plotted in Fig. 11. An increase in soda with increasing depth is apparent. The shallowest samples are from the Pah Canyon Member (Tpp) of the Paintbrush Tuff, (Fig. 11, left-hand diagram, open circles). These samples are very high in CaO and MgO, (Fig. 11, right-hand diagrams). The immediately subjacent top bed of the Topopah Spring Member (Tpt, open inverted triangles) is similar in composition but richer in K_2O and poorer in CaO. The base of the Topopah Spring Member has negligible MgO, higher Na_2O and K_2O contents, and lesser CaO content. The base of the Topopah Spring Member is very similar in chemical composition to the underlying tuff of

Calico Hills (Tht, open squares) but distinctly different from the upper beds of the Topopah Spring Member. All samples above 2,668 feet elevation are rich in CaO, (Figure 11, right-hand diagrams). All samples from the Prow Pass Member (Tcp, open diamonds) of the Crater Flat Tuff are very low in MgO and CaO, high in Na_2O, while K_2O is very low to moderate. No prominent change in chemical composition of the clinoptilolites occurs at the location of the present-day water table; strong changes in chemical composition are also not systematically related to stratigraphic boundaries. The compositions of the clinoptilolites, from the Pah Canyon Member (Tpp) of the Paintbrush Tuff and the tuff of Calico Hills (Tht), are grouped in the CaO-rich portions of the cross plots. The differences in chemical composition of the samples, from the top and bottom of the Topopah Spring Member (Tpt, open inverted triangles), are shown in the two right-hand diagrams of Fig. 11. The differences among the samples from the Prow Pass Member (Tcp, open diamonds) of the Crater Flat Tuff are shown in the two right-hand diagrams of Fig. 11. Especially notable is the difference among samples at the same elevation (2,031 feet, arrows, in Fig. 11). Very clearly this demonstrates that, even at the same elevation and below the water table, clinoptilolites can be out of equilibrium with one another even though in very close proximity to one another (same thin section?).

USW GU-3 & G-3

Boreholes USW GU-3 and G-3 are located along Yucca Ridge, south of the potential repository (Fig. 1). The ground surface elevation is 4,856.6 feet and the water table is at 2,397.7 feet of elevation (Table 2). Fifty-six samples of clinoptilolite, from 14

different elevations, were analyzed and the results are plotted in Fig. 12. Again, the samples from the Topopah Spring Member of the Paintbrush Tuff (Tpt, open inverted trianles) are very rich in CaO and moderately rich in MgO. A general increase in Na_2O is noted with increasing depth. Both CaO and K_2O vary irregularly but in a complementary fashion with respect to one another. The lowest concentration of CaO occurs in clinoptilolites from the Prow Pass Member (Tcp, open diamonds) of the Crater Flat Tuff at 2,871 feet elevation. MgO is generally low throughout most of these two boreholes. Large differences can be noted for the concentrations of Na_2O, CaO, and K_2O within the Bull Frog Member (Tcb, filled circles) of the Crater Flat Tuff (Fig. 12, right-hand diagrams). These substantial differences of clinoptilolite chemistry occur 60 to 100 feet below the present-day water table. K_2O is nearly absent at the deepest level (Tlr, 434 feet). Substantial changes in the chemical composition of clinoptilolites do not seem to be related to stratigraphic boundaries, but sample spacing is inadequate to determine if this is truly so. Clinoptilolites from the Prow Pass Member (Tcp, open diamonds) are more potash-rich and soda-poor than those from the Tram Member (Tct, filled triangles). Clinoptilolites from both members show that, within each stratigraphic unit, there are distinct differences in total alkali content. In each case the samples from lower elevations are richer in alkalis than those from upper elevations, and significant differences in the Na_2O to K_2O ratios occur within discrete horizons (for example, 2,871 feet for Tcp and 1,185 feet for Tct).

USW G-1

Borehole USW G-1 is located along the northern boundary of the potential repository in the central part of Yucca Mountain (Fig. 1). The ground surface elevation at this site is 4,348.6 feet and the present day water table is 2,471.1 feet (Table 2). Seventeen samples of clinoptilolite, from eleven different elevations, were analyzed. The results are presented in Fig. 13. The shallowest sample, from the Topopah Spring Member (Tpt) of the Paintbrush Tuff, is exceedingly rich in CaO and very poor in MgO, Na_2O, and K_2O. All samples from this borehole are low in MgO. There is a general increase of Na_2O with increasing depth. The deepest samples from the dacite flow breccia (Tfb) are very high in Na_2O but have negligible K_2O. Intermediate samples, from the tuff of Calico Hills (Tht) and the Prow Pass and Bull Frog members of the Crater Flat Tuff (Tcp and Tcb), are alkali-rich with large amounts of Na_2O and K_2O; CaO is generally low. No significant changes in the chemistry of clinoptilolites are obviously related to the present-day water table but there could be some significant changes in chemistry related to some of the litho-stratigraphic boundaries. The diversity of chemical composition of clinoptilolites from this borehole marks out at least a three-end member field in the right-hand diagram (Na_2O vs. K_2O) of Fig. 13. The samples from the Paintbrush Tuff (Tpt) and the flow breccia (Tfb) are markedly different in chemical composition from that of the glass (compare with Fig. 9). Some of the clinoptilolites from the tuff of Calico Hills (Tht) and from the Prow Pass Member (Tcp) of the Crater Flat Tuff, however, are not too different from the parent glass. The original chemical composition of the flow breccia is not known but the present-day composition of preserved glass does

accurately represent the original composition of the Topopah Spring Member (Tpt) of the Paintbrush Tuff, the tuff of Calico Hills (Tht), and the Prow Pass Member of the Crater Flat Tuff (Tcp).

USW G-4

Borehole USW G-4 is located in the central part of Yucca Mountain (Fig. 1). The ground surface elevation is 4,166.9 feet and the water table is 2,394.4 feet (Table 2). Fifty-nine samples of clinoptilolite from nine different elevations were analyzed. The results are presented in Fig. 14. Samples collected from below the water table are rich in CaO but contain only minor concentrations of MgO, Na_2O, and K_2O. Samples at and above the water table, however, are rich in Na_2O and K_2O and low in MgO and CaO. Chemical compositions of clinoptilolite, from the upper part of the Prow Pass Member (Tcp) of the Crater Flat Tuff, are very similar to those from the overlying beds of the tuff of Calico Hills but markedly different from clinoptilolite residing in lower beds of the Prow Pass Member. The pronounced chemical differences are not associated with stratigraphic boundaries and the overall trend is distinctly different from the trends in boreholes USW G-1, USW G-2, and USW G-3. The cross plots show the uniform character of the chemical composition of the clinoptilolites from the tuff of Calico Hills (Tht), which are not markedly different from the composition of glass (Fig. 9). Clinoptilolites from the Bull Frog Member (Tcb, filled circles) of the Crater Flat Tuff, however, are markedly enriched in CaO. The sharply contrasting chemical compositions of clinoptilolites, residing at different levels of the Prow Pass Member (Tcp, open diamonds) of the Crater Flat Tuff, are

shown in the right-hand diagram of Fig. 14. Samples from the upper elevation (2,405 feet) are alkali-rich while those from the lower elevations (2,035 to 1,928 feet) are lime-rich.

UE-25 a#1 & UE-25 b#1

Boreholes UE-25 a#1 and UE-25 b#1 are located in Drill Hole Wash, to the east of the potential repository site (Fig. 1). The ground surface elevation is 3,934.4 feet and the water table is at 2,397.7 feet (both values are for UE-25 a#1, Table 2). For the purpose of this report, these two drill holes are treated as one. Results of 86 analyses, from 15 different elevations are plotted in Fig. 15. Again, the uppermost samples of clinoptilolites from the Topopah Spring Member of the Paintbrush Tuff (Tpt, open inverted triangles) are rich in CaO, and the shallowest sample (2,655 feet) is exceedingly rich in MgO (Fig. 15, right-hand diagram). Most of the clinoptilolites from the Topopah Spring Member (Tpt) and the tuff of Calico Hills (Tht, open squares) are similar to one another and similar to most of the clinoptilolites from the Prow Pass Member (Tcp, open diamonds) of the Crater Flat Tuff. However, one of two samples from the tuff of Calico Hills (Tht, open square symbols at 2,469 feet) is richer in K_2O and lower in CaO than the other sample from the same elevation. Furthermore, one sample from the Prow Pass Member (open diamonds at 1,821 feet) is markedly low in CaO and high in Na_2O and K_2O (Fig. 15, right-hand diagrams). In terms of chemical composition, this sample is not very different from the parent glass (Fig. 9, left-hand diagram). The lowermost samples, from the Bull Frog Member of the Crater Flat Tuff (Fig. 15, right-hand diagram), are similar in chemical composition to most of the other samples from this borehole.

Marked changes in the chemical composition of clinoptilolites are related neither to stratigraphic boundaries nor to the present-day water table. Other than the previously mentioned anomalies, at this locality there is no pronounced trend of the chemical composition of the clinoptilolites with depth. Concentrations of MgO, Na_2O, and K_2O show some small variations but these oxides are consistently of low abundance.

UE-25 p#1

Borehole UE-25 p#1 is located south and east of the potential repository site (Fig. 1). The ground surface elevation is 3,654.6 feet and the water table is 2,466.6 feet (Table 2). Forty-eight samples of clinoptilolite, from seven different elevations, were analyzed and the results are presented in Fig. 16. All of these samples were collected from below the present-day water table. For these clinoptilolites, CaO is by far the most abundant cation oxide and shows a steady increase with increasing depth. In contrast, the concentrations of Na_2O and K_2O show a decrease with increasing depth. The concentration of MgO is very low and irregularly distributed with depth.

SUMMARY OF CHEMICAL HETEROGENEITY

The following six points summarize the chemical heterogeneity of clinoptilolites from of Yucca Mountain:

1. Most of the clinoptilolites are calcic in character, which differs markedly from the original composition of the parent glass which is alkalic in character.

2. In the southern and eastern parts of Yucca Mountain (boreholes UE-25 a#1, and b#1, and UE-25 p#1) the calcic clinoptilolites occur in all stratigraphic units from the Topopah Spring (Tpt) member of the Paintbrush Tuff to the tuff of Lithic Ridge (Tlr). Importantly, these alteration minerals are present both above and below the contemporary water table (Fig. 14).

3. In the northern and western parts of Yucca Mountain (boreholes USW G-1, G-2, and G-3 and GU-3), the calcic clinoptilolites are the abundant in upper parts of the stratigraphic section; i.e., within and above the Crater Flat Tuff. The occurrence of these clinoptilolites, however, is not restricted to the vadose zone. Instead, in all of the examined boreholes, calcic-rich clinoptilolites were found to be present hundreds to thousands of feet below the contemporary water table (Tht in Fig. 11, Tcb in Fig. 12, Tcb in Fig. 13).

4. At and near Yucca Mountain, the chemical composition of clinoptilolites is not uniform. Instead, these clinoptilolites display a remarkable degree of chemical diversity involving all of the major exchangable cations. Equally remarkable is the fact that, spatially, the chemical diversity persists at scales ranging from centimeters to kilometers.

5. For alteration observed at Yucca Mountain, the chemical composition of the original parent glass does not exclusively govern the composition of the alteration products (clinoptilolite). This is indicated by the fact that, for a given stratigraphic unit within a given borehole, the chemical compositions of clinoptilolites define two or more clusters, all with differing proportions of the exchangable oxides. Examples of such intra-stratigraphic clustering may be found in boreholes: USW G-2 (Tpt and Tcp Fig. 11); USW G-1 (Tht, Fig. 13); USW GU-3, G-3 (Tcp, Tcb, and Tct, Fig. 12); USW G-4 (Tcp, Fig. 14); and UE-25 a#1 and b#1 (Tpt, Tht, and Tcp, Fig. 15).

6. The large-scale diversity in chemical composition of the clinoptilolites does not exhibit any systematic relationship to lithostratigraphic boundaries or to the present-day water table.

Both the chemical character of the clinoptilolites (relative to the parent glass) and their chemical diversity (relative to each other) have important implications. First, the calcic composition of some of the clinoptilolites, if considered together with the fact that the host tuffs were originally alkalic in chemical composition, indicates that they must have been produced via interaction of metasomatic solutions with the vitric rock. In other words, the chemical solutions which brought about the alteration must have acquired their chemical character from sources other than the host tuffs.

Second, the pronounced diversity in chemical composition of the clinoptilolites at

both small and large spatial scales indicates that the metasomatic solutions were interacting with the host rock episodically over a prolonged period of time. In other words, the responsible alteration process must be regarded as polygenetic.

Third, the pronounced difference between the alkali-rich and calcic-rich clinoptilolites in the deeper parts of Yucca Mountain in the north and west as opposed to the southeast, respectively, indicates that the altering solutions must have acquired their chemical character from different sources and possibly by different processes. Again, the evidence suggests polygenesis.

Fourth, the similarity of the range of chemical diversity of clinoptilolites in both the vadose and the phreatic zones suggests that altering solutions of differing chemical character have intruded into rocks both above and below the present-day water table. This, in turn, suggests that the water level has undergone substantial flutuations in the past. These fluctuations may have occured at different places at different times and may or may not have been due to long term stands of stable regional water table but may in some places represent local incursions along faults or other permeable zones.

DISCUSSION

INTERPRETIVE OPTIONS

Iijima (1978) recognized five genetic developmental modes of zeolites in marine

deposits: 1) burial diagenesis; 2) contact metamorphism; 3) hydrothermal alteration; 4) submarine hydrothermal alteration; and 5) percolating groundwater alteration. In addition, he recognized zeolite accumulation in alkali saline lake environments (Iijima, 1975).

HYPOGENE VS. SUPERGENE

There are two opposing options for the interpretation of the alkaline earth zeolitic alteration at Yucca Mountain, the hypogene and the supergene (contemporary atmospheric precipitation infiltration through the vadose zone). With regard to the genetic mode of formation of the calcic clinoptilolites at Yucca Mountain, the range of viable interpretative options may be narrowed by considering the depositional history of this mountain. The following four points can be made. First, the tuff section at Yucca Mountain which contains the calcic clinoptilolites occurs between the topographic surface and a depth of about 1.2 km; thus, burial diagenesis similar to that affecting the several kilometer thick section described by Iijima (1978) can be ruled out. Second, the entire section was deposited strictly in a continental environment; thus, submarine hydrothermal alteration can be ruled out. Third, other than small basaltic dikes, there are no known occurrences of intrusive rocks at Yucca Mountain; thus, contact metamorphism can be ruled out. Fourth, the Yucca Mountain locality is definitely not an alkali saline lake. For Yucca Mountain , there are only two viable options, namely: (1) hydrothermal alteration; and (2) percolating groundwater alteration. Recognizing the fact that zeolitic alteration requires both the

presence of vitric material and abundant water over a long period of time, as described by Levy (1991, pg. 481) one may presume that the Iijima's percolating groundwater alteration option pertains to zeolitization below the water table where vitric rocks are subjected to prolonged exposure to aqueous solutions.

Within the context of the principal question that is being addressed by TRAC-NA (i.e., the long-term stability of the contemporary water table at Yucca Mountain), the hypogene alteration option does not differ fundamentally from the perched or percolation groundwater alteration option. Both of these options may be joined together under the banner of the so-called "hypogene hypothesis". This hypothesis calls on upwelling and lateral incursions of ground water from the phreatic zone, in response to perturbations introduced into the local flow system by tectonic factors and processes. In other words, the upwelling fluids have acted as an agent for the calcic-zeolitic alteration of the vitric tuffs as well as for the precipitation of the opal-calcite-sepiolite veins and calcretes, (see Hill et al., this Annual Report). Broxton et al. (1986) recognized this mode of formation for the calcic zeolite suite encountered below the contemporary water table in boreholes UE-25 p#1, UE-25 a#1, and UE-25 b#1. These authors expressed a viewpoint that these zeolites may have been formed by upwelling of hypogene fluids from the subjacent Paleozoic carbonates.

Recognition of the fact that, at Yucca Mountain, both the calcic zeolites and the opal-calcite-sepiolite veins are known to occur hundreds of meters above the contemporary water table and, at the same time, faithful adherence to traditional

hydrologic concepts (i.e., tectonic influence of the behavior of ground water systems is minimal) requires the assumption of a competing hypothesis. This so-called supergene hypothesis includes the deposition of eolian dust, derived from Paleozoic carbonates to provide calcium, and the direct infiltration of rain water to dissolve and transport the eolian components. Once introduced into the vadose zone, the infiltrating and chemically modified rain water acts as an agent for the calcic zeolitization and for the opal-calcite-sepiolite vein mineralization.

With regard to the calcic zeolites at Yucca Mountain, the following five remarks are appropriate to the hypogene-supergene debate First, the chemical composition of supergene fluids is not adequate to account for the chemical character of the alteration and mineralization in question. This composition is known based on the results of laboratory analyses of fracture-based fluids of the vadose zone from seeps into tunnels or from shallow boreholes at the Nevada Test Site. Winograd and Thordarson (1975) analyzed perched water encountered in test well 73-76, at depth intervals of 77-693 and 1565-1695 feet below the surface. The concentration of total dissolved solids in these waters are 327 and 985 mg/l, the Na + K concentrations are 105.4 and 428.4 mg/l, and the Ca + Mg concentrations are 14.0 and 4.0 mg/l, respectively. Similar relative concentrations of the major cations are evident in the results of chemical analyses reported by White et al. (1980) for the fracture-based fluids from the vadose zone at Rainier Mesa. For 36 samples of seeps into different segments of tunnels U12b, U12e, U12n, and U12t the average Na + K and Ca + Mg concentrations are 1.66 and 0.26 mmoles/l, respectively. For supergene fluids,

similar relative concentrations of the major cations were reported by Russell (1987), Kerrisk (1987), and Claassen (1985). Clearly, even allowing for a sufficiently rapid production of zeolitic alteration at temperatures of ~25° C, it is difficult to understand how the very weak alkalic (soda and potash) solutions may yield zeolitic alteration products which are alkaline earth-rich in character. To yield such products, solutions which (at least on relative basis) are enriched in the alkaline earth elements are required.

Direct observations indicate that such solutions are not being generated via interactions of meteoric precipitation with soil horizons and with alkalic tuffs. The results of chemical analyses of groundwater samples from and near the Nevada Test Site indicate that solutions with the required relative major cation concentrations exist, but only locally in areas that are associated with increased heat flow and positive vertical hydraulic gradients (Szymanski and Livingston,1993). These hypogene solutions acquire their chemical content through prolonged leaching of Paleozoic and older rocks underlying the Tertiary tuffs. The results of chemical analyses of Domenico (1972) and Claassen (1973 ,1985) indicate that such solutions are sharply enriched in total dissolved solids (in excess of 2,000 ppm) relative to supergene fluids, and that they carry sufficiently high concentrations of Ca + Mg cations relative to the concentrations of Na + K.

Second, the volume of the metasomatically altered tuffs at Yucca Mountain is measured in terms of at least a few km^3. To achieve this, a substantial mass of

alkaline earth elements must have been transported in water and sequestered in the tuffs. The average concentration of CaO in the altered tuffs is about 2% higher than in glass (Livingston, 1993) Within the context of a supergene origin, is such degree of CaO enrichment feasible? For a column of tuff 1 cm^2 in area and 50,000 cm in height (representative thickness of the altered tuff of Calico Hills and the Crater Flat Tuff combined), a 2% increase in the average concentration of CaO requires the addition of 2,200 g of calcium oxide. Although the long-term rate of the airborne supply of $CaCO_3$ is unknown for Yucca Mountain, it may be assumed that this rate does not exceed the mean value of 0.3 - 5.0 g/cm^2/10,000 years range proposed for eolian carbonate accumulation rates for soils on non-calcareous parent materials in the southwestern United States (D.O.E.,1993). The rate of the airborne supply of CaO, therefore, does not exceed 1.6 g/cm^2/10,000 years. The total accumulation of the airborne CaO, during a time span of 8.5 x 10^6 years (oldest known K/Ar age of the calcic clinoptilolites), is less than 1,360 grams. Presumably, only a fraction of the airborne CaO is sequestered in the vadose zone tuffs, and the remainder of it must be assumed to accumulate in the form of: a) petrocalcic soils (in the vicinity of Yucca Mountain there are calcite accumulations a few hundreds of feet thick; Carr and Parrish, 1985); b) the AMC breccia cements (Levy and Nasser, 1991); c) the calcite/opal veins (present throughout the 500m thick vadose zone); and the rest does not accumulate, but is transported in dissolved state into the phreatic zone. Although it is not known what fractions of the accumulated CaO are available to support each of these essential processes, the calculation suggests that the eolian source is insufficient to account for the observed degree of CaO enrichment of the tuffs and the calcite/silica deposits. According to a hypogene model, however, there

is no problem involving a sufficient source of Ca (and other elements). This is the same conclusion as arrived at by Hill et al. (this report; Source of Calcium section).

Third, an important chemical characteristic of the calcic zeolitization at Yucca Mountain is its pronounced spatial diversity. This chemical diversity is independent of stratigraphy and is expressed by spatially varying enrichments in alkaline earth elements relative to the composition of the parent glass. The degree of chemical diversity of such enrichment can be illustrated through a comparison of the concentrations of alkaline earth elements for stratigraphically equivalent sections at different localities. An example of such a comparison, for Ca, Sr, and Ba, is shown in Fig. 17. This figure is from Peterman et al. (1993) and involves the comparison of severely altered tuffs from boreholes UE-25 a#1 and b#1, with relatively unaltered tuffs exposed in Raven Canyon, at the southern end of Yucca Mountain. It was constructed by calculating the ratios of Ca, Ba, and Sr concentrations in the UE-25 a#1 and b#1 section relative to the concentrations in the Raven Canyon section. This figure shows that the stratigraphically equivalent tuffs of Calico Hills from boreholes UE-25 a#1 and b#1, relative to the Raven Canyon tuffs, are notably enriched in Ca, Sr, and Ba. The Ca enrichment is a factor of two to three; the Sr enrichment is a factor of 20; and locally, the Ba enrichment is as high as a factor of ten. Significantly, in boreholes UE-25a#1 and b#1, the altered tuffs of Calico Hills extends from about 200 feet above to 250 feet below the contemporary water table, and the vadose zone tuffs do not differ significantly in their composition from those of the phreatic zone. Within the context of the supergene hypothesis, there is no

plausible explanation for the sharply differential enrichment of the Calico Hills tuffs in the vadose zone. The opposite is true for the hypogene hypothesis. In that regard, the compositional similarities of the vadose and the phreatic zones tuffs alone indicate that the altered rocks of the vadose zone owes its chemical and mineralogical alteration to hypogene processes.

Fourth, in the northern and western sectors of Yucca Mountain (boreholes USW G-2, G-1, and G-3), the calcic clinoptilolites are developed selectively in the upper parts of the stratigraphic section. The underlying tuffs, however, contain clinoptilolites that are soda- and potash-rich, and the degree of alkaline earth element enrichment is significantly lower. It may be recalled that the overlying calcic clinoptilolites yield K/Ar ages younger than the ~10 Ma ages of the underlying sodic-potassic clinoptilolites. This spatio-temporal feature could be regarded as evidence favoring the supergene hypothesis. However, this is not necessarily the case because: (a) the depth-restricted development of calcic clinoptilolites is limited to the northern and western sectors of the mountain and, for the remaining sectors (boreholes USW G-4, UE-25 p#1, and UE-25 a#1 and b#1), the calcic clinoptilolites are present throughout the entire explored section and, (b) the spatial distribution of the calcic zeolites has a logical explanation which does not require adoption of a supergene hypothesis. Such an explanation has been offered by Szymanski (1992) and is summarized in Figs. 18 and 19. Within the context of the proposed explanation, the calcic clinoptilolites both above and below the contemporary water table have a common origin, as implied by their similar chemical compositions. This

is in contrast to the supergene hypothesis which does not allow for a common origin.

Fifth, it is also important to note that in addition to K/Ar ages similiar to those of illite-smectite the deeper clinoptilolites seem to be geochemically affiliated with the montmorillonite clays. Two points can be made: (1) the deeper clinoptilolites of the northern (boreholes USW G-1 and G-2) and south-western (borehole USW G-3/GU-3) sectors of Yucca Mountain record the event of alkali-rich metasomatism. From Figs. 10, 11, and 12, it may be recalled that the clinoptilolites are rich is potash and soda; the lime and magnesia content is relatively low. (2) the deep clinoptilolites occur in the sector of Yucca Mountain (boreholes USW G-1 and G-2) where higher grade montmorillonitic clays (allevardite, kalkberg, and illite) occur at a relatively shallow depth (Bish and Chipera, 1989, Bish, 1989, and Bish and Aronson, 1993). In addition to alteration temperature and duration of the thermal exposure, water chemistry plays an important role in controlling the formation of these clays; i.e., the smectite -> allevardite -> kalkberg -> illite transformations. Increasing concentration of potassium tends to promote these transformations (Bish and Aronson, 1993). The predominance of other cations (particularly Ca and Mg), however, tends to inhibit it (Howard, 1981). It is likely as with the older clinoptilolites that the argillitic alteration was produced by solutions carrying relatively high proportions of K + Na cations.

The above remarks, if considered together with the K/Ar ages, indicate that it is reasonable to consider the oldest potash-rich clinoptilolites and higher-grade

montmorillonite clays as members of an older paragenetic assemblage. Both the K/Ar ages and the proximity to the Timber Mountain caldera indicate that this assemblage may record active hydrothermal stages of this eruptive center. Clearly, the corresponding clinoptilolites are neither deuteric nor supergene in origin.

Much more important and problematic are the clinoptilolites yielding K/Ar ages significantly younger than 10 Ma. By comparing Fig. 5 with Figs. 11 through 16, it can be noted that these younger clinoptilolites reside in metasomatically altered tuffs which (relative to the parent glass) are enriched in alkaline earth elements. It is likely therefore that the dated clinoptilolites themselves were also similarly enriched. Should this expectation be confirmed by further analyses, then two important points follow. (1) Even after allowing for some losses of radiogenic argon and resetting of the K/Ar radiometric clock, the shallower, lime-rich clinoptilolites must be regarded as younger that the deeper, potash-soda-rich clinoptilolites. These lime-rich clinoptilolites are neither deuteric in origin nor formed in association with hydrothermal activity of the Timber Mountain Caldera. (2) Both the K/Ar ages and the results of NaCl and BaCl exchange experiments (WoldeGabriel, 1991) indicate polygenetic formation of the lime rich clinoptilolites. This confirms the independent conclusion based on the chemical diversity of these clinoptilolites.

POSSIBLE LINKAGE OF CALCIC ZEOLITES WITH CALCITE/SILICA DEPOSITS

Within the strategy adopted by TRAC-NA to address the potential significance of a

variety of hydro-tectonic interactions at Yucca Mountain (Szymanski et al., 1993), the genetic mode of formation of the post-Timber Mountain Caldera clinoptilolites is of direct regulatory concern. The reasons for this concern are: (1) The apparent ages of the younger clinoptilolites may be mixed or average ages of younger and older clinoptilolite which would suggest a very young age for the latest event of clinoptilolite formation. (2) Being clearly of the post-Timber Mountain caldera age, the calcic clinoptilolites may be expressing hydro-tectonic processes and/or hydrothermal events that have been previously unrecognized by D.O.E. project scientists. In this regard, the clinoptilolites, as well as other zeolites from the calcic series, may lead to the establishment of a rational framework within which it is possible to seek a reliable resolution of the controversy that surrounds the origin (either hypogene or supergene) of the opal-calcite-sepiolite veins and calcretes (Hill, et al., in this report). These controversial deposits are geochemically affiliated with the calcic zeolites and, consequently, may be cogenetic with them. (3) Although the K/Ar ages of the calcic zeolites may be considered by some to be unreliable, Peterman et al. (1993), there is less doubt about the ages of the controversial veins and calcretes. In that regard both directly observed geologic relationships and U/Th ages conclusively indicate that the precipitation of these deposits occurred during at least the late Quaternary. (4) The presence of numerous, up-to-30-feet thick, layers of calcrete in the first ~1500 feet of the section penetrated by borehole VH-2, both above and below the Rainier Mesa member of the Timber Mountain tuff (Carr and Parrish, 1985), indicates that the opal-calcite-sepiolite calcretes were formed intermittently throughout the entire Plio-Quaternary time span. If the K/Ar ages of

the post-Timber Mountain caldera clinoptilolites are taken as reliable, then these clinoptilolites, may display a temporal affinity with the opal-calcite-sepiolite veins and calcretes. In other words it is possible that the calcic zeolitization and the opal-calcite-sepiolite veins and calcretes at Yucca Mountain are connected temporally as well as compositionally.

CONCLUSIONS

(1) The chemical composition of most clinoptilolites at Yucca Mountain is rich in calcium and markedly different from their parental alkali rhyolite tuffs. This fact indicates that enormous quantities of calcium, as well as other elements, have been introduced into the interior of Yucca Mountain subsequent to the deposition and lithification of the tuffs. This fact further indicates that the calcium-rich alteration of the tuffs is epigenetic rather than diagenetic.

(2) The occurrence of locally discrete clinoptilolites with chemical compositions distinctively different from that of immediately adjacent clinoptilolites indicates that the zeolitic alteration is not an equilibrium assemblage and therefore must be polygenetic.

(3) The small spatial scaled chemical diversity of clinoptilolites further indicates that at least some of the alteration was introduced through locally permeable zones such as faults, fractures, and breccias.

(4) Apparent K/Ar ages of clinoptilolites suggest that some of the alteration has continued into the Plio-Quaternary time.

(5) The diagenetic and supergene modes of formation of the zeolitic alteration in the vadose zone, as advocated by workers of the U. S. Department of Energy Yucca Mountain Project, do not adequately account for the remarkably heterogeneous spatial and chemical diversity of clinoptilolite from Yucca Mountain tuffs. This heterogeneity and diversity seems best explained as a product of the polygenetic and epigenetic incursions of hypogene solutions, geothermal in nature or otherwise.

(6) The relatively late stage, epigenetic, calcic metasomatism at Yucca Mountain may possibly be temporally continuous with the controversial calcite/opal mineralization (see next section of this Annul Report by Hill et al.).

REFERENCES

Aronson, J. L. and D. L. Bish, 1987. *Distribution, K/Ar Dates, and Origin of Illite/Smectite in Tuffs from Cores USW G-1 and USW G-2, Yucca Mountain, Nevada, A Potential High-Level Radioactive Waste Repository.* Clay Mineral Society, 24th Annual Meeting, Socorro, New Mexico.

Bish, D. L., 1989. *Evaluation of Past and Future Alterations in Tuff at Yucca Mountain, Nevada, Based on the Clay Mineralogy of Drill Cores USW G-1, G-2, and G-3.* LA-10667-MS, Los Alamos National Laboratory, Los Alamos, New Mexico.

Bish, D. L. and S. J. Chipera, 1989. *Revised Mineralogic Summary of Yucca Mountain, Nevada.* LA-11497-MS, Los Alamos National Laboratory, Los Alamos, New Mexico.

Bish, D.L. and J.L. Aronson, 1993. *Paleogeothermal and Paleohydrologic Conditions in Silicic Tuff from Yucca Mountain, Nevada.* Clays and Clay Minerals, Vol. 41, pg.148-161.

Bish, D. L. and D. T. Vaniman, 1985. *Mineralogic Summary of Yucca Mountain, Nevada. LA-10543-MS,* Los Alamos National Laboratory, Los Alamos, New Mexico.

Broxton, D. E., R. G. Warren, R. C. Hagan, and Gary Luedemann, 1986. *Chemistry of Diagenetically Altered Tuffs at a Potential Nuclear Waste Repository, Yucca Mountain, Nye County, Nevada.* LA-10802-MS, Los Alamos National Laboratory, Los Alamos, New Mexico.

Broxton, D. E., D. L. Bish, and R. G. Warren, 1987. *Distribution and Chemistry of Diagenetic Minerals at Yucca Mountain, Nye County , Nevada.* Clays and Clay Minerals, Vol. 35, No. 2, pp. 89-110.

Carr, W. J., and L. D. Parrish, 1985. *Geology of Drill Hole USW VH-2, and Structure of Crater Flat, Southwestern Nevada.* USGS Open-File Report 85-475, Denver, Co.

Claassen, H. C., 1973. *Water Quality and Physical Characteristics of Nevada Test Site Water-Supply Wells.* USGS Open-File Report 474-158, Denver, Co.

Claassen, H. C., 1985. *Sources and Mechanisms of Recharge for Groundwater in the West-Central Amargosa Desert, Nevada* - A Geochemical Interpretation. USGS Professional Paper 712.

Chipera, S. J., and D. L. Bish, 1988. *Mineralogy of Drill Hole UE-25p#1 at Yucca Mountain, Nevada.* LANL Report LA-11292-MS.

Coombs, D. S., 1970. *Present Status of the Zeolite Facies.* Am. Chem. Soc. Adv. Chem. Ser. 101.

Coombs, D. S., A. J. Ellis, W. S. Fyle, and A.M. Taylor, 1959. *The Zeolite Facies with Comments on the Interpretation of Hydrothermal Synthesis.* Geochimica at Cosmochimica Acta, 17.

Craig, R. W. and K. A. Johnson, 1984. *Geohydrologic Data for Test Well UE-25p#1, Yucca Mountain Area, Nye County, Nevada.* U.S. Geological Survey Open File Report 84-450.

DOE (U.S. Department of Energy), 1993. *Report on the Origin of Calcite-Silica Deposits at Trench 14 and Busted Butte and Methodologies Used to Determine Their Origin.* The U.S. Department of Energy, Office of Civilian Radioactive Waste Management, Washington, D.C.

Domenico, P. A., 1972. *Concepts and Models in Groundwater Hydrology.* Earth and Planetary Sciences, McGraw-Hill International Series.

Hoover, D. L., 1968. *Genesis of Zeolites, Nevada Test Site.* Geol. Soc. Am., Memoir 110, pp. 275 to 284.

Howard , J. J., 1981. *Lithium and Potassium Saturation of Illite/Smectite Clays from Interlaminated Shales and Sandstones.* Clays and Clay Minerals, 29.

Iijima, A., (1975). *Effect of Pore Water to Clinoptilolite-Analcime-Albite Reaction Series.* J. Fac. Sci. Univ. Tokyo, Sec. II 19. 133-147.

Iijima, A. (1978). *Geologic Occurrences of Zeolites in Marine Environments: In Natural Zeolites: Occurrence, Properties.* Use, L. B. Sand and F. A. Mumpton, eds., Pergamon Press, Elmsford, New York, 175-198.

Iijima, A. (1980). *Geology of Natural Zeolites and Zeolitic Rocks.* In Proc. 5th Int. Conf. on Zeolites, Naples, 1990, L. V. C. Rees, ed., Heyden, London, 103-118.

Kerrisk, J. G., 1987. *Groundwater Chemistry at Yucca Mountain, Nevada, and Vicinity.* LANL Report LA-10929-MS.

Levy, S. S., 1991. *Mineralogic Alteration History and Paleohydrology at Yucca Mountain, Nevada.* High Level Radioactive Waste Management, Proceedings of the Second International Conference, Las Vegas, Nevada, April 28 - May 3, 1991. American Nuclear Society, La Grange, Ill. and American Society of

Civil Engineers, New York, N.Y.

Levy, S. S. and C.W. Naeser, 1991. *Bedrock Breccias Along Fault Zones Near Yucca Mountain, Nevada.* Draft report submitted for publication by the U.S. Geological Survey. Los Alamos National Laboratory. Los Alamos, New Mexico.

Livingston, Donald E.,1992. *Some Aspects of Alteration and Metasomatism at Yucca Mountain, Nevada.* Presentation to: The Association o f Engineering Geologists, Southwestern Section. Las Vegas, Nevada, Nov. 10, 1992.

Livingston, Donald E., 1993a. *A Review of the Major Element Geochemistry of Yucca Mountain, Nevada.* Report No. 4, Quarterly Report submitted to the Nuclear Waste Project Office of the State of Nevada,. Technical and Resource Assessment Corporation, Boulder, Colorado, 89 pp.

Livingston, Donald E., 1993b. *The Spatial and Chemical Diversity of Zeolitic Alteration at Yucca Mountain, Nye County, Nevada.* Report No. 5, Quarterly Report submitted to the Nuclear Waste Project Office of the State of Nevada. Technical And Resource Assessment Corporation,. Boulder, Colorado. 84 pp.

Maldonado, Florian and S. L. Koether, 1983. *Stratigraphy, Structure, and Some Petrographic Features of Tertiary Volcanic Rocks at the USW G-2 Drill Hole, Yucca Mountain, Nye County, Nevada.* U.S. Geological Survey Open File Report 83-732.

Marshall, B. D., Z. E. Peterman, and J. S. Stuckless, 1993. *Strontium Isotopic Evidence for a Higher Water Table at Yucca Mountain.* High Level Radioactive Waste Management, Proceedings of The Fourth International Conference, Las Vegas, Nevada, April 26-30. American Nuclear Society, La Grange, Ill. and American Society of Civil Engineers, New York, N.Y.

NAS/NRC, 1992. *Ground Water at Yucca Mountain, How High Can It Rise?* Final Report of the Panel on Coupled Hydrologic/Tectonic./Hydrothermal Systems at Yucca Mountain. National Research Council, National Academy Press, Washington, D.C.

Peterman, Z. E., R. W. Spengler, F. R. Singer, and R. P. Dickerson, 1993. *Isotopic and Trace Element Variability in Altered and Unaltered Tuffs at Yucca Mountain, Nevada.* High Level Radioactive Waste Management, Proceedings of the Fourth International Conference, Las Vegas, Nevada, April 26-30. American Nuclear Society, La Grange, Ill. and American Society of Civil Engineers, New York, N.Y.

Russell, C. E., 1987. *Hydrogeologic Investigations of Flow in Fractured Tuffs, Rainier Mesa, Nevada Test Site.* M. S. Thesis, University of Nevada-Reno, Reno, Nevada.

SAIC, 1992. *Report of Early Site Suitability Evaluation of the Potential Repository Site at Yucca Mountain, Nevada.* SAIC-91/8000, prepared for the Office of Civilian Radioactive Waste Management, Science Applications International Corporation, Las Vegas, Nevada.

Scott, R. B. and Mayra Castellanos, 1984. *Stratigraphic and Structural Relations of Volcanic Rocks in Drill Holes USW GU-3 and USW G-3, Yucca Mountain, Nye County, Nevada.* U.S. Geological Survey Open File Report 84-491,

Spengler, R. W., F. M. Byers Jr., and J. B. Warner, 1981. *Stratigraphy and Structure of Volcanic Rocks in Drill Hole USW G-1, Yucca Mountain, Nye County, Nevada.* U. S. Geological Survey Open File Report 84-491.

Szymanski, J. S., 1989. *Conceptual Considerations of the Yucca Mountain Groundwater System with Special Emphasis in the Adequacy of this System to Accommodate a High-Level Nuclear Waste Repository.* DOE Internal Report. U.S. Department of Energy, Las Vegas, Nevada.

Szymanski, J. S., 1992. *The Origin and History of Alteration and Carbonization of the Yucca Mountain Ignimbrites.* DOE Internal Report, U.S. Department of Energy, Las Vegas, Nevada.

Szymanski, J. S. and D. E. Livingston, 1993. *Dialogs by Jerry Szymanski Regarding the Yucca Mountain Controversy from December, 1990 to March, 1991.* Special Report No. 9 submitted to the Nuclear Waste Project Office of the State of Nevada. Technology and Resource Assessment Corporation, Boulder, Colorado.

Szymanski, J. S., C. M. Schluter, D. E. Livingston, M. R. Somerville, and J. B. Davies, 1993. *Annual Report.* Annual Report No. 1 submitted to the Nuclear Waste Project Office of the State of Nevada. Technology and Resource Assessment Corporation, Boulder, Colorado.

Vaniman, D. L .,1993. *Calcite Deposits in Fractures at Yucca Mountain, Nevada.* High Level Radioactive Waste Management, Proceedings of the Fourth International Conference, Las Vegas, Nevada, April 26-30. American Nuclear Society , La Grange, Ill. and American Society of Civil Engineers, New York, N.Y.

Vaniman, D., D. Bish, D. Broxton, F. Byers, G. Heiken, B. Carlos, El Semarge, F. Caporuscio, and R. Gooley, 1984. *Variations in Authigenic Mineralogy and Sorptive Zeolite Abundance at Yucca Mountain, Nevada, Based on Studies*

of Drill Cores USW GU-3 and G-3. LA-9707-MS, Los Alamos National Laboratory, Los Alamos, New Mexico.

White, A. C., H. C. Claassen, L. V. Benson, 1980. *The Effect of Dissolution of Volcanic Glass on the Water Chemistry in a Tuffaceous Aquifer, Rainier Mesa, Nevada.* USGS-WSO1536-Q, Water Supply Paper, Washington, D.C.

Winograd, I. J., and W. Thordarson, 1975. *Hydrogeologic and Hydrochemical Framework, South-Central Great Basin, Nevada-California, with Special Reference to the Nevada Test Site.* USGS Professional Paper 712-C, pp. C1-C126, Washington, D.C.

WoldeGabriel, Giday, 1991. *Diagenetic Minerals, K/Ar Data, and Alteration History in the Yucca Mountain, Nevada: A Candidate High-Level Radioactive Waste Repository.* Draft Report, Los Alamos National Laboratory, Los Alamos, New Mexico.

WoldeGabriel, Giday, D. E. Broxton, D. L. Bish and S. T. Chipera, 1992. *Preliminary Assessment of Clinoptilolite K/Ar Results from Yucca Mountain, Nevada: A Potential High-Level Radioactive Waste Repository Site.* 7th Symposium on Water-Rock Interaction, International Association of Geochemistry and Cosmochemistry, July 9-23, 1992, Park City, Utah.

TABLE 1. STRATIGRAPHIC UNITS

Formation	Member	Symbol	Reference
Paintbrush Tuff	Tiva Canyon	Tpc	Broxton *et al.* 1986
	Yucca Mountain	Tpy	Broxton *et al.* 1986
	bedded tuff	Tb	Broxton *et al.* 1986
	Pah Canyon	Tpp	Broxton *et al.* 1986
	Topopah spring	Tpt	Broxton *et al.* 1986
Tuff of Calico Hills		Tht	Broxton *et al.* 1986
Crater Flat Tuff	Prow Pass	Tcp	Broxton *et al.* 1986
	Bullfrog	Tcb	Broxton *et al.* 1986
	Tram	Tct	Broxton *et al.* 1986
Dacite flow breccia		Tfb	Broxton *et al.* 1986
Lithic Ridge Tuff		Tlr	Broxton *et al.* 1986
	bedded tuff	Tb	Broxton *et al.* 1986
Older tuffs and lavas		Tot	Broxton *et al.* 1986
Conglomerate		Tcgl	Craig and Johnson, 1984
Older tuff		To	Craig and Johnson,1984
Tuff of Yucca Flat		Tyf	Craig and Johnson, 1984
Lone Mountain Dolomite and Roberts Mountain Formation		Pal	Craig and Johnson,1984

TABLE 2. LOCATIONS FOR BOREHOLES AND BOREHOLE DATA

Borehole	North	East	G.L. Elev.	Tot. Depth	W.T. Depth	W.T.Elev
	(Nevada State Coordinates)		(ft.)	(ft.)	(ft.)	(ft.)
J-12	740,969.26	611,766.08	3,128.40	887.00	741.40	2,387.00
J-13	749,209.00	579,651.00	3,318.00	3,488.00	928.24	2,387.84
UE-25 a#1	764,900.20	566,349.90	3,934.40	2,501.00	1,538.32	2,397.68
UE-25 b#1	765,243.40	566,416.40	3,939.00	4,002.00	1,541.60	2,397.68
UE-25 p#1	756,171.20	571,484.50	3,654.60	5,923.00	1,187.36	2,466.5
USW G-1	770,500.20	561,000.50	4,348.60	6,000.00	1,876.16	2,471.11
USW G-2	778,824.20	560,503.90	5,098.40	6,006.00	1,722.00	3,375.12
USW G-3	752,779.80	558,483.10	4,856.50	5,031.00	2,460.00	2,397.68
USW GU-3	752,690.10	558,501.30	4,856.60	2,644.00	*	*
USW G-4	765,807.10	563,081.60	4,166.90	3,003.00	1,771.20	2,394.40
USW H-3	756,542.10	558,451.70	4,866.40	4,000.00	2,466.56	2,400.96
USW H-4	761,643.60	563,911.10	4,096.50	4,000.00	1,699.04	2,394.40
USW H-5	766,634.30	558,908.70	4,850.80	4,000.00	2,305.84	2,542.00
USW H-6	763,298.90	554,074.90	4,270.60	4,002.00	1,727.00	2,544.00
USW WT-1	753,940.60	563,739.20	3,942.50	1,689.00	1,545.00	2,397.00
USW WT-2	760,660.50	561,923.60	4,269.70	2060.00	1,874.00	2,396.00

TABLE 3A, SAMPLE DISTRIBUTION, GLASS
(Number of analyses)

Borehole	Stratigraphic Unit													Sum
	Tpc	Tpy	Tb	Tpp	Tpt	Tht	Tcp	Tcb	Tct	Tfb	Tlr	Tb	Tot	
USW G-1	*	*	*	*	*	*	*	*	*	*	*	*	*	0
USW G-2	*	9	5	3	*	*	*	*	*	*	*	*	*	17
USW GU-3	3	*	*	*	19	5	1	*	*	*	*	*	*	28
USW G-4	*	*	*	*	*	3	*	*	*	*	*	*	*	3
USW H-3	*	*	*	*	*	*	*	*	*	*	*	*	*	0
USW H-4	*	*	*	*	*	6	*	*	*	*	*	*	*	6
USW H-5	4	*	*	*	1	6	3	*	*	*	*	*	*	14
UE-25 a#1	2	*	16#	*	1	*	1	*	*	*	*	*	*	20
UE-25 b#1	*	*	*	*	*	*	*	*	*	*	*	*	*	0
UE-25 p#1	*	*	*	*	*	*	*	*	*	*	*	*	*	0
J-13	*	*	*	*	8	5	*	*	*	*	*	*	*	13
Prow Pass	*	*	*	*	11	*	*	*	*	*	*	*	*	11
Sum	9	9	21	3	40	25	5	*	*	*	*	*	*	112

Includes 7 high alumina (13.4 % or greater) and low silica (70.5 % or less) samples

TABLE 3B, SAMPLE DISTRIBUTION, WHOLE ROCK
(Number of analyses)

Borehole	Stratigraphic Unit													Sum
	Tpc	Tpy	Tb	Tpp	Tpt	Tht	Tcp	Tcb	Tct	Tfb	Tlr	Tb	Tot	
USW G-1	*	*	*	*	*	*	*	*	*	*	*	*	*	0
USW G-2	*	*	*	1	*	2	2	2	2	1	11	1		13
USW GU-3 & USW GU-3	*	*	*	*	*	1	2	1	2	*	4	*	2	12
USW G-4	*	*	*	*	1	2	2	1	1	*	*	*	*	7
USW H-3	*	*	*	*	*	*	*	*	*	*	*	*	*	0
USW H-4	*	*	*	*	*	*	*	*	*	*	*	*	*	0
USW H-5	*	*	*	*	*	*	*	*	*	*	*	*	*	0
UE-25 a#1	*	*	*	*	2	3	1	1	*	*	*	*	*	7
UE-25 b#1	*	*	*	*	*	*	*	2	4	*	1	*	*	7
UE-25 p#1	*	*	*	*	*	*	3	3	*	*	*	*	2	8
J-13	*	*	*	*	*	2	2	1	2	*	*	*	*	7
Prow Pass	*	*	*	*	*	2	*	*	*	*	*	*	*	2
Sum	0	0	0	1	3	12	12	11	11	1	6	1	5	63

TABLE 3C, SAMPLE DISTRIBUTION, CLINPOTILOLITE
(Number of analyses)

Borehole	Stratigraphic Unit													Sum
	Tpc	Tpy	Tb	Tpp	Tpt	Tht	Tcp	Tcb	Tct	Tfb	Tlr	Tb	Tot	
USW G-1	*	*	*	*	1	7	4	1	*	4	*	*	*	
USW G-2	*	*	*	17	3	18	16	*	*	*	*	*	*	54
USW G-3	*	*	*	*	6	*	20	10	18	*	2	*	*	56
USW G-4	*	*	*	*	*	18	31	10	*	*	*	*	*	59
USW H-3	*	*	*	*	*	*	5	*	*	*	*	*	*	5
USW H-4	*	*	*	*	*	16	7	*	*	*	*	*	*	23
USW H-5	*	*	*	*	2	14	4	*	*	*	*	*	*	20
UE-25 a#1	*	*	*	*	11	28	25	*	*	*	*	*	*	64
UE-25 b#1	*	*	*	*	*	*	*	22#	*	*	*	*	*	22
UE-25 p#1	*	*	*	*	*	15	18	*	3	*	12#	*	*	48
J-13	*	*	*	*	22	14	*	*	*	*	*	*	*	36
Prow Pass	*	*	*	*	8	24	*	*	*	*	*	*	*	32
Sum	0	0	0	17	53	154	130	43	21	4	14	0	0	436

All high alumina (14.5 % or greater) and high lime (5.5 % or greater) samples

Figure 1
BOREHOLE AND SURFACE SAMPLE LOCATIONS
Yucca Mountain, Nevada

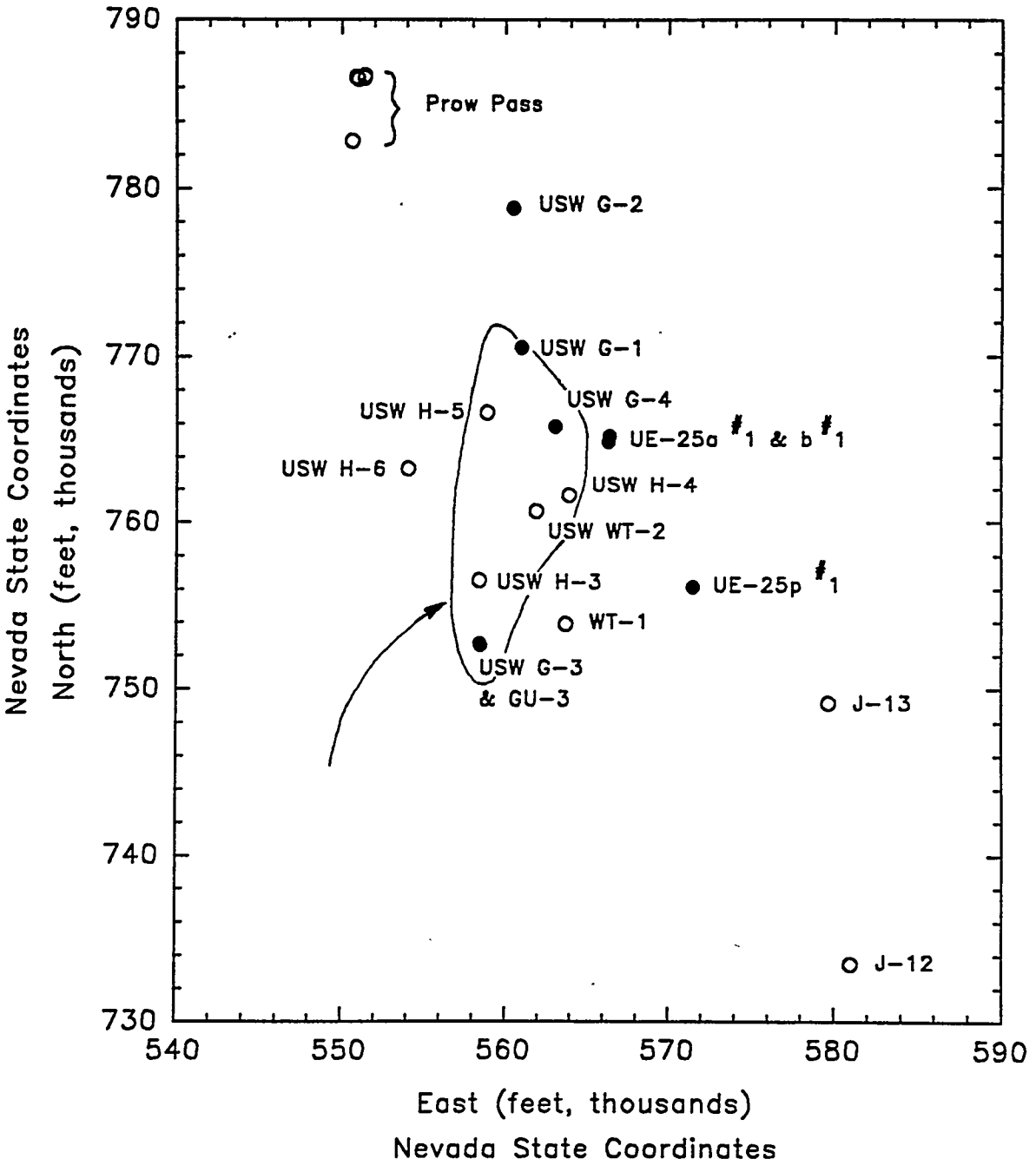

Figure 1. Borehole and surface sample locations, Yucca Mountain, Nevada. Solid circles indicate boreholes examined in this report. Open circles indicate boreholes and surface sites for which chemical (Broxton et al., 1986) and mineralogical (Bish and Chipera, 1989) data have been reported. The approximate area of the potential repository is also shown.

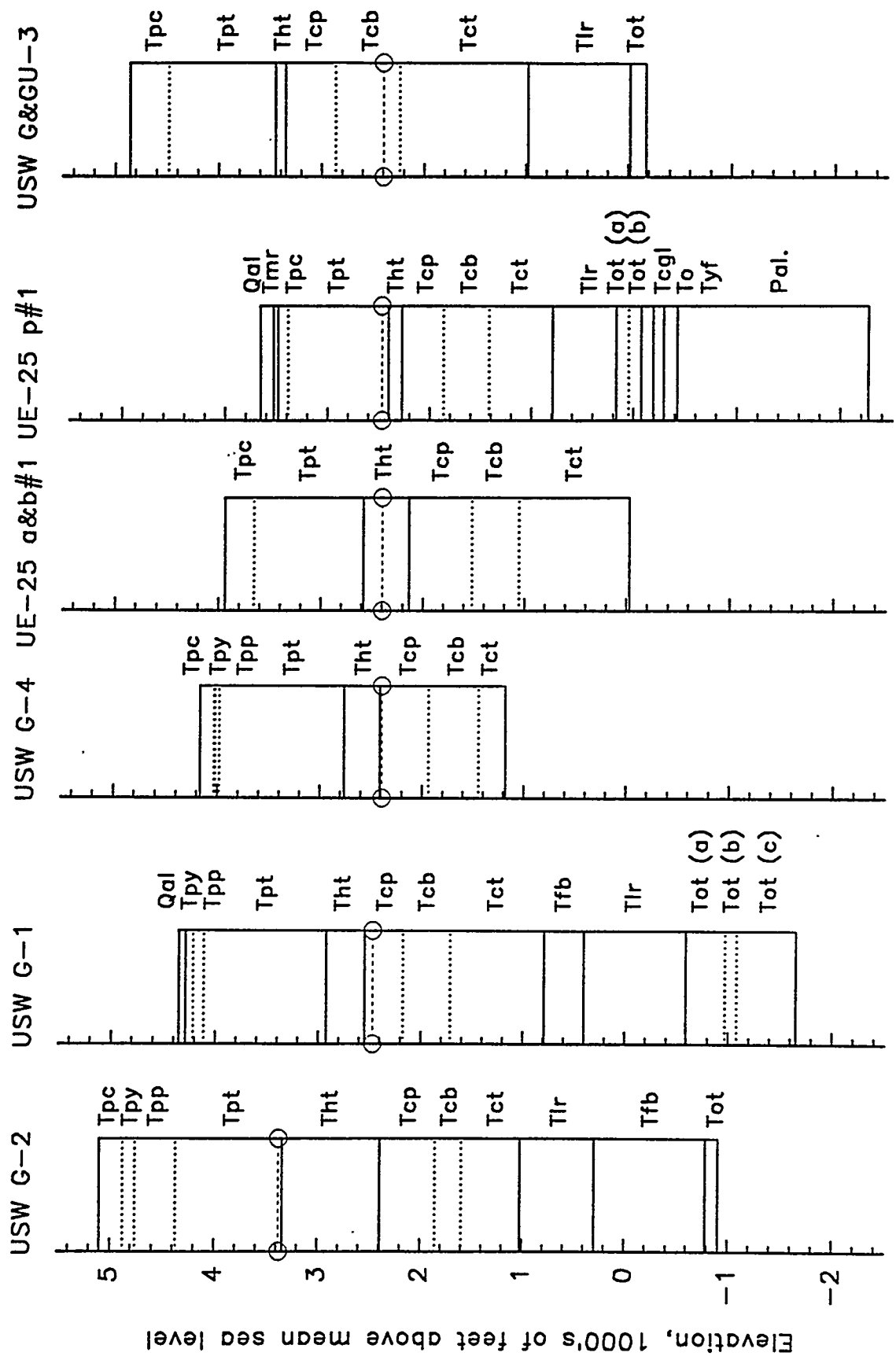

Figure 2. Simplified stratigraphic diagram of boreholes at Yucca Mountain. The statigraphic symbols are the same as given in Table 1. The surface and total depth are indicated by the upper and lower horizontal solid lines, other solid horizontal lines indicate formation boundaries. Dotted horizontal lines indicate member boundaries. The present-day water table is indicated by the dashed horizontal line with open circles at the left and right sides of each borehole. The source of stratigraphic infomation is given in the text. Elevations are given in feet in keeping with the pagoda diagrams of Bish and Chipera (1989) and sample locations of Broxton et al. (1986). Boreholes UE-25 p#1, a#1, and b#1 are substantially eastward from the other boreholes (see Fig. 1).

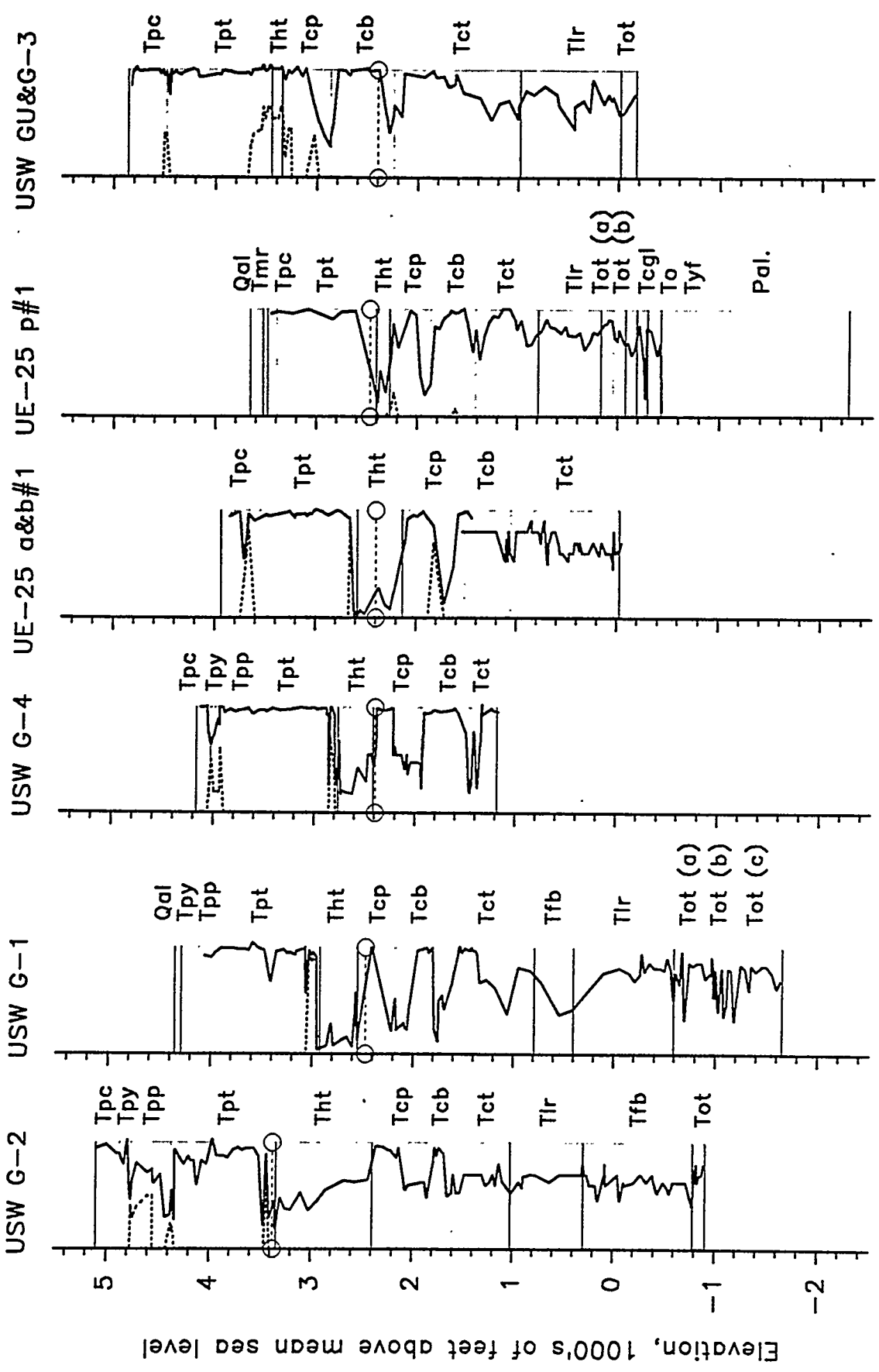

Figure 3. Abundance of glass (dashed curves) and the sum of glass, quartz, tridymite, cristobalite, and alkali feldspar (solid curves). Deficiencies from 100% (right hand border) approximate the total abundance of all alteration minerals. Where the solid line approaches 100% the rock are but slightly chemically altered or unaltered. Devitrified densely welded tuffs that have not been chemically altered can be noted by their high (~100%) abundance of the three silica polymorphs (quartz, tridymite, and cristobalite) and alkali feldspar. They occur in the Tiva Canyon (Tpc), Topopah Spring (Tpt), Prow Pass (Tcp), Bullfrog (Tcb) and Tram (Tct) members of the Paintbrush and the Crater Flat tuffs. The vitropheres at the top and bottom of the Topopah Spring (Tpt) can be noted by their high abundance of glass (USW G-2, G-1, G-4, and UE-25 a#1). The scale for each diagram is zero (left) to 100% (right).

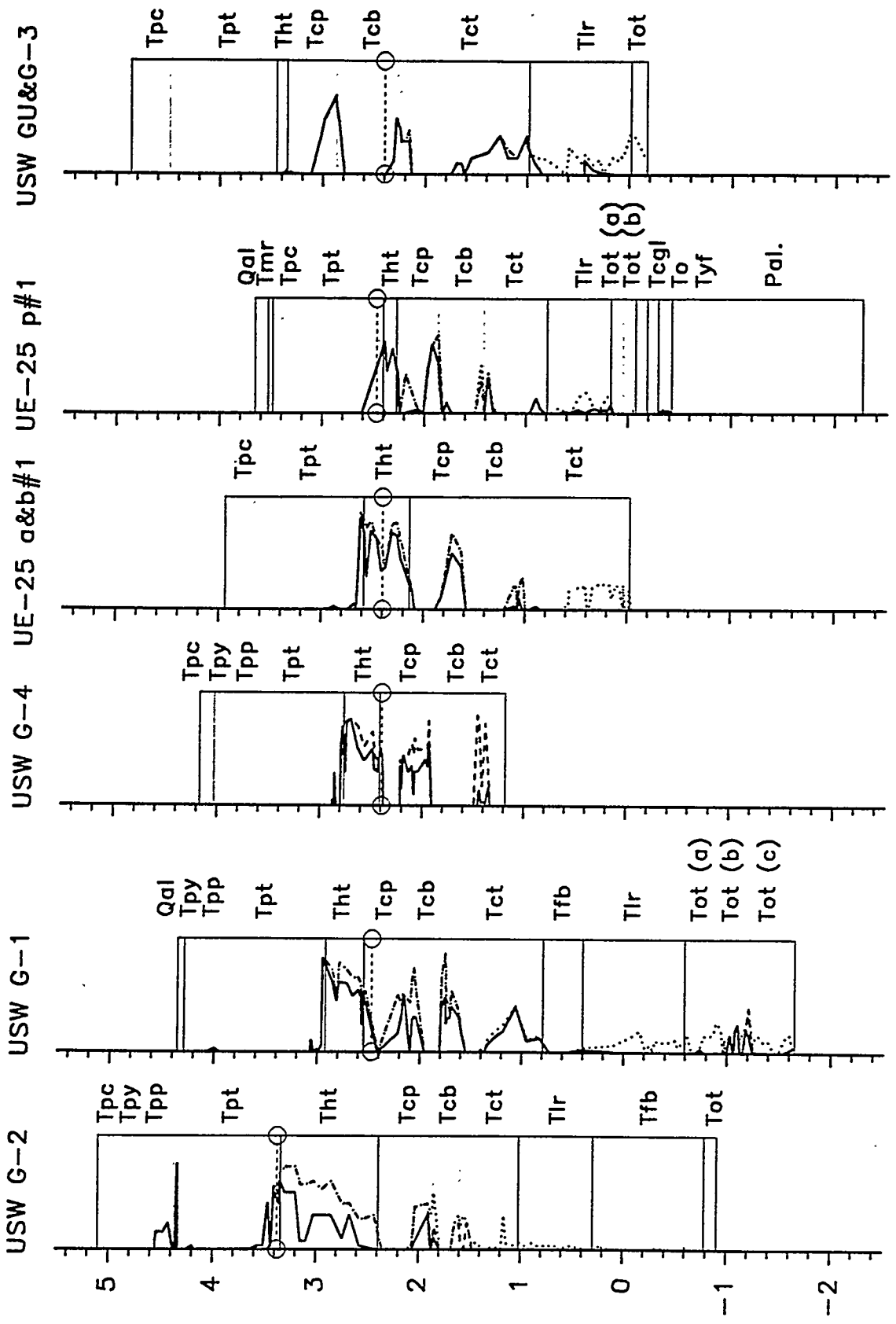

Figure 4. The distribution of zeolites in boreholes at Yucca Mountain. Solid curve = clinoptilolite, dashed curve = clinoptilolite + mordenite, dotted curve = clinoptilolite + mordenite + analcime The scale for each diagram is 0 -100%, left to right. A general trend of clinoptilolite to mordenite to analcime is noted with increasing depth for most boreholes. No analcime is reported for USW G-4 and no analcime is reported for USW GU-3 except at an elevation of 1,184.6 ft.. Note that clinoptilolite occurs well below the highest occurrence of analcime in USW G-1 (-1250 to -1000 ft.) and UE-25 p#1 (-400 to -300 ft.).

Figure 6. Comparison of normalized and non-normalized oxides for glass, whole rock, and clinoptilolite. In the top row of diagrams the oxide concentrations (wt.%) are plotted as reported by Broxton et al. (1986). In the second row the oxide concentrations are normalized to the sum of the reported metal oxides (volatile-free). In the third row the data are converted to molar concentrations and normalized to the sum of SiO_2, Al_2O_3, MgO, CaO, K_2O, and Na_2O. The dotted diagonals in the top three rows are lines of constant Al_2O3 / SiO_2. In the bottom row the Al_2O_3 (moles/g) is plotted against the sum of Na_2O, K_2O, MgO, and CaO (moles/g). The diagonal dotted line is the line of equal abundance.

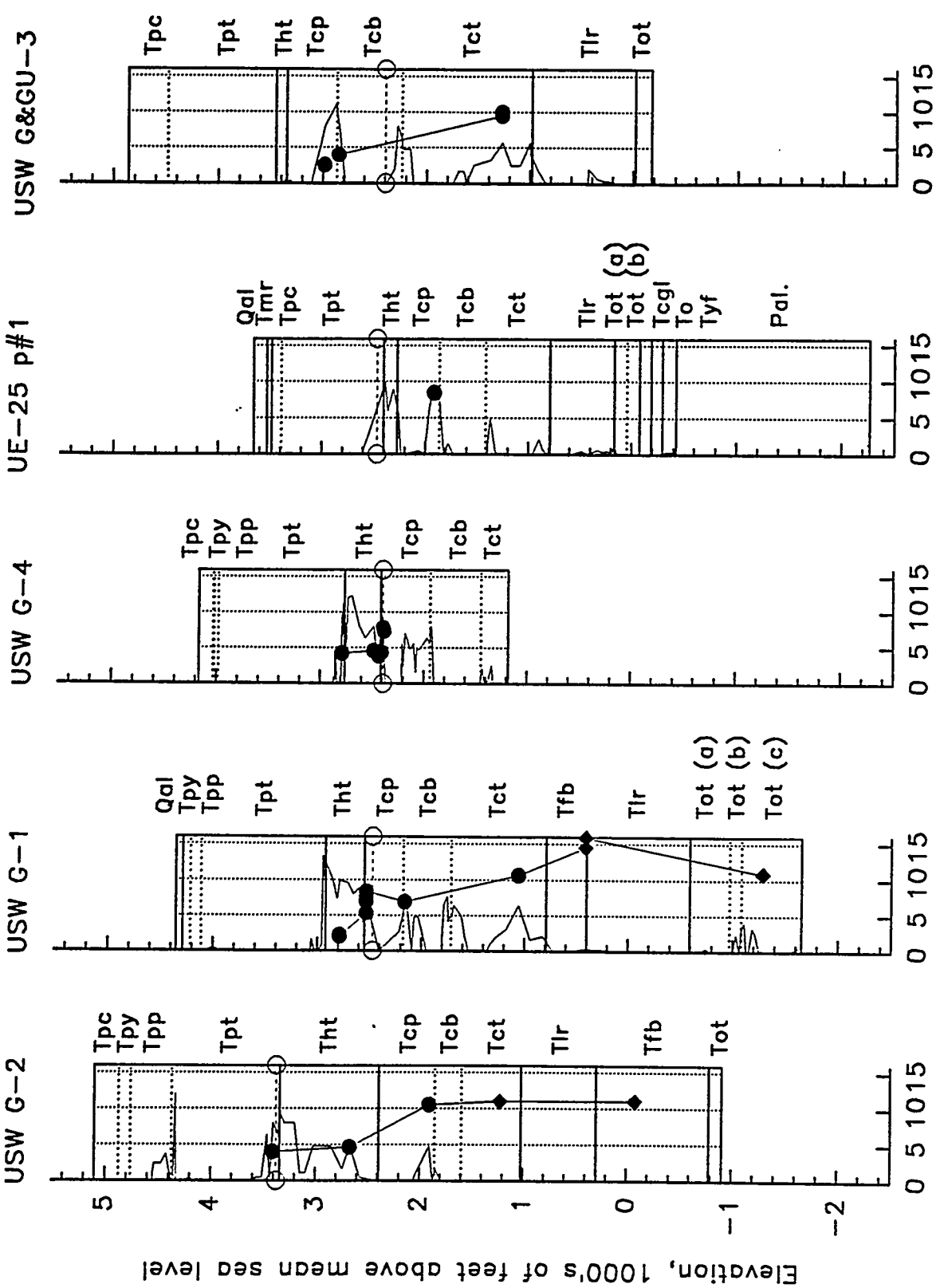

Figure 5. Potassium-argon ages of alteration minerals. Solid circles = clinoptilolite, solid diamonds = illite-smectite.

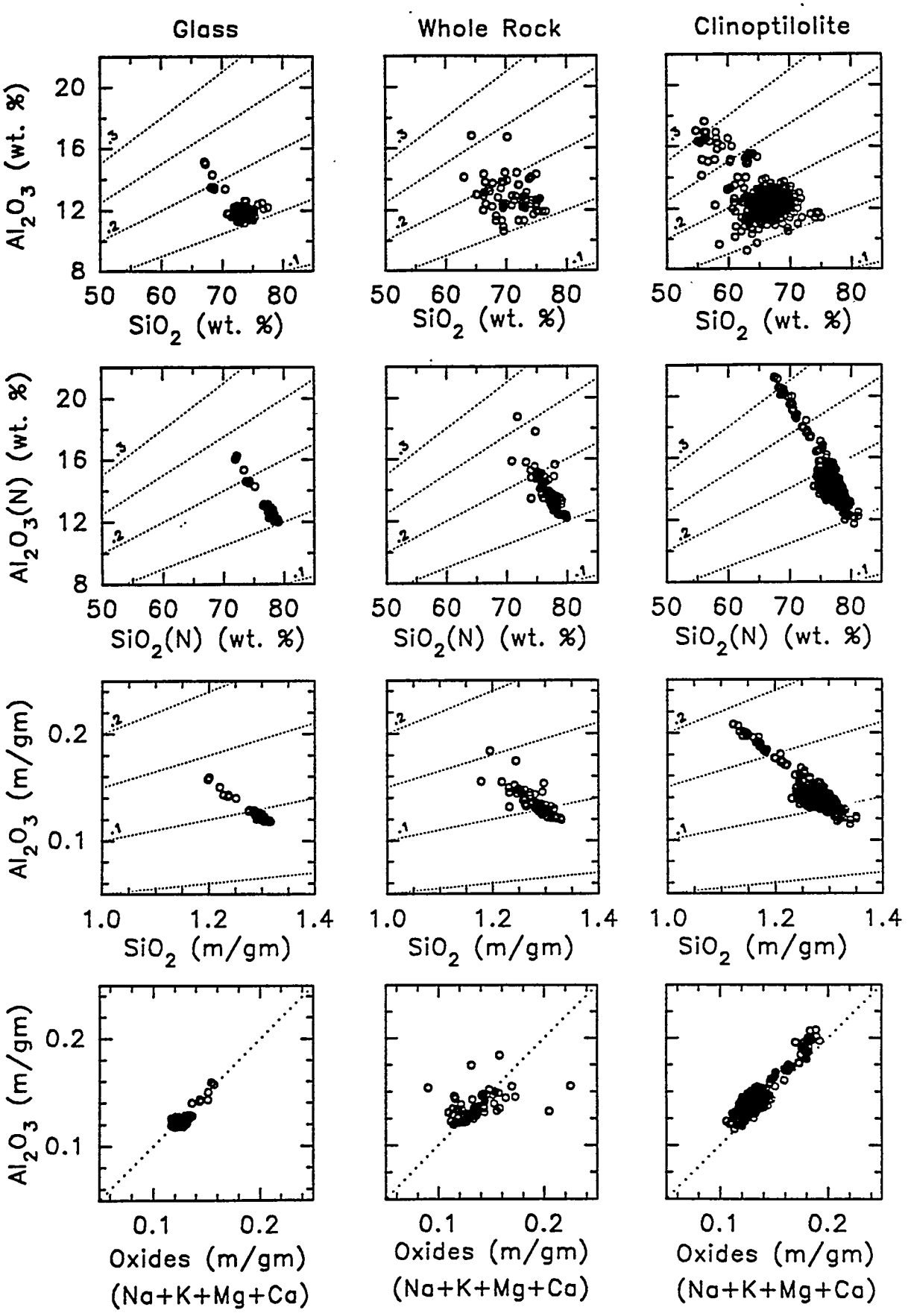

Figure 6. Comparison of normalized and non-normalized oxides for glass, whole rock, and clinoptilolite.

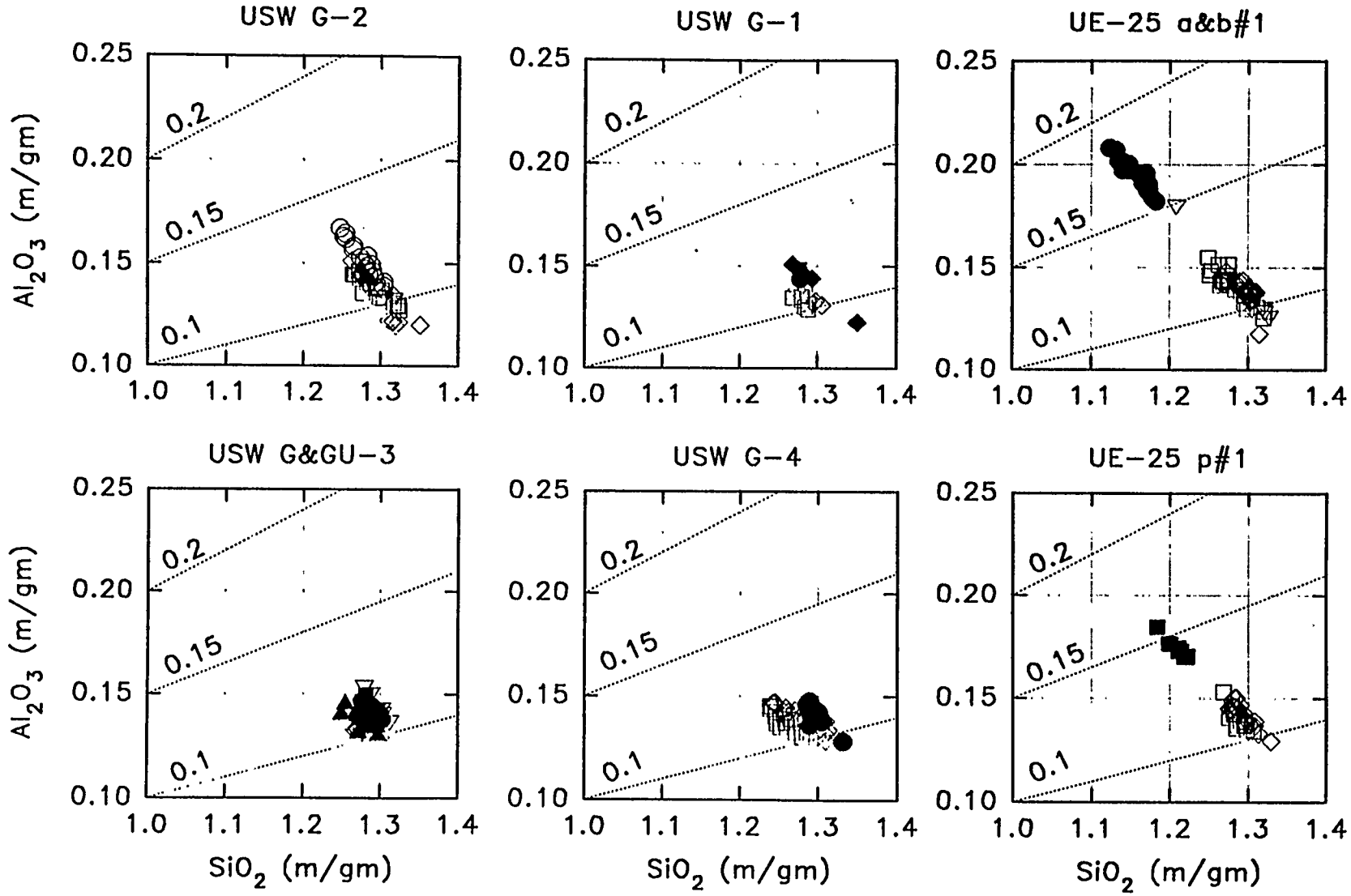

Figure 7. Silica and alumina abundances of clinoptololites. Values are normalized to the six major oxides (silica, alumina, soda, potash, lime and magnesia) for six selected boreholes at Yucca Mountain. Dotted diagonals are lines of equal alumina / silica ratio. Symbols as in Fig. 7. Particulary note the bimodal distribution in boreholes UE-25 p#1, a#1, and b#1. This distribution is in sharp contrast with the tight clusters in boreholes USW GU-3, G-3, and G-4. Different symbols represent different stratigraphic units (see Fig. 7).

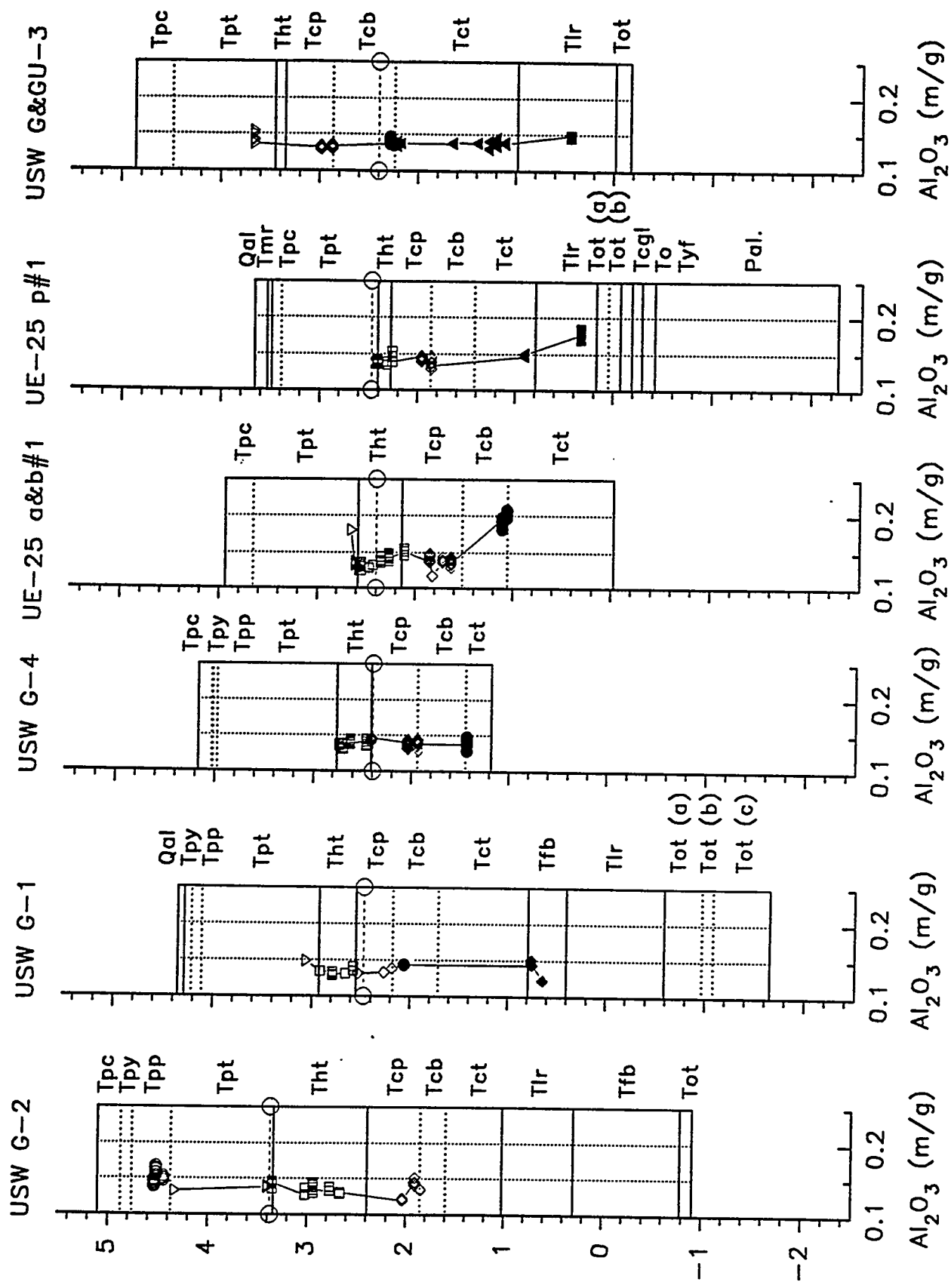

Figure 8. Logs of normalized alumina distribution of clinoptilolites within selected boreholes. Different symbols represent different stratigraphic units and are the same as given in Fig. 6. Especially note that high alumina concentrations show no systematic relationship to stratigraphy.

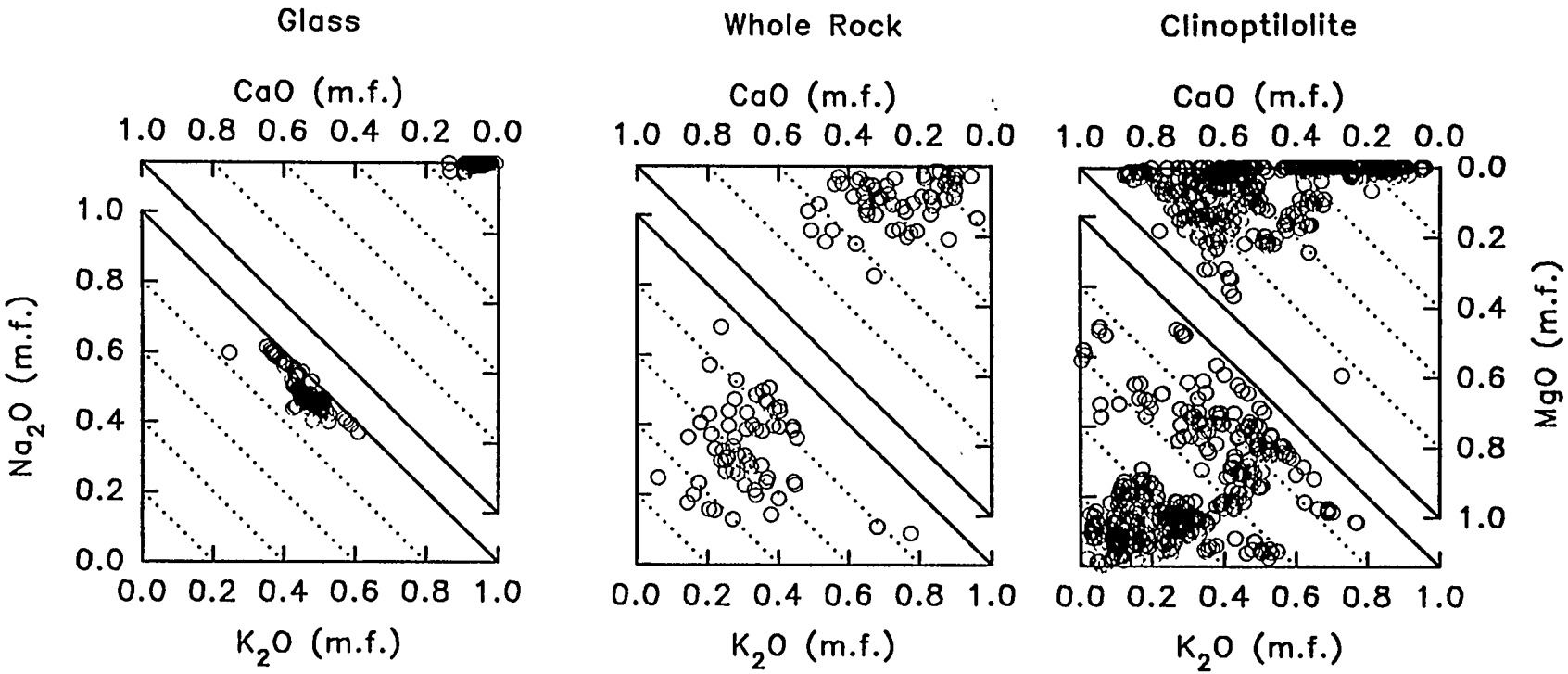

Figure 9. Normalized soda, potash, lime, and magnesia for glass, whole rock, and clinoptilolite at Yucca Mountain, Nevada.

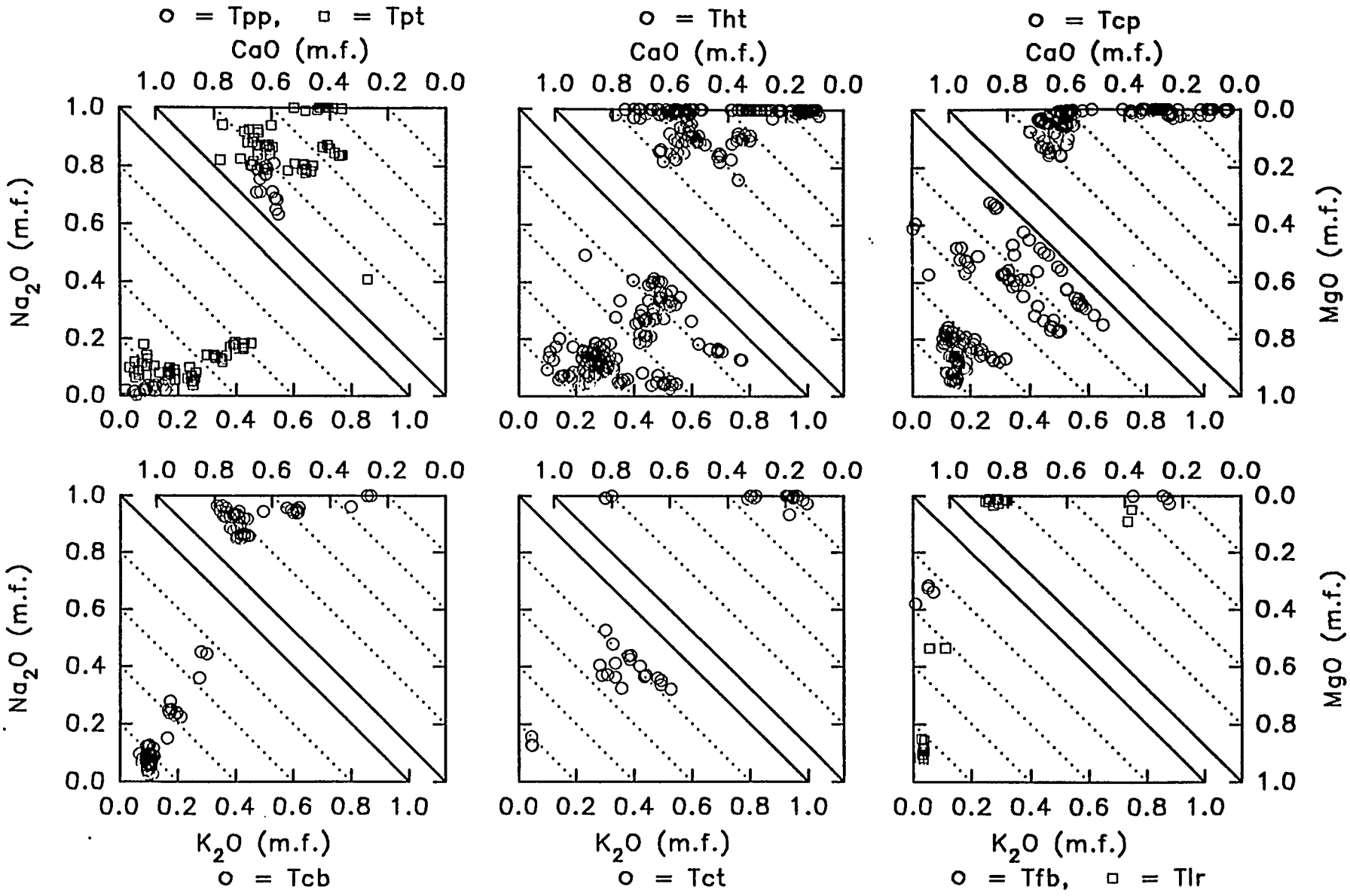

Figure 10. The normalized abundance of soda, potash, lime, and magnesia of clinoptilolites arranged by statigraphic unit at Yucca Mountain, Nevada.

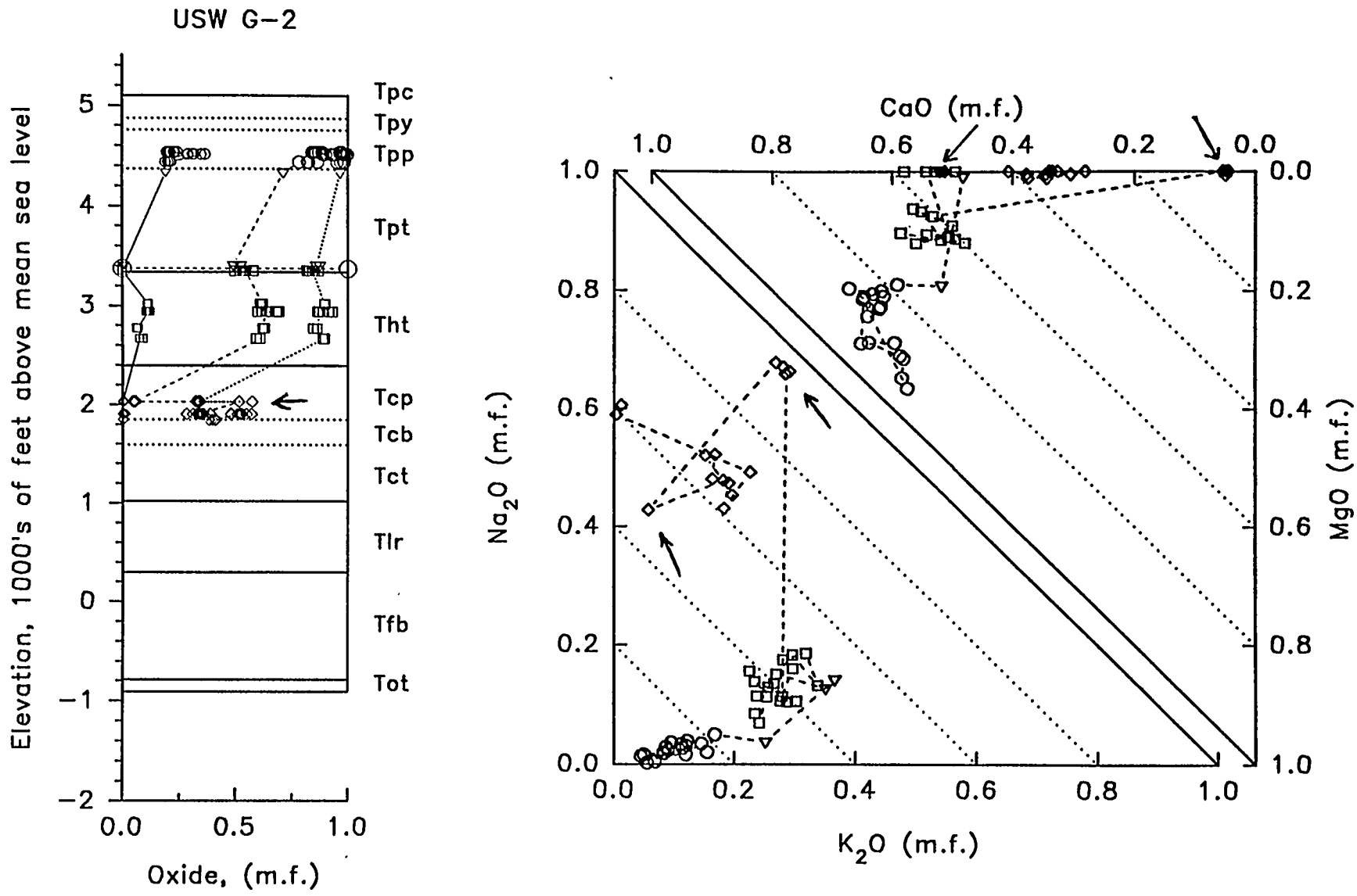

Figure 11. The spatial distribution and chemical diversity of exchangeable oxides in borehole USW G-2. Solid curve = MgO, dashed curve = MgO + CaO, dotted curve = MgO + CaO + K_2O.

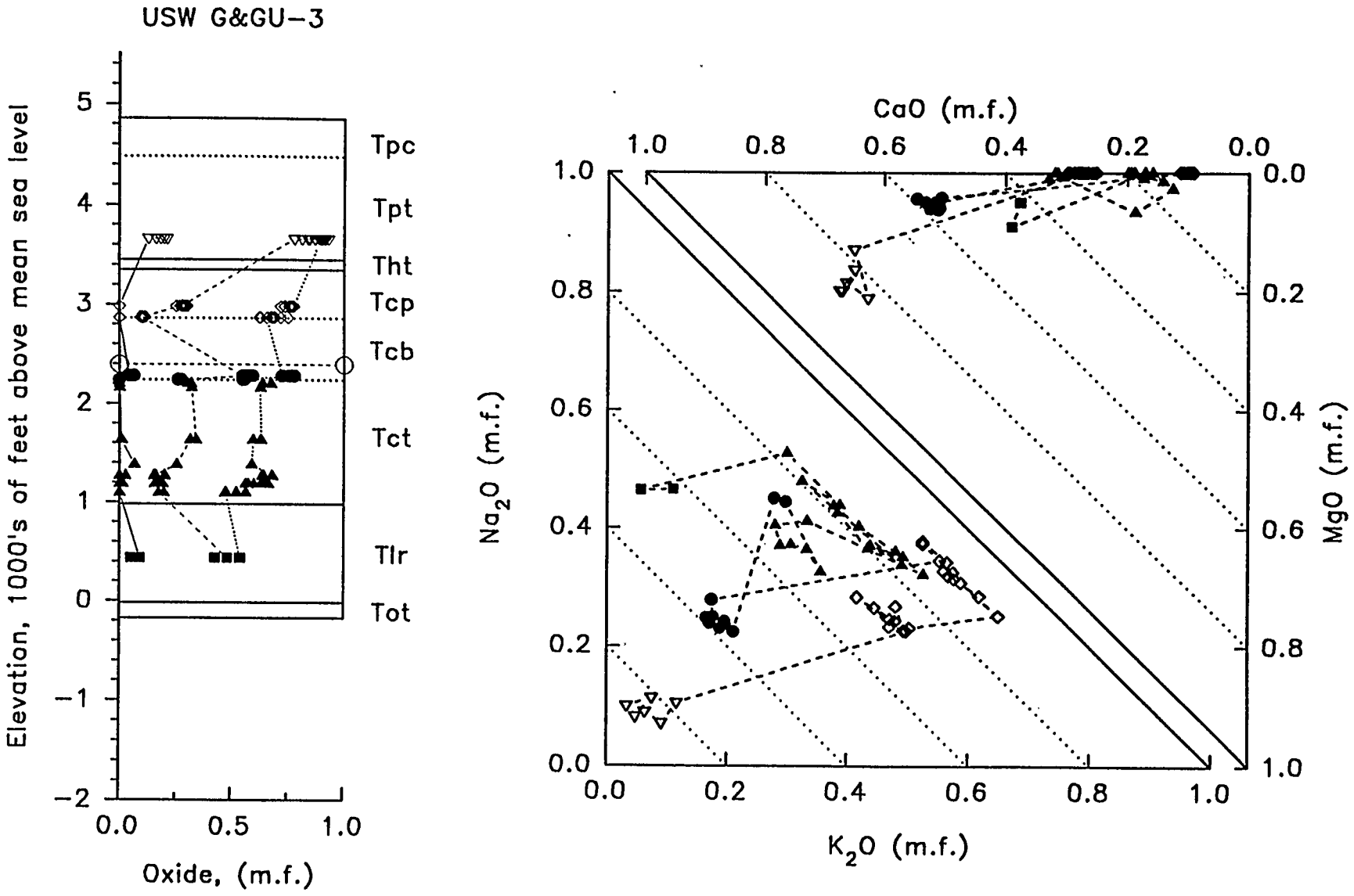

Figure 12. The spatial distribution and chemical diversity of exchangeable oxides in boreholes USW GU-3 and G-3. Solid curve = MgO, dashed curve = MgO + CaO, dotted curve = MgO + CaO + K_2O.

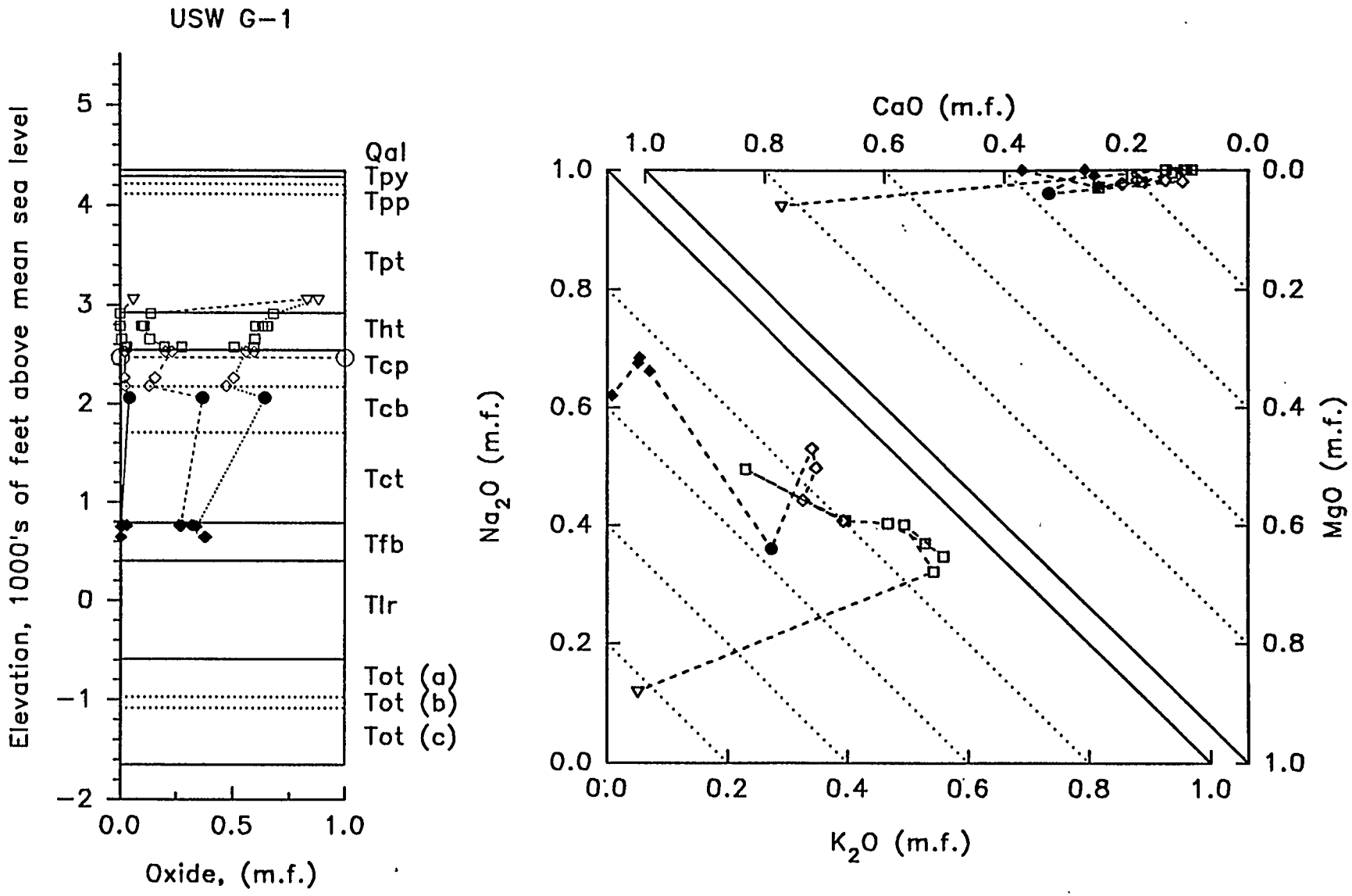

Figure 13. The spatial distribution and chemical diverstiy of exchangeable oxides in borehole USW G-1. Solid curve = MgO, dashed curve = MgO + CaO, dotted curve = MgO + CaO + K_2O.

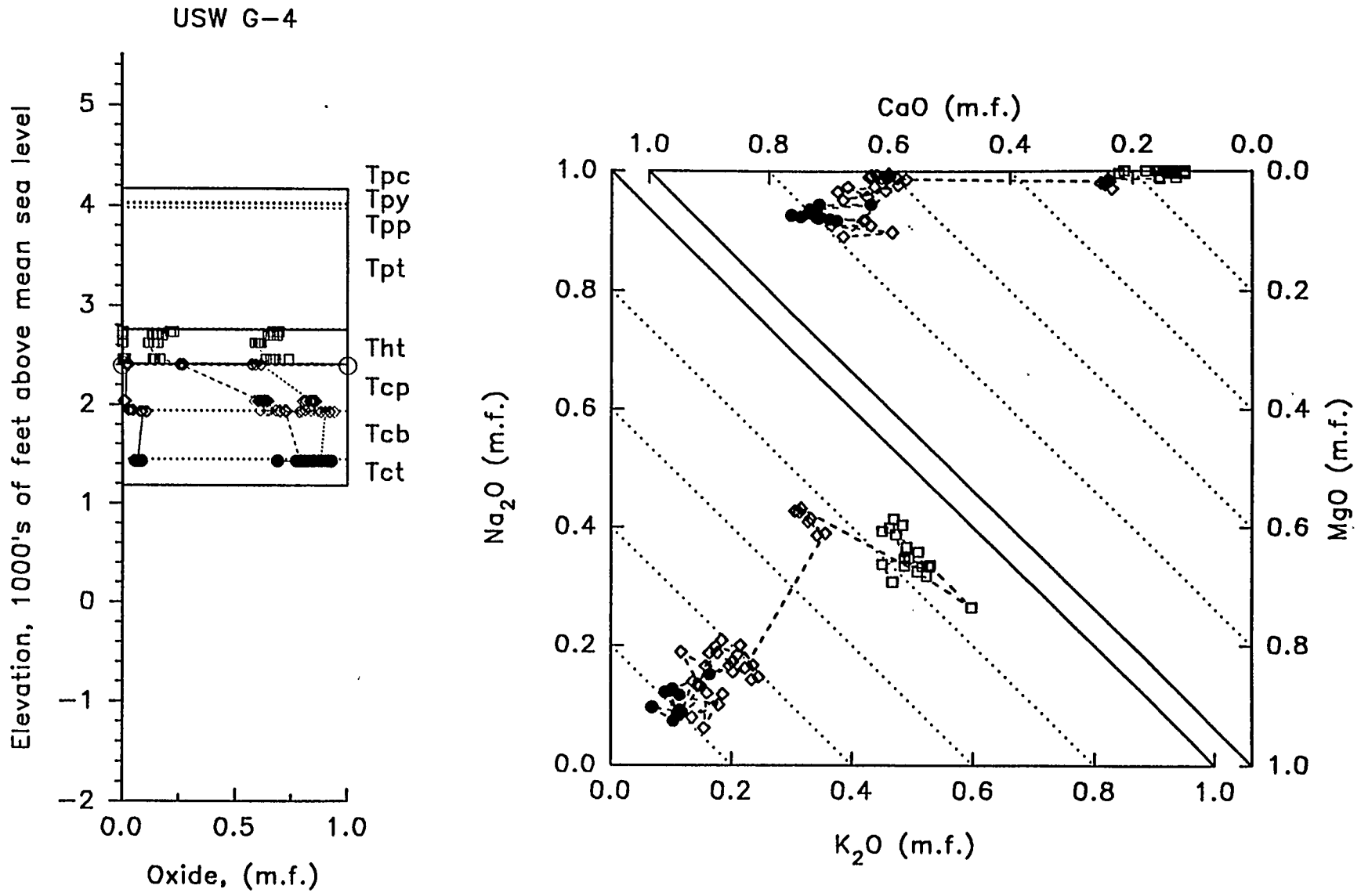

Figure 14. The spatial distribution and chemical diverstiy of exchangeable oxides in borehole USW G-4. Solid curve = MgO, dashed curve = MgO + CaO, dotted curve = MgO + CaO + K_2O.

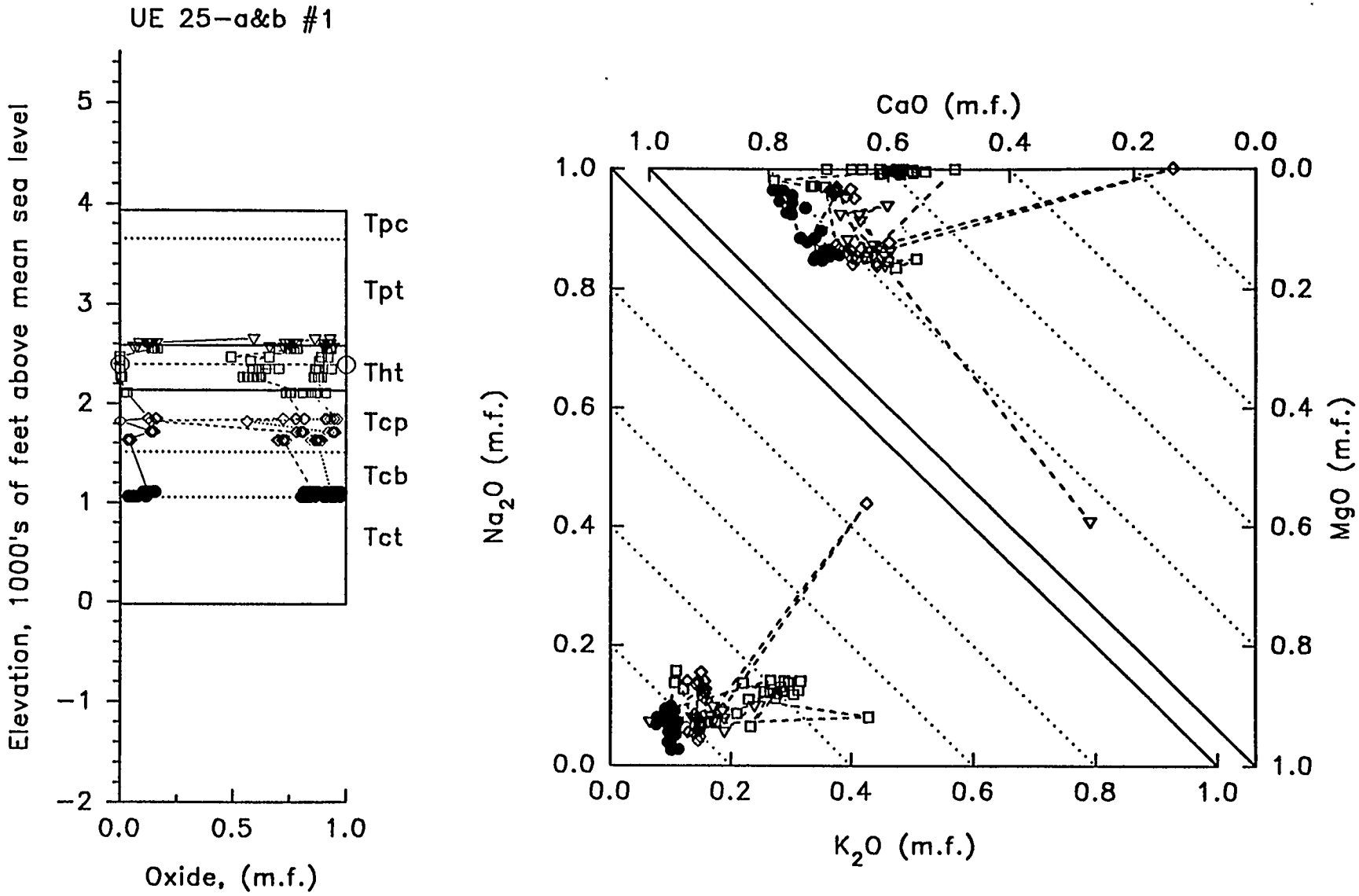

Figure 15. The spatial distribution and chemical diverstiy of exchangeable oxides in boreholes UE-25 a#1, and UE-25 b#1. Solid curve = MgO, dashed curve = MgO + CaO, dotted curve = MgO + CaO + K_2O.

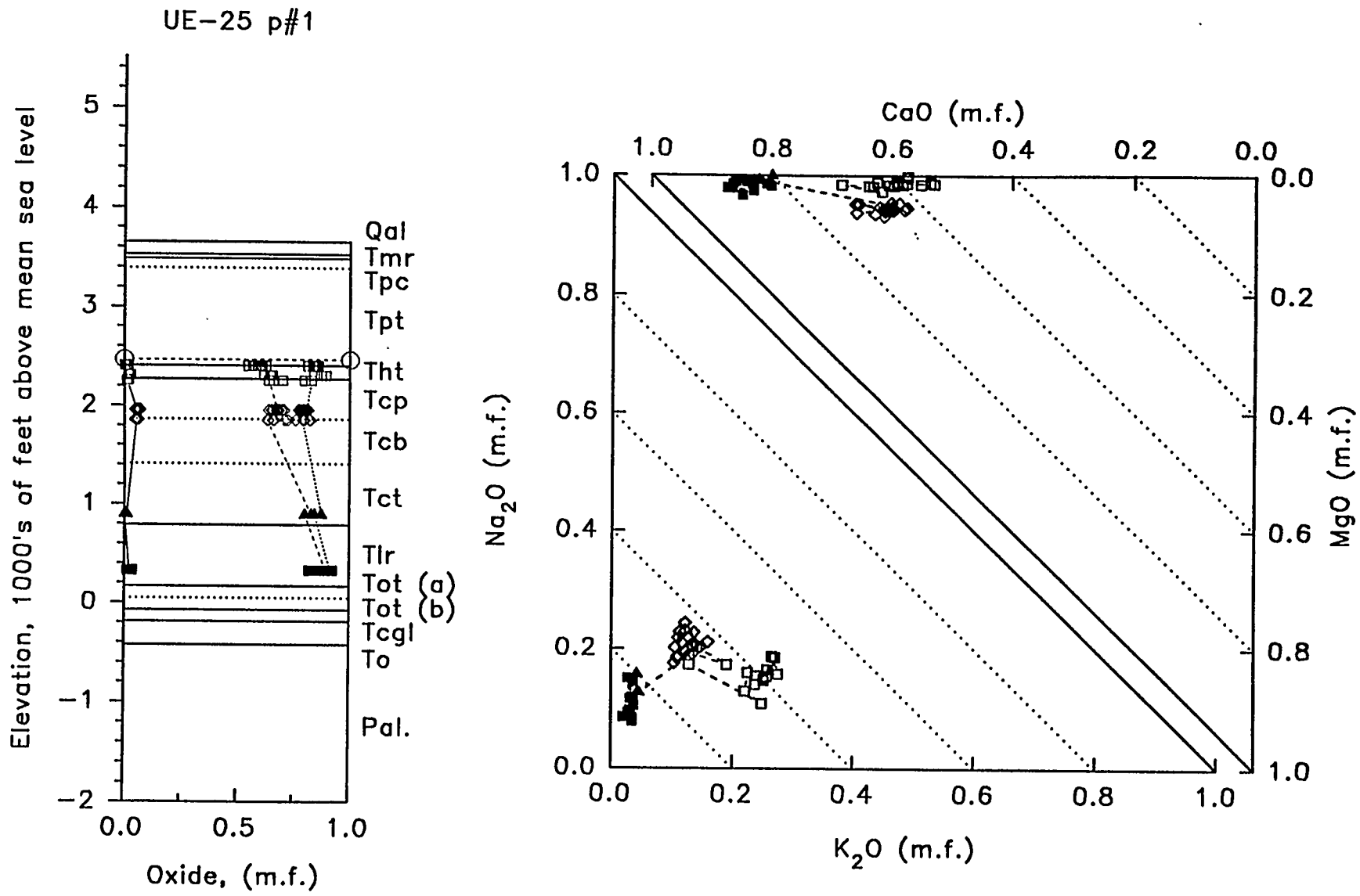

Figure 16. The spatial distribution and chemical diverstiy of exchangeable oxides in borehole UE-25 p#1. Solid curve = MgO, dashed curve = MgO + CaO, dotted curve = MgO + CaO + K_2O.

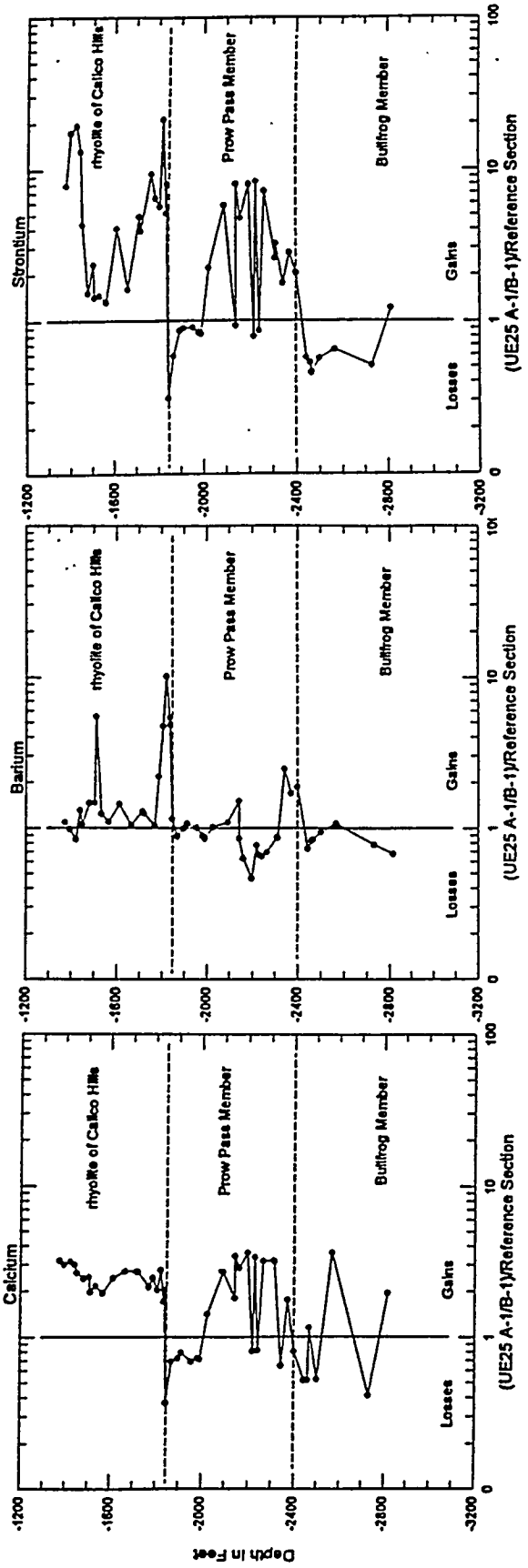

Figure 17. The enrichment of calcium, strontium and barium in boreholes UE-25 a#1 and b#1. From Peterman et al. (1993).

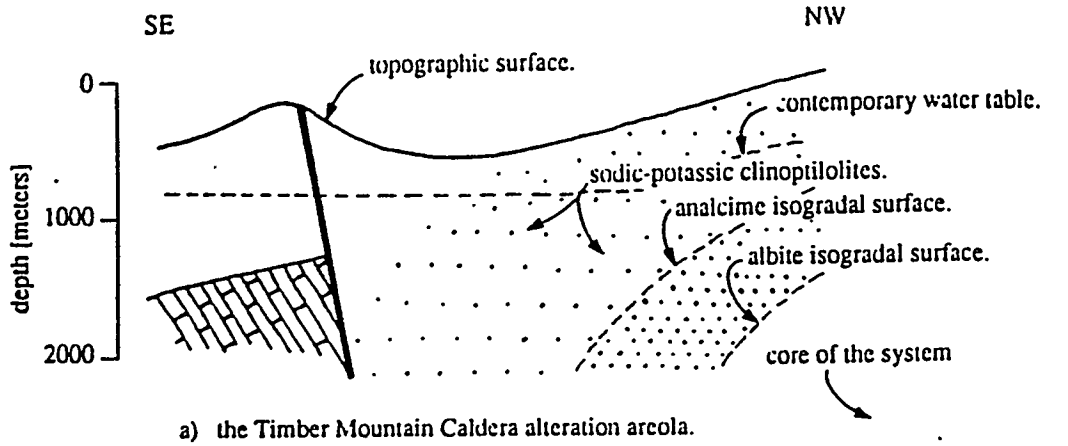

a) the Timber Mountain Caldera alteration areola.

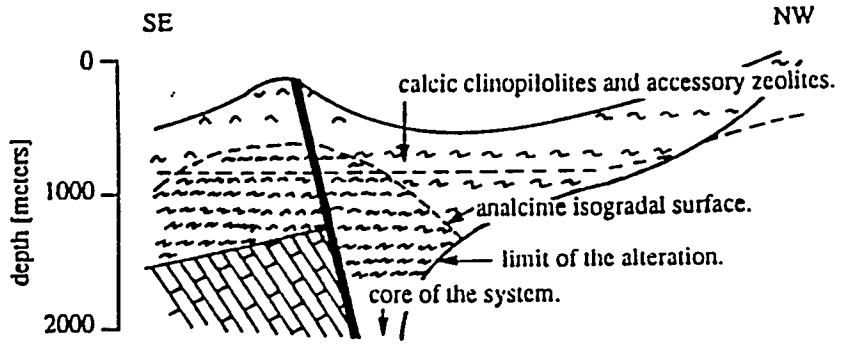

b) the alteration areola of the fault-based hydrothermal system.

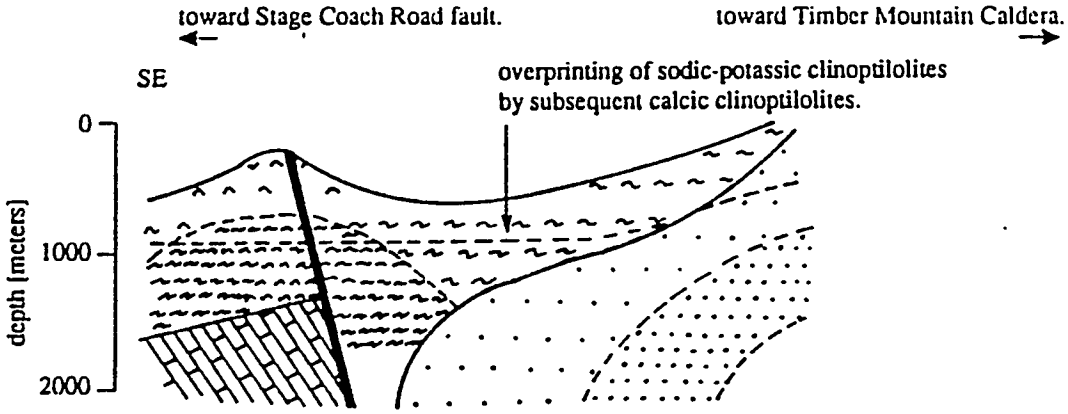

c) the presently observed juxtaposition of the alteration areolas.

Figure 18. Schematic diagram illustrating the interpretation of the spatial distribution of the chemical and temporal characteristics of alteration minerals at Yucca Mountain, Nevada. From Szymanski (1992).

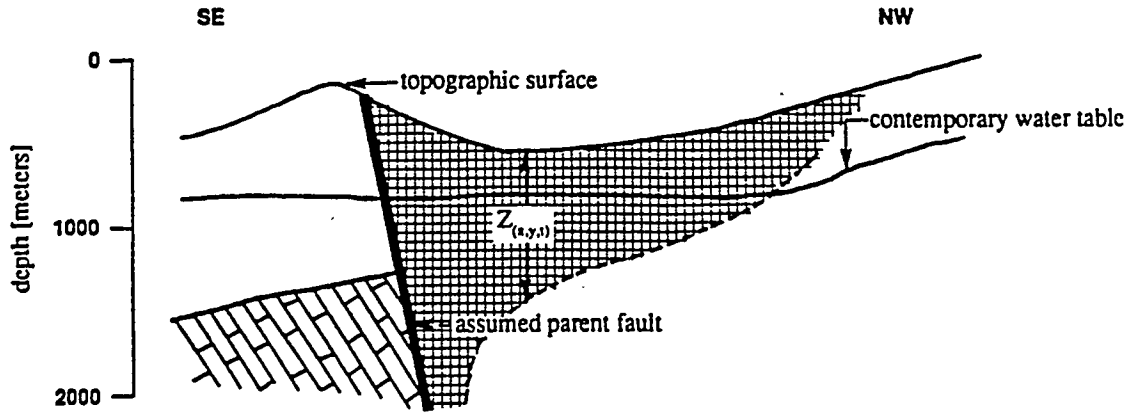

a) schematic diagram showing principal elements of the fault-based upwelling.

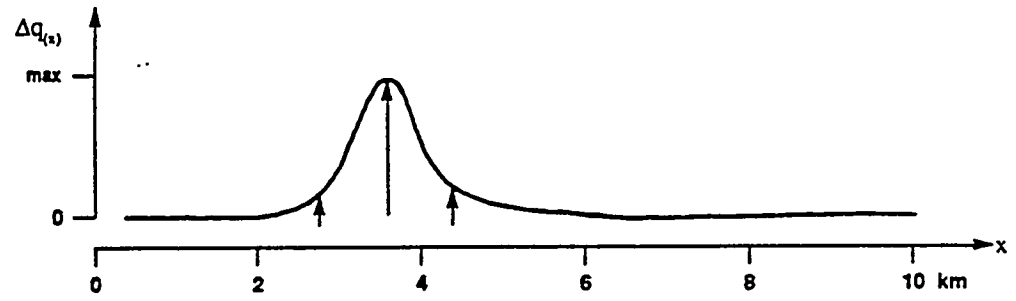

b) spatial distribution of the upward fluid flux increase - $\Delta q_{(x)}$.

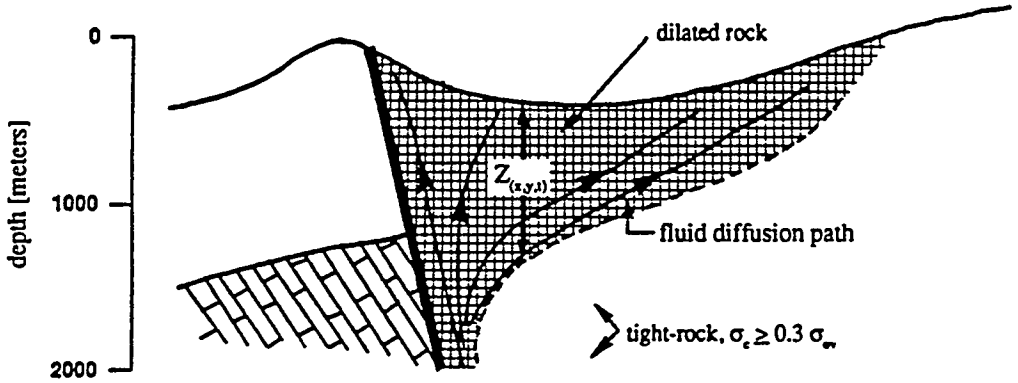

c) spatial distribution of the fluid diffusion path.

Figure 19. Schematic diagram illustrating the explanation of the spatial distribution of calcic zeolites. From Szymanski (1992).

PART II: GEOLOGY AT YUCCA MOUNTAIN

Section B: Calcite/Opal Deposits At Yucca Mountain, Nevada: Pedogenic Or Hypogene?

By C. A. Hill, C. M. Schluter, R. S. Harmon, H. C. Monger, Y. G. Liu, and R. A. Schmitt

CALCITE/OPAL DEPOSITS AT YUCCA MOUNTAIN, NEVADA:

PEDOGENIC OR HYPOGENE?

By: Carol A. Hill, Christine M. Schluter, Russell S. Harmon,

H. Curtis Monger, Roman A. Schmitt, and Y.-G. Liu

TABLE OF CONTENTS

LIST OF TABLES

LIST OF FIGURES

INTRODUCTION

This study is part of the research program of the Yucca Mountain Project intended to provide the State of Nevada with a detailed assessment of the geology and geochemistry of Yucca Mountain and adjacent regions. The purpose of this paper is to consider all of the geological and geochemical data available for the calcite/opal deposits at Yucca Mountain and to ascertain whether this data favors a pedogenic or hypogene origin for these deposits. Far from being of esoteric concern, this subject is of paramount importance to the debate which rages around the suitability of Yucca Mountain as a high-level radioactive waste repository site. It is also the purpose of this paper to serve as a foundation for a lengthy feature article to be submitted for publication in 1994.

It has often been stated in the published literature that the evidence "precludes" the involvement of upwelling waters in the deposition of the calcite/opal deposits at Yucca Mountain (e.g., Marshall and Mahan, 1991, p. A118; Stuckless et al., 1991a, p. 553). In addition, a stand has been taken by the National Research Council of the National Academy of Sciences (NAS/NRC, 1992) against the upwelling-water model (a vote of 17 to 0 against), and this same panel report has concluded that "there is no compelling evidence for the repetitive flooding of the environment by expulsion of groundwater" and that "instead, the evidence strongly supports the idea that the near-surface mineral deposits resulted from percolating rainwater, which carried soil minerals down into rock fractures" (*Science*, April 18, 1992, p. 247). Based on such

information the Department of Energy has stated that it "finds no basis to continue to study the origin of these specific deposits" (DOE, 1993, p. ii).

This study, based upon many different independent lines of evidence, reaches the opposite conclusion and instead favors a hypogene spring-travertine origin for the controversial calcite/opal deposits at Yucca Mountain. This study recognizes a pedogenic carbonate component at Yucca Mountain, but argues that this component is distinct from, and sometimes intermixed with, the calcite/opal deposits.

THE PROBLEM

One of the main reasons why the pedogenic-hypogene debate rages on is because the existing data is often contradictory and non-definitive when considered in isolation. This ambiguity applies particularly to the isotopic data (e.g., Quade and Cerling, 1990 versus Szymanski et al., 1993) but it also characterizes other evidence such as petrographic textures and mineralogy. For example, vesicles (observed in some of the calcite/opal deposits; Hill and Schluter, 1993) are usually indicative of degassing, but they can also occur in pedogenic caliches. Laminations are common in pedogenic deposits, but they can also occur in hypogene deposits. Sepiolite can form pedogenically, or it can be of hydrothermal origin and related to faults (Hill, 1993a). Calcrete deposits can be a mixture of pedogenic and non-pedogenic components, thus making the origin of some of these deposits indeterminable (Bachman and Machette, 1977).

This confusion has been compounded by studies based upon possible wrong assumptions. For example, Quade and Cerling (1990, p. 1550) sampled five "Holocene-age soils" in the vicinity of Trench 14 and assumed that these were laced with "pedogenic" carbonate but did not consider that these soils might instead be laced with hypogenic carbonate which had ascended up the fault. Marshall et al. (1990, p. 922) also assumed that the calcretes at Trench 14 and Busted Butte were "pedogenic" deposits. These two sets of authors further assumed that since the carbon-oxygen and strontium isotopes of the vein material at Trench 14 and Busted Butte matched the carbon-oxygen composition of these presumed "pedogenic" soil carbonates, that the veins must therefore also be of pedogenic origin. This presumptive logic, using carbon-oxygen and strontium isotopes, has continued to be applied to fracture calcites down to depths of ~400 m into the subsurface (e.g., Marshall et al., 1993); furthermore, it has been applied to rare earth element (REE) analyses in the subsurface (Vaniman, 1993). In other words, from this single, unquestioned and therefore untested assumption, it is now being claimed that "pedogenic" deposits of calcite/opal/sepiolite can be found as deep as 400 m beneath Yucca Mountain, a highly questionable conclusion.

Another problem has revolved around the retrievability of data that does exist on the calcite/opal deposits at Yucca Mountain. In many reports only general locations are given; or, if a specific location is given, the exact collection site and detailed description of the deposit at that location may not be given, so that the data is sometimes almost meaningless and collection sites are not relocatable. An example

of this is the Department of Energy's report (DOE,1993, p. A-19) where uranium-series dates obtained from Busted Butte carbonates are listed. The interested person is not given the general location (were the samples collected from west or east Busted Butte?), nor is it possible to know if these samples were collected from vein or slope travertine, or if the A, B, C, and D represent a collection from a number of different places or a top to bottom sampling of the calcrete at a specific place. In addition, in many of the papers that have been published on Yucca Mountain, there are no data charts listing citations for reused data. This has made it extremely difficult to obtain a complete data set that is free from duplication. Finally, availability of data and cores from the Department of Energy has been both slow and limited.

However, the most critical problem that concerns the calcite/opal deposits at Yucca Mountain has been the lack of definition of what is "pedogenic" versus what is "non-pedogenic." This is not surprising since this subject has never before been adequately addressed. While the literature on pedogenic calcrete deposits is abundant, the literature on non-pedogenic or hypogene calcrete deposits is sparse to almost non-existent (Hill et al., 1993). It seems that our study at Yucca Mountain may actually be one of the first to address the issue of supergene versus hypogene calcretes. This lack of definition has created a myriad of problems. If samples collected from Yucca Mountain are of mixed origin (i.e., both pedogenic and non-pedogenic), then how should the strontium and carbon-oxygen isotope data be interpreted? If trees and plants can grow in both pedogenic soils and hypogene-spring travertine, then how should the root casts in the calcite/opal deposits at Yucca

Mountain be interpreted? If "true" pedogenic deposits have little, or no, opal in them, then how should the laminated/banded calcite/opal textures be interpreted?

The solution is to try and find answers to these questions through a co-ordinated, multi-disciplinary study. In particular, the following needs to be done:

1. Consider all of the aspects of the controversial calcite/opal deposits -- from their regional geologic setting down to their finest microscopic textures. Only by considering the whole picture can one understand how the ambiguous parts fit together.

2. Determine whether or not the calcite/opal deposits consist of a single genetic component or whether they might be of mixed origin and be a product of multiple end-member components. If of mixed origin, separate the "true" pedogenic end-member component from the hypogene end member component. This can only be accomplished through a consideration of field, petrographic, and geochemical/isotopic data that leads to internally consistent interpretations regarding the origin of the components. Only by establishing criteria for "true" pedogenic deposits can one distinguish them from presumed "pedogenic" deposits which may be hypogene or mixed pedogenic-hypogene. Establishing such criteria is not only essential to a correct understanding of the calcite/opal deposits at Yucca Mountain, but it is also important to the field of soil science.

3. Compile and evaluate all of the data that has been produced for the calcite/opal deposits at Yucca Mountain. Hill and Schluter (1994) have attempted to compile all of the data in their most recent report to the State of Nevada, but it is estimated that perhaps only two-thirds of the data that does exist is included in this report because of the difficulty of retrievability. This annual report is an attempt to evaluate all of the data on the calcite/opal deposits at Yucca Mountain. The data used in this annual report is from the data charts of Hill and Schluter (1994)

REGIONAL GEOLOGY

Yucca Mountain, Nevada, is located in the southern Great Basin, a tectonically-active area characterized by north-trending linear mountain ranges flanked by extensive alluvial fans and separated by broad alluvial basins (Fig. 1). The climate of the region is arid and vegetation is limited to sparse desert plants. Yucca Mountain is situated within the Basin and Range Province between the Sierra Nevada Batholith on the west and the Colorado Plateau on the east. The region is currently undergoing rapid crustal extension. This crustal extension is responsible for Quaternary to Holocene volcanism, faulting, active seismicity, and high heat flow in Yucca Mountain region.

The Yucca Mountain fault block is composed of a thick sequence of ash-flow tuffs, lavas, and bedded tuffs that were erupted primarily from the Timber Mountain-Oasis

Valley cauldron complex between 11-15 Ma (Caporuscio et al., 1982). The thickness of these volcanic units exceeds 1800 m and may extend to 3000 m. Nearby rhyolitic volcanics of the Calico Hills and Shoshone Mountain are ~8-9 Ma, and younger basaltic volcanism ranges from 8 Ma to less than 1 Ma. The most recent volcanic features in the region are a series of volcanic cones in Crater Flat, located just west of Yucca Mountain (Fig. 1). The age of Red Cone in Crater Flat is 1.0-1.5 Ma, the age of Little Cone is 1.11 Ma, and the age of Black Cone is 1.07-1.09 Ma (Wells et al., 1990). Lathrop Wells Cone, the youngest of the series, has been dated at 119±11 to 141±10 Ka (Turrin and Champion, 1991).

Faulting also dates from the Quaternary to Holocene. Four to six faults along the Furnace Creek fault system ~30 km west of Yucca Mountain, and three or more faults in the Death Valley fault system (~40 km west of Yucca Mountain) have experienced movement along them during the last 200-2,000 yrs (Brogan et al., 1991). Two faults along the east side of Bare Mountain (located ~15 km west of Yucca Mountain, Fig. 2) have experienced recurrent movement during the last 10 Ka; these range-front faults contain extensive infillings of secondary calcite and silica that commonly exhibits slickensides (Reheis, 1986). Latest movement on the Paintbrush Canyon fault at Busted Butte, Yucca Mountain, was sometime in the late Quaternary (Whitney and Muhs, 1991), and latest movement on the Yucca fault is <35 Ka (Knauss, 1981). Other Quaternary faults in the Yucca Mountain area are shown in Fig. 2.

Earthquakes are common occurrences in the Yucca Mountain region. In the Rock Valley seismic zone, just southeast of Yucca Mountain, there is strong evidence for a major earthquake sometime prior to about 12 Ka, which earthquake was followed by a smaller event in the early Holocene, probably between 5-12 Ka (Szabo et al., 1981). Several earthquakes recorded from 1978 to 1984 had epicenters located along the range-front faults on the east side of Bare Mountain (Reheis, 1986), and, a swarm of about 20 earthquakes occurred over a short period of time in 1976 along the southern part of the Rock Valley fault system (just north of U.S. Highway 95; Szabo et al., 1981). The most recent earthquake activity in the Yucca Mountain area occurred on June 29, 1992. This earthquake measured 5.6 on the Richter scale and had its epicenter at Little Skull Mountain located just 18 km southeast of the proposed high-level waste repository. Considerable damage was done to the Yucca Mountain Project Operations Center on the Nevada Test Site by this earthquake.

Heat flow in the Yucca Mountain area is also considerable because of rapid crustal extension. Simonds (1980) reported a heat flow value of 135 mWm^{-2} for the UE-25 a#3 drill hole located in the Calico Hills just northeast of Yucca Mountain. This value is significantly above Basin and Range heat-flow averages of 80 to 100 mWm^{-2}. Such high heat flow is responsible for the many hot springs in the region (Horton, 1964). Thermal springs discharging from Ash Meadows have temperatures of 20-34°C (Winograd and Pearson, 1976); water at Devils Hole is 34°C (Hoffman, 1988), and water at Oasis Hot Springs (northeast of Beatty) is 43°C (Castor et al., 1989).

FIELD RELATIONSHIPS

Field work by the various authors of this report over the period of 1992-1993 has encompassed the sampling and study of approximately 50 separate localities in and around Yucca Mountain. Key localities visited have been the Bare Mountains, Yucca Mountain, Calico Hills, Skeleton Hills, Busted Butte, Harper Valley, Red Cliff Gulch, Wahmonie Hills, Crater Flat, Fortymile Wash, Midway Valley, Big Dunes, Amargosa Playa, Red Cone, Lathrop Wells Cone, and Devils Hole (Fig. 1). Over 125 kg (275 lbs) of rock/calcite/opal/soil samples have been collected during these field trips. The purpose of this field work was to obtain field observations and samples relevant to the origin of the controversial calcite/opal deposits at Yucca Mountain.

The following general field observations are pertinent to these deposits:

General occurrence

A variety of types of calcite and/or silica deposits exist at and in the immediate vicinity of Yucca Mountain: (1) petrocalcic horizons, (2) small veins and fracture fillings in subsurface rock, (3) large veins and calcrete masses deposited along surface faults, and (4) spring deposits. The main controversy revolves around whether types (2) and (3) are of pedogenic origin as is (1), or if instead they are fracture fillings and spring deposits (4) entirely, or in part, of hypogene origin.

Localization along faults

Secondary carbonate/silica deposits are commonly associated with Quaternary faults at Yucca Mountain (e.g., Szabo and O'Malley, 1985). In this and a previous study (Hill, 1993a), faults were defined in the field by the presence of offset beds (e.g., Harper Valley), well-exposed and slickensided surfaces (e.g., the Wailing Wall, Fig. 3), or by brecciated and mineralized zones (e.g., Calico Hills). In places where faults are well-exposed, the calcite/opal mineralization occurs primarily as seams or veins along or near the fault plane, and either dies out away from the fault (e.g., the Wailing Wall; Fig. 3) or forms travertine-like deposits downslope from the faults and veins (e.g., at Busted Butte; Fig. 4). A number of calcite/opal deposits are located along major faults. For example, the calcite/opal at Trench 14 is located along the Bow Ridge fault; at Busted Butte along the Paintbrush Canyon fault; at the Wailing Wall, Trench 8, New Trench, and at drill pad WT-7 along the Solitario Canyon fault; and at the CF1 and CF2 trenches along the Windy Wash fault (Fig. 2). The nearly universal association of the calcite/opal deposits with faults implies that the mineralization has a fault-related origin. If the calcite/opal were pedogenic in origin it should occur universally around Yucca Mountain and not be by-in-large restricted to, and localized along, fault zones.

Vein geometry

The calcite/opal deposits often display a vein morphology where observed along faults and where vertically exposed by trenching or by valley downcutting. This vein geometry is well illustrated at Trench 14 (Fig. 5) and at the fault scarp exposed north of Site 106, but is most dramatic on the west and east sides of Busted Butte where

valley erosion has dissected sand ramps (Fig. 6A). As fully exposed in the sand ramps at Busted Butte, the veins narrow towards the base but thicken and splay out into multiple veins near (within a few meters of) the sand-ramp ground surface (Fig. 6B). Travertine-like calcite/opal then continues downslope from these feeder veins, sometimes reaching or surpassing the toe of slope of the sand ramp (Fig. 4). At Trench 14 calcite/opal veins crosscut soil horizons and also earlier veins (Fig. 5). Hill (1993a) recognized at least five crosscutting episodes of vein mineralization exposed at Trench 14.

The vein geometry shown by the calcite/opal at Yucca Mountain is an important criteria for considering that these have a hypogene origin. Epithermal mineral deposits characteristically display a vein morphology, where feeder veins bifurcate or splay out near the ground surface and where these veins crosscut soil layers and earlier mineral deposits (e.g., Berger and Eimon, 1982; Fig. 7). If formed from the surface downward through pedogenic processes, it is essential to ask why is it that the calcite/opal deposits occur in the form of sub-vertical, feeder and splayed vein systems, instead of as sub-horizontal, laminated forms as is typical of intrasoil pedogenic deposits? Even if it is hypothesized that the vein morphology was caused by faults having filled with pedogenic calcite/opal, this origin seems improbable at Busted Butte where the calcite/opal veins are located in sand ramps. How could slowly-accumulating, pedogenic, calcite/opal fill faults in sand? Why wouldn't the faults fill with sand long before the calcite/opal could accumulate pedogenically?

Relationship to stratigraphic units or rock types

Calcite/opal at Yucca Mountain has been observed along fault zones in Paleozoic limestone (e.g., Bonanza King Limestone, Pull Apart fault), in rhyolitic tuffs (e.g., bedded member of Paintbrush Tuff, Busted Butte), and even in unconsolidated tuff-derived sand (e.g., Busted Butte sand ramps). Thus, the source of calcium does not appear to be related to the amount of calcium in the host rock, but rather to a subsurface travel route in which solutions acquired enhanced contents of calcium along the flow path somewhere between recharge and discharge.

Relationship to mining districts

Yucca Mountain is sandwiched in between two zones of epithermal mineralization, the Bare Mountain Mining District ~11 km to the west and the Wahmonie Mining District ~20 km to the east (Fig. 1). The Wahmonie Mining District was mined primarily for silver (Quade and Tingley, 1983), but also has a high concentration of cobalt, chromium, and gold; the Bare Mountain Mining District was primarily mined for gold, fluorite, and mercury (Tingley, 1984), but also has a high concentration of arsenic, cadmium, lead, and zinc. Time of metal enrichment in these mining areas was most probably related to mid-Tertiary volcanism (14-11 Ma; Weiss et al., 1993). While metal enrichment is much less at Yucca Mountain than in the mining districts directly to the west and east of it, this does not mean that the calcite/opal deposits at Yucca Mountain did not form by a hypogene process. It may only mean that the bulk of metal enrichment was mid-Tertiary, but that hydrothermal mineralization has continued to the present, with lesser amounts of metal enrichment. Yucca Mountain,

viewed from a field perspective, should be considered as an integral part of the same regional, hypogene, epithermal system as Bare Mountain and Wahmonie.

MINERALOGY

The controversial deposits in the Yucca Mountain area are composed primarily of calcite/opal, with minor amounts of sepiolite and quartz, and in one locality, gypsum. Trace amounts of pyrite/chalcopyrite have been found in the calcite/opal.

Calcite/opal

Almost invariably the deposits are a mixture of calcite and opal, with typical values of carbonate ranging from ~20-75%, and with silica ranging from ~25-80% (DOE, 1993). Only rarely is pure calcite found in these deposits -- not even secondary accumulations of pure calcite. This in itself is unusual for pedogenic deposits which are usually composed solely of calcite and which usually have secondary accumulations of carbonate material on the undersides of clasts, sometimes in a speleothemic manner (Fig. 8). Pure hyalite opal layers often exist within the calcite/opal deposits at Yucca Mountain (Fig. 9). This opal is uraniferous (Szabo and Kyser, 1985) and fluoresces a brilliant yellow-green to green under ultraviolet light. According to Vaniman et al. (1988) the opal is of two varieties: "opal-A" (amorphous opal) and "opal CT" (cristobalite-tridymite).

The proportion of calcite or opal in the calcite/opal mixture can vary at different

localities. On the surface, near drill site UE-25 p#1, opal is predominant (even root casts are silicified), while at Trench 14 and Busted Butte the percentage of silica is somewhat less (on the average, about 50% carbonate, 50% opal; DOE, 1993). At Site 199 (Figs. 1 and 10), the spring deposits are composed predominantly of carbonate, while at the nearby Diatomaceous Earth site (Figs. 1 and 11), the spring deposits are composed predominantly of silica. Why such differences in mineralogy should occur is not clear, especially if all of the deposits are of pedogenic origin. Rather, the expectation would be that all such deposits in a region of similar bedrock geology and climate, formed through a common process, should exhibit similar textures and have the same mineralogy and chemical composition. However, a hypogene origin, in which textures resemble those present in epithermal mineral and hot spring deposits and in which the chemical character of the ascending fluids is controlled by subsurface lithology, could readily explain this otherwise perplexing distribution. For example, fluids depositing the carbonate tufa at Site 199 could have travelled primarily through Paleozoic carbonates and Precambrian metamorphic rock on their ascent to the spring, whereas fluids depositing the diatomaceous (silica) earth could have travelled primarily along Tertiary volcanic rock on their way to that spring location.

The occurrence of pure to mixed opal in the controversial deposits at Yucca Mountain is considered highly significant. Pedogenic calcretes generally do not contain continuous veins of opal; instead, opal in pedogenic deposits has been reported mainly as localized coatings and void fillings (e.g., McGrath, 1984; Sowers,

1985; Chitale, 1986). Thus, the critical question is: How could the pure, uraniferous opal have been derived from pedogenic processes and yet have been concentrated into discrete bands and seams within the calcite/opal mass?

Gypsum

Gypsum has been found at only one locality in the Yucca Mountain area, at the Wahmonie mound which is located ~25 km east of Yucca Mountain (Fig. 12). This lack of gypsum in all of the other calcite/opal deposits may be significant since pedogenic calcretes in the arid southwestern United States often contain gypsum (Bachman and Machette, 1977). For example, both gypsum and sepiolite exist in surficial calcic (Ka) horizons in Kyle Canyon, Nevada (Sowers et al., 1988).

The gypsum at Wahmonie mound is not pure gypsum, but is intermixed with carbonate (calcite $\cong$ 70-80%, gypsum $\cong$ 20-30%; Hill and Schluter, 1993). The mound is located within the Wahmonie Mining District along a prominent N30° E-trending fault. Precious-metal mineralization in the Wahmonie district occurs in a system of N30° E veins with a similarly-oriented 8 km x 4 km elliptical alteration halo containing strongly oxidized, argillized, and silicified rock (Castor et al., 1989). The Wahmonie travertine/gypsite mound locality is important for two reasons:

1. It demonstrates the principle: "What's on top reflects what's below" (Hill, 1993a). Quade and Tingley (1983) attributed the mineralization at the Wahmonie Mining District to a sulfide-rich intrusive body in the subsurface.

The Wahmonie surface mound is along the same fault as the mining district and so it is likely that the gypsum derived from oxidation of sulfides at depth along the fault zone. This relationship, in turn, implies ascending water along the fault rather than the sulfate being deposited by descending water (i.e., the gypsite is not of pedogenic origin). And while the Wahmonie mound, per se, has not been presumed to be "pedogenic," it still cannot be dismissed because the mound occurs at an altitude of about 1400 m elevation in an area where the water table is at about 1000 m elevation. Thus, its likely "spring" origin cannot be explained as easily as the spring deposits of Site 199 and Diatomaceous Earth site (Paces et al., 1993). The Wahmonie mound, by itself, seems to challenge the notion of a quiescent steady-state hydrologic system.

2. Because the mound is composed of a mass of very friable calcite and soluble gypsum, it should be quite young (assuming that the volume of the deposits was not considerably larger than they are now), otherwise it would have been eroded away. This possibility of a very-young deposit associated with a deep water table suggests that ascending fluids arising from hydrotectonic interactions may have continued until recent times.

Quartz

Quartz does occur at Yucca Mountain, both as vug fillings in the Tertiary rock, and also within the controversial calcite/opal deposits. An example of vug-filling quartz is

the drusy quartz at Trench 14 which occurs within cavities of the Tiva Canyon Member and is no doubt contemporary with volcanism (Vaniman et al., 1988). However, other, minor deposits of quartz have been found within the controversial calcite/opal deposits that are likely not to be syndepositional or detrital in origin. Harmon (1993) discussed three occurrences of this quartz: at WT-7, the Wailing Wall, and Pull Apart Fault.

WT-7

Samples collected from WT-7 consist predominantly of carbonate in which there are numerous sub-parallel veinlets of quartz. Under high magnification the quartz veinlets are zoned, the central portions consisting of clear euhedral quartz and the outer portions being comprised of fine-grained opal. Some of the quartz veinlets contain tubular structures of undetermined composition; these could be organic or they could represent low-temperature, epithermal flow structures. The latter explanation is preferred as there are mammillated surfaces on some of the voids which appear to consist of similar material. These same samples contain very small grains and microveinlets of pyrite and chalcopyrite, which also suggests an origin related to an epithermal environment.

Wailing Wall

Samples collected from the Wailing Wall are mixed calcite/opal deposits containing numerous small void spaces infilled with secondary silica. This silica is zoned, with an earlier, microcrystalline opal episode and a later, clear-crystalline quartz episode.

The quartz forms subhedral to euhedral crystals with doubly-terminated bipyramidal forms. Microveinlets of chalcopyrite were observed to cut across some of the quartz crystals; this association with sulfides again strongly suggests an epithermal origin.

Pull Apart Fault

Samples collected from Pull Apart fault consist of mixed calcite/opal that contains three distinct types of quartz: (a) solitary crystals with bipyramidal form, (b) veins of fibrous quartz, and (c) euhedral crystals infilling vugs. The bipyramidal quartz crystals were found to have rounded inclusions of glass in them which undoubtedly makes them of magmatic (volcanic) and detrital origin. The other two types of quartz, the fibrous and vug-filling quartz, are probably not of volcanic/detrital origin (Harmon, 1993).

Sepiolite

Sepiolite, a hydrated Mg-rich silicate clay mineral, has been reported from a number of localities in the Yucca Mountain area: from Trench 14 and Busted Butte (Vaniman et al., 1988; Levy and Naeser, 1991), and from the southern Striped Hills, Crater Flat, Jackass Divide, and Mercury Valley (Jones, 1983). It occurs locally within surface exposures of calcite/opal and also in fractures with subsurface calcite and opal in the unsaturated zone beneath Yucca Mountain (Vaniman, 1993).

The sepiolite at Yucca Mountain has been attributed to a supergene-pedogenic origin: e.g., Vaniman et al. (1988, p. 18) stated that "the commonest occurrences of

sepiolite in southern Nevada appear to be either playa-formed or pedogenic." Sepiolite can certainly be of pedogenic origin (Bachman and Machette, 1977), but it can also be of hypogene origin and related to faults (Hill, 1993b). Bachman and Machette (1977, p. 93) reported that pedogenically-formed sepiolite occurs in soils "only where palygorskite is dominant and montmorillonite is relatively depleted." In addition, these authors reported that sepiolite is a late-stage product of pedogenesis where the mineral usually occurs in the medial portion of a calcic soil profile, suggesting that its occurrence may be a function of depth of soil-water infiltration. In contrast to this occurrence of definitely-pedogenic sepiolite are the sepiolite deposits at Yucca Mountain which occur as fracture and vesicle fillings in a mixed calcite/opal matrix along surface fault zones and deep within the subsurface.

A review of the literature on sepiolite in the Basin and Range Province indicates that sepiolite in this setting is usually related to hydrothermal water upwelling along fault zones (Hill, 1993b). Ehlmann et al. (1962) described sepiolite from four mining districts in Utah and Nevada and in all of these occurrences the sepiolite was attributed to low-temperature, hydrothermal solutions. Post (1978, p. 58) described four other occurrences of sepiolite in the Las Vegas area and was of this opinion concerning the origin of these deposits: "Each of the sepiolite deposits appears to be formed in a somewhat different manner, although they all appear to be brought about by groundwater movement in areas of high Mg concentration...the mineral source in each case must have been derived from some depth in circulating groundwater." For all of these Basin and Range deposits, the universal source of Mg and Si for the formation of sepiolite has been reported to be dolomite and volcanic

rock in the subsurface.

Closer to Yucca Mountain, sepiolite is found along the Eleana thrust fault just northeast of Yucca Mountain, and in the Amagorsa Flat playa just south of Yucca Mountain. Jones (1983, p. 4) attributed the Eleana sepiolite and associated carbonate mineralization to "spring waters brought to the surface along a thrust of quartzite over argillite in the Mississippian Eleana Formation." Regis (1978, p. 31) said of the Amagorsa Flat sepiolite: "Introduction of late Pleistocene and recent hot-spring activity and subsequent faulting did much to produce the clay mineral assemblage occurring here and also the high magnesium content of the clays. This (sepiolite) deposit is probably the result of the alteration of Tertiary volcanic sediment by hot, magnesium-rich water." Hay et al. (1986) found that the Amargosa sepiolite deposits were concentrated along fault zones and attributed the mineralization to groundwater seeping upward from Paleozoic dolomite aquifers. In addition, these authors found that the difference in $\delta^{18}O$ values of co-existing silica and calcite corresponded to an equilibrium temperature of about 27 ° C and formation from water having a $\delta^{18}O$ value near -10.0. This low-temperature, hydrothermal origin of sepiolite at Amargosa playa is not consistent with a pedogenic origin where water temperatures should be <20°C.

The pertinent questions to be asked relative to the sepiolite deposits at Yucca Mountain are: If many or most of the sepiolite deposits in the Basin and Range Province are of a hydrothermal, spring- and fault-related origin, then why should the fault-related Trench 14 and Busted Butte sepiolite be considered not to be

hypogene? And, if the sepiolite is hypogene rather than pedogenic, then how can the intimately-associated and intermixed calcite/opal be considered to be supergene-pedogenic? And, if the source of Mg and Si for the Basin and Range sepiolite is dolomite and volcanic rock, then why should the Paleozoic dolomite and volcanic rock in the subsurface at Yucca Mountain not be the source of Ca, Mg, and Si for the calcite/opal/sepiolite deposits there?

FLUID INCLUSIONS

The extremely fine-grained nature of the calcite in the surficial calcite/opal deposits at Yucca Mountain precludes examining this mineral for fluid inclusions. However, some of the quartz crystals described above in the mineralogy section have been found to contain fluid inclusions large enough for microscopic examination and thermometric analyses (Harmon, 1993), and some of the calcite in the subsurface is also suitable for fluid inclusion analysis (Bish, 1989).

Fluid inclusions in quartz

In the WT-7 calcite/opal samples, clear euhedral quartz crystals are totally lacking in fluid inclusions except for a few very small (<1μm) monophase (?) inclusions. In the Wailing Wall samples, the quartz crystals contain abundant, but minute (<1 μm) fluid inclusions not suitable for thermometric analysis. Two kinds of inclusions appear to be present in the Wailing Wall samples: a monophase gaseous type and a two-phase liquid-vapor variety which have a high degree of fill (i.e., a ratio of liquid to

total volume of about 0.9).

In the Pull Apart fault samples, the solitary, bipyramidal quartz crystals (of probable volcanic, detrital origin) were heated to 400°C, but neither movement of the vapor bubble nor a change in phase proportions was noted. The fibrous quartz samples are inclusion-free, but the euhedral quartz crystals filling vugs in the calcite/opal mass contain fluid inclusions of adequate size for thermometric analysis. However, even in these samples, fluid inclusions are small and relatively rare, so that only 22 were located that were suitable for analysis. The heating measurements were confined to the temperature of homogenization of the inclusion (T_h), which always occurred by the disappearance of the vapor bubble. The freezing measurements were confined to a recording of the last melting temperature of the ice formed inside the inclusions upon freezing.

Thermometric analysis of the liquid inclusions of the euhedral, vug-filling quartz at Pull Apart fault yielded homogenization temperatures in the range of 118 to >216°C, with a mean of 147°C (Fig. 13). The T_h determinations are considered accurate to about ± 3°C, given the small size of the inclusions. Although the fluid inclusions within the euhedral quartz at the Wailing Wall were not of adequate size to permit thermometric analysis, the similarity of the quartz in this sample to that at Pull Apart fault, and the similar degree of fill of the inclusions, suggests a similar range of homogenization temperatures for the two sites. Only two inclusions were located in the Pull Apart fault sample which were of adequate size for freezing studies:

salinities of 0.1 and 0.5 wt % (NaCl equivalent) were obtained for these two inclusions. No evidence of boiling was observed in the inclusions in quartz at Pull Apart fault. Therefore, the T_h values measured represent a minimum temperature for epithermal activity. A pressure-based temperature correction, which would be controlled by the depth of formation, is necessary to define precise fluid inclusion filling temperatures. However, a rough approximation of the depth of formation of the quartz at Pull Apart fault (i.e., the depth necessary to prevent boiling of the fluid) is ~150 m.

Fluid inclusions in calcite

Calcite, opal, and sepiolite have all been encountered in the subsurface at Yucca Mountain by a number of drill holes. The calcite from these drill cores has been subjected to strontium (Fig. 28), carbon-oxygen (Fig. 32), and fluid inclusion analyses (Fig. 14). According to Bish (1989) and Bish and Aronson (1993), calcite encountered in USW G-2 has reported fluid inclusion T_h = 94-115°C (at 1640 m depth), 147°C (at 1756 m), 202-239°C (at 1774 m); and calcite encountered in USW G-3 has T_h = 101-227°C (at 31 m depth), 125-170°C (at 131 m), and 97°C (at 1464 m).

The fluid inclusion temperatures on calcite are important for three reasons:

1. The calcite from which the fluid inclusion data were obtained is the same type of fracture-filling calcite selected for the strontium and carbon-oxygen

isotopic analyses, the samples sometimes being collected in the same core and at the same depth (but the very same calcite pieces were not necessarily used for each type of analyses). For example, in drill hole USW G-2, at the 131 m depth level, the calcite was analyzed for fluid inclusion temperatures, strontium isotopes, and carbon-oxygen isotopes (Hill and Schluter, 1994). This is significant because it has been assumed, and then subsequently asserted as fact by such investigators as Peterman et al. (1992) and Marshall et al. (1993), that the calcite in the unsaturated zone is "pedogenic." Yet, seemingly, this "pedogenic" calcite may have high temperatures of formation. As discussed in The Problem section, this basic assumption of what is truly pedogenic is highly suspect.

2. The age of this high-temperature calcite may be very young. Again using the USW G-2, 131 m-depth example: calcite in fracture fillings have a T_h = 125-170°C, and other fracture calcite in this same drill hole and at the same depth was determined to have a U-series age of 26 ± 20 Ka (Szabo and Kyser, 1985; 1990).

3. It is interesting that the fluid inclusion filling temperatures for calcite in USW G-2 at 31 m and 131 m is between 101-227°C, and that for the quartz at Pull Apart fault it is between 118 to >216°C. These temperature ranges are approximately the same for approximately the same depths (0-150 m), suggesting a common origin for the fracture-filling calcite present in the drill

cores and in the surficial calcite/opal in the Yucca Mountain region.

TRACE ELEMENT ANALYSES AND CORRELATIONS

Trace element analyses and element correlations have been performed on the calcite/opal samples in the Yucca Mountain region (Hill and Livingston, 1993; Schmitt, 1993).

Trace element analyses

In general, the calcite/opal deposits at Yucca Mountain are not significantly enriched in trace metal content (Weiss et al., 1992, 1993), but there are important exceptions to this rule. Relatively-high barium was found at Pull Apart fault (440 ppm) and Site 199 (190 ppm), and relatively-high arsenic was found at Pull Apart fault (50 ppm) (Hill and Livingston, 1993). Relatively-high concentrations of zinc have been found in the calcite/opal deposits at Trench 8 (166 ppm), New Trench (90 ppm), and Wailing Wall (90 ppm) (Hill and Livingston, 1993); at Trench 14 (north wall), calcite/opal has measured zinc concentrations of 130 ppm and 210 ppm (DOE, 1993). How could this amount of metal enrichment have been supplied by a supergene-pedogenic process with a limestone dust source, when limestone typically has As values of 1 ppm, Ba values of 10 ppm, and Zn values of 20 ppm (Krauskopf, 1967)? It seems highly unlikely. Rather, the high metal levels at these various locations seem to indicate that the calcite/opal formed from fluids originating at depth that developed enhanced trace metal abundances as a result of water-rock interaction at elevated

temperatures. Subsequently, the fluids rose upwards along fractures and precipitated the calcite/opal deposits in various forms (veins, fracture fillings, spring travertine) across the Yucca Mountain region. The close proximity of silicified faults suggest that these faults were "feeders" for these calcite/opal depositing solutions.

There is also additional mineralogical and textural evidence that the calcite/opal at Yucca Mountain is tied to a regional epithermal system. Harmon (1993) reported quartz from three sites at Yucca Mountain and associated with this quartz are small amounts of sulfide minerals (see discussion in Mineralogy section). At WT-7 relatively abundant, very small grains and microveinlets of pyrite and chalopyrite exist with the quartz. The pyrite tends to occur as small, discrete grains scattered throughout the sample, whereas the chalcopyrite occurs either as solitary grains or as microveinlets. All of the sulfides are on the order of a few microns in diameter. Some of the microveinlets exhibit a clear association with zones of brecciation in the carbonate host. Small pyrite grains are also present at the Wailing Wall, scattered throughout the host carbonate/silica groundmass, and microveinlets of chalopyrite cross cut some of the euhedral-subhedral quartz crystals. Possible pyrite or chalcopyrite was also observed in several liquid inclusions within vug-filling quartz at Pull Apart fault. The association of these sulfide minerals with quartz points to a hydrothermal environment with a low-temperature character (i.e., an epithermal origin for the deposits).

Although the amount of sulfide mineralization within the calcite/opal is small, it is still

important. Studies done by the Department of Energy (e.g., Castor et al., 1992) have argued that pyrite disseminated in tuffs in the subsurface is of lithic or xenocrystic origin and provides no evidence of hydrothermal activity. However, based on textural, thermal, and stratigraphic information, Weiss et al. (1993) explained the pyrite as simply being the result of *in situ* sulphidation by aqueous solutions containing reduced sulfur. This reduced sulfur could have easily come from a hypogenic source, but not a pedogenic source.

Trace element correlations

Correlation of elements have been performed on five different calcite/opal deposits at Yucca Mountain. A total of 46 calcite/opal samples collected from these five sites were submitted for INAA (Instrumental Neutron Activation Analyses): 26 from Trench 14, three from west Busted Butte, three from Stagecoach Road north-trench A, six from Site 199, and eight from Wahmonie mound. Elemental abundances of these 46 samples were compared to the average abundance of these elements in soil and ped fines from Trench 14. The INAA procedure was the same as reported by Laul and Schmitt (1973) and Liu and Schmitt (1990). The data from these analyses is shown in tabular and graphic form in Appendix 1.

The following important trends can be seen from the INAA analyses:

1. Using Th as a representative detrital indicator, the detritus content of the calcite/opal vein samples varies from 0.2-25% at Trench 14, ~25% at West

Busted Butte, 20-35% at Stagecoach Road north-trench A, 8-90% at Site 199, and 0.8-80% at Wahmonie mound. These values are comparable to detritus values reported by the DOE (1993).

2. The slope calcrete and vein samples at Trench 14 are similar in their elemental analyses. This similarity supports a common genesis for both types of samples; i.e., the vein and slope deposits have derived from the same source. This is the exact same conclusion as reached from the strontium and carbon-oxygen isotopic data. The controversy is: are they both pedogenic or are they both hypogene?

3. Significant enrichments of trace elements (over soil-ped fines at Trench 14) were observed for all five sites: Co, Ni, Br, As, Sb, W, Au, and U are enriched in the Trench 14 vein/calcrete samples; Br, As, Sb, W, Au, and U are enriched in the west Busted Butte and Stagecoach Road north-trench A samples; Br, As, Sb, Au, and U are enriched in the Site 199 and Wahmonie mound samples (in both the calcite and gypsum fractions). In addition, the travertine calcite at Wahmonie mound exhibits extraordinarily high Mn, Ba, Zr, Hf, Th, and LREE (e.g., La = 138 ppm). The abundance of elements at all five sites is similar (see graphs and tables in Appendix 1).

The elemental correlations are important to the pedogenic/hypogene debate for the following reasons:

1. The significant enrichments over that found in the soil suggests that the

calcite/opal deposits were not derived from pedogenic soil processes but instead derived from an epithermal, metal-rich source (i.e., from the Precambrian basement by a hypogene process). This conclusion must be considered preliminary since the soil-ped fraction was analysed only from Trench 14 and not from the other four sites.

2. Similar elemental enrichments and abundances for the calcite/opal/gypsum deposits at all five sites implies a common mechanism for their emplacement. This is important because Site 199 and Wahmonie mound have been considered to be spring deposits (Paces et al, 1993, and Vaniman et al., 1988, respectively). If all of these deposits were formed by a common mechanism, then the Trench 14, Busted Butte, and calcite/opal from Stagecoach Road north-trench A must also be considered to have a spring (hypogene) origin.

PETROGRAPHIC TEXTURES

Texture refers to the size, shape, and arrangement (packing and fabric) of the physical constituents (grains, crystals) of a rock or mineral. The crystal size of the Yucca Mountain calcite/opal deposits is always extremely fine-grained. Most of the calcite (>95%) is micrite (<5 μm); the coarsest crystals are anhedral, void-filling calcites of 100-200 μm (Vaniman, 1993). This is in contrast to pedogenic carbonates

which are nearly always aggregates of silt-size calcite crystals (Dixon and Weed, 1989).

While the crystal size and mineralogy of the controversial deposits at Yucca Mountain is simple and consistent, textures of the deposits are diverse. Hill and Schluter (1993) identified 15 textural types in ~200 samples of calcite/opal collected from the approximately 50 localities studied across the Yucca Mountain region. These textural types are: pure (Fig. 15), mixed (Figs. 15, 16, and 17), banded/laminated (Figs. 16 and 17), massive (Figs. 15 and 18), powdery (Fig. 19), patchy, brecciated (Fig. 20), flow (Figs. 17 and 20), vesicular/ phenocrystic (Figs. 15 and 21), veined, invasive (Fig. 22), botryoidal, algal/ooidal, root-cast (Fig. 23), and speleothemic. Of these, the mixed and banded/laminated are by far the most common textural types. Ooidal texture is also common in some localities.

Mixed texture consists of a mixture of calcite and opal (and locally, minor sepiolite). The mixture varies in density and color depending on the relative amounts of calcite and opal. The denser, darker-tan samples contain more opal, and the less-dense, lighter-colored samples contain more calcite. Samples which display a mixed texture never fluoresce as do the pure-textured, hyalite opal (Fig. 15B). Vaniman et al. (1988, p. 20) reported that the dense, buff-colored, silica component of this mixture is opal CT.

Banded/laminated texture describes repeated layered sequences of calcite/opal,

calcite/opal. Calcite/opal sequences contain layers composed of various amounts of mixed-textured calcite/opal, and they can also contain layers of pure opal. Layering can vary in thickness from millimeters (laminations) to centimeters (bands) (Fig. 17), and it can vary in orientation from the horizontal to the vertical (Fig. 16). Layers can be concisely or roughly banded/laminated, with layers aligned perfectly parallel to one another or roughly sub-parallel to one another.

Ooidal texture is common in calcite/opal from the Busted Butte and Harper Valley area. The ooids of this textural type are spherical, about 1mm in diameter, and embedded in a matrix of micrite and fine-grained clastics. The ooids are especially noticeable where samples have been exposed to, and etched by, weathering. The ooids are whiter than the matrix and composed largely of carbonate that coats detrital grains, although many ooids contain no apparent nucleus. The surfaces of a few hand samples collected from the Harper Valley area were covered by black lichens which grew in semispherical pods, also about 1mm in diameter, and which may be related to the formation of some of the ooids. The ooids associated with opaline samples from Busted Butte were more opaline than ooids associated with carbonate samples.

Less common, but important, textures described by Hill and Schluter (1993) are flow texture, invasive texture, and vesicular texture. Flow texture is where darker and lighter bands of calcite/opal exhibit a marbly or wavy pattern (Figs. 17 and 20). These undulatory bands give the appearance that the calcite/opal groundmass was

once in a plastic or fluid state. Vesicular texture is where the groundmass displays vesicles or holes (sometimes filled with calcite, opal, and/or quartz, but more often not filled). The holes may be randomly spaced within the calcite/opal matrix or they may be aligned in rows along roughly-banded sequences or flow texture (Fig. 21). The holes themselves can be ellipsoidal, the ellipsoids being elongated in the direction of the flow bands or layering. Rarely, the holes are aligned in swirl-shaped rows. Holes usually occur in a dense, mixed-textured, calcite/opal groundmass, but they can also occur in a powdery- or massive-textured groundmass. Invasive texture is where a "blob" or "finger" of calcite/opal material penetrates the main mass of calcite/opal (Fig. 22). The invasive material can be distinguished from the matrix material by its lighter (or darker) color and by its more calcitic (or opalitic) composition.

Petrographic textures of the calcite/opal deposits in the Yucca Mountain area have the following important field relationships (Hill and Schluter, 1993):

1. There appears to be little correlation between location and textural type. Different textural types are found throughout the Yucca Mountain region -- including the Bare Mountain Mining District to the west of Yucca Mountain. The one exception to this rule is root cast texture: it appears to be especially abundant in the calcite/opal deposits on east and west Busted Butte.

2. Different textural types can exist in close proximity to one another. For

example, samples collected at Plug Hill display powdery, laminated, and patchy texture within centimeters of each other.

3. Various textures do not appear to have any relationship to host-rock type. These textures are features of fault-related calcite/opal, whether the occurrence is in Tertiary volcanic rock, Paleozoic carbonate rock, Precambrian metamorphic rock, or sand in sand ramps.

The textural types are important in that they are critical indicators of origin. The diversity and heterogeneity of texture displayed by the calcite/opal deposits, even within centimeters of each other, favor a dynamic fluid system. It is difficult to imagine how flow and brecciated textures could have been produced by pedogenic processes. For example, in Fig. 20, how could the breccia fragments have been moved sideways from their original position by pedogenic processes? Invasive texture suggests penetration of later fluids of slightly different composition after sections of the calcite/opal matrix had either solidified or partly solidified, and vesicular texture suggests gas cavities created by the degassing of fluids out of which the calcite/opal precipitated.

Banded/laminated texture is a common feature of pedogenic calcretes, and this type of texture may seem to favor a pedogenic origin for the calcite/opal deposits at Yucca Mountain. However, the banded/laminated texture of these Yucca Mountain deposits differs from laminated pedogenic calcretes in a number of important ways

(Hill et al., 1993):

1. In pedogenic calcretes the soil is microlaminated with respect to alternating carbonate/sand/silt/clay layers; in the Yucca Mountain calcite/opal there are no alternating sand/silt/clay layers.

2. The banding of the Yucca Mountain samples consists of repeated calcite/opal sequences, with mixed amounts of calcite and opal occurring in each band and with different proportions of the two minerals being variable from band to band. This is in contrast to reported pedogenic deposits which contain mostly (or only) calcite (calcrete) or opal (silcrete). It is of interest that petrographic features in other reported laminar silcrete deposits (e.g., Graaff, 1983) do not resemble the calcite/opal deposits at Yucca Mountain.

3. The thickness of the bands/laminations of the Yucca Mountain calcite/opal is much greater (often centimeters) than that reported for pedogenic calcrete/caliche deposits (usually millimeters or smaller).

4. The total thickness of a laminated/banded sequence of the Yucca Mountain calcite/opal are often on the scale of meters, not on the scale of centimeters as is characteristic of pedogenic deposits.

5. The calcite/opal laminated sequences at Yucca Mountain commonly bear no relationship to plugged horizons, petrocalcic horizons, or bedrock, conditions

which are supposedly responsible for the formation of laminar horizons in pedogenic deposits (Gile et al., 1966).

6. The banded/laminated sequences at Yucca Mountain are not necessarily oriented along soil horizons or parallel to the land surface as is characteristic of laminated pedogenic deposits. Many of the Yucca Mountain sequences cut across soil horizons and can be oriented in the vertical to near-vertical direction.

"TRUE" PEDOGENIC DEPOSITS

Criteria for recognition of pedogenic deposits

In order to distinguish between what is really pedogenic at Yucca Mountain and what may be hypogene, and in order to correctly interpret the isotopic data on the calcite/opal deposits, it is first necessary to compare the physical, textural, mineralogical, and geochemical characteristics of the calcite/opal deposits with the criteria that characterizes "true" pedogenic deposits (Hill et al., 1993). As defined by a number of soil scientists (e.g., Gile, 1961; Gile et al., 1965, 1966, 1981; Bachman and Machette, 1977; Machette, 1985; Soil Science of America, 1987), pedogenic deposits:

1. Occur as petrocalcic horizons which are oriented approximately parallel to, and a few meters or less down from, the land surface (Fig. 24).

2. Usually are laterally continuous, having a very large areal extent that can frequently be traced over tens to hundreds of square kilometers.

3. Typically consist of two major components, a calcareous fraction and a detrital or noncalcareous fraction (i.e., the "soil matrix"; Fig. 25b).

4. Have a rate of accumulation in desert soils which is very slow. A young (<100 Ka) geomorphic surface may have soils without petrocalcic horizons or in the first stage of petrocalcic morphologic development (Stage I), but more mature horizons (a meter or more in thickness) should be hundreds of thousands or even millions of years old (Fig. 24).

5. Have a morphological development which follows a six-stage sequence as described by Gile et al. (1966) and Machette (1985): (I) a first stage of filaments or faint coatings of carbonate on detrital grains, (II) a second stage of continuous pebble coatings and carbonate nodule development, (III) a third stage containing an essentially continuous horizon of carbonate composed of coalesced nodules and interpebble fillings, (IV) a fourth stage where the soil horizon becomes plugged to downward-moving solutions and laminar layers develop, (V) a fifth stage where laminar layers occur on the upper surface of the plugged horizon and where pisolites begin to form, and (VI) a sixth and most advanced stage which consists of massive, multilaminar, and strongly-cemented calcrete containing multiple generations

of brecciation and recementation (Fig. 25b).

Basin and Range Province

Older soils which have been exposed to pedogenesis longer should contain more pedogenic carbonate and thus follow the morphogenetic stages described above (i.e., stages I, II, III, IV, V, and VI). In the Basin and Range Province of the western United States, older soils commonly occur on the topographically highest alluvial fans which are inset by younger alluvium (Bull, 1991; Seager, 1981). An example of this pattern is given in Fig. 25a. The alluvial fans at and near Mercury follow this pattern, as do the fans in the Fortymile Wash area. Thus, the soils at the Nevada Test Site appear to follow the general trend of many southwestern arid soils, whereby progressively more complex carbonate horizons are associated with soils of progressively older geomorphic surfaces. One of the oldest surfaces in southern New Mexico is the upper La Mesa, which is approximately one million years old (Machette, 1985). Yet, this soil has a carbonate accumulation, including laminated pipes, of only two meters in thickness (Gile et al., 1981).

Yucca Mountain

There are carbonate deposits at Yucca Mountain that do meet the criteria for pedogenesis, but these are <u>not</u> the same as the controversial calcite/opal vein and travertine deposits located along fault zones. "True" pedogenic carbonate deposits at Yucca Mountain meet the criteria outlined above: they are laminated parallel to the land surface, they are widely distributed, and they are limited in thickness. Soils

with petrocalcic horizons often display (in descending order): (1) a thin layer of desert pavement containing pebbles and pieces of carbonate material, (2) a vesicular A horizon less than a few centimeters to 20 cm thick, (3) an argillic horizon up to a half a meter thick (only in some locations), and (4) a petrocalcic horizon up to a meter or so thick (Fig. 26). Pieces of carbonate material interdispersed between volcanic pebbles in the desert pavement surface represent fragments of the petrocalcic horizon which have worked their way up to the surface along with the pebbles (McFadden et al., 1987).

The thickness of petrocalcic horizons at Yucca Mountain corresponds to the geologic age of the geomorphic surface on which these horizons are developed (i.e., Fig. 25a). For example, at the gravel pit along Highway 95 (at the turnoff to Site 199), the gravels occur in a very young, late Quaternary geomorphic surface; these deposits have not accumulated any carbonate except for a faint discoloring of the soil. In Harper Valley, a petrocalcic horizon about 15 cm thick is located about 0.3 m beneath the soil surface (except for where it is exposed by gullying); this pedogenic layer has been dated at ~170 Ka (Hill and Schluter, 1994). Older geomorphic surfaces, such as the 1.0-1.5 my old surface at Red Cone, have well-developed petrocalcic horizons (Fig. 26).

The calcite/opal deposits at Yucca Mountain (e.g., those presumed to be "pedogenic" by Quade and Cerling, 1990 and others), however, do not meet the criteria for pedogenesis. Typically, these deposits are not laminated parallel or sub-

parallel to the land surface (many are vertical veins), they are not laterally continuous (they have a very restricted occurrence being localized along, or downgradient from, faults; Fig. 4), and they do not display pebble coatings, nodular/glaebular/pisolitic texture, or plugged laminar horizons that are characteristic of "true" pedogenic deposits (Hill et al., 1993). Sometimes the soil-matrix clastic fraction of these deposits is small to non-existent. Furthermore, the controversial calcite/opal deposits do not display the morphologic development sequence expected of pedogenic deposits (Stages I to IV), and the age of many of these deposits can be very young (Fig. 38). This also applies to so-called "pedogenic" deposits within the unsaturated zone at Yucca Mountain: these also have ages as young as ~30 Ka (Fig. 38).

Description of "true" pedogenic deposits at Yucca Mountain

"True" pedogenic deposits were collected from five locations in the Yucca Mountain area, and, for a regional perspective, two samples were collected from the River Mountains (east of Las Vegas) which has a rhyolitic terrain similar to Yucca Mountain (Lattman, 1973). Criteria for the recognition of pedogenic deposits was closely adhered to in the collection of all seven samples. The preliminary microscopic observations of these seven deposits is listed in Table 1, and are as follows:

1. "True" pedogenic carbonate deposits do not appear to display the same textures as the presumed "pedogenic" calcite/opal deposits, with the exception of powdery, ooidal, veined, and speleothemic texture. They do not

display pure, mixed, banded/laminated, massive, patchy, brecciated, flow, vesicular/phenocrystic, invasive, or root-cast texture (Figs. 15-23). In addition, "true" pedogenic deposits display nodular texture whereas the controversial calcite/opal deposits do not (Table 1).

2. "True" pedogenic deposits do not contain opal -- either pure opal (pure texture) or opal mixed with carbonate (mixed texture). In some of the samples a few pieces of detrital opal were observed (Table 1).

3. "True" pedogenic deposits are not nearly as fine-grained as the presumed "pedogenic" calcite/opal deposits. Crystal size of the controversial calcite/opal is always extremely fine-grained; most of it is <5 μm (microns) and crystals are not distinguishable under high magnification (50x). In contrast, individual calcite crystals in the "true" pedogenic carbonates were always observable under microscopic examination; even the tiniest calcite crystals could be distinguished by their high birefringence. Calcite crystals in the "true" pedogenic deposits were observed to range in size from ~5μm to 0.2mm, with a common size of ~10-100 μm. Thus, the "true" pedogenic calcite crystals are typically 10-1000x (or more) larger than the calcite/opal crystals in the controversial deposits. This is consistent with the observations of Dixon and Weed (1989, p. 281) who stated that pedogenic carbonates are "nearly always aggregates of silt-size crystals." This difference in size between "true" pedogenic deposits and the controversial calcite/opal deposits may be an important indicator of the hypogene origin of the

calcite/opal; i.e., the deposits cooled very quickly.

4. Some of the crystals within "true" pedogenic deposits can be quite large (1-2mm in size). These are calcite crystals which have been formed by secondary processes; i.e., remobilization of pedogenic carbonate and redeposition within the mass. This is in contrast to the controversial calcite/opal deposits which never display large crystals (this is why it is almost impossible to get fluid inclusion determinations for them).

5. Carbonate in "true" pedogenic deposits acts as the matrix material for silt-, sand-, and pebble-size clasts (Fig. 25b; Table 1). This is in contrast to some of the controversial calcite/opal deposits which contain little or no clastic material (DOE, 1993).

6. Some of the "true" pedogenic deposits at Yucca Mountain fit into the Stages I to III morphogenetic categories of Gile et al. (1966). These stages do not match the maturity of the category that the banded/laminated calcite/opal deposits would have to be placed into (i.e., Stages V to VI; Hill et al., 1993).

To summarize, there are "true" pedogenic horizons at Yucca Mountain, but these are not the same as the controversial calcite/opal vein and calcrete deposits. However, a pedogenic (supergene) component is no doubt superimposed over the calcite/opal deposits so it is imperative that these two components be differentiated in the field

and in the laboratory.

SOURCE OF CALCIUM

Another question of major importance with respect to the pedogenic-hypogene debate and this discussion is: What is the source of calcium for the calcite constituent of the calcite/opal deposits at Yucca Mountain? Five possible sources of calcium exist for the calcite/opal deposits at Yucca Mountain: rain water, eolian dust, tuffaceous bedrock, Paleozoic carbonates, and Precambrian basement rocks. And three mechanisms or processes exist for the emplacement of these deposits: water descending from the surface, capillary rise from shallow groundwater, and ascension of groundwater from depth due to hydrotectonic interactions.

Rain water is a potential source of carbonate as rain contains dissolved salts (6-7 ppm Ca; Goudie, 1973; Birkeland, 1984). According to most authors, this is a relatively low figure. Goudie (1973, p. 139) reported that with an annual rainfall of 325 mm (much higher than that at Yucca Mountain) it would take as much as five million years to build up 60 cm of calcrete by this mechanism. However, Gile et al. (1981, p. 63) estimated that rain water could form about 1.5 g of pedogenic carbonate/square meter/year whereas eolian dust could supply only 0.35-0.55 g/square meter/year of carbonate.

Calcareous dust and Ca^{2+} dissolved in rain water have been the best explanations

for the origin of carbonates in many arid soils (Reeves, 1976; Bachman and Machette, 1977; Gile et al., 1981; Machette, 1985). This is especially true where soil carbonates are laterally continuous across the landscape, the parent material is unweathered and low in calcium, and where there is no apparent communication between the groundwater and land surface. The ten-year dust trap data of Gile and Grossman (1979) provided supporting evidence for the calcareous dust theory. It appears, however, that the process of carbonate accumulation is more complicated than calcareous dust blanketing the landscape and infiltrating into the soils. For example, based on isotopic and pollen studies on the Fort Bliss Military Reservation in western Texas and southern New Mexico, the carbonate appears to be primarily generated *in situ* as the result of Ca^{2+} in the soil solution combining with bicarbonate generated by root and microbial respiration (Monger, 1993).

The source of calcium for many calcretes is limestone or dolomite. However, there are no surface exposures of limestone or dolomite in the Yucca Mountain area, only Paleozoic carbonate rocks in the subsurface below Tertiary volcanic rock. The tuffaceous bedrock at Yucca Mountain is very low in both calcium (usually only a few percent) and carbonate (<2%; Hill and Livingston, 1993). For this and other reasons (mostly isotopic) it is agreed on by most researchers that the tuffs at Yucca Mountain cannot be the source of calcium to the calcite/opal deposits (see the strontium isotope discussion).

Early workers thought that calcium for caliche deposits was brought from depth to

the surface by the capillary rise of groundwater (Reeves, 1976). However, the major soil process for calcrete deposits is actually the leaching of carbonates from upper soil horizons by downward percolating water (Bachman and Machette, 1977). The model of rising capillary water, if it were a major mechanism (which it is not), is also not appropriate for Yucca Mountain since the water table is presently ~400-600 m below the ground surface.

The argument involving Yucca Mountain revolves around whether the calcium is supplied by eolian limestone dust via descending water ("per descensum" model), or whether the calcium is supplied by water ascending from subsurface Paleozoic carbonate and Precambrian rocks. The pedogenic proponents (e.g., Stuckless et al., 1991a) insist that eolian limestone dust is brought into the region in sufficient quantities to provide enough calcium for the calcite of the calcite/opal deposits. Opponents of the pedogenic model (e.g., Szymanski et al., 1993) have argued that this source is insufficient, and therefore ascension of groundwater due to hydrotectonic interactions must have occurred.

A pertinent question with regard to the source of calcium is: Is there volumetrically enough wind-blown dust at Yucca Mountain to have supplied all of the calcite for the extensive calcite/opal deposits there? A study especially pertinent to this question is that of Lattman (1973) who found that alluvial fans flanking the Las Vegas Basin of southern Nevada are composed of detritus which may be dominantly carbonate, andesite-basalt, rhyolite and rhyolitic tuff, or siliceous sedimentary rock -- yet all fans

have been cemented by calcium carbonate to some degree. The carbonate and andesite fans show the best-developed cementation and the rhyolitic fans and those composed dominantly of siliceous sediments have markedly less well-developed cementation. Calcic horizons ranging from pebble coatings to plugged and laminar horizons, sequence steps I to VI in the formation of mature calcic horizons (Gile et al., 1966), were found on alluvial-fan deposits of carbonate and andesite lithologies, but only thin pebble coatings, discontinuous strings of calcareous cement, or weak calcic horizons were found on rhyolite, rhyolitic tuffs (like at Yucca Mountain) and noncalcareous sediments, even where large quantities of calcareous dust were available (Lattman, 1973). Lattman's study is pertinent to our findings at Yucca Mountain. There should be pebble coatings and some petrocalcic horizon development at Yucca Mountain from a wind-blown dust source, but not extensive calcite/opal deposits that extend up to 400 m into the subsurface.

The final two possible sources of calcium for the calcite/opal deposits at Yucca Mountain are Paleozoic carbonate and Precambrian rock in the subsurface, which rock supplies the calcium for the calcite/opal deposits on the surface and in the unsaturated zone by the ascension of groundwater. Proof of this source and process requires a discussion of the isotopic evidence.

STRONTIUM ISOTOPES

Strontium is an alkaline earth element with a geochemical behavior similar to

calcium except that in most geological situations it occurs as a trace element and, therefore, its distribution and isotopic composition can be used as petrogenetic tracers. Because carbonate minerals form essentially free of Rb, the $^{87}Sr/^{86}Sr$ ratio of a carbonate will not change as a result of radioactive decay which produces ^{87}Sr from the decay of the parent nuclide ^{87}Rb. Because there is no mass-dependent fractionation of the Sr isotope during geochemical processes, such as dissolution and precipitation, the isotopic composition of Sr incorporated in a secondary carbonate or silica precipitate will be identical to that of the dissolved constituents in the parent fluid. Hence, the $^{87}Sr/^{86}Sr$ ratio measured for such materials will directly reflect the ultimate source or sources from which the Sr in aqueous solution was derived.

A large amount of Sr-isotope data has been produced for the calcite/opal deposits at Yucca Mountain (Marshall et al., 1990, 1991, 1993; Marshall and Mahan, 1991; Peterman et al. 1991, 1992; Spengler and Peterman, 1991; Stuckless et al.,1991a,b; 1992; Ludwig et al.,1993; and Peterman and Stuckless,1993). In all of these studies the same basic assumption has been made: namely, that deposits presumed to be "pedogenic" in origin have a Sr-isotope character which is similar to the calcite/opal vein, travertine, and subsurface deposits, and that therefore these must also be "pedogenic." For example, Marshall et al. (1991) collected nine samples of presumed "pedogenic" carbonate from three trenches in Crater Flat (Trench 8, CF1, and CF2) and said that these matched the Sr-isotope composition of the Trench 14, 14a, and Busted Butte calcite/opal deposits in $^{87}Sr/^{86}Sr$. But each of these Crater

Flat trenches were dug along a fault zone: Trench 8 is located on the Solitario Canyon fault and Trenches CF1 and CF2 on the Windy Wash fault. Trench 8 is covered with pedogenic soils, but it also contains calcite/opal vertically emplaced along the fault. So how can it be presumed that the carbonate material at Trench 8 is not of hypogene or of mixed pedogenic-hypogene origin? The same reasoning applies to Trench CF1 where supposedly pedogenic carbonate material ~4 m thick is crosscut by a calcite/opal vein along the Windy Wash fault. The important point to be considered is that previous studies have not attempted to first examine the physical characteristics of the variety of carbonate deposits that occur in the Yucca Mountain area and then classify the samples into different types based upon occurrence and texture before undertaking sophisticated chemical and isotopic analyses. Rather, they have presumed an origin for some samples and then argued that any other samples having an equivalent isotopic character must have had the same origin. Although this second step of the chain of reasoning is correct, the presumption upon which it is based has not been demonstrated (or even evaluated). No attempt has been made to insure that the reference carbonates are pedogenic in origin; this critical point has just been assumed.

Strontium data compiled by Hill and Schluter (1994) has been plotted in Fig. 27 and shows the following trends:

1. All of the calcite/opal deposits at Yucca Mountain fall within a narrow range of $^{87}Sr/^{86}Sr$ ratios, with averages which are remarkably constant (0.71221-0.71240). A few of these deposits have much lower Sr-isotope ratios (dots,

Trench 14, Fig. 27)

2. Calcite/opal at Pull Apart fault and Bare Mountain fall within the same range of $^{87}Sr/^{86}Sr$ ratios as the texturally-similar calcite/opal deposits at Yucca Mountain.

3. Paleozoic limestone in the Yucca Mountain area has been significantly altered and has much higher $^{87}Sr/^{86}Sr$ ratios than unaltered limestone (e.g., the Spring Mountains, Fig. 27). This is especially true for the Paleozoic limestones at Black Marble Hill and, to a lesser extent, for other limestone localities in the Yucca Mountain area.

4. The calcite/opal deposits fall within the range of altered Paleozoic carbonate rock at Yucca and Bare Mountains, but are on the high side of this range and have much higher average values than the carbonate rock.

5. The Tertiary rock at Black Marble Hill has also been significantly altered, even more so than other Tertiary rock in the Yucca Mountain area (Fig. 27). In this regard it is important to realize that Black Marble Hill is located in an area where Paleozoic carbonate rock has been thrust-faulted over Tertiary rock (Cornwall and Kleinhampl, 1961), and that this thrust faulting continues all the way past the Diatomaceous Earth site to Site 199 (Swadley and Carr, 1987).

6. Suspected "spring" deposits, as shown in Fig. 27, have a slightly higher range of $^{87}Sr/^{86}Sr$ values than do the calcite/opal vein and travertine-like deposits at Yucca Mountain. In this category are the spring deposits of Site 199 and Diatomaceous Earth site (Paces et al., 1993), the Highway 95 "marsh" deposits of Marshall et al. (1993), and Devils Hole, which is part of the spring discharge system at Ash Meadows. It is not clear if Site 106 should be placed into the spring category (when only the highest 16 values are averaged), or if it should be placed into the calcite/opal category (when all of the 18 values are averaged; Fig. 27).

7. The Wahmonie travertine/gypsite mound is isotopically distinct (Fig. 27). This very low value may possibly be explained by the fact that gypsum has an affinity for strontium, and that a large influx of unradiogenic strontium would lower the $^{87}Sr/^{86}Sr$ ratio of the travertine/gypsite. The source of this unradiogenic strontium is unknown, but is probably important to the correct interpretation of the source of gypsum at Wahmonie mound.

8. The $^{87}Sr/^{86}Sr$ values of the drill-hole calcite increases from the saturated zone to the unsaturated zone to the surface, and approaches, but rarely exceeds, the range of values for the controversial surficial calcite/opal deposits. This trend of strontium ratios is not linear, but consists of four separate groups of strontium isotope values (A, B, C, D; Fig. 28).

The data trends discussed above will now be interpreted with respect to a hypogene versus pedogenic source for the calcite/opal deposits.

$^{87}Sr/^{86}Sr$ of calcite/opal

The similar range and average $^{87}Sr/^{86}Sr$ values for the various calcite/opal deposits across the Yucca Mountain region implies that all of these deposits derived from the same source. The fact that the Pull Apart fault calcite/opal falls within this same range of values is highly significant because of the high fluid inclusion temperatures, sulfide-bearing character, and metal enrichment of these deposits. The fact that the Pull Apart fault calcite/opal is most probably epithermal in origin implies that other, similar calcite/opal deposits at Yucca Mountain are epithermal, or at the very least, contain components which have an epithermal origin.

The spring deposits of calcite and silica are slightly higher in $^{87}Sr/^{86}Sr$ than the calcite/opal vein and calcrete deposits at Yucca Mountain. The reason for this is not clear but may be related to an increase in both Sr concentration and $^{87}Sr/^{86}Sr$ ratios from north to south and downgradient in the flow system; i.e., as was documented by Peterman et al. (1991) and Peterman and Stuckless (1993) for the nearby Ash Meadows groundwater system. Such Sr-isotope ratios and Sr concentrations implies the presence of high ^{87}Sr-enriched source rocks also having high elemental Sr abundances somewhere along the flow path: either Precambrian crystalline basement rocks, and/or younger clastic rocks derived from the Precambrian basement, and/or metasomatized Paleozoic and Tertiary rock which have been altered by fluids derived from the Precambrian basement. The location of Site 199

and Diatomaceous Earth along this flow path, and the higher $^{87}Sr/^{86}Sr$ ratios of these spring deposits, may not be fortuitous. Both of these sites are located where Paleozoic carbonate rock has been thrust up over Tertiary volcanic rock (Swadley and Carr, 1987), and where both types of rocks have been highly altered and brecciated (Fig. 29). Water ascending from depth along this thrust belt could have picked up radiogenic strontium from the Precambrian basement thus causing the higher $^{87}Sr/^{86}Sr$ ratios of the Paleozoic carbonate rock, Tertiary volcanic rock, and the spring deposits (Fig. 27).

$^{87}Sr/^{86}Sr$ ratios with depth

The trend of decreasing $^{87}Sr/^{86}Sr$ ratios with depth and the clustering of this data into four groups (Fig. 28) needs explanation. Spengler and Peterman (1991) noted an increase in strontium concentration in tuffaceous rock at Yucca Mountain from about 30 ppm in the Topapah Spring Member of the Paintbrush Tuff to almost 300 ppm in the older tuffs, with conspicuous local high concentrations of Sr. These authors also noted an increase of $^{87}Sr/^{86}Sr$ ratios upwards in the units above the Bullfrog Member of the Crater Flat Tuff. This progressive tenfold increase in Sr with depth, coupled with the similarity of $^{87}Sr/^{86}Sr$ values within the Bullfrog Member and older units to those of Paleozoic marine carbonates, are consistent with a large influx of Sr from water derived from the Paleozoic carbonate aquifer.

Spengler and Peterman's (1991) results are applicable to our discussion of decreasing Sr-isotope ratios with depth for calcites at the surface, in the unsaturated

zone, and in the saturated zone at Yucca Mountain (Fig. 28) A large influx of water derived from an unaltered Paleozoic aquifer would lower $^{87}Sr/^{86}Sr$ ratios to values commensurate with normal limestone (i.e., 0.708-0.709) and calcites precipitated from these waters would reflect these low values (Fig. 28, A). The gradual increase of strontium ratios in calcites of group A reflects the distance from the Paleozoic aquifer: samples collected deeper and closer to this aquifer more readily reflect the lower values of this aquifer versus higher values in the above-lying Tertiary aquifer.

The similarity in $^{87}Sr/^{86}Sr$ ratios between calcite fracture fillings in the 100 m interval immediately above the water table (Fig. 28, B) and the mean groundwater value of the Cenozoic aquifer (Fig. 28, arrow), may indicate that the calcite in the zone intermediate between the saturated and unsaturated zone formed primarily from water derived from Tertiary rock at a time when the water table was considerably higher than it is at the present (60-130 m; ~85 m, Fig. 30; Peterman et al., 1992; Marshall et al., 1993). Similarity, studies of the distribution of both zeolitized and vitric tuff and tridymite indicated to Levy (1991) a water table position ~60 m higher than the present water table.

While Groups A and B in Fig. 28 can be adequately accounted for, groups C and D are more difficult to explain. The similarity in strontium isotope values between these two groups (C and D) implies either that the calcite in the unsaturated zone (down to ~400 m) is "pedogenic" similar to surficial calcite/opal deposits (the USGS's presumed position) or that both must be hypogene (our position). The proper

interpretation of the $^{87}Sr/^{86}Sr$ ratios of these deposits depends on the determination of the source of the strontium.

Source of strontium

There are four possible sources of strontium for the controversial calcite/opal deposits at Yucca Mountain (i.e., groups C and D of Fig. 28). These are, from top to bottom stratigraphically: (1) eolian dust, (2) Tertiary volcanic rock, (3) Paleozoic carbonate rock, and (4) Precambrian basement rock.

Eolian dust

A number of investigators have proposed that eolian limestone dust is the source of calcium and strontium for the controversial calcite/opal deposits at Yucca Mountain (e.g., Stuckless et al., 1991a; 1992). According to this scenario, meteoric water dissolves and washes dust high in carbonate into permeable zones such as fractures or porous soils; this carbonate then precipitates within these voids and the force of crystallization pushes the deposits apart, causing bands of calcite and opal to form.

From the composite Sr-isotope diagram (Fig. 27), this eolian interpretation seems highly unlikely for the following reasons:

1. Eolian limestone dust is not nearly sufficiently enriched in ^{87}Sr to be the only source of strontium for the controversial calcite/opal deposits at Yucca

Mountain. Notice in Fig. 27 that only the limestone with the very highest strontium ratios (i.e., from Black Marble Hill) could be an eolian source of strontium for these deposits; other local limestones (e.g., mainly the Bonanza King) do not have sufficiently high $^{87}Sr/^{86}Sr$ ratios (n = 6, avg. = 0.71024) even though they have been somewhat enriched in ^{87}Sr relative to "normal" limestones (0.708-0.709). Thus, even if a completely local source of limestone dust is claimed (as was proposed by Marshall et al., 1991), eolian dust cannot have been the only source of strontium to the calcite/opal deposits.

2. It is more likely that eolian dust should be a mixture of both local and regional limestone as well as any other lithologies which outcrop and contain Sr. If this is the case, then it even further discredits an eolian source for the controversial calcite/opal deposits because Sr-isotope ratios should be even lower for such mixtures. Limestone in the Spring Mountains, located west of Las Vegas, has $^{87}Sr/^{86}Sr$ ratios of 0.708-0.7092 (0.70852 avg.; Fig. 27) typical of "normal" limestones (Faure, 1986); such "normal" limestones have much-too-low Sr-isotope ratios to account for the high Sr-isotope ratios (0.7112-0.7128) of the calcite/opal deposits at Yucca Mountain.
3. Some calcite/opal deposits in groups C and D of Fig. 28 have high fluid inclusion temperatures (see previous discussion on fluid inclusions). Therefore, an eolian-dust, pedogenic source is not considered reasonable for these deposits.

While eolian dust cannot be the entire source of strontium to the controversial calcite/opal deposits at Yucca Mountain, it may be a partial source. Note in Fig. 27 that the highest eolian $^{87}Sr/^{86}Sr$ values are equivalent to the lowest values of the calcite/opal deposits. Also note that a few of the calcite/opal samples plot much lower on Fig. 27 than do the others (e.g., the dots along the lines for Trench 14, Diatomaceous Earth, and Site 106). These values suggest that eolian carbonate may be one end-member that contributes Sr and Ca to the calcite/opal (Marshall et al., 1991; Marshall and Mahon, 1991). If true, then what is the source of the other, more-dominant, end member of the controversial calcite/opal deposits?

Tertiary volcanic rock

Tertiary volcanic rock in the vicinity of Yucca Mountain has been highly altered in some locations, with $^{87}Sr/^{86}Sr$ ratios as high as 0.71897 (Fig. 27). K-Ar dating of zeolites in these rocks yields a wide spectrum of ages (from ~10.6-2.0 Ma) suggesting that the rock mass has continued to be susceptible to low-temperature alteration long after the main episode of diagenesis (Peterman et al., 1993). However, even though some of the rock is altered and has relatively high Sr-isotope ratios (Fig. 27), water derived exclusively from the Tertiary aquifer in the immediate vicinity of Yucca Mountain could not have been entirely involved in the generation of the calcite/opal deposits because its $^{87}Sr/^{86}Sr$ average is only 0.71092 (Stuckless et al., 1991a; Fig. 28, arrow). This is one of the main reasons for not favoring a strictly-Tertiary volcanic, "per descensum" model for the controversial calcite/opal deposits. Another reason is the inability of the Tertiary rock to supply enough calcium

necessary for the formation of these abundant deposits (see discussion on source of calcium). However, the Tertiary rock, either by ascending or descending (or both) water, could have supplied the opal for these deposits.

Paleozoic carbonate rock

A number of studies have claimed that the calcite/opal deposits at Yucca Mountain could not have derived from the Paleozoic aquifer since unaltered limestone should have $^{87}Sr/^{86}Sr$ values between 0.7078-0.7093 (e.g., Marshall et al., 1990). This is true for unaltered limestone, but it is also apparent from Fig. 27 that much of the limestone at Yucca Mountain has been highly altered, and that this altered limestone could have been at least a partial source for the ^{87}Sr enrichment observed in the calcite/opal deposits. A Paleozoic carbonate source makes sense because this rock would have been able to supply all of the calcium and magnesium needed for the calcite and sepiolite in the controversial deposits; however, Paleozoic limestone cannot be the entire source because only the highest values of Sr-isotope ratios (e.g., a few of the limestones at Black Marble Hill) overlap with the calcite/opal (Fig. 27).

Precambrian basement rock

None of the three sources so far discussed is adequate to explain the high Sr-isotope ratios of the calcite/opal deposits (groups C and D, Fig. 28). These three may be partial sources for the deposits, however. There is only one source that could have supplied the required ^{87}Sr enrichment: the Precambrian basement.

would pick up high $^{87}Sr/^{86}Sr$ ratios from this rock; then, as convecting geothermal fluids flowed through the above-lying Paleozoic carbonate and Tertiary rocks higher in the stratigraphic section, they would pick up calcium and silica and also become lighter in their $^{87}Sr/^{86}Sr$ ratio. Finally, these equilibriated fluids, upon reaching the near-surface (unsaturated zone) or surface, would experience a loss of gas and pressure and the calcite/opal would precipitate. Finally, this hypogenic calcite/opal would be modified by meteoric water and a "true" pedogenic component. This carbonate component would build up in the surface soil with time and descend along fractures (as it is remobilized by meteoric water) to become superimposed over the hypogene component, thus causing a lowering of the $^{87}Sr/^{86}Sr$ ratios of some of the calcite/opal deposits.

It is therefore concluded that the strontium isotopic data does not "preclude" the precipitation of vein and other carbonates from ascending waters (Stuckless et al., 1991, p. 553). On the contrary, an examination of all of the data indicates that water ascending from the Precambrian basement is the only reasonable source of strontium to the calcite/opal deposits at Yucca Mountain. This conclusion is in accord with that of Johnson and DePaolo (1993, p. 20) who stated from their modelling of Yucca Mountain Sr isotope data: "The upward-flow scenario modeled here is consistent with the vein calcite data."

CARBON-OXYGEN ISOTOPES

The stable isotopes of carbon and oxygen are useful as geochemical tracers because fractionation of the light stable isotopes occurs during physio-chemical processes in the natural environment, but isotope ratios do not change as a function of time. Hence, different environments tend to be characterized by distinct stable isotope compositions, and isotopic fractionation in stable isotope systems can be diagnositc of particular geologic processes. Also, because isotope fractionation between coexisting phases at equilibrium is temperature dependent, there is an important potential for geothermometry. The stable isotopes of carbon and oxygen are also useful in determining terrestrial paleoclimatic conditions involved in the deposition of pedogenic carbonates (Cerling, 1984; Amundson et al., 1989; Quade et al., 1989; Kelly et al., 1991; Mack et al., 1991).

Carbon-oxygen isotope studies on the calcite fraction of the controversial calcite/opal deposits at Yucca Mountain have been performed by Szabo and Kyser (1985, 1990), Quade and Cerling (1990), and Whelan and Stuckless (1991, 1992). These authors have again taken the approach that because calcrete deposits presumed to be pedogenic have stable isotopic compositions which are similar to those of the calcite/opal vein deposits, that these latter must also be pedogenic. These authors have not considered the possibility that their presumed "pedogenic" deposits may really be hypogene in origin, and that this is the reason why these deposits and the calcite/opal veins are isotopically similar.

The carbon-oxygen data compiled by Hill and Schluter (1994) is plotted in Fig. 31 and shows the following trends:

1. All of the Yucca Mountain calcite/opal deposits fall within a fairly narrow field of carbon-oxygen isotopic compositions (i.e., the solid ellipse of Fig. 31 labelled "controversial calcite/opal").

2. All of the calcite/opal deposits that plotted within the calcite/opal field in terms of their $^{87}Sr/^{86}Sr$ ratios (Fig. 27) also plot within the ellipse of Fig. 31, with the exceptions of Trench 8 (TR8) and Pull Apart fault (PAF), which plot to the right of the solid ellipse.

3. The spring deposits at Site 199 plot between the $\delta^{13}C$-$\delta^{18}O$ ellipse and mammillary calcite at Devils Hole.

4. Calcite/opal along faults at Bare Mountain plots with the Yucca Mountain calcite/opal in terms of its C- and O- isotope composition (Fig. 31), just as it did in its Sr- strontium isotope composition (Fig. 27).

5. The Wahmonie travertine/gypsite plots with the Yucca Mountain calcite/opal deposits in its C- and O- isotope composition (Fig. 31), but varied radically from these deposits in its Sr-isotopic composition (Fig. 27).

6. The calcite/opal deposits at Busted Butte (open circles, Fig. 31) have considerably higher $\delta^{13}C$ and $\delta^{18}O$ values than do the calcite/opal deposits at Trench 14 (x, Fig. 31).

7. Values of "true" pedogenic deposits at Kyle Canyon are indicated by the rectangles in Fig. 31. The highest elevations at Yucca Mountain are ~1300 m, so that "true" pedogenic deposits at Yucca Mountain should plot within rectangles 1 and 2, but not 3 and 4, assuming that the conditions for forming pedogenic deposits throughout southern Nevada are approximately the same.

8. The pedogenic carbonate coating overlying clasts at Lathrop Wells Cone (LWC, Fig. 31, ~ 800 m elevation), lies well outside of the calcite/opal $\delta^{13}C$-$\delta^{18}O$ ellipse, and instead lies within the Kyle Canyon ~800 m elevation field.

9. There is a distinct increase in $\delta^{13}C$ and $\delta^{18}O$ values with depth in drill holes UE-25 a#1, b#1 and USW G-1, G-2, G-3, and G-4, but there is much variation of isotopic composition with depth within this general trend (see data for these drill holes; Hill and Schluter, 1994). In addition, this trend can be divided into two groups (A and B, dashed ellipsoids, Fig. 31): group A representing most (but not all) of the calcites in the saturated zone and group B representing most (but not all) of the calcites in the unsaturated zone. Thus, this trend is similar to that for strontium isotopes (Fig. 28) in that the

saturated and unsaturated zones have largely separate isotopic signatures, and in that the isotopic values within the unsaturated zone merge with those of the surficial calcite/opal deposits.

10. The stable isotopic composition of the Devils Hole mammillary calcite plots mostly within the field of the saturated zone carbonates (Fig. 31), or near the boundary between the saturated and unsaturated zone carbonates. This is consistent with the shallow water-table position of this precipitated calcite.

11. C-, O-, and Sr-isotopic compositions of the Paleozoic limestone show that this limestone is highly altered (Figs. 27 and 31). "Normal" marine limestone/dolomite should plot in the hatched area of Fig. 31; instead, the four LS values of Fig. 31 have somewhat lower $\delta^{13}C$ values than unaltered limestone/dolomite and much lower $\delta^{18}O$ values than unaltered limestone/dolomite (see middle and upper left of Fig. 31).

The $\delta^{13}C$ and $\delta^{18}O$ trends discussed above will now be interpreted in light of the conclusions drawn in the strontium isotope section.

1. All of the controversial calcite/opal deposits fall within a fairly narrow range of C-, O-, and Sr-isotope compositions because they all derived from the same source (this is the same conclusion as reached in the Sr- isotope section). This narrow range of values favors a hypogene groundwater origin over a

surface pedogenic origin for the calcite/opal deposits. The formation of soil calcretes and other pedogenic carbonate deposits is strongly dependent on evaporation. This is a process in which the fractionation effects become progressively greater in an exponential manner as the process continues (i.e., as the degree of evaporation becomes greater). Thus, a large amount of stable isotope variation in any suite of pedogenic samples should not be the same for all samples and a range of values should occur. Groundwaters, however, are subject to much less O-isotope variation than meteoric precipitation which exhibits huge annual ranges in desert regions and which is subjected to large modifications via evaporation.

2. The carbon-oxygen values of all the carbonates, however, appear to be more variable than the strontium isotope values, both on the surface and in the trend with depth. This variation may be caused by a number of factors: climate, vegetation type, or the amount of "true" pedogenic material which may be superimposed on, or mixed with, the calcite/opal deposits. For example, the range and average of $^{87}Sr/^{86}Sr$ values for the Busted Butte calcite/opal are nearly identical to those at Trench 14 (Fig. 27); yet, they are lighter in their $\delta^{13}C$ and $\delta^{18}O$ values (Fig. 31). Why should this be so? It may be that the Busted Butte samples, and also the Pull Apart fault (PAF) and Trench 8 (TR8) samples were more contaminated by "true" pedogenic material. Or perhaps, during the climatic periods in which each of these were deposited, different vegetation and atmospheric conditions existed, so that

the resulting carbon-oxygen values have been variable over time for different calcite/opal deposits around Yucca Mountain.

3. The difference in carbon-oxygen isotopic ratios for Site 199 and Devil's Hole is interesting because these sites fall within the same "spring" category in Fig. 27, having approximately the same $^{87}Sr/^{86}Sr$ ratios. From the difference in $\delta^{18}O$ values (but not $\delta^{13}C$ values which are not strongly temperature dependent), it may be that the water which deposited the Devil's Hole calcite had a somewhat higher temperature than the water which deposited the Site 199 spring mound, or Site 199 may have been subjected to post-depositional leaching.

4. The Bare Mountain calcite/opal has the same carbon-oxygen composition as the Yucca Mountain calcite/opal (BM, Fig. 31). This, in combination with equivalent $^{87}Sr/^{86}Sr$ ratios, the same petrographic textures (Hill and Schluter, 1993), the same trace element abundances (Hill and Livingston, 1993), and the fact that the deposits in both locations occur along fault zones, suggests that they have the same origin and source.

5. The Wahmonie travertine/gypsum has the same carbon-oxygen signature as the Yucca Mountain calcite/opal (WM, Fig. 31). This is important because from previous discussions (see Mineralogy section) it was emphasized that the Wahmonie gypsum is probably a surface expression of sulfides at depth, ascending water being the means by which this oxidized sulfur was brought

to the surface. The similarity in C- and O-isotopic composition at Wahmonie to the calcite/opal deposits at Yucca Mountain implies that these deposits also derived from ascending water.

6. Calcite within the saturated zone (group A, Fig. 31) has a stable isotope composition which reflects both the depth of formation and the influence of the unaltered Paleozoic limestone aquifer (as was the case with the strontium isotopes). The $\delta^{18}O$ values become lower with depth because the temperature increases, and $\delta^{13}C$ values become higher with depth because of the increased rock-water interaction with the unaltered Paleozoic limestone (see the unaltered Paleozoic limestone/dolomite regime, hatched area, Fig. 31).

7. The $\delta^{13}C$ and $\delta^{18}O$ values for limestone at or near Yucca Mountain (LS, Fig. 31) show that the Paleozoic limestone in many locations has been highly altered from "normal" marine limestone (hatched area, Fig. 31). This is in accord with the strontium isotopic data (Fig. 27).

The model of origin proposed in the strontium isotope section can be applied to the carbon-oxygen isotope data.

Carbon isotopes

Carbon isotopes can be used in the study of pedogenic carbonates. Pedogenic

carbonates record the isotopic signature of soil CO_2 which, in turn, is controlled primarily by the relative abundance of C_3 and C_4 plants (Cerling, 1984; Quade et al., 1989). Soils having abundant C_3 plants, which respire isotopically light CO_2, produce pedogenic carbonates with lower $\delta^{13}C$ values (approximately -12 ‰) than soils dominated by C_4 plants (approximately +2 ‰) (Boutton, 1991). Thus, a shift from high $\delta^{13}C$ values to lower $\delta^{13}C$ values with time indicates a decline in C_4 plants or an increase in C_3 plants (Wang et al., 1993). Conversely, a shift from low to higher $\delta^{13}C$ values is evidence for a C_4 increase that suggests warm-season rainfall and/or higher temperatures (Wang et al., 1993).

According to Quade and Cerling (1990) the local vegetation at Yucca Mountain is dominated by C_3 shrubs such as black bush and cresote, but mixed with some C_4 plants. This mix should produce $\delta^{13}C$ values in soil carbonates of -7 to -4‰. The values of $\delta^{13}C$ for the controversial calcite/opal deposits fall within a range of -8 to -3, the Busted Butte values falling toward the higher end of the $\delta^{13}C$ range and the Trench 14 values lying toward the lower end of this range (Fig. 31). From the Trench 14 $\delta^{13}C$ values, which are somewhat higher than values for the vegetation in the area, Quade and Cerling (1990, p. 1550) came to the conclusion that: "The Trench 14 carbonates did not form in equilibrium with the modern vegetation in the area, but vegetation zones were displaced about 1000 m downward during the last full-glacial period (16,000-19,000 years ago)". One problem with this interpretation is that the dates on the calcite/opal deposits at Trench 14 cover the time frame of 38 Ka to >400 Da, (Fig. 38) and as such would cover full-glacial and interglacial periods and

therefore should be expected to vary widely instead of falling within such a narrow range of $\delta^{13}C$ values.

An alternate view to that of Quade and Cerling's is to consider (from the strontium isotope discussion) that the $\delta^{13}C$ values may be from a mainly hypogene source; i.e., values representative of Precambrian rock modified by Paleozoic carbonate and Tertiary rock, further modified by a pedogenic signature. Typically, in the pristine state, prior to CO_2 degassing and resulting ^{13}C diffusional enrichment, hydrothermal, hypogene fluids contain dissolved igneous CO_2 carrying values of $\delta^{13}C$ from about -8 to -5 (Faure, 1986). Calcites formed under such non-equilibrium conditions, where CO_2 is degassing and precipitating calcite, would carry the observed range of $\delta^{13}C$ = -9 to -3 such as exhibited by the controversial calcite/opal deposits (Szymanski et al., 1993).

Oxygen isotopes

A large number of O-isotope ratio determinations have been performed on the calcite of the Yucca Mountain calcite/opal deposits (Fig. 31), but only four analyses of co-existing opal have been made (Harmon, 1993; Table 2).

Opal

Oxygen values (SMOW) for four carbonate-opal pairs were determined for samples collected from Pull Apart fault, Bare Mountain, Wailing Wall, and Busted Butte (Table 2). Assuming that two co-existing phases have been deposited under conditions of

O-isotope equilibrium from a common fluid phase, then the distribution of ^{18}O between the two phases will be a direct function of the temperature at which the precipitation of the minerals occurred (Fig. 32).

Of the four samples tested, only one of the four (from Pull Apart fault) seems to have deposited under conditions of O-isotope equilibrium. If this was in fact the case, then the depositional temperature was 50-60°C (Harmon, 1993; Fig. 32, PAF). The displacement of the other three samples far to the left of the 25°C isotherm in Fig. 32 implies isotopic disequilibrium between opal and calcite in these samples. However, three of the four samples (all but the Busted Butte sample) have practically identical $\delta^{18}O$ values for opal, and this suggests that the Bare Mountain and Wailing Wall samples were deposited under essentially equivalent environmental conditions as the Pull Apart sample; that is, from an isotopically similar epithermal solution (assuming that deposition occurred at this same temperature).

Quartz and opal are known to be essentially insensitive to post-depositional isotope exchange under low-temperature conditions, whereas fine-grained calcite will readily undergo isotopic exchange. Therefore the O-isotope relationships displayed in Fig. 32 are interpreted to indicate that the carbonate components of the Bare Mountain, Wailing Wall, and Busted Butte samples (and also other carbonate vein/travertine samples of similar composition) have been affected by post-depositional O-isotope exchange with a fluid phase having significantly lower ^{18}O (SMOW) content than that which precipitated the coexisting opal; i.e., meteoric precipitation (Harmon, 1993).

Calcite

The above discussion is crucial to understanding the oxygen isotope values of the controversial calcite/opal deposits at Yucca Mountain. Note in Fig. 31 that the Bare Mountain (BM), Busted Butte (circles), and Wailing Wall (WW) samples all plot within the calcite/opal ellipse and are essentially equivalent to the Trench 14 (x's) samples in terms of their O-isotope composition. This means that probably all of these samples have undergone isotopic exchange with meteoric water and have partially equilibriated with meteoric water (i.e., precipitation average $\delta^{18}O \cong -9$, SMOW, Fig. 33). This same principle also applies to the other surficial calcite/opal and hydrothermal spring deposits in the area: many have probably undergone isotopic exchange with meteoric water to some extent (e.g., the $\delta^{18}O$ value of Site 199 may not plot with the Devil's Hole calcite because of its fine-grained nature and isotopic exchange with meteoric water). Under laboratory conditions such an exchange process occurs quite readily (days to weeks), but the process is grain size, flow rate, temperature, and composition dependent.

If the oxygen isotope values of the surficial, fine-grained calcite/opal deposits at Yucca Mountain have undergone isotopic exchange with meteoric water, then what might have been the values of the originally-precipitated hypogene calcite? To obtain relatively unexchanged oxygen isotope values one must look to the Devils Hole calcite. As discussed in the strontium isotope section, the Devils Hole mammillary calcite probably represents that which was derived from both the Paleozoic and Precambrian aquifers, and as such, this calcite very likely represents water out of

which the controversial calcite/opal formed. Also, again note in Fig. 31 that $\delta^{18}O$ values for calcite from Devils Hole to the unsaturated zone and to the surface continually increase and approach the values for the surficial calcite/opal deposits. This trend may be caused by the increased amount of isotopic exchange of calcites with meteoric water as they approach the surface, and it may also be a reflection of the very fine-grained nature of the surficial calcite/opal deposits versus the less fine-grained nature of the calcite in the unsaturated zone.

In this regard, it is interesting to compare $\delta^{18}O$ values of the surficial calcite/opal deposits at Yucca Mountain with $\delta^{18}O$ values of "true" pedogenic deposits in the southwestern United States and elsewhere. The amount of ^{18}O in pedogenic carbonate is inherited from local meteoric water (Cerling, 1984). Because the isotopic composition of meteoric water is a function of the mean annual temperature (Dansgaard, 1964; Rozanski et al., 1992), pedogenic carbonates contain information about air temperatures that existed when calcite crystals precipitated (Hays and Grossman, 1991). Thus, a change from high $\delta^{18}O$ (SMOW) values to lower $\delta^{18}O$ values is evidence for a decrease of $\delta^{18}O$ values in meteoric water resulting from (a) increased winter relative to summer precipitation, (b) decrease in local temperature, and (c) a change in global mean temperature (Wang et al., 1993). In contrast, a shift from low to higher $\delta^{18}O$ (SMOW) values is evidence for (a) increased summer relative to winter precipitation, (b) increase in local temperature, or (c) a change in global mean temperature (Wang et al., 1993). Additionally, enrichment of ^{18}O may occur in the soils due to evaporation (Schlesinger et al.,

1989).

On a worldwide scale, pedogenic calcretes have characteristic $\delta^{13}C$ values ranging from -12 to +4‰ (average -4‰) and $\delta^{18}O$ values ranging from -9 to +3‰ (average -5‰, PDB) (Talma and Netterberg, 1983). From Fig. 31, it can readily be seen that the controversial calcite/opal deposits at Yucca Mountain fall within this worldwide range of carbon isotope values (but are somewhat lower than the average of -4‰), but do not fall within the pedogenic range in oxygen isotope values (except for only one of the Trench 14 samples, four of the Busted Butte samples, and the Trench 8 and Pull Apart fault samples). Also, according to Talma and Netterberg (1983), in arid climates (annual rainfall <250 mm) $\delta^{13}C$ values of less than -6‰ were rare (only two out of 90 samples) and $\delta^{18}O$ values of less than -5‰ did not occur at all. Therefore it would appear that the calcite/opal deposits at Yucca Mountain are anomalous with respect to other known pedogenic calcretes around the world. In contrast, Talma and Netterberg (1983) found that groundwater calcretes exhibited more consistent isotopic contents and had lower $\delta^{13}C$ values than pedogenic calcretes from the same region.

A study of soils in south-central New Mexico has revealed $\delta^{18}O$ values consistent with those in the worldwide study of Talma and Netterberg (1983). Monger (1993) reported $\delta^{18}O$ values between -7 to -2‰ for samples ranging in age from approximately 0.1-40 Ka (Fig. 34). However, Amundson et al. (1989) measured $\delta^{18}O$ values of calcretes at Kyle Canyon, Nevada, and found a range from approximately -

1.5 to -13.5‰ for elevations varying from ~800 to 2200 m (Fig. 31). It is not known why the Kyle Canyon samples are isotopically lighter than other reported pedogenic samples; perhaps these were collected at a higher elevation than the other samples.

LEAD ISOTOPES

Lead isotope studies have been performed on the calcite/opal veins and calcretes at Trench 14 and Busted Butte by Zartman and Kwak (1991, 1993). Lead contained in the silicate (opal) fraction of these deposits has an isotopic composition of $^{206}Pb/^{204}Pb$ = 18.09 - 18.84, and a $^{208}Pb/^{204}Pb$ = 38.51 - 39.16, whereas the carbonate (calcite) fraction has a isotopic composition of $^{206}Pb/^{204}Pb$ = 18.11 - 18.24 and $^{208}Pb/^{204}Pb$ = 38.70 - 39.15.

These investigations have identified two sources of lead in the calcite/opal deposits at Yucca Mountain. The lead component dominating the silicate phase was derived mainly from volcanic rocks which have a similar lead isotope composition as the calcite/opal deposits. The lead component dominating the carbonate phase has a variable isotopic composition which generally has higher $^{206}Pb/^{204}Pb$ values than the volcanic rock, but which has similar $^{208}Pb/^{204}Pb$ to the volcanic rocks and silicate phases. This carbonate component was considered by Zartman and Kwak (1993, p. 1953) to derive from Paleozoic and Precambrian rocks which "contain lead with an isotopic composition strongly suggesting them to be a major source of lead

at Trench 14 in the carbonate phase of carbonate-silica veins and nearby surficial calcrete deposits." Zartman and Kwak (1991) speculated that eolian dust derived from Paleozoic and Later Proterozoic marine carbonate rocks exposed in surrounding mountains provided the best explanation for the "pedogenic" carbonate and its contained lead, but Zartman and Kwak (1993, p. 1957-58) were not so sure of the eolian contribution: "Although we had hoped that the samples of eolian dust would reveal an isotopically intermediate step in the pedogenic processes leading to the formation of calcretes and vein deposits, their relatively high lead contents and isotopic homogeneity defy obvious interpretations." Nevertheless, these authors stuck to the position that (p. 1958): "the Trench 14 shallow vein system and adjacent calcretes can be satisfactorily accounted for by a continuing influx of windblown particulate matter derived from the erosion of surrounding marine carbonate rock (Paleozoic and Precambrian)....neither carbonate nor silica transport by an ascending fluid is required to explain the Trench 14 carbonate-silica veins."

Despite this conclusion, the calcite/opal vein and calcrete system can <u>also</u> be satisfactorily accounted for by a hypogene model where solutions equilibriated with Paleozoic, Tertiary, and Precambrian rock. As stated by Zartman and Kwak (1993), the too-low Th/U for marine carbonate rocks can be easily reconciled by the inclusion of some lead derived from clastic sedimentary rocks or igneous and metamorphic crystalline rocks in the carbonate fraction -- i.e., a lead source from

Precambrian rock, exactly the same conclusion as indicated by the Sr- isotope data. In addition, preliminary results by Zartman and Kwak (unpublished data, 1992, cited in Zartman and Kwak, 1993) obtained on secondary carbonate from core samples reveal that a lead isotopic behavior similar to that observed for surface calcrete samples extends downward through the unsaturated zone to near the present water table (~500 m in depth). This observation is again analogous to the strontium isotope data -- that the isotopic composition of lead and strontium in the surface calcite/opal deposits continues down into the unsaturated zone.

Therefore, the same questions as posed for the Sr- isotope isotope data can be posed for the Pb- isotope data:

1. Does it make sense that a small wind-blow dust fraction (which should create "true" pedogenic horizons not more than a meter or so thick) should extend its influence down to ~500 m in the subsurface?

2. If the strontium isotope data preclude an entirely eolian dust source of calcium and strontium for the calcite/opal deposits (see discussion on strontium isotopes and source of calcium), and instead favor an involvement of the Precambrian basement by ascending water, then why should the lead isotope data be interpreted any differently?

It is our interpretation that the Paleozoic and Precambrian rocks contain lead with an isotopic composition that strongly suggests that they are a major source of lead to the calcite/opal deposits at Yucca Mountain, because they are the source of this lead -- not indirectly through eolian dust but directly by ascending water from the basement.

URANIUM ISOTOPES

Uranium isotopic studies have been done in order to: (1) date the micritic veins and affiliated calcretes by the U-series disequilibrium method, and (2) determine the $^{234}U/^{238}U$ ratios (activity ratios) of the veins and calcretes. Each of these are important to understanding the origin of the calcite/opal deposits at Yucca Mountain.

$^{234}U/^{238}U$ ratios

The isotopic character of uranium incorporated in various calcareous deposits, both at Yucca Mountain and from the larger surrounding area, have been studied by Szabo et al. (1981), Szabo and O'Malley (1985), Szabo and Kyser (1985), and Winograd et al. (1985). $^{234}U/^{238}U$ ratios have been determined both for the calcite/opal deposits at Yucca Mountain and for calcite veins whose hypogene/spring origin is known with certainty.

As shown in Fig. 35, the isotopic character of uranium incorporated in the micritic veins and affiliated calcretes (the calcite/opal deposits) is characterized by values of the $^{234}U/^{238}U$ ratio ranging from 1.0 to seldom more than 1.5. These deposits at Yucca Mountain may be compared with known hypogene deposits from Devils Hole, Amargosa Basin, and Furnace Creek Wash. From Figs. 36a and 36b it is observed that the calcite/opal deposits from Yucca Mountain plot with the Furnace Creek travertine veins but not with the Devils Hole mammillary coatings or the Amargosa Basin travertine. Also note in Fig. 35 that the $^{234}U/^{238}U$ of subsurface veins at Yucca Mountain plot in nearly the same position as the Yucca Mountain surficial veins and calcretes -- that is, as for the strontium, carbon-oxygen, and lead isotopes there seems to be a connection between surficial deposits and those in the unsaturated zone.

The answer to the above trends in uranium isotopes is similar to the explanation of the oxygen isotope trends: the controversial calcite/opal deposits have been subjected to post-depositional alteration by meteoric water. It is feasible to estimate parent fluids from $^{234}U/^{238}U$ ratios, but only for deposits behaving as a closed system. For a coarse-grained (i.e., macrocrystalline) deposit submerged in a fluid saturated with respect to $CaCO_3$ (e.g., the Devils Hole and Amargosa Basin calcites) the assumption of closed system behavior seems appropriate. In this setting vulnerable ^{234}U atoms, which are contained in a previously precipitated part of a travertine vein, are shielded by continuous precipitation of $CaCO_3$.

In the vadose zone, however, the circumstances are markedly different because the carbonate deposits are exposed to open system conditions and leaching of ^{234}U residing in radiation-damaged sites within the calcite crystal lattice by downward percolating vadose moisture. Intermittent flushing by infiltrating rainwater may lead to preferential removal of ^{234}U atoms, resulting in the lowering of the actual value of the $^{234}U/^{238}U$ ratio. In terms of Fig. 36, this means that the travertine deposits exposed at Yucca Mountain and Furnace Creek have been subjected to leaching by meteoric water (the same conclusion as reached in the oxygen-isotope discussion), but that the Devils Hole and Amargosa Basin spring deposits have not been subjected to this vadose leaching since they were deposited at, or beneath, the water table. Therefore, $^{234}U/^{238}U$ values for these two sites plot higher on Fig. 36 than do the controversial calcite/opal deposits. Rather than indicating a supergene-pedogenic origin for the controversial deposits as proposed by Stuckless et al. (1991a), the $^{234}U/^{238}U$ data simply indicates the open system behavior for some of these deposits (Szymanski et al., 1993).

Harmon (1993) came to the same conclusion as Szymanski et al. (1993) based on ten samples of calcite/opal submitted for U-series analysis. A negative correlation between $^{234}U/^{238}U$ and $^{230}Th/^{234}U$ ratios and U concentrations, and $^{230}Th/^{234}U$ ratios that were too high, suggested to Harmon that some of the calcite/opal deposits at Yucca Mountain have experienced post-depositional leaching of U. Of the ten

samples analyzed, five (red dots, Fig. 37) appear to have remained closed systems to radionuclides migration since their time of deposition; the other five appear to have been subjected to variable degrees of fluid-rock interaction which leached U from the samples. For the five pristine samples, calculated $^{234}U/^{238}U$ ratios fall between 2.2 and 3.2 (Fig. 37). These values bracket the $^{234}U/^{238}U$ activity ratios of 2.5 to 3.0 for deep carbonate groundwaters that periodically supplied springs near the southern end of Crater Flat during the Late Pleistocene (Paces et al., 1993).

Uranium-series dates

A number of the calcite/opal deposits in the region of Yucca Mountain have been dated by the U-series disequilibrium technique, and these dates seem to cluster into discrete age groups (Fig. 38). Szabo and Kyser (1990) and Vaniman (1993) reported three age groupings for the deposits: at ~28 Ka, ~170 Ka, and ~280 Ka. In addition, Paces et al. (1993) identified three age groupings for the spring deposits at Site 199 and Diatomaceous Earth site: at 18±1 Ka, 30±3 Ka, and 45±4 Ka. Considering all of the dates performed on the various carbonate (but not opal) deposits in the Yucca Mountain area (see data charts of Hill and Schluter, 1994), these six groupings appear to be real, but also other groupings may exist at ~75 Ka, ~95 Ka, and ~320 Ka (Fig. 38). It is important to note in Fig. 38 that within each age-group there can exist the controversial calcite/opal deposits, known carbonate/siliceous spring deposits, and calcite found deep in the subsurface at Yucca Mountain (e.g., see the 30 Ka group).

There seems to be observable breaks between some of the age groups (Fig. 38, dashed lines), but in other groupings the breaks are more gradual (Fig. 38, no dashed lines). The more gradual breaks may be real or they may be due to the very approximate nature of some of the dates (open-ended dates designated by question marks, or dates with very large ±'s). It is important to keep in mind that the uncertainties given with a U-series age determination are the $\pm 1\sigma$ uncertainties (i.e., 67% confidence level) based upon only the counting statistics. At the $\pm 2\sigma$ level (i.e., the 99% confidence level), the stated uncertainty doubles. If the U-series age distribution is considered in this context, then there is no grouping of ages as shown in Fig. 38. The data will have to be analyzed further before these age groups can be discussed in a meaningful way.

In addition, the possibility of open-system behavior, as suggested by the oxygen isotope data and the $^{234}U/^{238}U$ ratios, has profound implications for the U-series geochronology. The basic assumption that one has to make in accepting the number that is calculated from a measurement of ^{238}U, ^{234}U, and ^{230}Th activities as a meaningful age with geological significance is that the isotopic system has remained closed with respect to the isotopic species of interest since the time of deposition. Any addition, removal, or exchange of one or more isotopic species invalidates this basic assumption and makes the calculated age meaningless. Thus, it has yet to be resolved whether the U-series age data has been significantly affected by open-system behavior.

CONCLUSIONS

A number of conclusions can be made concerning the calcite/opal deposits and hypogene-pedogenic debate at Yucca Mountain:

1. The proposed high level nuclear waste repository site at Yucca Mountain is located in a tectonically-active area of volcanism, faulting, earthquake activity, high heat flow, and thermal springs. The calcite/opal deposits should be considered in the context, and as an integral part, of this regional geologic framework.

2. The nearly universal association of the calcite/opal with faults, and the vein geometry displayed by these deposits, should be considered as evidence favoring an epithermal, hypogene origin.

3. "True" pedogenic deposits exist at Yucca Mountain, but these are not the same as the presumed "pedogenic" calcretes described by Quade and Cerling (1990) and others. "True" pedogenic deposits occur in soil horizons near, and parallel to, the surface and are composed of aggregates of silt-size particles of carbonate material intermixed with a soil matrix which displays mainly powdery or nodular textures. Presumed "pedogenic"

deposits are composed of an extremely fine-grained mixture of calcite, opal, and sepiolite which exhibit a wide range of textures not displayed by the "true" pedogenic deposits.

4. Mineralogy of the calcite/opal samples is simple: calcite, opal, sepiolite (minor), quartz (rare), pyrite/chalcopyrite (trace), and gypsum (at one locality only). The presence of high amounts of opal (sometimes pure, sometimes mixed) is considered significant because "true" pedogenic deposits at Yucca Mountain contain no opal (or only tiny shards of detrital opal).

5. Non-detrital or non-syndepositional quartz occurs in the calcite/opal deposits but is rare. Its presence is significant because this quartz has high fluid inclusion temperatures and is associated with microveinlets of pyrite and chalcopyrite. Such a high-temperature mineral association definitely suggests an origin related to an epithermal environment.

6. A review of the literature on sepiolite in the Basin and Range Province (including sites near Yucca Mountain) reveal that sepiolite in this setting is usually a low-temperature, hydrothermal (epithermal) mineral that occurs along faults. Since the sepiolite at Yucca Mountain occurs intimately intermixed with the calcite/opal along fault zones, it implies that the calcite/opal is also epithermal.

7. Fluid inclusions in non-detrital, non-syndepositional, surficial quartz and in fracture-filling, subsurface calcite have high fluid inclusion temperatures. These high temperatures imply that the calcite/opal hosting these minerals is not "pedogenic" as has been presumed.

8. Trace element analyses and correlations indicate that while the calcite/opal deposits at Yucca Mountain are not significantly enriched in metal, they can contain anomalous amounts of As, Au, Ba, Br, Co, Ni, Sb, U, W, Zn and other elements. These enrichments at various locations around Yucca Mountain favor an epithermal origin for the calcite/opal deposits. Similar elemental enrichment for controversial sites (e.g., Trench 14) and known spring sites (e.g., Site 199) implies a common mechanism (i.e., a hypogene, epithermal, spring origin) for all of the calcite/opal deposits at Yucca Mountain.

9. Petrographic textures of the calcite/opal deposits are diverse, widespread, and independent of location and rock type. These various textural types are critical indicators of origin because they do not match the textures of "true" pedogenic deposits at Yucca Mountain, and because the various types and heterogeneity of textures (even within centimeters of each other) favor a dynamic fluid system. For example, it cannot be visualized how flow texture,

vesicular texture, and invasive texture could have been caused by pedogenic processes.

10. The strontium isotopic data does not "preclude" the precipitation of the calcite/opal from ascending water; rather, this data indicates that water ascending from the Precambrian basement is the only reasonable source of the high Sr-isotope ratios in the calcite/opal. Other partial sources of strontium for these deposits could be Paleozoic carbonate rock, Tertiary volcanic rock, and eolian dust. Strontium supplied by eolian dust may represent a pedogenic end-member component in an otherwise hypogene-derived system.

11. All of the calcite/opal deposits fall within a fairly narrow range of C-, O-, and Sr-isotopic compositions which suggests that all of the calcite/opal in the Yucca Mountain region came from the same source. The narrow range of carbon-oxygen isotope values favors a hypogene groundwater origin over a surface pedogenic origin for the calcite/opal deposits because the formation of soil calcretes is strongly dependent on evaporation. This evaporation should produce a much larger amount of stable isotope variation than that exhibited by the calcite/opal deposits.

12. The similarity in C-, O-, and Sr-isotope values of the calcite/opal at WT-7,

Bare Mountain, and New Trench with those at Trench 14 suggests that all of these deposits have the same origin. Since the WT-7 calcite/opal was found to have the mineral association quartz/pyrite/chalcopyrite, since the Bare Mountain calcite/opal is in the Bare Mountain Mining District, and since the New Trench calcite/opal has relatively-high zinc concentrations (90 ppm), this implies that all four have the same epithermal origin. The similarity in Sr-isotope values of the calcite/opal at Pull Apart fault with those at Trench 14 suggests an epithermal origin for both of these sites, since the Pull Apart deposits have high fluid inclusion temperatures and trace metal enrichments, and the similarity in carbon-oxygen isotope values of the Wahmonie travertine/gypsite spring mound to the calcite/opal at Trench 14 implies a hypogene, spring origin for both of these sites. From these various isotopic connections, it is deduced that the Trench 14 calcite/opal is most likely of epithermal, hypogene origin.

13. Preliminary O-isotope investigations of carbonate-opal pairs indicates a possible epithermal (~50-60°C) origin for at least some of the calcite/opal deposits in the Yucca Mountain region.

14. Oxygen isotopes and $^{234}U/^{238}U$ ratios indicate that some of the surficial calcite/opal deposits have probably undergone at least some leaching by,

and isotopic exchange with, meteoric water (i.e., these deposits have been exposed to open system conditions). It has yet to be determined how such an open system has affected the U-series systematics.

15. The U-series dates seem to cluster in at least six (and maybe nine) groups, but these groupings need to be further analyzed to see if they are "real."

16. The lead isotope data suggests that Paleozoic and Precambrian rocks are a major source of lead to the calcite/opal deposits at Yucca Mountain and does not rule out an origin by ascending water.

17. The most important conclusion of this report is that a number of lines of evidence, consisting of geologically independent data, all point to the same internally consistent interpretation: the controversial calcite/opal deposits at Yucca Mountain are of hypogene origin.

ACKNOWLEDGEMENTS

Strontium isotope analyses were made by thermal ionization mass spectrometry in the laboratory of Professor S. Moorbath, Oxford University, United Kingdom; carbon-oxygen isotope analyses were made by gas-source mass spectrometry in the stable isotope laboratory of Professor Dr. J. Hoefs, University of Göttingen, Germany; U-series dates were made by alpha spectrometry in the laboratory of Professor D. C.

Ford, McMaster University, Canada; fluid inclusion studies were conducted by Dr. D. M. H. Alderton, University of London, United Kingdom; Instrumental Neutron Activation Analyses were performed by Drs. Y. G. Liu and R. A. Schmitt, Oregon State University, USA; and trace element analyses were performed by Chemex Laboratory, Reno, Nevada, USA. Funding for this project was received from the Nuclear Waste Project Office, State of Nevada.

REFERENCES

Amundson, R. G., Chadwick, O. A., Sowers, J. M., and Doner, H. E., 1989, *The Stable Isotope Chemistry of Pedogenic Carbonates at Kyle Canyon, Nevada:* Soil Science Society of America, Journal, v. 53, pp. 201-210.

Bachman, G. O., and Machette, M. N., 1977, *Calcic Soils and Calcretes in the Southwestern United States:* U. S. Geological Survey, Open File Report 77-794, 163 pp.

Berger, B. R., and Eimon, P., 1982, *Comparative Models of Epithermal Gold-Silver Deposits*: Society of Mining Engineers, Reprint 82-13, 25 pp.

Birkeland, P. W., 1984, *Soils and Geomorphology:* Oxford University Press, New York, 372 pp.

Bish, D. L., 1989, *Evaluation of Past and Future Alterations in Tuff at Yucca Mountain, Nevada, Based on the Clay Mineralogy of Drill Cores USW G-1, G-2, and G-3*, Los Alamos National Laboratories, Report LA-10667-MS, 40 pp.

Bish, D. L., and Aronson, J. L., 1993, *Paleogeothermal and Paleohydrologic Conditions in Silicic Tuff from Yucca Mountain, Nevada*: Clays and Clay Minerals, v. 41, no. 2, pp. 148-161.

Boutton, T. W., 1991, *Stable Carbon Isotope Ratios of Natural Materials: II. Atmospheric, Terrestiral, Marine, and Freshwater Environments; in Coleman, D., and Fry, B, eds., Carbon Isotope Techniques:* Academic Press, New York, pp. 173-186.

Brogan, G. E., Kellogg, K. S., Slemmons, D. B., and Terhune, C. L., 1991, *Late Quaternary Faulting Along the Death Valley-Furnace Creek Fault System, California and Nevada:* U. S. Geological Survey, Bulletin no. 1991, 23 pp.

Bull, W. B., 1991, *Geomorphic Responses to Climate Change:* Oxford University Press, New York, 326 pp.

Caporuscio, F., Vaniman, D., Bish, D., Broxton, D., Arney, B., Heiken, G.,Byers, F., Gooley, R., and Semarge, E., 1982, *Petrologic Studies of Drill Cores USW G-2 and UE25b-1H, Yucca Mountain, Nevada:* Los Alamos National Laboratory, Report LA-9255-MS, 111 pp.

Castor, S. B., Feldman, S. C., and Tingley, J. V., 1989, *Mineral Evaluation of the Yucca Mountain Addition, Nye County, Nevada:* Nevada Bureau of Mines and Geology-Desert Research Institute, Reno, Nevada, 80 pp + appendix.

Castor, S. B., Tingley, J. V., and Bonham, H. F., 1992, *Subsurface Mineral Resource Analysis, Yucca Mountain, Nevada, Preliminary Report 1; Lithologic Logs:* Nevada Bureau of Mines and Geology, Open File Report 92-4, 11 pp + appendices.

Cerling, T. E., 1984, *The Stable Isotopic Composition of Modern Soil Carbonate and Its Relationship to Climate:* Earth and Planetary Science Letters, v. 71, pp. 229-240.

Chitale, J. D., 1986, *Study of Petrography and Internal Structures in Calcretes of West Texas and New Mexico:* Unpublished PhD dissertation, Texas Tech University, Lubbock, Texas, 107 pp.

Cornwall, H. R., and Kleinhampl, F. J., 1961, *Geologic Map of the Bare Mountain Quadrangle, Nevada:* U. S. Geological Survey, Map GQ-157, scale 1:62,500.

Dansgaard, W., 1964, *Stable Isotopes in Precipitation:* Tellus, v. 16, pp. 436-468.

DOE, 1993, *Report on the Origin of Calcite-Silica Deposits at Trench 14 and Busted Butte and Methodologies Used to Determine Their Origin:* U. S. Department of Energy, Yucca Mountain site characterization project, Report YMP193-11-R, 64 pp + references + glossary + appendices.

Dixon, J. B., and Weed, S. B., 1989, *Minerals in Soil Environments:* Soil Science of America, Madison, Wisconsin, 1244 pp.

Ehlmann, A. J., Sand, L. B., and Regis, A. J., 1962, *Occurrences of Sepiolite in Utah and Nevada:* Economic Geology, v. 57, pp. 1085-1094.

Faure, G., 1986, *Principles of Isotope Geology:* John Wiley and Sons, New York, 464 pp.

Gile, L H., 1961, *A Classification of Ca Horizons in Soils of a Desert Region, Dona Ana County, New Mexico:* Soil Science Society of America, Proceedings, v. 25, no. 1, pp. 52-61.

Gile, L. H., and Grossman, R. B., 1979, *The Desert Project Soil Monograph, Document PB80-13504*, National Technical Information Service, Springfield, Virginia, 984 pp.

Gile, L. H., Peterson, F. F., and Grossman, R. B., 1965, *The K Horizon: A Master Soil Horizon of Carbonate Accumulation:* Soil Science, v. 99, no. 2, pp. 74-82.

Gile, L. H., Peterson, F. F., and Grossman, R. B., 1966, *Morphological and Genetic Sequences of Carbonate Accumulation in Desert Soils:* Soil Science, v. 101, no. 5, pp. 347-360.

Gile, L. H., Hawley, J. W., and Grossman, R. B., 1981, *Soils and Geomorphology in the Basin and Range Area of Southern New Mexico: Guidebook to the Desert Project:* New Mexico Bureau of Mines and Mineral Resources, Memoir 39, 222 p.

Goff, F., Wollenberg, H. A., Brookins, D. C., and Kistler, R. W., 1991, *A Sr-Isotopic Comparison Between Thermal Waters, Rocks, and Hydrothermal Calcites, Long Valley Caldera, California:* Journal of Volcanology and Geothermal Research, v. 48, pp. 165-281.

Goudie, A., 1973, *Duricrusts in Tropical and Subtropical Landscapes:* Clarendon Press, Oxford, 174 pp.

Graaff, W. J., 1983, *Silcrete in Western Australia: Geomorphological Settings, Textures, Structures, and Their Genetic Implications*; *in Wilson, R. C., ed., Residual Deposits: Surface Related Weathering Processes and Materials:* Geological Society of London, Oxford, pp. 159-166.

Harmon, R. S., 1993, *Isotopic and Fluid Inclusion Study of Yucca Mountain Samples: Quarterly Report No. 6*, submitted to the Nuclear Waste Project Office, State of Nevada, 38 pp.

Hay, R. L., Pexton, R. E., Teague, T. T., and Kyser, T. K., 1986, *Spring-Related Carbonate Rocks, Mg Clays, and Associated Minerals in Pliocene Deposits of the Amargosa Desert, Nevada and California:* Geological Society of America, Bulletin, v. 97, pp. 1488-1503.

Hays, P. D., and Grossman, E. L., 1991, *Oxygen Isotopes in Meteoric Calcite Cements as Indicators of Continental Paleoclimate:* Geology, v. 19, pp. 441-444.

Hill, C. A., 1993a, *Field Trip Report: Observations Made at Yucca Mountain, Nye County, Nevada: Special Report No. 2*, submitted to the Nuclear Waste Project Office, State of Nevada, March, 30 pp.

Hill, C. A., 1993b, *The Origin of Sepiolite, Yucca Mountain, Nevada: Special Report No. 6*, submitted to the Nuclear Waste Project Office, State of Nevda, June, 12 pp.

Hill, C. A., and Livingston, D. E., 1993, *Chemical Analyses of Rocks, Minerals, and Detritus, Yucca Mountain -- Preliminary Report: Special Report No. 11*, submitted to the Nuclear Waste Project Office, State of Nevada, September, 24 pp.

Hill, C. A., and Schluter, C. M., 1993, *Petrographic Description of Calcite/Opal Samples Collected on Field Trip of December 5-9, 1992: Special Report No. 7*, submitted to the Nuclear Waste Project Office, State of Nevada, June, 20 pp.

Hill, C. A., and Schluter, C. M., 1994, *Data Chart, Yucca Mountain and Vicinity: Report* submitted to the Nuclear Waste Project Office, State of Nevada, January, 38 pp.

Hill, C. A., Schluter, C. M., and Monger, H. C., 1993, *Criteria for the Recognition of Pedogenic/Supergene and Nonpedogenic/Hypogene Deposits and Their Relationship to the Origin of Calcite/Opal Deposits at Yucca Mountain: Special Report No. 14*, submitted to the Nuclear Waste Project Office, State of Nevada, October, 37 pp.

Hoffman, R. J., 1988, *Chronology of Diving Activities and Underground Surveys in Devils Hole and Devils Hole Cave, Nye County, Nevada, 1950-1986*: U. S. Geological Survey, Open File Report 88-93, 12 pp.

Horton, R. C., 1964, *Hot Springs, Sinter Deposits, and Volcanic Cinder Cones in Nevada:* Nevada Bureau of Mines, Map 25, scale 1:1,000,000.

Ingraham, N. L., Jacobson, R. L., Hess, J. W., and Lyles, B. F., 1990, *Stable Isotopic Study of Precipitation and Spring Discharge on the Nevada Test Site:* Department of Energy, Report DOE/NV10845-03, 55 pp.

Johnson, T. M., and DePaolo, D. J., 1993, *Interpretation of Sr Isotope Data from Yucca Mountain: Modeling the Effects of Water-Rock Interaction:* Lawrence Berkeley Laboratory, University of California, LBL-33000, UC-403, pp. 18-20.

Jones, B. F., 1983, *Occurrence of Clay Minerals in Surficial Deposits of Southwest Nevada*; in Nahon, D., ed., Colloquie Nationale Research Sciences: Colloquium on Petrology of Weathering and Soils, Paris, 13 pp.

Kelly, E. F., Amundson, R. G., Marino, B. D., and DeNiro, M. J., 1991, *Stable Carbon Isotopic Composition of Carbonate in Holocene Grassland Soils:* Soil Science Society of America, Journal, v. 55, pp. 1651-1658.

Knauss, K. G., 1981, *Dating Fault-Associated Quaternary Material from the Nevada Test Site Using Uranium-Series Methods:* Lawrence Livermore Laboratories, University of California, Report UCRL-53231, 51 pp.

Krauskopf, K. B., 1967, *Introduction to Geochemistry:* McGraw-Hill, New York, 721 pp.

Lattman, L. H., 1973, *Calcium Carbonate Cementation of Alluvial Fans in Southern Nevada:* Geological Society of America, Bulletin, v. 84, pp. 3013-3028.

Laul, J. C., and Schmitt, R. A., 1973, *Chemical Composition of Luna-20 Rocks and Soil and Apollo 16 Soils:* Geochemica Cosmochemica Acta, v. 37, pp. 927-942.

Levy, S. S., 1991, *Mineralogic Alteration History and Paleohydrology at Yucca Mountain, Nevada:* High Level Radioactive Waste Management Conference, Proceedings, April 28-May 3, Las Vegas, Nevada, pp. 477-485.

Levy, S. S., and Naeser, C. W., 1991, *Bedrock Breccias Along Fault Zone Near Yucca Mountain, Nevada,* Draft report submitted for publication by the U. S. Geological Survey-Los Alamos National Laboratories, 25 pp.

Liu, Y.-G., and Schmitt, R. A., 1990, *Cerium Anomolies in Western Indian Ocean Cenozoic Carbonates, Leg 105;* in Duncan, R. A., et al., eds., Proceedings of the Ocean Drilling Program: Scientific Results, v. 115, pp. 709-714.

Ludwig, K. R., Peterman, Z. E., Simmons, K. R., and Gutentag, E. D., 1993, *$^{234}U/^{238}U$ as Ground-Water Tracer, Southwest Nevada-Southeast California:* International High Level Radioctive Waste Management Conference, Proceedings, April 26-30, Las Vegas, Nevada, pp. 1567-1572.

Machette, M. N., 1985, *Calcic Soils of the Southwestern United States; in Weide, D. L., Soils and Quaternary Geology of the Southwestern United States:* Geological Society of America, Special Paper 203, pp. 1-21.

Mack, G. H., Cole, D. R., Giordano, T. H., Schaal, W. C., and Barcelos, J. H., 1991, *Paleoclimatic Controls on Stable Oxygen and Carbon Isotopes in Caliche of the Abo Formation (Permian), South-Central New Mexico, USA:* Journal of Sedimentary Petrology, v. 61, pp. 458-472.

Marshall, B. D., and Mahan, S., 1991, *A Model for the Formation of Pedogenic Carbonate Based on Strontium Isotope Data from Southwest Nevada (abstract):* Geological Society of America, Abstracts with Programs, v. 23, p. A118.

Marshall, B. D., Peterman, Z. E., Futa, K., Stuckless, J. S., Mahan, S. A., Downey, J. S., and Gutentag, E. D., 1990, *Origin of Carbonate Deposits in the Vicinity of Yucca Mountain, Nevada: Preliminary Results of Strontium-Isotope Analyses:* International High Level Radioactive Waste Management Conference, Proceedings, April 8-12, Las Vegas, Nevada, pp. 921-923.

Marshall, B. C., Peterman, Z. E., Futa, K., and Stuckless, J. S., 1991, *Strontium Isotopes in Carbonate Deposits at Crater Flat, Nevada:* International High Level Radioactive Waste Mangagment Conference, Proceedings, April 28-May3, Las Vegas, Nevada, pp. 1423-1428.

Marshall, B. D., Peterman, Z. E., and Stuckless, J. E., 1993, *Strontium Isotopic Evidence for a Higher Water Table at Yucca Mountain:* International High Level Radioactive Waste Management Conference, Proceedings, April 26-30, Las Vegas, Nevada, pp. 1948-1951.

McFadden, L. D., Wells, S. G., and Jercinovich, M. J., 1987, *Influence of Eolian Pedogenic Processes on the Origin and Evolution of Desert Pavement:* Geology, v. 15, pp. 504-508.

McGrath, D. A., 1984, *Morphological and Mineralogical Characteristics of Indurated Caliches of the Llano Estacado:* Unpublished MS thesis, Texas Tech University, Lubbock, Texas, 210 pp.

Milne, W. K., Benson, L. V., and McKinley, P. W., 1987, *Isotope Content and Temperature of Precipitation in Southern Nevada,* August 1983-August 1986: U.S. Geological Survey, Open File Report 87-463, 32 pp.

Monger, H. C., 1993, *Soil-Geomorphic and Paleoclimatic Characteristics of the Fort Bliss Maneuver Areas, Southern New Mexico and Western Texas: Historic and Natural Resources Report No. 10,* Environmental Management Office, Fort Bliss, Texas, in press.

NAS/NRC, 1992. *Ground Water at Yucca Mountain How High Can It Rise?,* Final Report of the Panel on Coupled Hydrologic/Tectonic/Hydrothermal Systems at Yucca Mountain, National Research Council, National Academy Press, Washington, D.C., 148 pp + appendices.

Paces, J. B., Taylor, E. M., and Bush, C., 1993, *Late Quaternary History and Uranium Isotopic Compositions of Ground Water Discharge Deposits, Crater Flat, Nevada:* International High Level Radioactive Waste Management Conference, Proceedings, April 26-30, Las Vegas, Nevada, pp. 1573-1580.

Peterman, Z. E., and Stuckless, J. S., 1993, *Isotopic Evidence of Complex Ground-Water Flow at Yucca Mountain, Nevada, USA:* International High Level Waste Management Conference, Proceedings, April 26-30, Las Vegas, Nevada, v. 2, pp. 1559-1566.

Peterman, Z. E., Stuckless, J. S., Mahan, S., Gutentag, E. D., and Downey, J. S., 1991, *Strontium Isotope Characterization of Ground-Water Flow Systems in Southern Nevada (abstract):* Geological Society of America, Abstracts with Programs, v. 23, p. A117.

Peterman, Z. E., Stuckless, J. S., Marshall, B. D., Mahan, S. A., and Futa, K., 1992, *Strontium Isotope Geochemistry of Calcite Fracture Fillings in Deep Core, Yucca Mountain, Nevada -- A Progress Report:* International High Level Radioactive Waste Management Conference, Proceedings, April 12-16, Las Vegas, Nevada, pp. 1582-1586.

Peterman, Z. E., Spengler, R. W., Singer, F. R., and Dickerson, R. P., 1993, *Isotopic and Trace Element Variability in Altered and Unaltered Tuffs at Yucca Mountain, Nevada:* International High Level Radioactive Waste Management Conference, Proceedings, April 26-30, Las Vegas, Nevada, pp. 1940-1947.

Post, J. L., 1978, *Sepiolite Deposits of the Las Vegas, Nevada Area:* Clays and Clay Minerals, v. 26, no. 1, pp. 58-64.

Quade, J., and Cerling, T. E., 1990, *Stable Isotopic Evidence for a Pedogenic Origin of Carbonates in Trench 14 Near Yucca Mountain, Nevada: Science,* v. 250, pp. 1549-1552.

Quade, J., Cerling, T. E., and Bowman, J. R., 1989, *Systematic Variations in Carbon and Oxygen Isotopic Composition of Pedogenic Carbonate Along Elevation Transects in the Southern Great Basin, United States:* Geological Society of America, Bulletin, v. 101, pp. 464-475.

Quade, J., and Tingley, J. V., 1983, *A Mineral Inventory of the Nevada Test Site and Portions of Nellis Bombing and Gunnery Range, Southern Nye County, Nevada:* Nevada Bureau of Mines, Report DOE/NV/10295-1, Reno, Nevada, pp. 31-34.

Reeves, C. C., 1976, *Caliche: Origin, Classification, Morphology and Uses:* Estacado Books, Lubbock, Texas, 233 pp.

Regis, A. J., 1978, *Mineralogy, Physical and Exchangeable Chemistry Properties of Bentonites from the Western United States, Exclusive of Montana and Wyoming:* U. S. Bureau of Land Management, Technical note, v. 315, 35 pp.

Reheis, M. C., 1986, *Preliminary Study of Quaternary Faulting on the East Side of Bare Mountain, Nye County, Nevada:* U. S. Geological Survey, Open File Report 86-576, 14 pp.

Rozanski, K., Araguas-Araguas, L., and Gonfiantini, R., 1992, *Relation Between Long-Term Trends of Oxygen-18 Isotope Composition of Precipitation and Climate:* Science, v. 258, pp. 981-985.

Schlesinger, W. H., Marino, G. M., and Fonteyn, P. J., 1989, *Stable Isotope Ratios and the Dynamics of Caliche in Desert Soils;* in Rundel, P. W., et al., eds., Ecological studies volume 68: Stable isotopes in ecological research, Springer-Verlag, New York, pp. 309-317.

Schmitt, R. A., 1993, Technical Report, Radiation Center Project no. 926; in Livingston, D. E., *Trace Element and REE Compostion of Five Samples of the Yucca Mountain Calcite/Silica Deposits:* Special Report no. 8, submitted to the Nuclear Waste Project Office, State of Nevada, 18 pp.

Seager, W. R., 1981, *The Geology of the Organ Mountains and Southern San Andres Mountains, New Mexico:* New Mexico Bureau of Mines and Mineral Resources, Memoir 39, 97 pp.

Simonds, F. W., 1980, *Geology and Hydrothermal Alteration in the Calico Hills, Southern Nevada:* Unpublished MS thesis, University of Colorado, 103 pp.

Soil Science of America, 1987, *Glossary of Soil Science Terms:* Soil Science of America, Madison, Wisconsin, 44 pp.

Sowers, J. M., 1985, *Pedogenic Calcretes of Kyle Canyon Alluvial Fan, Southern Nevada: Morphology and Development:* Unpublished PhD dissertation, University of California, Berkeley, 160 pp.

Sowers, J. M., et al., 1988, *Geomorphology and Pedology on the Kyle Canyon Alluvial Fan, Southern Nevada;* in Weide, D. L., and Faber, M. L., eds., This extended land, geological journeys in the southern Basin and Range: Geological Society of America, Cordilleran Section Meeting, Field Trip Guidebook, Las Vegas, Nevada, pp. 137-157.

Spengler, R. W., and Peterman, Z. E., 1991, *Distribution of Rubidium, Strontium, and Zirconium in Tuff from Two Deep Coreholes at Yucca Mountain, Nevada:* International High Level Radioactive Waste Management Conference, Proceedings, April 28-May 3, Las Vegas, Nevada, pp. 1416-1422.

Stuckless, J. S., 1991, *An Evaluation of Evidence Pertaining to the Origin of Vein Deposits Exposed in Trench 14, Nevada Test Site, Nevada:* International High Level Radioactive Waste Management Conference, Proceedings, April 28-May 3, Las Vegas, Nevada, pp. 1429-1438.

Stuckless, J. S., Peterman, Z. E., and Muhs, D. R., 1991a, *U and Sr Isotopes in Ground Water and Calcite, Yucca Mountain, Nevada: Evidence Against Upwelling Water:* Science, v. 254, pp. 551-554.

Stuckless, J. S., Peterman, Z. E., Whelan, J. F., and Muhs, D. R., 1991b, *Isotopic Evidence for a Per Descensum Origin for Hydrogenic Veins in Faults Near Yucca Mountain, Nevada (abstract):* Geological Society of America, Abstracts with Programs, v. 23, p. A118.

Stuckless, J. S., Peterman, Z. E., Forester, R. L., Whelan, J. F., Vaniman, D. T., Marshall, B. D., and Taylor, E. M., 1992, *Characterization of Fault-Filling Deposits in the Vicinity of Yucca Mountain, Nevada:* Rough Draft, Proceedings of Waste Management /92, to be held in Tucson, Arizona, March 1-5, 1992.

Swadley, W. C., and Carr, W. J., 1987, *Geologic Map of the Quaternary and Tertiary Deposits of the Big Dune Quadrangle, Nye County, Nevada, and Inyo County, California:* U. S. Geological Survey, Miscellaneous Investigations Map I-1767, scale 1:48,000.

Szabo, B. J., and Kyser, T. K., 1985, *Uranium, Thorium Isotopic Analyses and Uranium-Series Ages of Calcite and Opal, and Stable Isotopic Compositions of Calcite from Drill Cores UE25a#1, USW G-2 and USW G-3/GU-3, Yucca Mountain, Nevada:* U. S. Geological Survey, Open File Report 85-224, 25 pp.

Szabo, B. J., and Kyser, T. K., 1990, Ages and Stable-Isotope *Compositions of Secondary Calcite and Opal in Drill Cores from Tertiary Volcanic Rocks of the Yucca Mountain Area, Nevada:* Geological Society of America, Bulletin, v. 102, pp. 1714-1719.

Szabo, B. J., and O'Malley, P. A., 1985, *Uranium-Series Dating of Secondary Carbonate and Silica Precipitates Relating to Fault Movements in the Nevada Test Site Region and of Caliche and Travertine Samples from the Amargosa Desert:* U. S. Geological Survey, Open File Report 85-47, 12 pp.

Szabo, B. J., Carr, W. J., and Gottschall, W. C., 1981, *Uranium-Thorium Dating of Quaternary Carbonate Accumulations in the Nevada Test Site Region, Southern Nevada:* U. S. Geological Survey, Open File Report 81-119, 35 pp.

Szymanski, J. S., Schluter, C. M., Livingston, D. E., Somerville, M. K., and Davis, J. B., 1993, *Investigations of Natural Groundwater Hazards at the Proposed Yucca Mountain High Level Nuclear Waste Repository: Part A, Geology at Yucca Mountain,* submitted to the Nuclear Waste Project Office, State of Nevada, May, 81 pp.

Talma, A. S., and Netterberg, F., 1983, *Stable Isotope Abundances in Calcretes;* in Wilson, R. C., ed., Residual deposits: surface related weathering processes and materials: Geological Society of London, Oxford, pp. 221-233.

Tingley, J. V., 1984, *Trace Element Associations in Mineral Deposits, Bare Mountain (fluorine) Mining District, Southern Nye County, Nevada:* Nevada Bureau of Mines and Geology, Report 39, 28 pp.

Turrin, B. D., and Champion, D. E., 1991, *40Ar/39Ar Lasar Fusion and K-Ar Ages from Lathrop Wells, Nevada and Cima, California: The Age of the Latest Volcanic Activity in the Yucca Mountain Area:* High Level Radioactive Waste Management Conference, Proceedings, America Nuclear Society, La Grange Park, Illinois, pp. 68-75.

Vaniman, D. T., 1993, *Calcite Deposits in Fractures at Yucca Mountain, Nevada:* International High Level Radioactive Waste Management Conference, Proceedings, April 26-30, Las Vegas, Nevada, pp. 1935-1939.

Vaniman, D. T., Bish, D. L., and Chipera, S., 1988, *A Preliminary Comparison of Mineral Deposits in Faults Near Yucca Mountain, Nevada,* with possible Analogs: Los Alamos National Laboratories, Report LA-11289-MS, 54 pp.

Wang, Y., Cerling, T. E., Smith, G. A., Quade, J., Lindsay, E. H., and Bowman, J. R., 1993, *Stable Isotopes of Paleosols and Fossil Teeth as Paleoecology and Paleoclimate Indicators:* an example from the St. David Formation, Arizona; in Swart, P. K., et al., eds., Climate change in continental isotopic records: Geophysical Mongraph Series, v. 78, pp. 241-248.

Weiss, S. E., Noble, D. C., and Larson, L. T., 1992, Task 3: *Evaluation of Mineral Resource Potential, Caldera Geology, and Volcano-Tectonic Framework at and Near Yucca Mountain:* report for October, 1991-September, 1992: Center for Neotectonic Studies, University of Nevada-Reno, 44 pp.

Weiss, S. I., Noble, D. C., and Larson, L. T., 1993, Task 3: *Evaluation of Mineral Resource Potential, Caldera Geology, and Volcano-Tectonic Framework at and Near Yucca Mountain:* report for October 1992-September 1993: Center for Neotectonic Studies, University of Nevada-Reno, 41 pp.

Wells, S. G., McFadden, L. D., Renault, C. E., and Crowe, B. M., 1990, *Geomorphic Assessment of Late Quaternary Volcanism in the Yucca Mountain Area, Southern Nevada:* implications for the proposed high-level radioactive waste repository: Geology, v. 18, pp. 549-553.

Whelan, J. F., and Stuckless, J. S., 1991, *The $\delta^{18}C$ and $\delta^{18}O$ Values of Epigenetic Calcite within Yucca Mountain, Nevada:* paleohydrologic implications (abstract): Geological Society of America, Abstracts with Programs, v. 23, p. A117.

Whelan, J. F., and Stuckless, J. S., 1992, *Paleohydrologic Implications of the Stable Isotopic Composition of Secondary Calcite within the Tertiary Volcanic Rocks of Yucca Mountain, Nevada*; High Level Radioactive Waste Management Proceedings, American Nuclear Society, La Grange Park, Illinois, pp. 1572-1581.

Whitney, J. W., and Muhs, D. R., 1991, *Quaternary Movement on the Paintbrush Canyon-Stagecoach Road Fault System, Yucca Mountain, Nevada (abstract):* Geological Society of America, Abstracts with Programs, v. 23, p. A119.

Winograd, I. J., and Pearson, F. J., 1976, *Major Carbon-14 Anomaly in a Regional Carbonate Aquifer: Possible Evidence for Megascale Channelling, South Central Great Basin:* Water Resources Research, v. 12, no. 6, pp. 1125-1143.

Winograd, I. J., Szabo, B. J., Coplen, T. B., Riggs, A. C., and Kolesar, P. T., 1985, *Two-Million-Year Record of Deuterium Depletion in Great Basin Ground Waters:* Science, v. 227, pp. 519-522.

Zartman, R. E., and Kwak, L. M., 1991, *Lead Isotopes in the Carbonate-Silica Veins of Trench 14, Yucca Mountain, Nevada (abstract):* Geological Society of America, Abstracts with Programs, v. 23, pp. A117-118.

Zartman, R. E., and Kwak, L. M., 1993, *Lead Isotopic Composition of Paleozoic and Late Proterozoic Marine Carbonate Rocks in the Vicinity of Yucca Mountain, Nevada:* International High Level Radioactive Waste Management Conference, Proceedings, April 26-30, Las Vegas, Nevada, pp. 1953-1959.

Table 1. Petrographic Description of "True" Pedogenic Deposits.

Location	Sample #	Elevation	Occurrence	Petrographic texture	% Carbonate/ soil fraction	Carbonate grain size	Opal %
River Mtn							
Boulder Beach; rhyolite terrain	RM-1	500m	Stage I-II carb. matrix filling interstices bet. pebbles, silt, sand; coatings over clasts. Weak petrocalcic horiz.	Powdery; nodular structure not well-developed	~10-50% as matrix in soil ~90% as coatings over clasts	Fine-grained 1-10μ	None observed
East side, roadcut, rhyolite terrain	RM-2	500m	Stage II horizon ~0.5m thick, carb. coating of clasts	Ooidal; ooids ≅0.5 mm; Xline calcite fills fractures	~45% carb. ~50% silt ~5% gypsum	Fine-grain except for fracture-filling calcite	None observed
Yucca Mtn							
Road stop on way to FOC	JR-1	1150 m	Carbonate sheet horizon ~15cm below desert pavement + carb. pieces in des.pav.	Ooidal; ooids≅0.1-1mm	~70% carb. ~25% silt ~5% basalt fragments	1μ-0.2mm calcite xls = lg. grains	Few pieces of opal? Detrital?
Fortymile Wash-Midway Vly, TR-1	FMV-1	1250 m	Petrocalcic horizon ~1.5m below A-horizon. Krotovina in calcic horizon	Powdery; coatings over sand grains	~30% carb. ~70% silt, sand, pebbles	1μ-0.1mm calcite xls = lg. grains	None observed
Fortymile Wash-Midway Vly, TR-2	FMV-3	1250 m	Petrocalcic horizon ~1.5m thick below A-horizon; fossil soil horizon	Powdery; coatings over sand grains	~30% carb. ~70% silt, sand, pebbles	1μ-0.1mm 10μ is common	Few pieces of opal? Detrital?
Rk Valley fault, roadcut	RVF-1	830m	Desert pavement, vesicular A horiz., petrocalcic horizon well-indurated.	Powdery, carb. matrix coats sand grains; spel-eothemic tx.	~50% carb. ~50% silt and sand	1μ-0.1 mm; 10μ is common	Few pieces of opal? Detrital?
Red Cone; slope of volcano	RC-5	960m	Desert pavement, vesicular A horiz. petrocalcic horizon Stage III; coalesced nodules in friable& disem. carb. matrix	Powdery, good nodular texture	~40% carb. ~60% eolian sand grains	10μ-1mm 0.1mm is common	None observed

Table 2. Measured Values of $\delta^{18}O$ for Opal/Carbonate Pairs.

Location	$\delta^{18}O$ (‰ SMOW)	$\delta^{18}O$ (‰ SMOW)	$\delta^{18}O$ opal-carb (‰)
Pull Apart fault	28.17	23.36	4.81
Bare Mountain	28.19	20.27	7.92
Wailing Wall	28.17	19.84	8.33
Busted Butte	29.91	20.23	9.68

BEATTY, NEVADA—CALIFORNIA

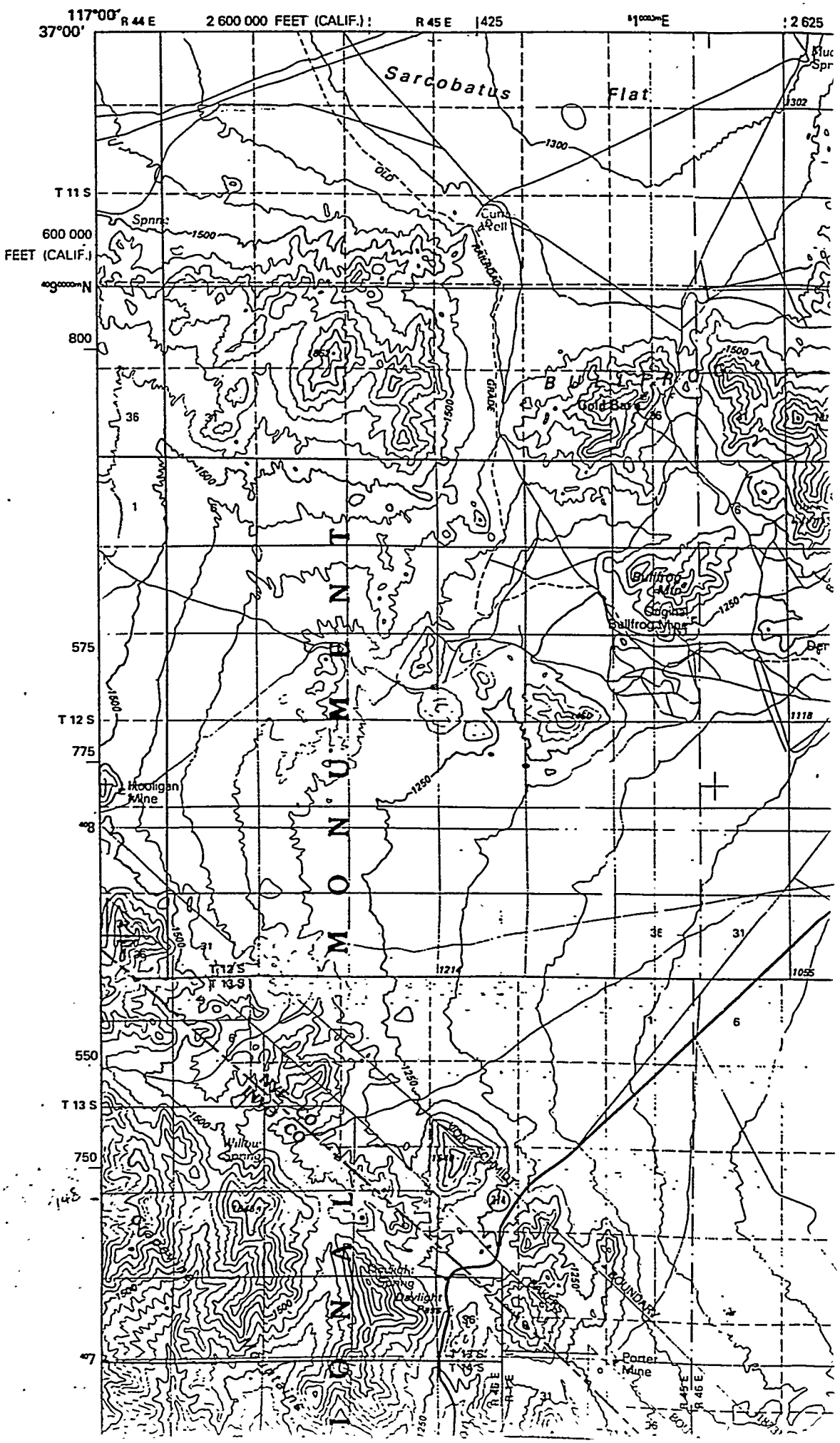

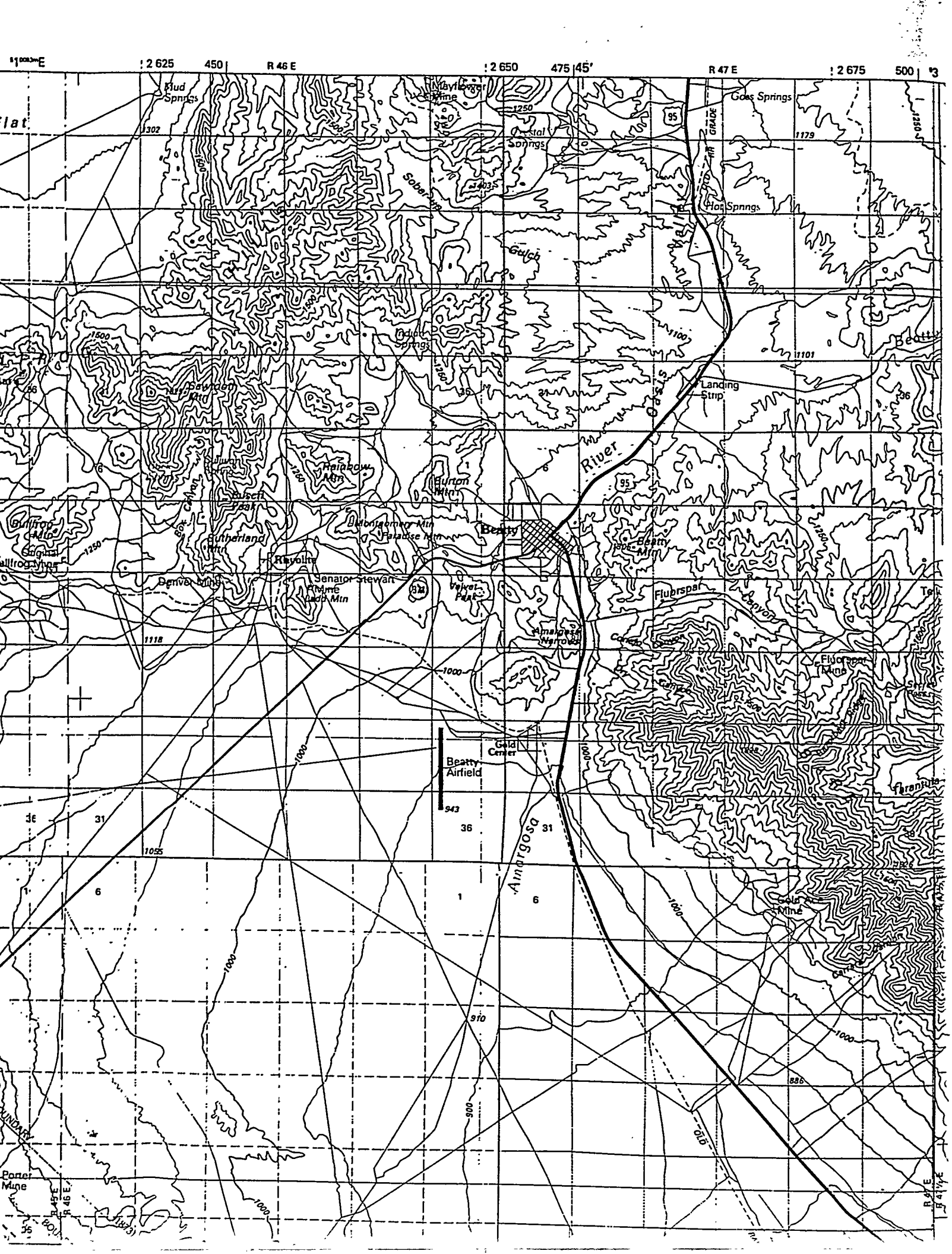
R 46 E
R 47 E
2 625
450
2 650
475
45'
2 675
500
Mud Springs
Mayflower Mine
Crystal Springs
Goss Springs
Hot Springs
Gulch
Idiot Springs
Beatty
Landing Strip
Amargosa River
Rainbow Mtn
Burton Mtn
Bullfrog Mtn
Bullfrog Mine
Sutherland Mtn
Montgomery Mtn
Paradise Mtn
Beatty Mtn
Rhyolite
Denver Mine
Senator Stewart Mine
Lead Mtn
Velvet Peak
Fluorspar Canyon
Fluorspar Mine
Gold Center
Beatty Airfield
Gold Bar Mine
Porter Mine
1118
1055
943
910
886
1179
1101
1000
900

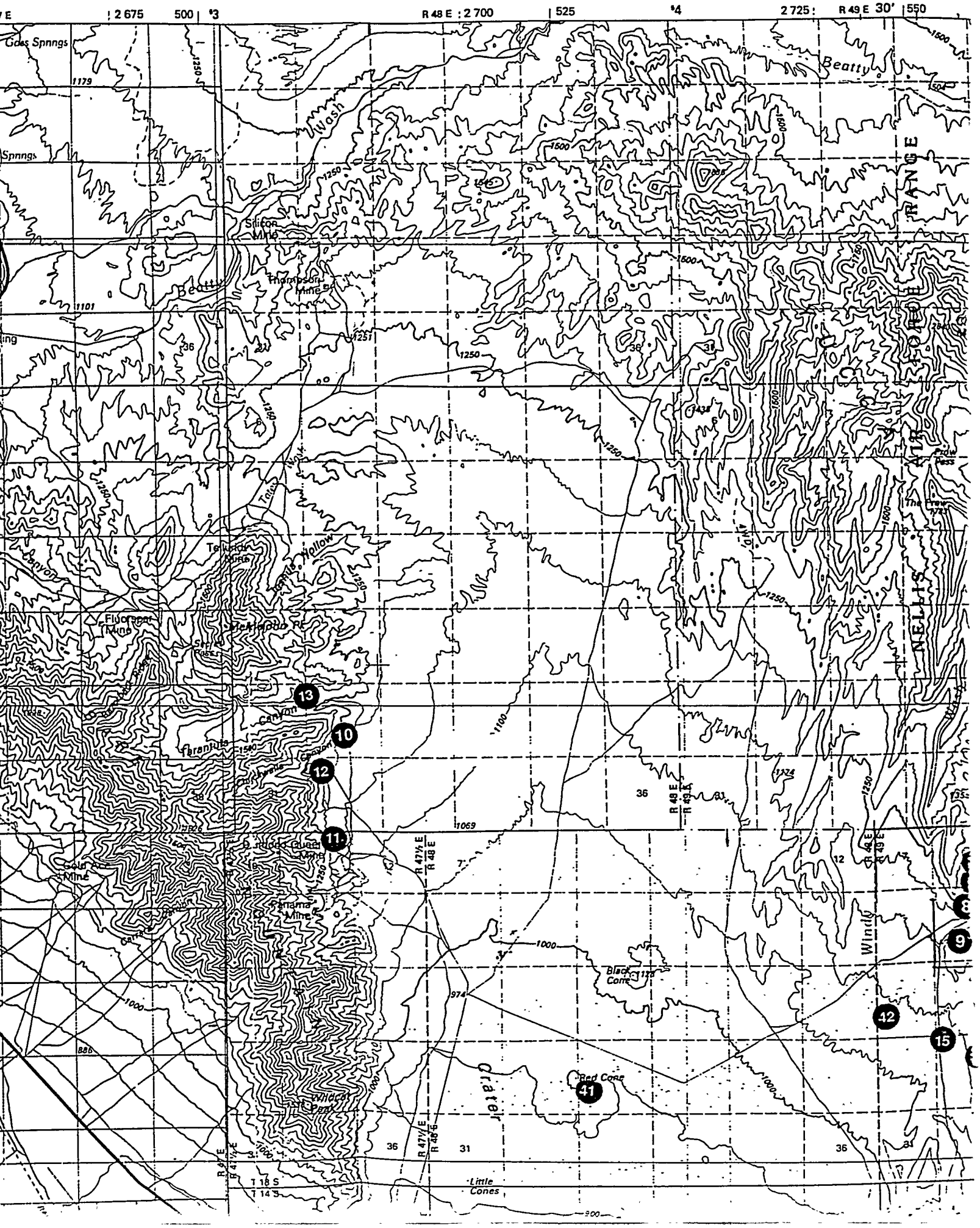
R 48 E
2 700
525
4
2 725
R 49 E
30'
550
Beatty
Wash
Silicon Mine
Thompson Mine
Beatty
Funeral Mts
Tarantula Canyon
Tarantula Hollow
Fluorspar Mine
Striped Rocks
Canyon
Fluorspar Canyon
Tarantula
Gold Ace Mine
Panama Mine
Crater
Wildcat Peak
Black Cone
Red Cone
Little Cones
Windy
Nellis Air Force Range
R 47½ E
R 48 E
R 49 E
T 18 S
T 14 S
13
10
12
11
9
42
15
41

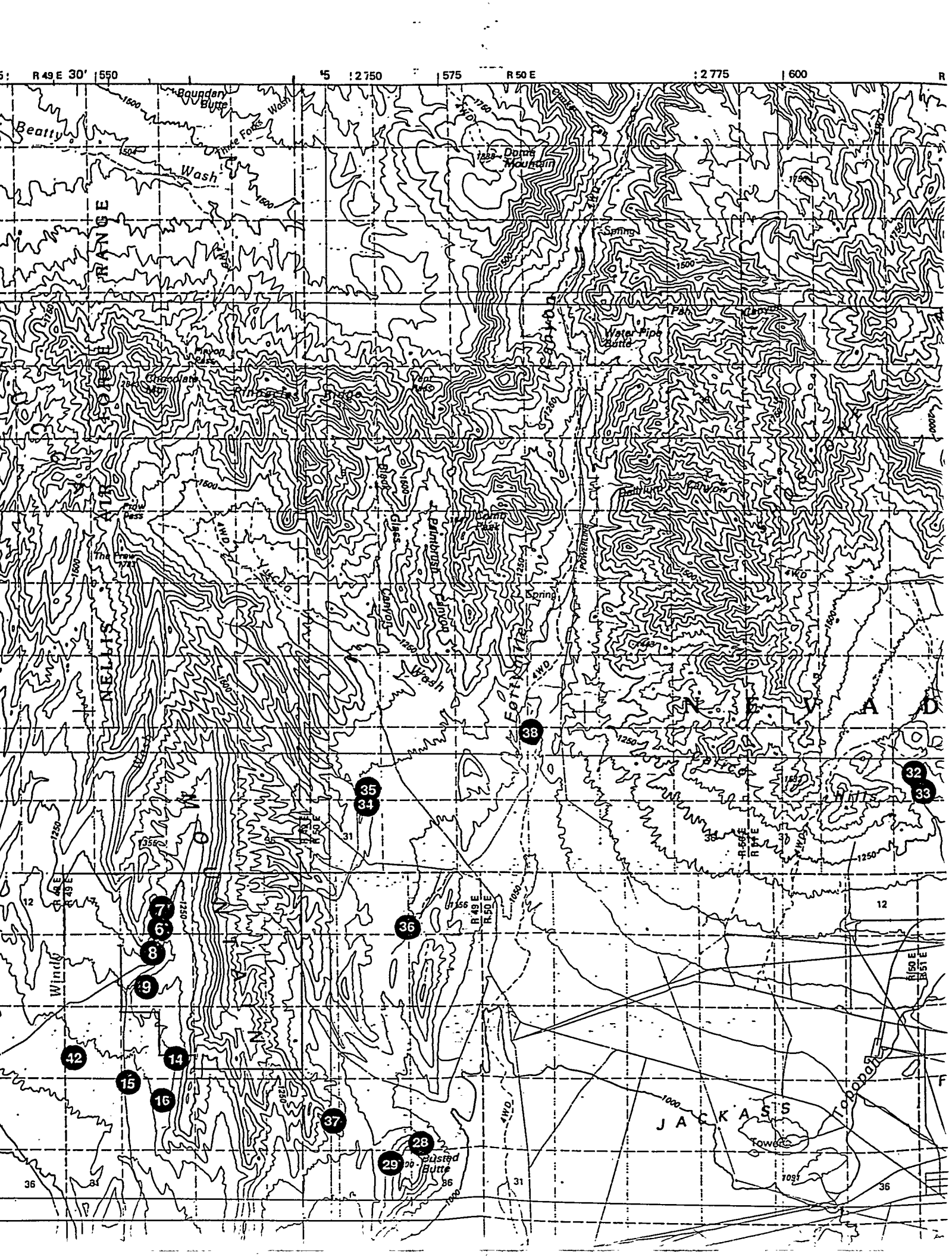
R 49 E 30'
550
'5
2750
575
R 50 E
2775
600
Boundary Butte
Beatty
Three Forks Wash
Wash
Dome Mountain
Spring
RANGE
FORTY MILE
Canyon
Pah Canyon
Water Pipe Butte
Pinnacle Ridge
Chocolate Mtn
Pinyon Pass
Yucca
Prow Pass
The Prow
Black Glass Canyon
Paintbrush Canyon
Camp Peak
Spring
POWERLINE
Jet Ridge
Wash
Fortymile
4WD
NELLIS
Calico Hills
N E V A D
Yucca
Windy Wash
JACKASS
Tower
Busted Butte
Topopah
1500
1250
1000
1750
R 49 E
R 50 E
R 50 E
R 51 E
12
31
36
38
35
34
32
33
7
6
8
9
36
42
14
15
16
37
28
29

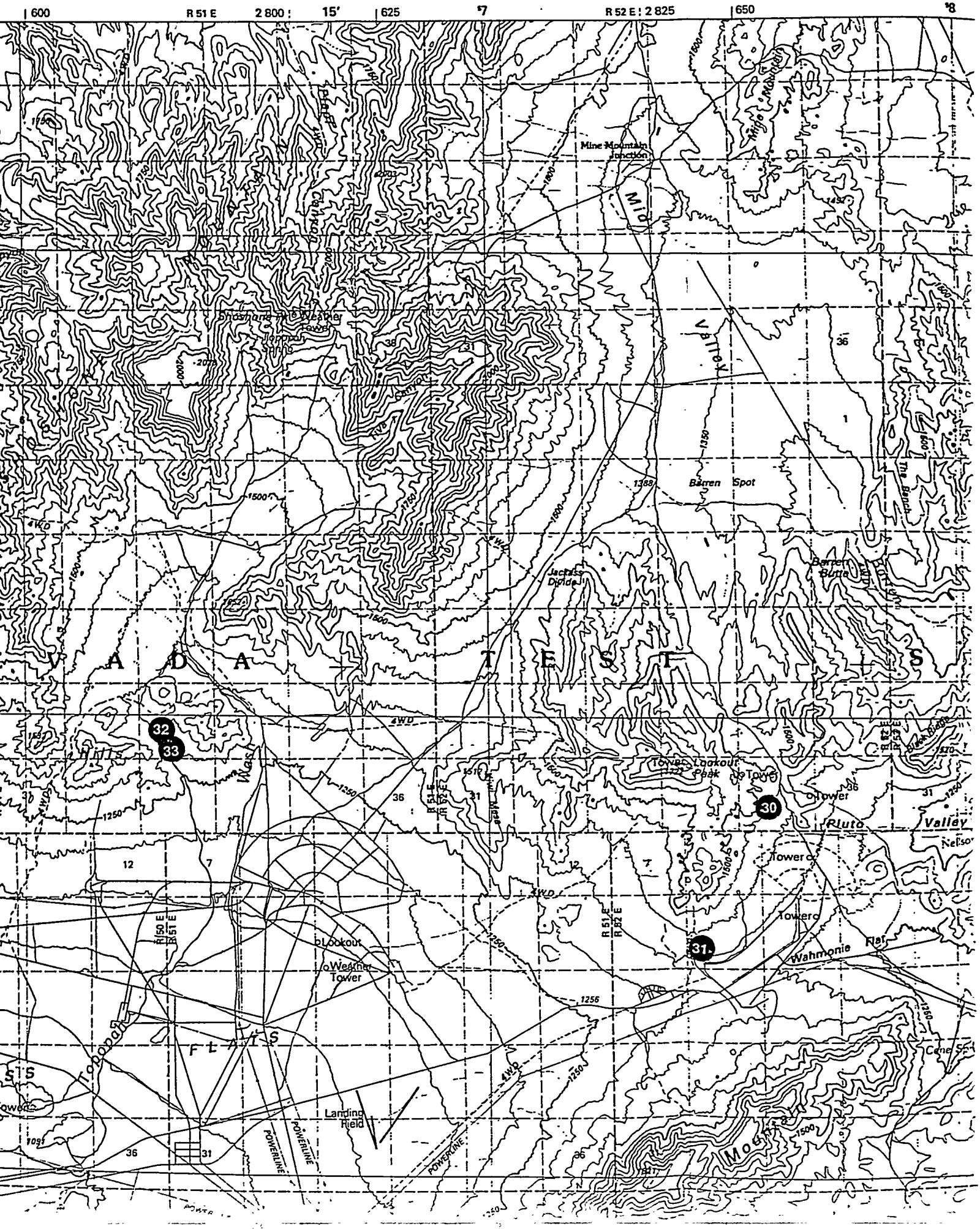
600
R 51 E
2 800 :
15'
625
7
R 52 E : 2 825
650
8
Mine Mountain Junction
Mine Mountain
Valley
Barren Spot
Jackass Divide
Barren Butte
The Bench
Black Ridge
Tower
Lookout Peak
Pluto
Valley
Nelson
Wahmonie
Flat
Weather Tower
Landing Field
POWERLINE
Mo
Cone
4WD
Wash
Hills
FLATS
T E S T
V A D A
32
33
30
31

30X60 MINUTE SERIES (TOPOGRAPHIC)

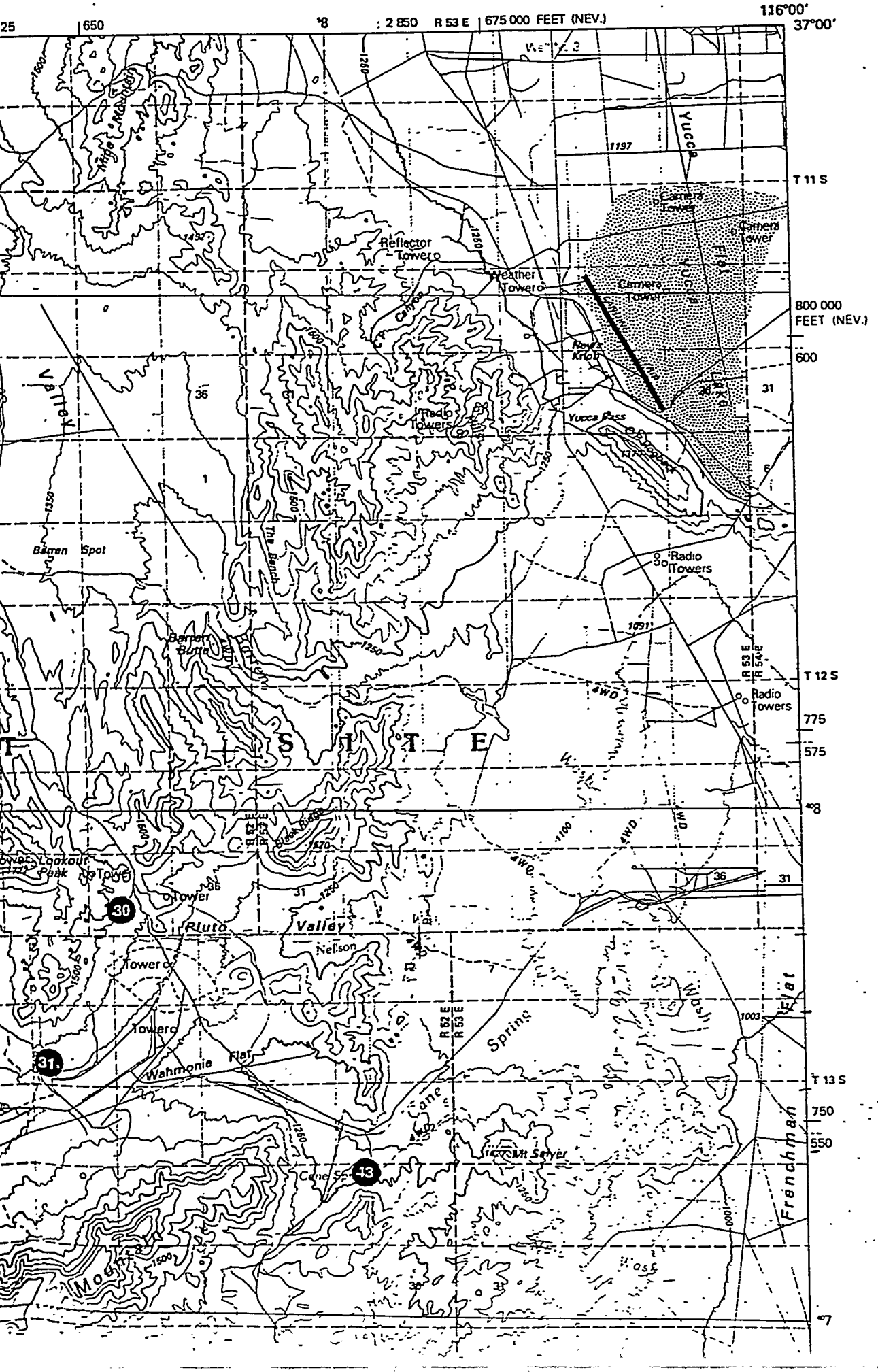

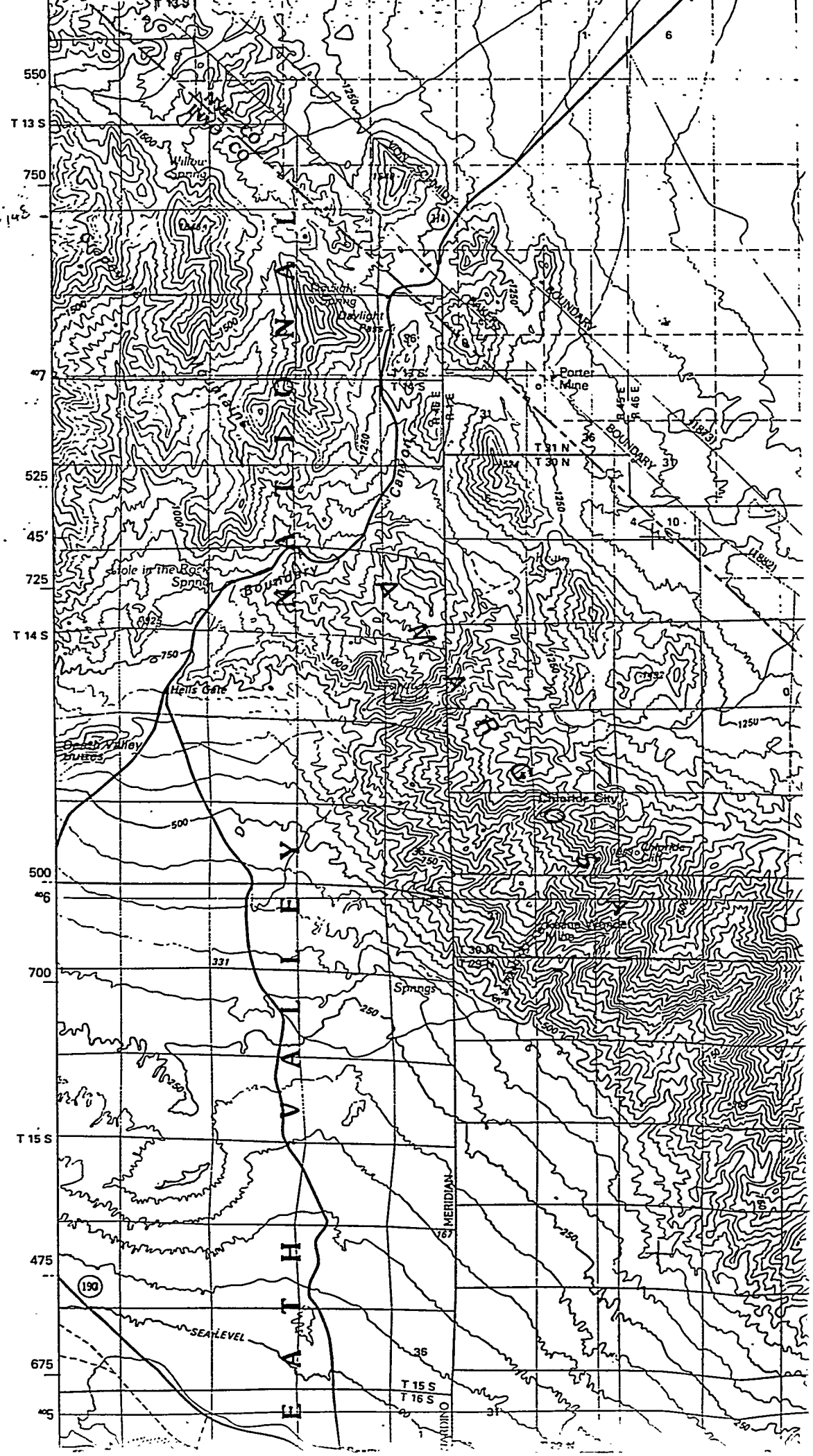
550
T 13 S
750
525
45'
725
T 14 S
500
700
T 15 S
475
675
SEA LEVEL
DEATH VALLEY
Willow Spring
Daylight Pass
Porter Mine
Stole in the Rock Spring
Hells Gate
Boundary
Canyon
Springs
MERIDIAN
T 15 S
T 16 S
T 31 N
T 30 N
R 45 E
R 46 E
BOUNDARY

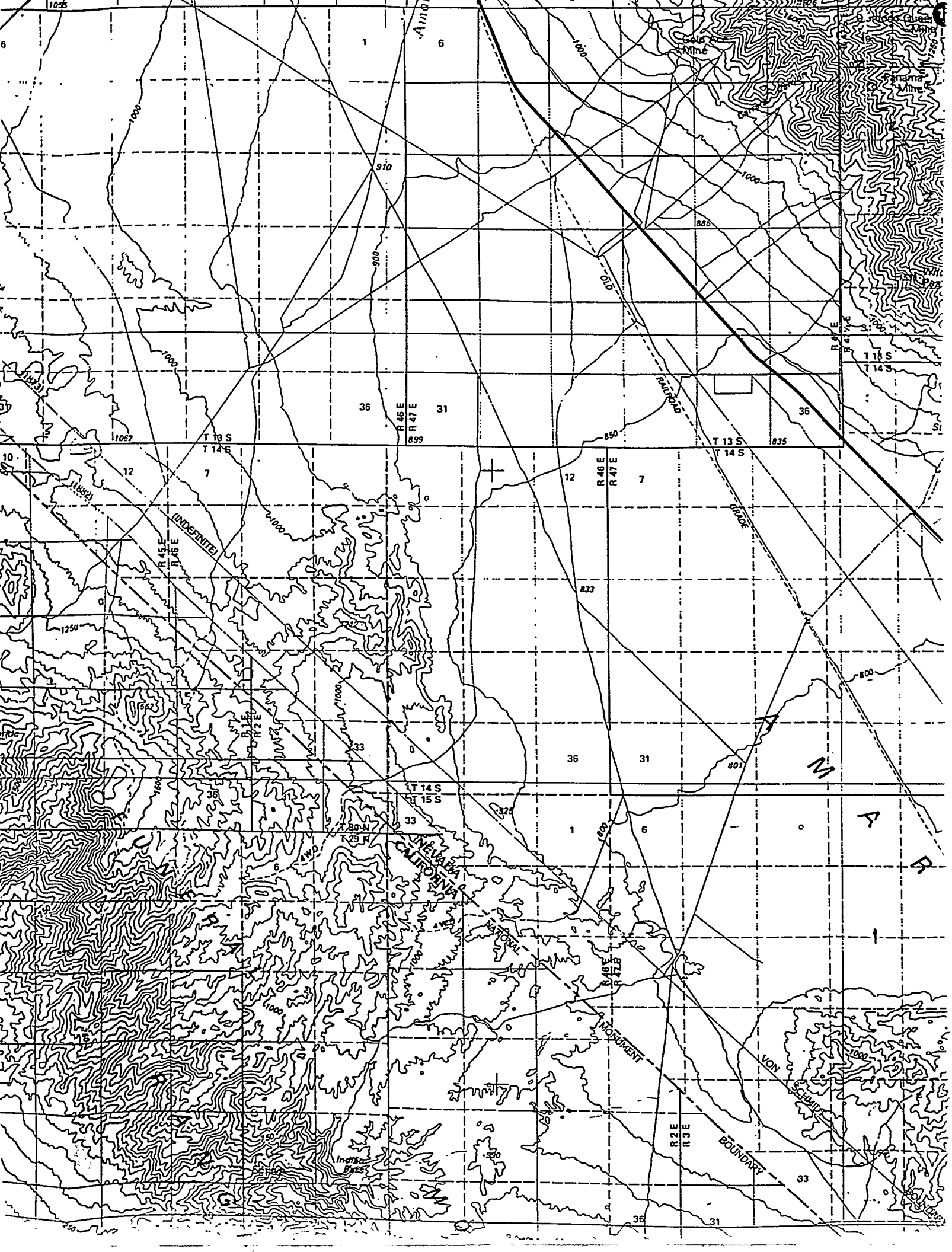
Gold Ace Mine
Panama Mine
RAILROAD
GRADE
(INDEFINITE)
T 13 S
T 14 S
T 14 S
T 15 S
R 45 E
R 46 E
R 47 E
R 48 E
R 1 E
R 2 E
R 2 E
R 3 E
CALIFORNIA
NEVADA
NATIONAL
MONUMENT
VON SCHMIDT
BOUNDARY
4WD
Indian Basin
1000
900
910
886
850
899
1067
835
833
801
825
800
1250
1500
1050

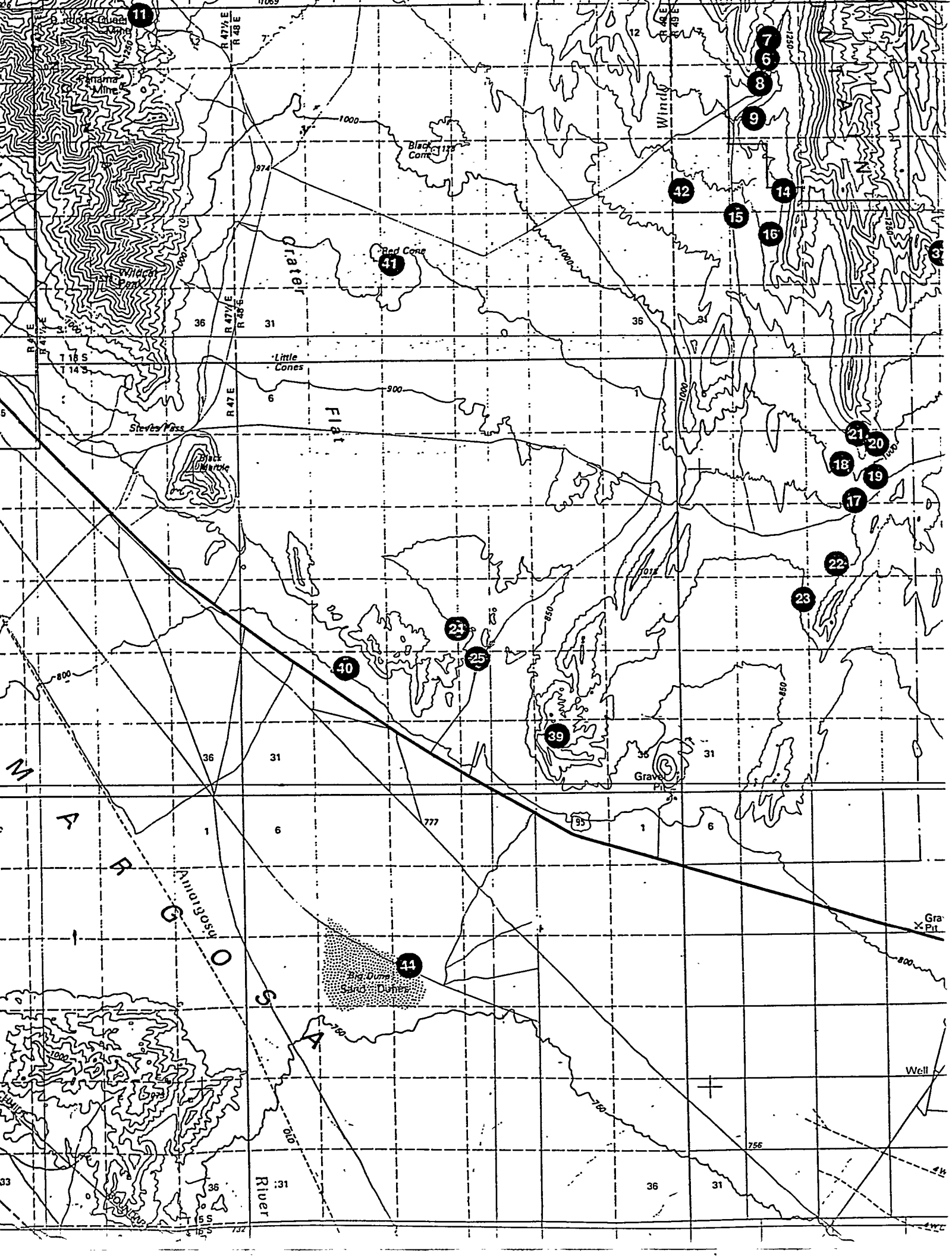
11
7
6
8
9
42
14
15
16
41
21
20
18
19
17
22
23
24
25
40
39
44
Crater
Flat
Red Cone
Black Cone
Little Cones
Steves Pass
Black Butte
Wildcat Hill
Panama Mine
Big Dune
Sand Dunes
Gravel Pit
Amargosa River
MARGOSA
Windy
R 47½ E
R 48 E
T 16 S
T 15 S
36
31
1
6

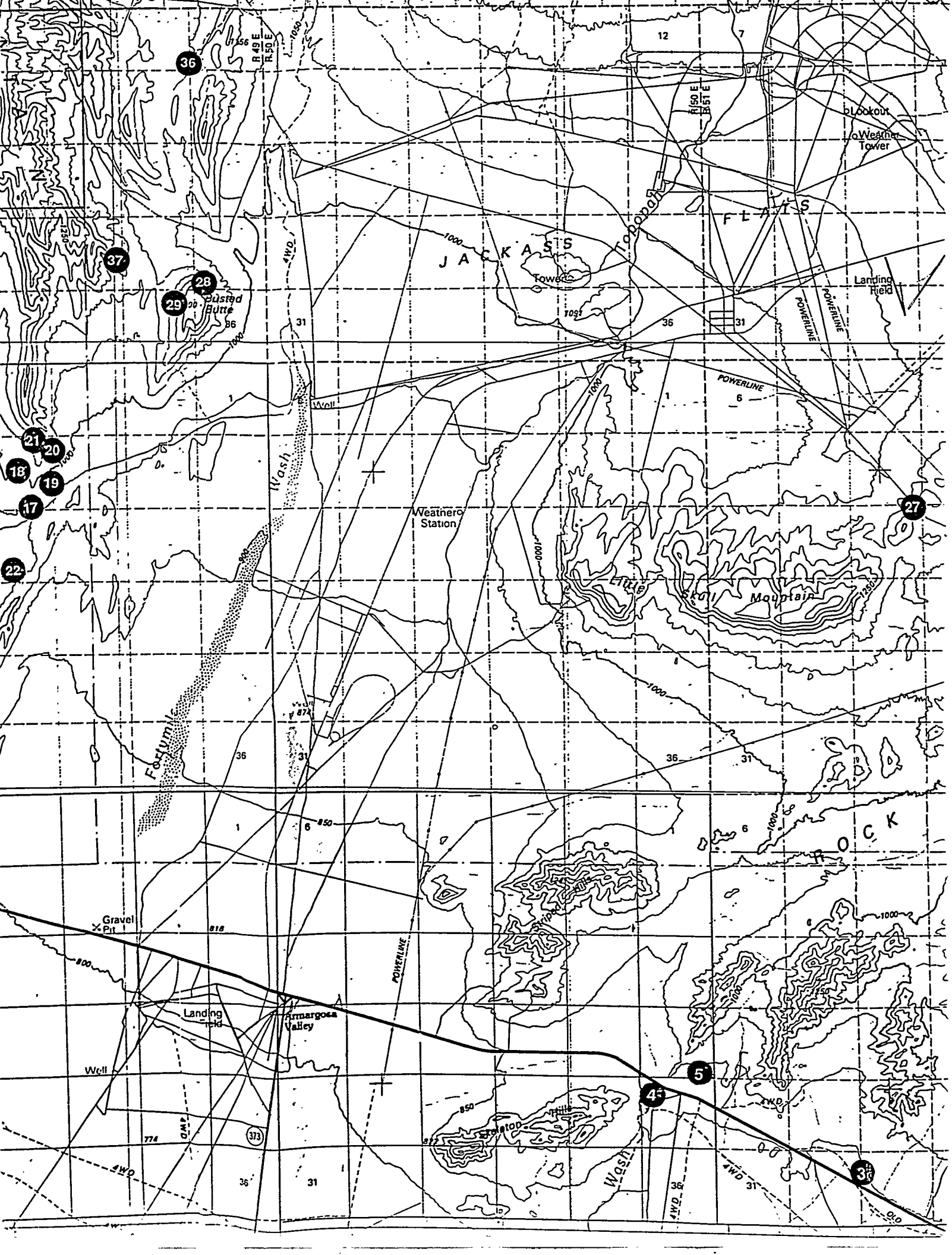
36
37
28
29
Busted Butte
21
20
18
19
17
22
27
Wash
Well
Weathero Station
Little Skull Mountain
Lookout
Weather Tower
Landing Field
POWERLINE
Gravel Pit
Landing Field
Amargosa Valley
Tolicha Peak
Skeleton Hills
5
4
3
373
JACKASS FLATS
ROCK

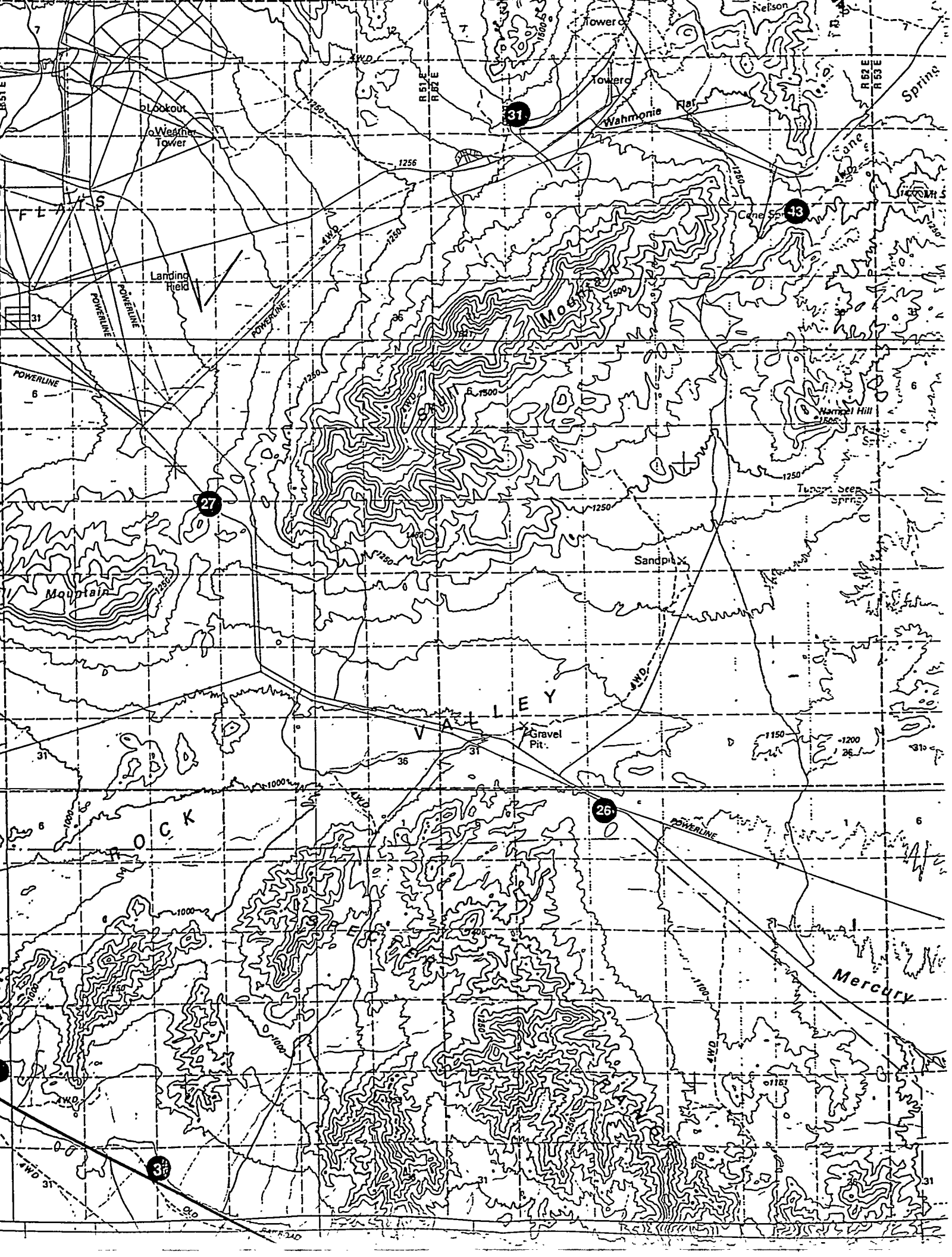
Nelson
Tower
Tower
Wahmonie
Flat
Lookout
Weather Tower
Landing Field
POWERLINE
POWERLINE
POWERLINE
POWERLINE
4WD
Mountain
Sandpit
Tunnel Seep
Spring
Gravel Pit
VALLEY
ROCK
Mercury
31
13
27
26
31
R51E
R52E
R53E
T8S
T9S
1250
1256
1500
1000
1100
1150
1200

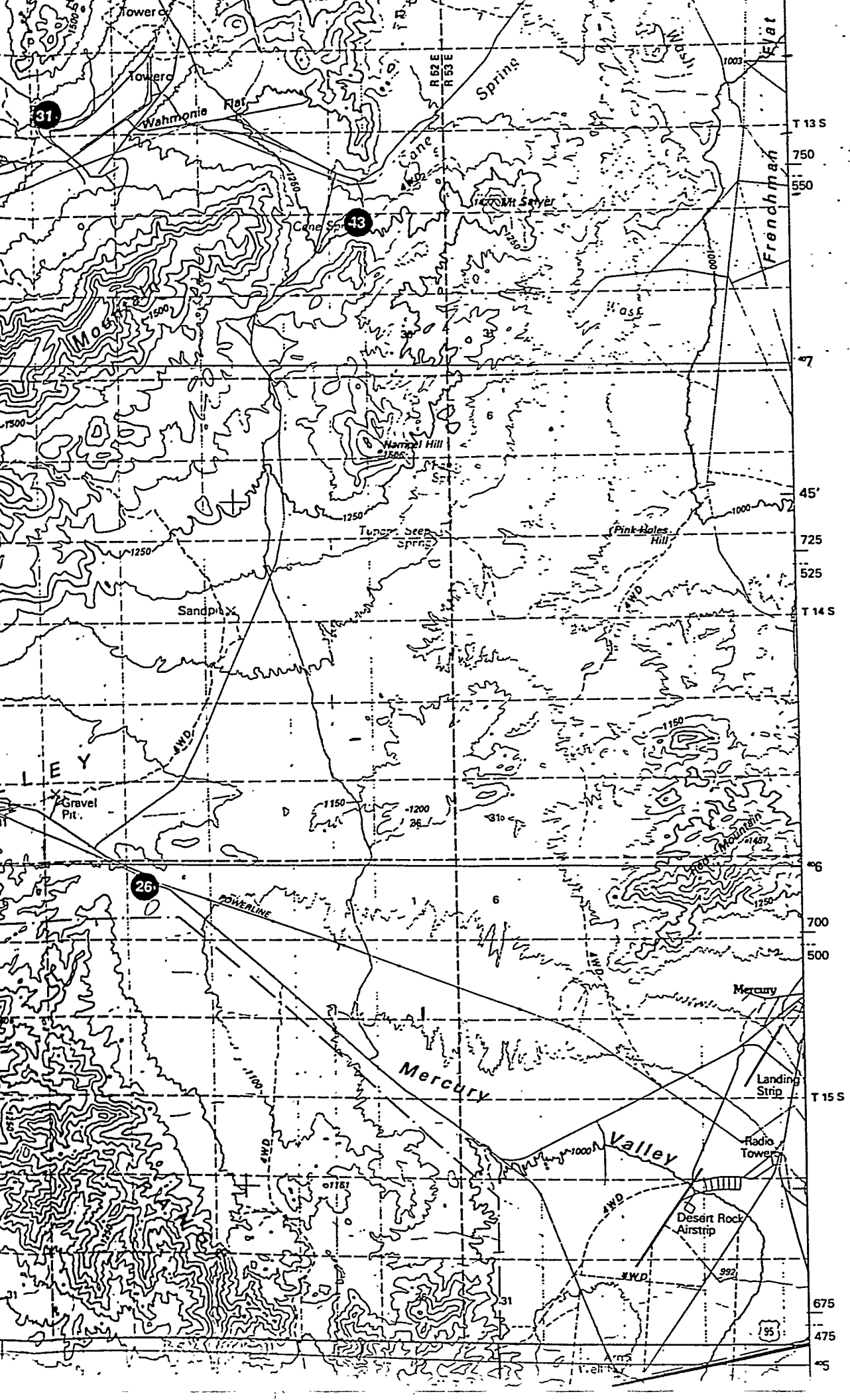
Tower
Tower
Wahmonie Flat
Cane Spring
Mt Sayer
Cane Spring
Frenchman Flat
Mountain
Hannel Hill
Tunnel Seep
Spring
Pink Holes Hill
Sandpit
Gravel Pit
Fran Mountain
POWERLINE
Mercury
Mercury Valley
Landing Strip
Radio Towers
Desert Rock Airstrip
4WD
T 13 S
T 14 S
T 15 S
750
550
725
525
700
500
675
475
45'
31
43
26
95

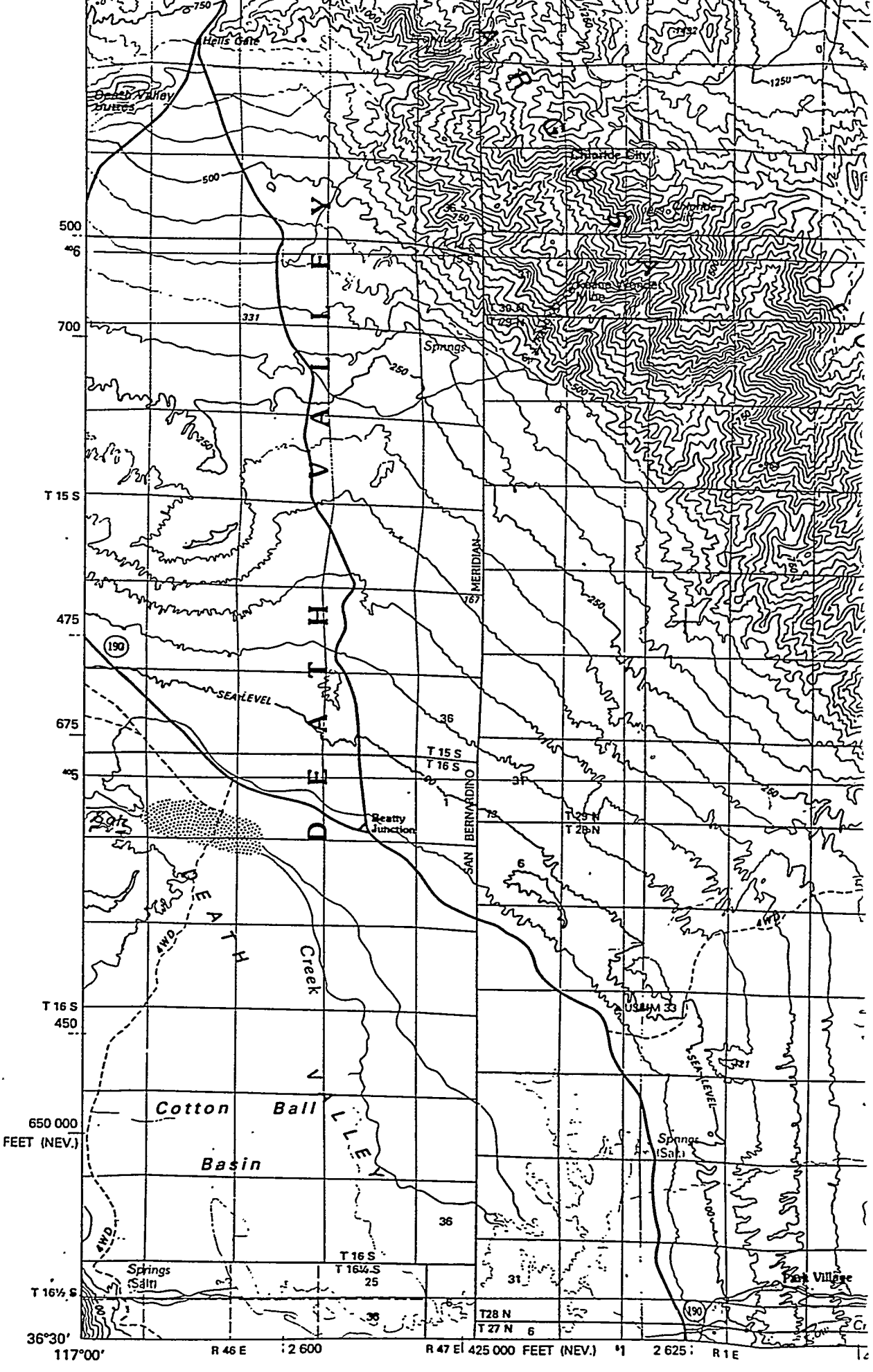

● INTERIOR—GEOLOGICAL SURVEY, RESTON, VIRGINIA— 1968

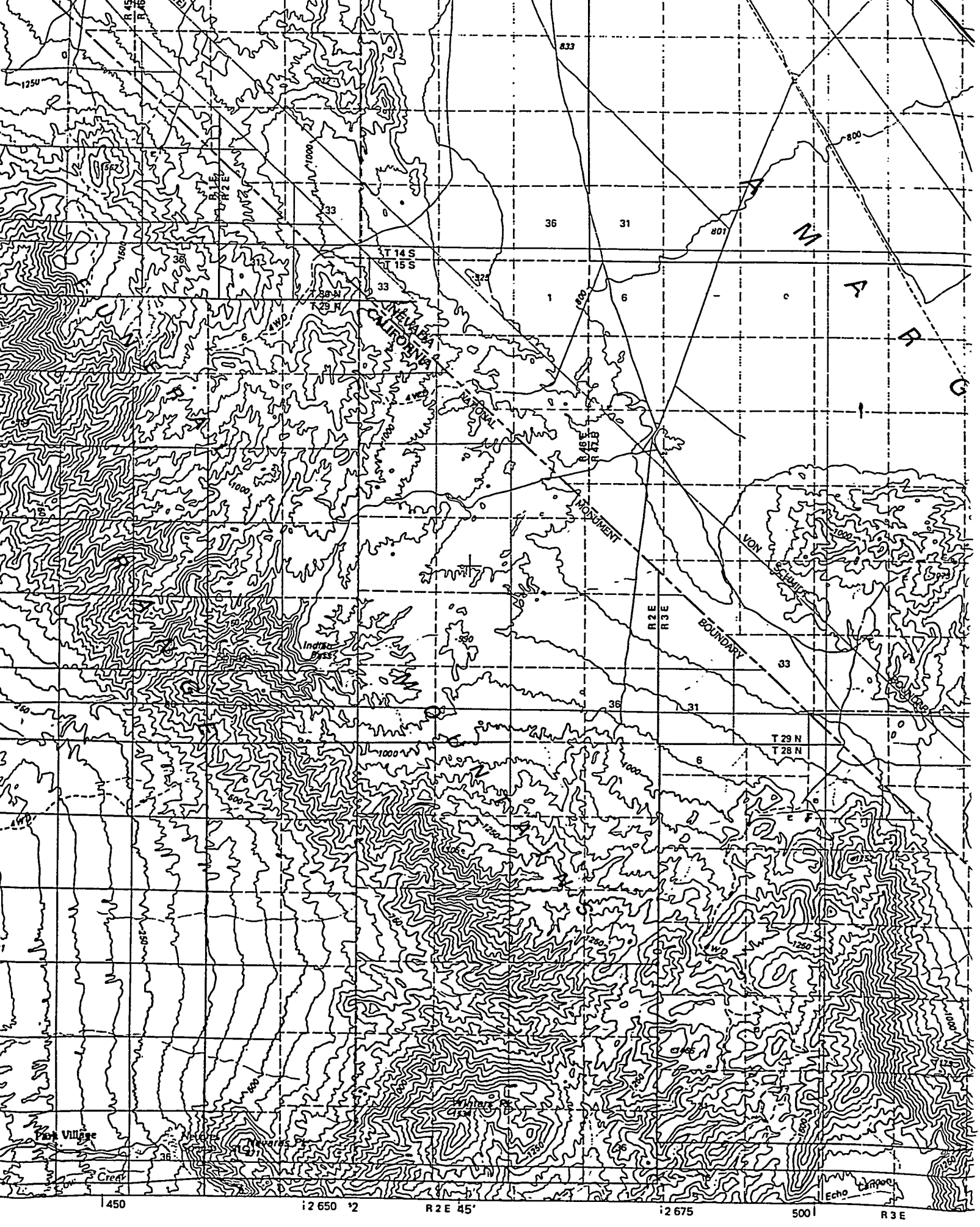
T 14 S
T 15 S
T 30 N
T 29 N
T 29 N
T 28 N
R 45 E
R 46 E
R 1 E
R 2 E
R 46 E
R 47 E
R 2 E
R 3 E
CALIFORNIA
NEVADA
MONUMENT
BOUNDARY
VON SCHMIDT
Indian Pass
Park Village
Navares Pk
Echo
Canyon
Crest
4WD
1000
800
600
400
200
1250
1500
1750
2000
2250
2500
2750
3000
3250
3500
36
31
33
6
1
450
2 650
2 675
500
R 2 E 45'
R 3 E
KILOMETERS 1
0 1 2 3 4 5 6 7 8 9 10 11 12 13
MILES 1
0 1 2 3 4 5 6 7

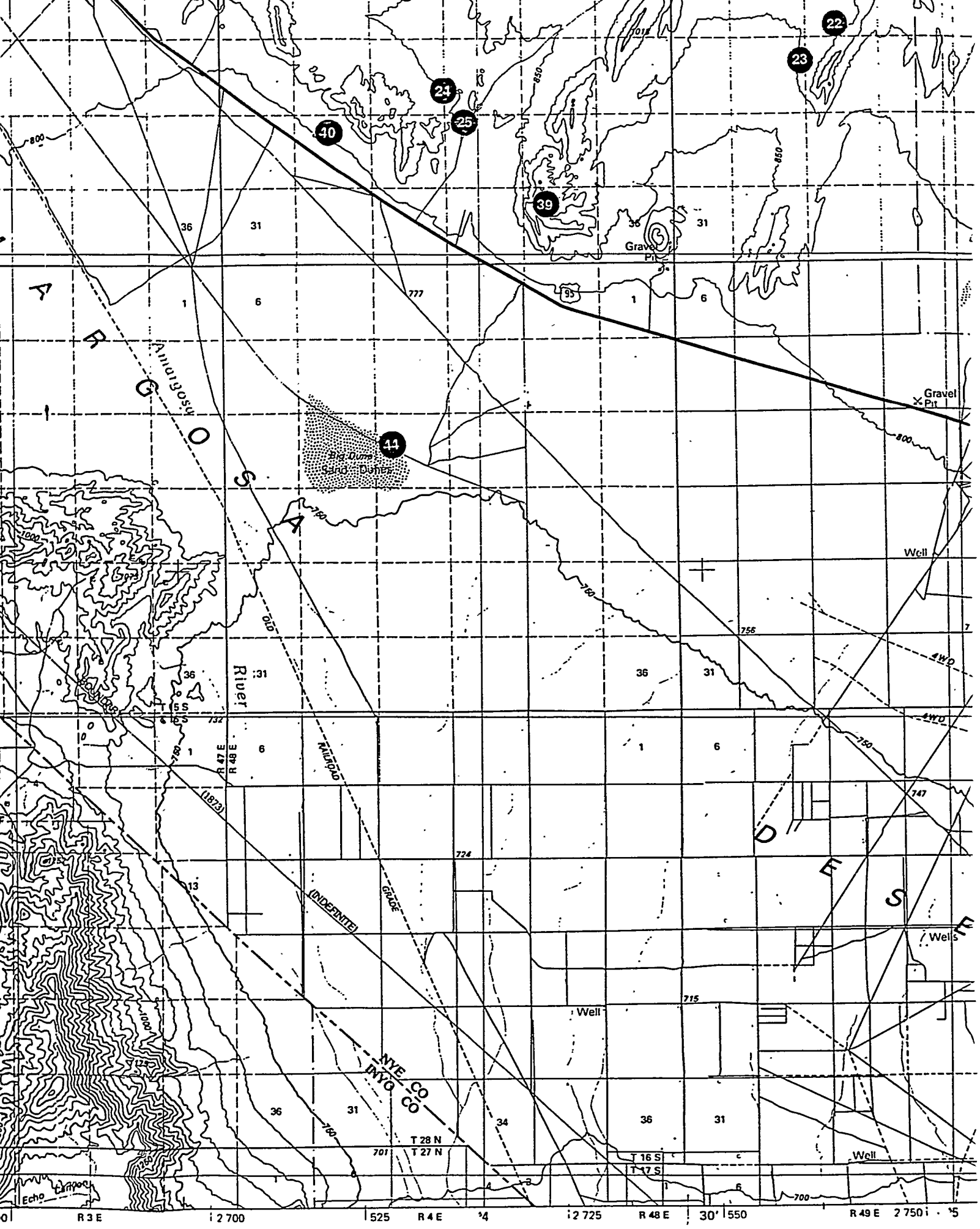

SCALE 1:100 000

1 CENTIMETER ON THE MAP REPRESENTS 1 KILOMETER ON THE GROUND

CONTOUR INTERVAL 50 METERS

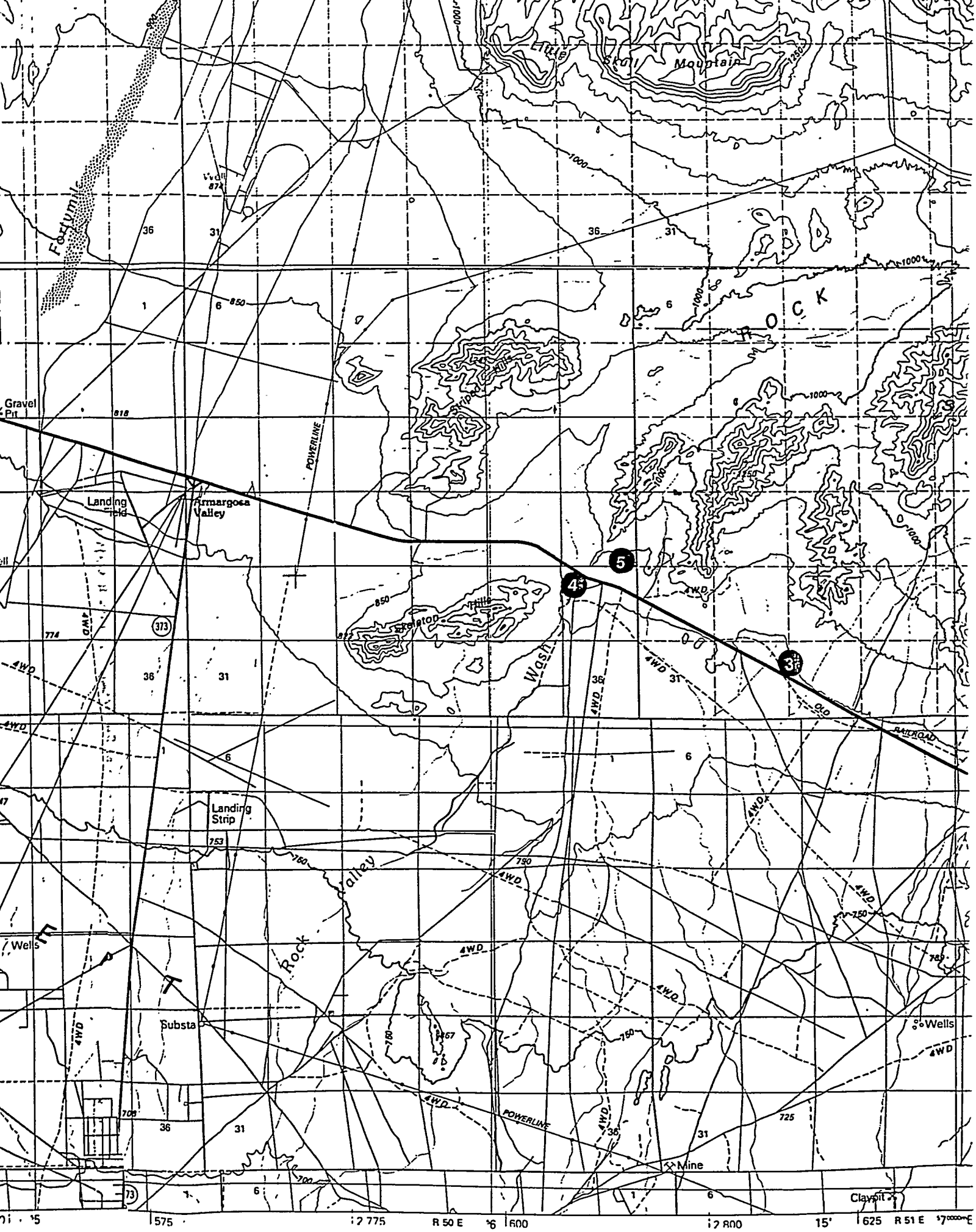
Little Skull Mountain
Fortymile Wash
ROCK
Gravel Pit
POWERLINE
Landing Field
Armargosa Valley
Skeleton Hills
Wash
OLD RAILROAD
Landing Strip
Rock Valley
Wells
Substa
Mine
Claypit
5
4
3
4WD
R 50 E
R 51 E
1000 0 5000 10000 15000

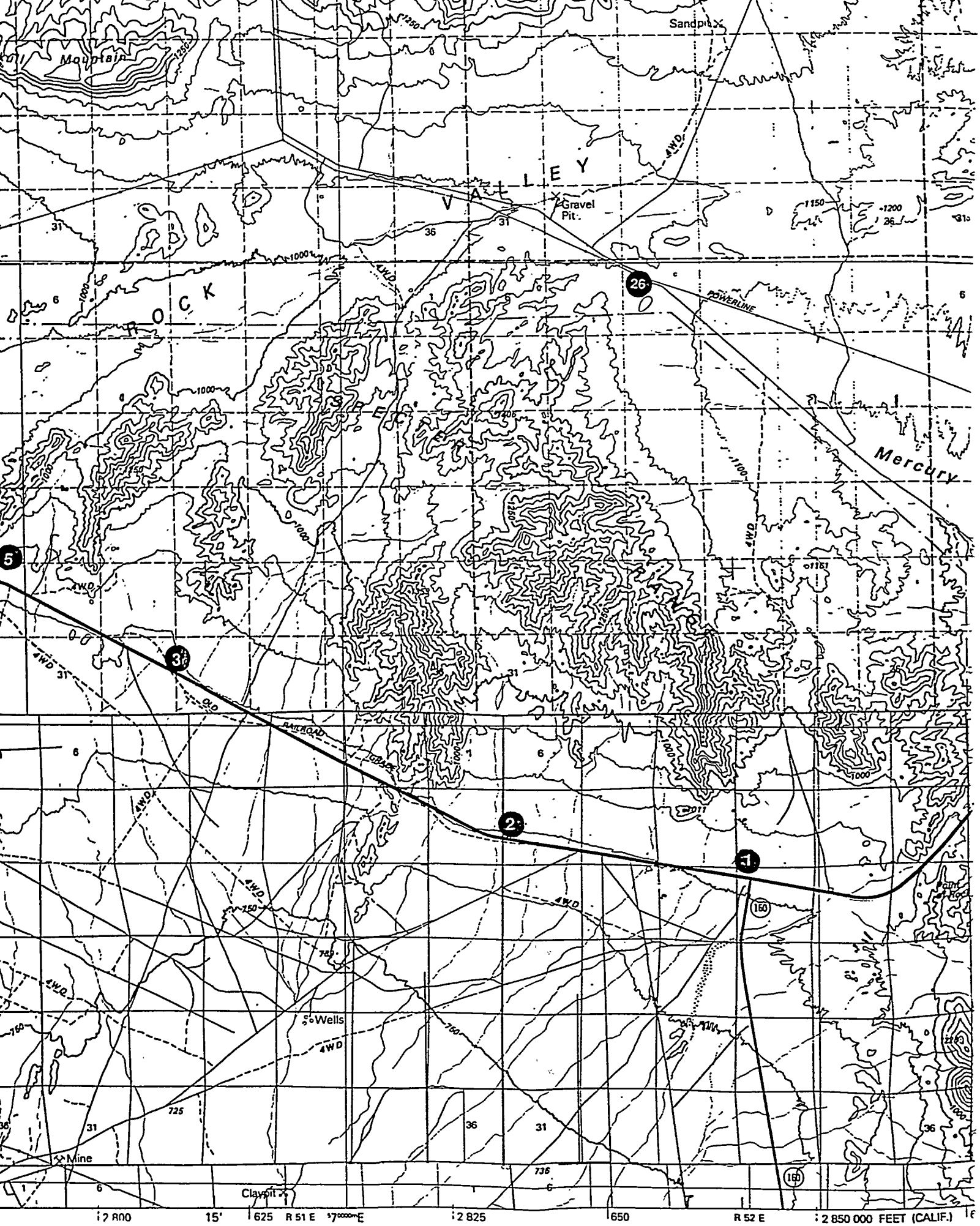
Sandpit
Mountain
VALLEY
Gravel Pit
ROCK
SPRING
POWERLINE
Mercury
RAILROAD
Wells
Mine
Claypit
4WD
26
5
3
2
1
160
15'
R 51 E
R 52 E
2 800
625
2 825
650
2 850 000 FEET (CALIF.)
15 000
20 000 METERS
BEATTY

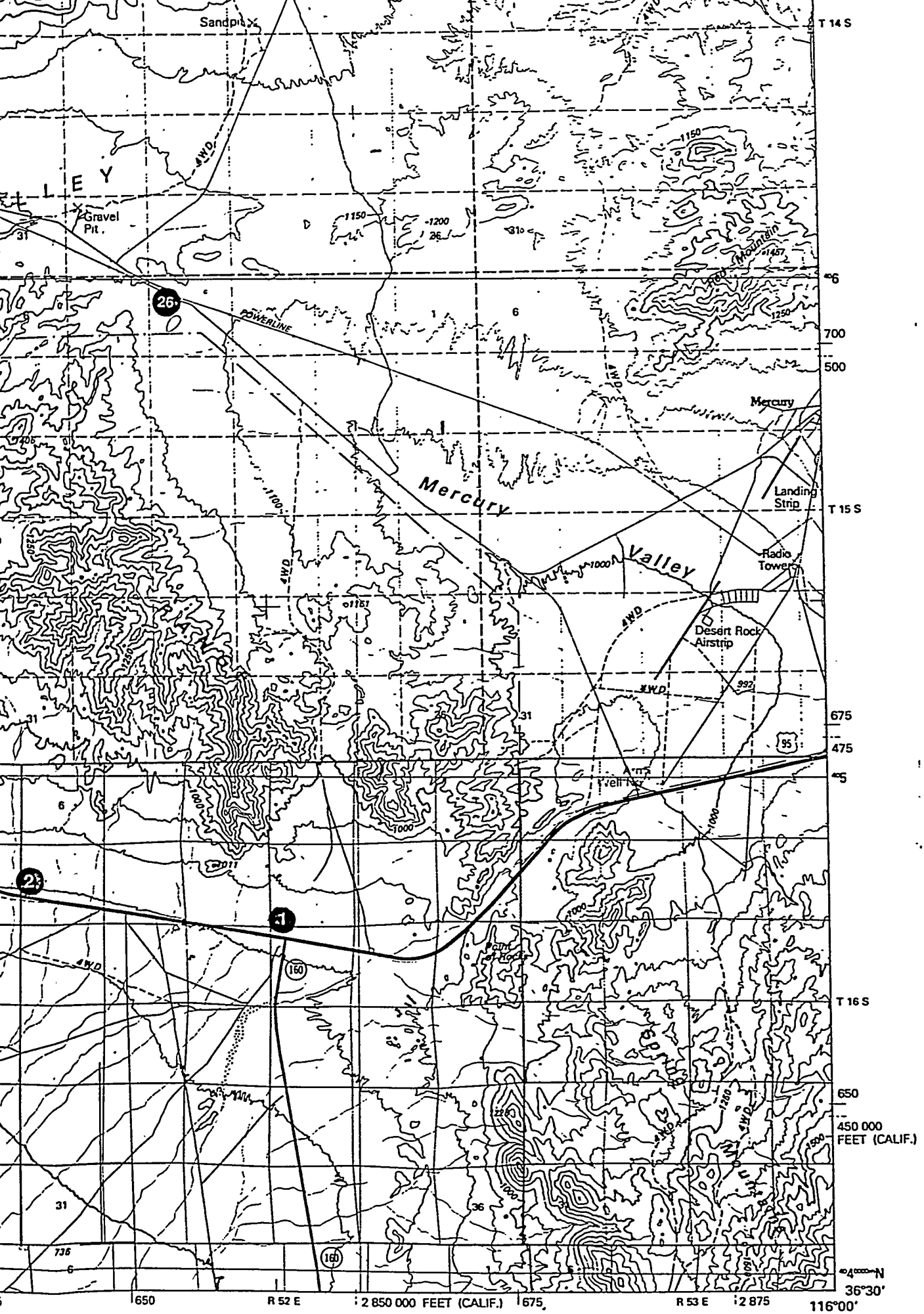

BEATTY, NEVADA—CALIFORNIA

36116-E1-TM-100

List of locations refer to Figure 1.

SITE#	LOCATION
1	US Hwy 95, mile 10
2	US Hwy 95, mile 12.47
3	US Hwy 95, mile 18.8
4	Pull Apart fault
5	Rock Valley fault
6	WT-7
7	USW H-6
8	WT-7, roadside
9	Plug Hill
10	Bare Mountain
11	Diamond Queen Mine
12	Chuckwalla Canyon
13	Tarantula Canyon
14	Trench 8
15	Trench 8, roadside
16	New Trench
17	Site 106
18	Livingston Scarp
19	Wailing Wall
20	roadside ("scarp")
21	Red Cliff Gulch
22	North Trench A at Stagecoach Road fault
23	South Trench at Stagecoach Road fault
24	Site 199
25	Site 199, roadside
26	Jackass Flats Road
27	Jackass Flats Road
28	East Busted Butte
29	West Busted Butte
30	Wahmonie Mound
31	Wahmonie Mines
32	Calico Hills
33	Shoshone Mountain road
34	Trench 14
35	Trench 14A
36	UE25 p#1
37	Harper Valley
38	Forty Mile Wash
39	Lathrop Wells Cone
40	Diatomaceous Earth
41	Red Cone
42	Trench CF-1
43	Cane Springs
44	Big Dunes

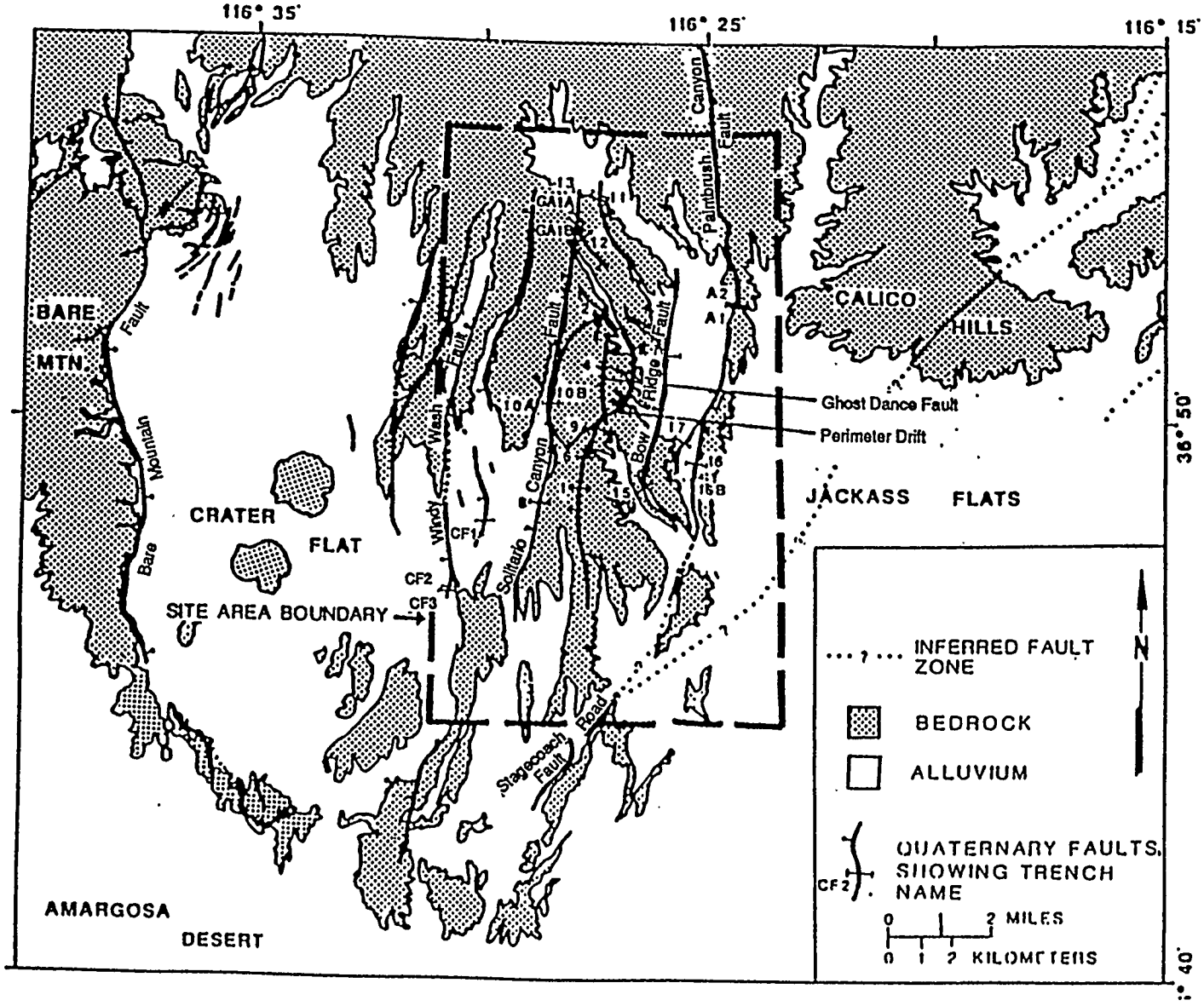

Figure 2. Location of faults in the Yucca Mountain area.

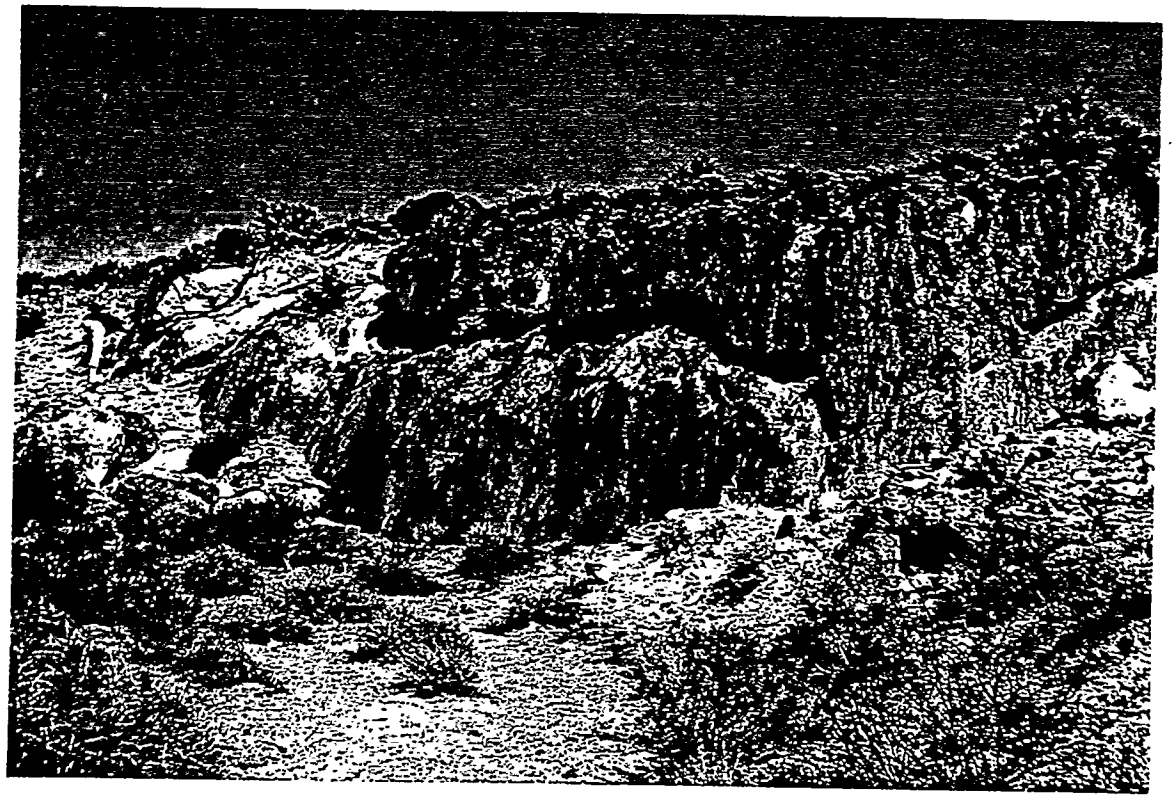

Figure 3. Calcite/opal (white material) directly along fault, Wailing Wall. Away from the fault the carbonate material dies out. The fault is part of the Stagecoach Road fault system and is recognizable by slickensides and offset beds. Photo: Carol A. Hill.

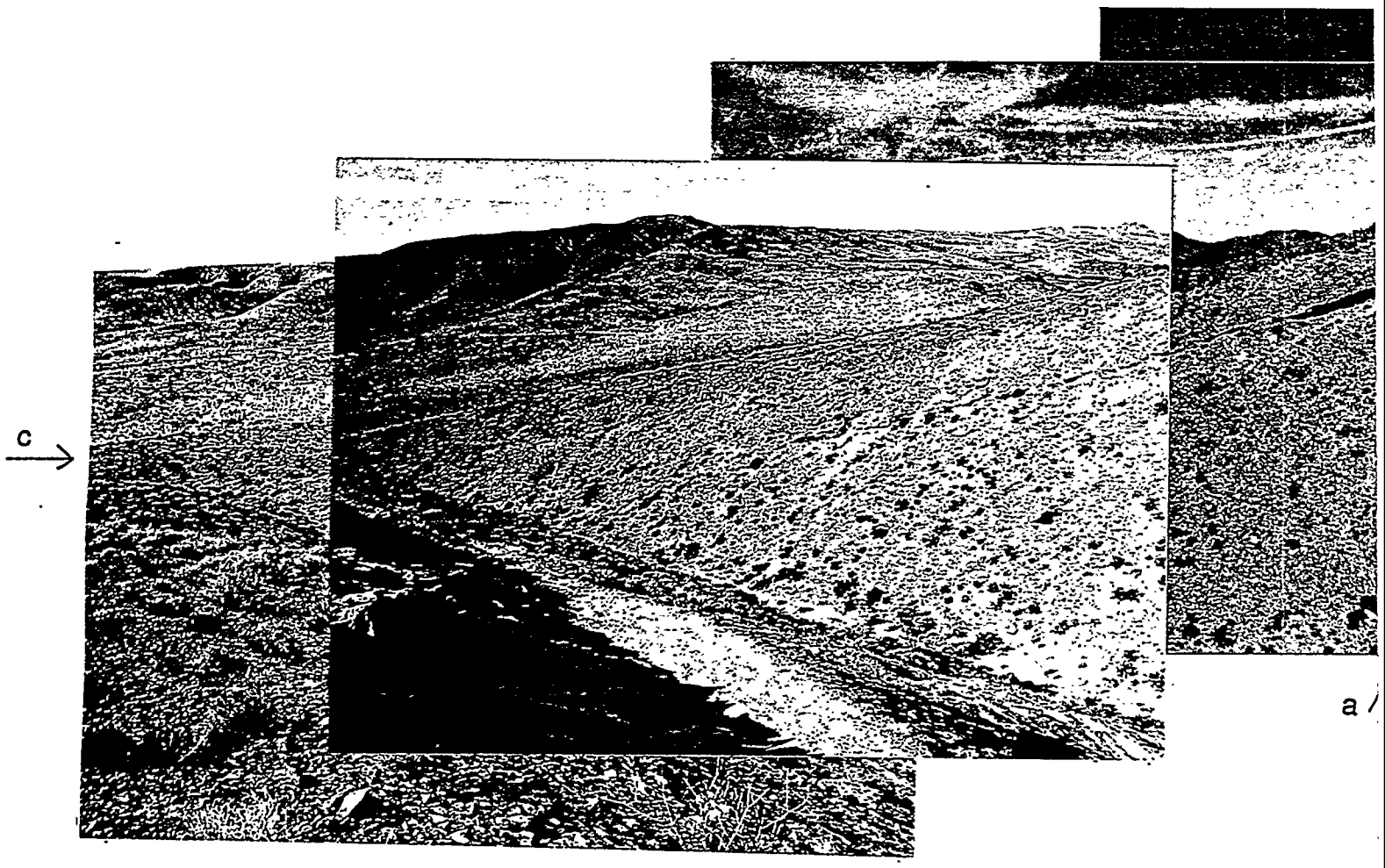

Figure 4. Composite photo of dissected sand ramp, west Busted Butte, showing calc
and travertine which emanates from the vein and continues down slope to
material that can be found on the surface of this sand ramp is at (b_2). It i
are not found along sand ramps which have not been cut across by faults
occur everywhere on Busted Butte.

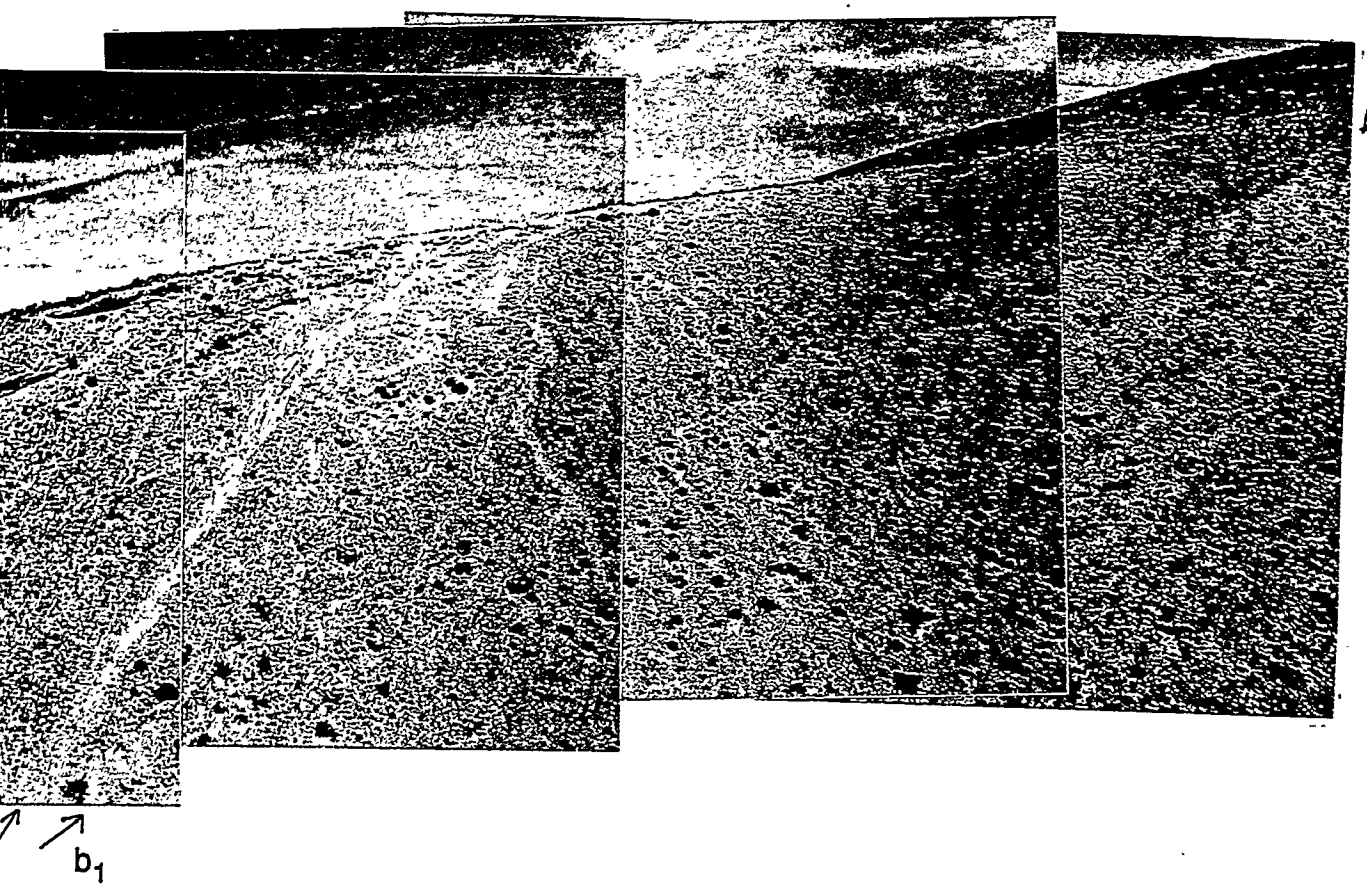

te/opal vein along the fault (a) and at an angle from fault (b_1, $_2$), the toe of slope and beyond (c). The highest calcrete travertine extremely important that such calcite/opal veins and travertines If this travertine was pedogenic in origin (as claimed) it should

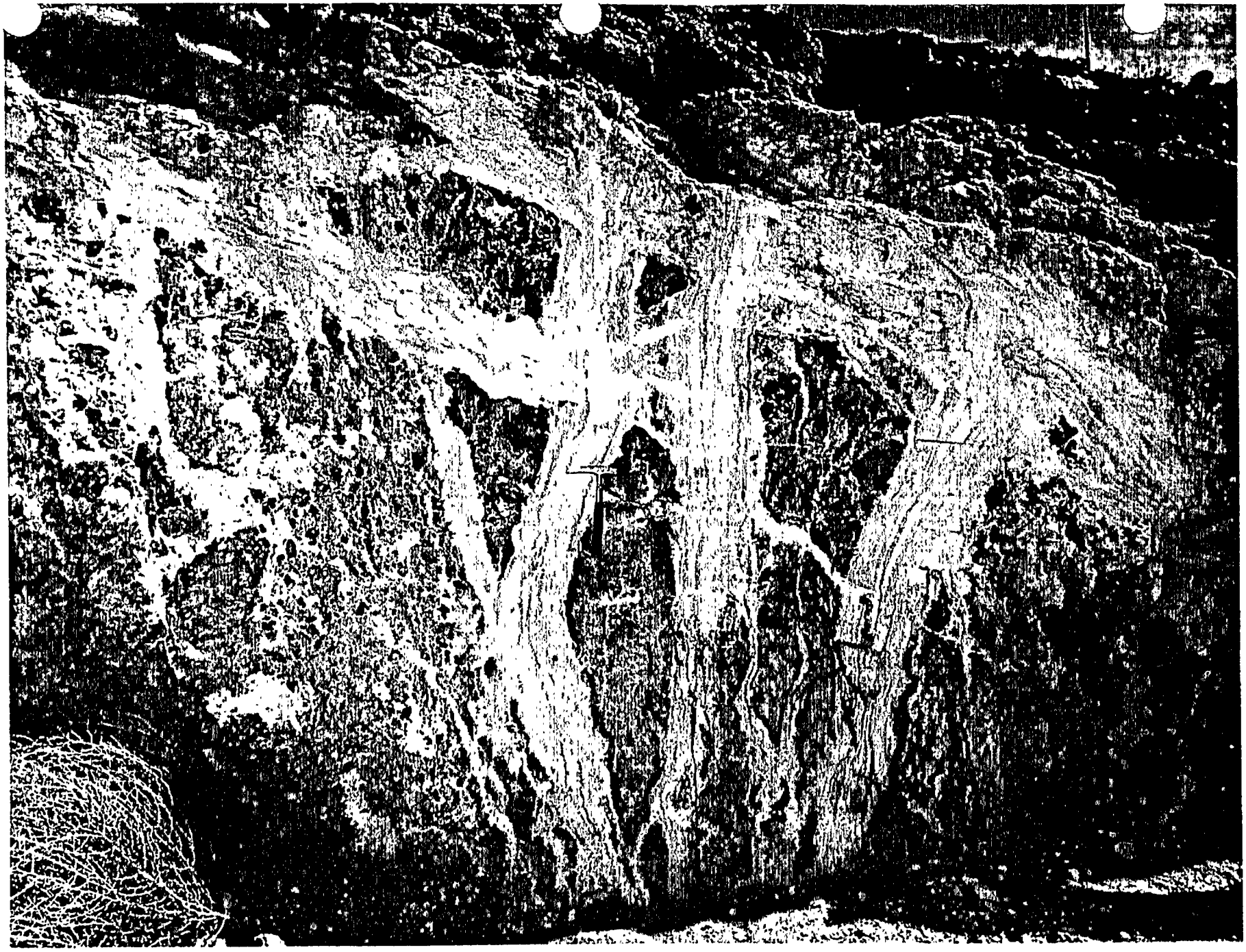

Figure 5. Actual photograph of the south wall of Trench 14 showing a cross section of at least five episodes of crosscutting mineralization. Taken from an unclassified, United States Department of Energy negative - No. YM-284.

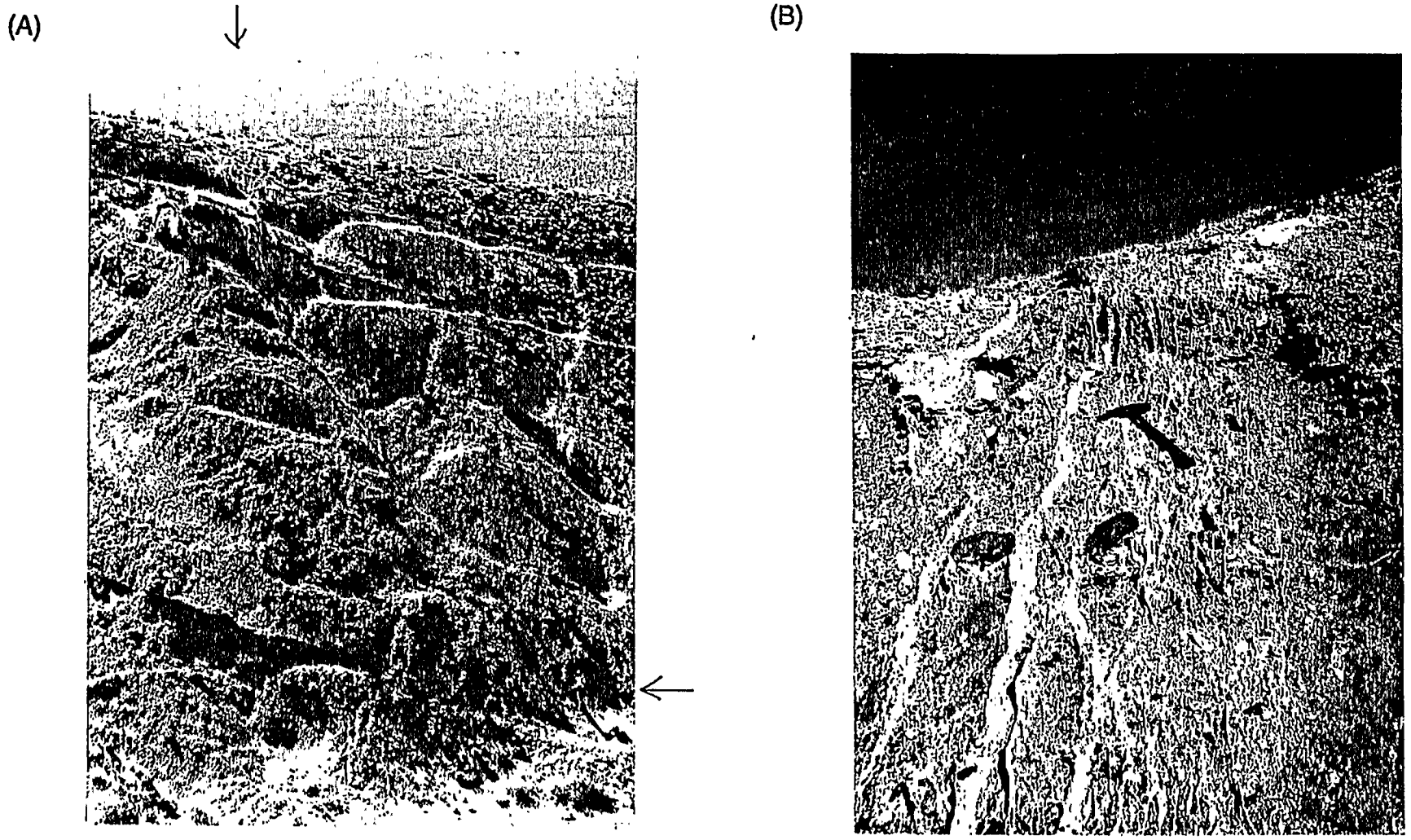

Figure 6. (A) Vein of calcite/opal along fault, looking southward along downcut sand ramp, west Busted Butte. The calcite/opal follows directly along the fault and is about 70 m in vertical extent (it continues beyond this into the subsurface). Note the person for scale (horizontal arrow) and how the vein splays out near the top of the sand ramp (vertical arrow). (B) Close-up of splayed veins, north side of same dissected sand ramp. Photos: Carol A. Hill.

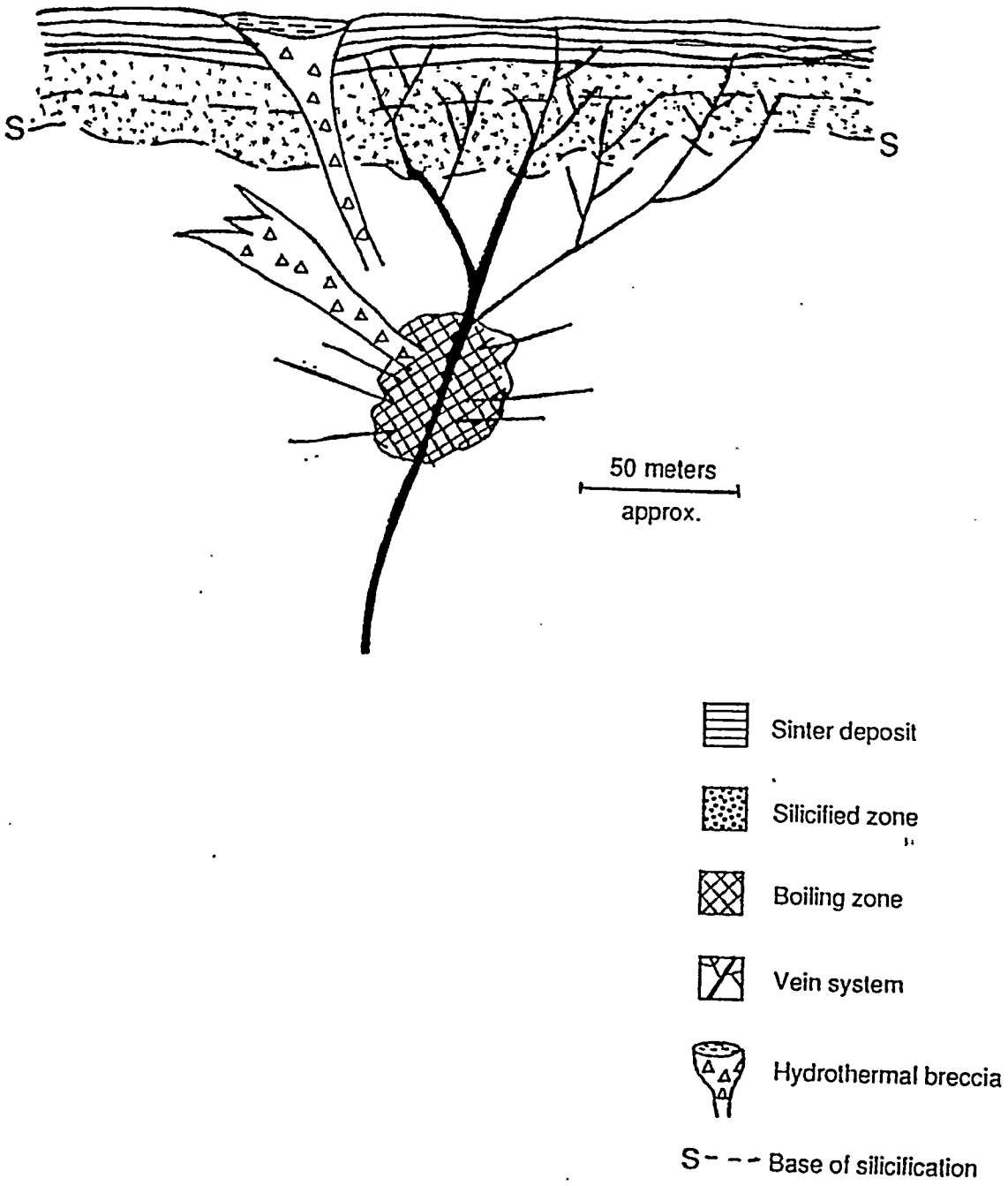

Figure 7. Schematic cross-section of epithermal vein deposits, after Berger and Eimon (1982). Calcite/opal deposits at Yucca Mountain have a similar morphology of a feeder vein bifurcating near the surface into multiple smaller veins and they also consist of surface sinter (calcite and opal travertine) and disseminated metal enrichment. Breccias at Yucca Mountain, such as the AMC breccias, may be hydrothermal breccias as shown in this diagram.

Figure 8. Pedogenic carbonate coating the undersides of a pebble in speleothemic fashion, River Mountains, just east of Las Vegas, Nevada. The rhyolitic terrain in the River Mountains is similar to that at Yucca Mountain. Photo: Carol A. Hill.

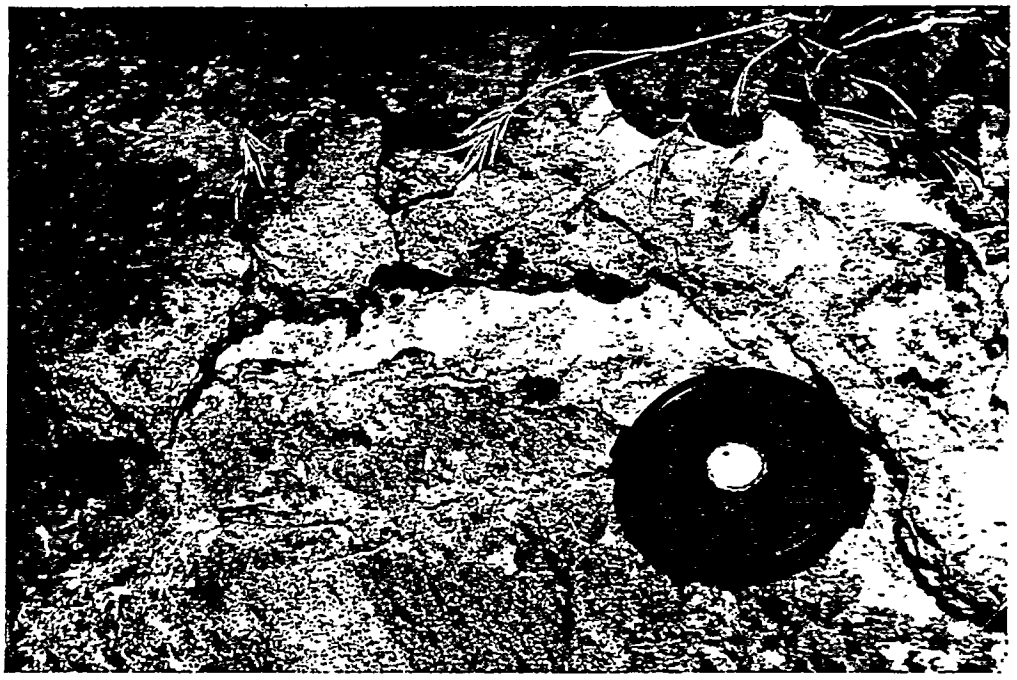

Figure 9. Opal and calcite/opal overlying the Tiva Canyon Member of the Paintbrush Tuff, west Busted Butte. The layer of pure hyalite opal directly overlies the volcanic rock and is overlain by the mixed texture calcite/opal. Photo: Carol A. Hill.

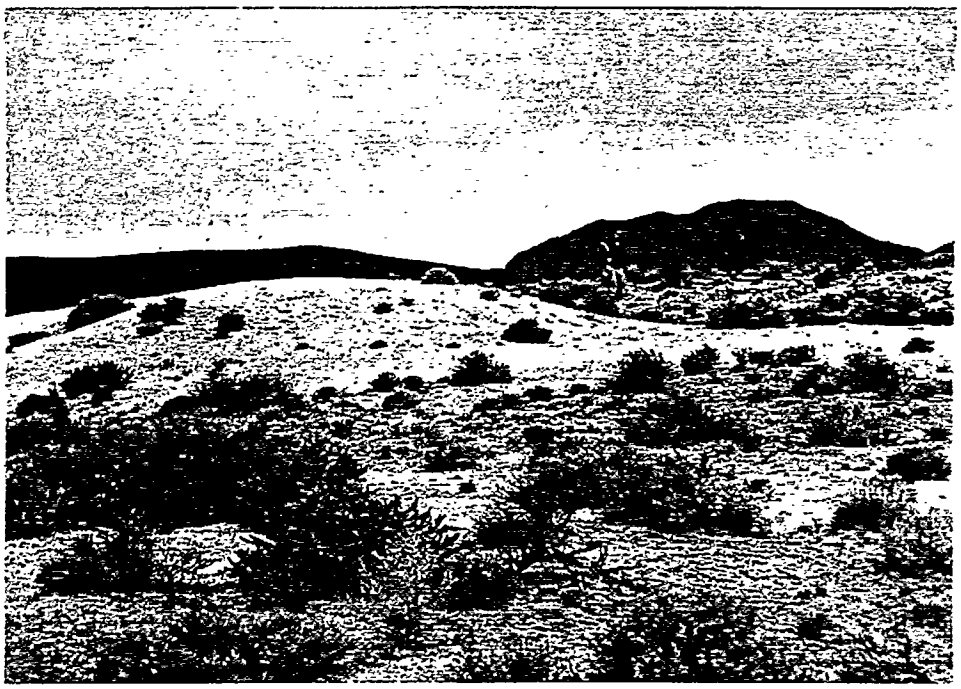

Figure 10. Spring mound of primarily carbonate material, Site 199. Photo: Carol A. Hill.

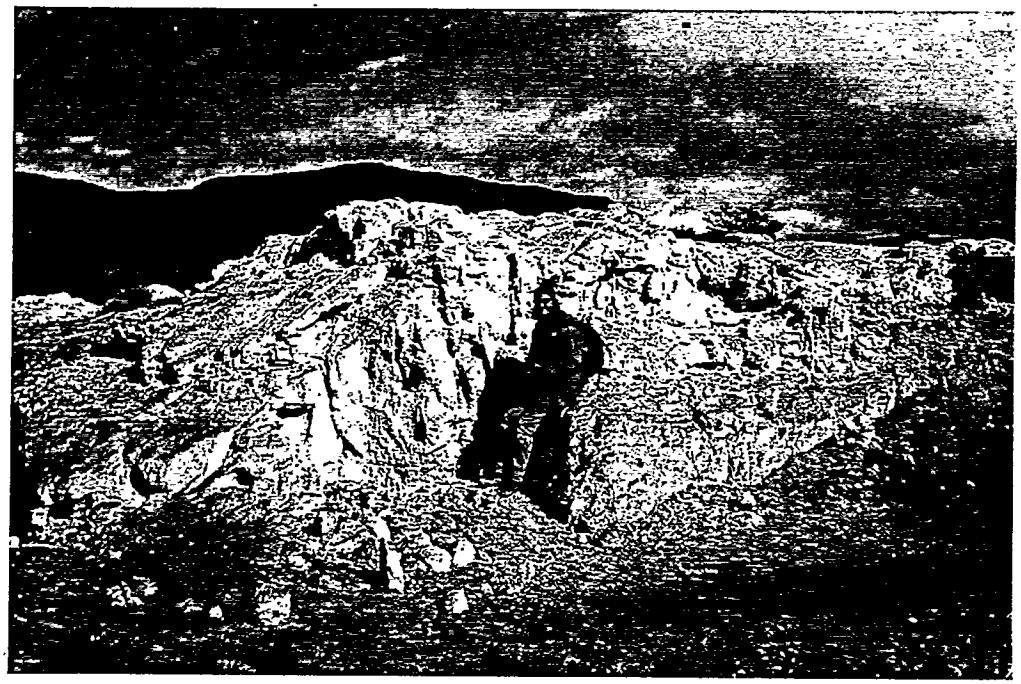

Figure 11. Spring mound composed primarily of silica, Diatomaceous Earth site. Photo: Carol A. Hill.

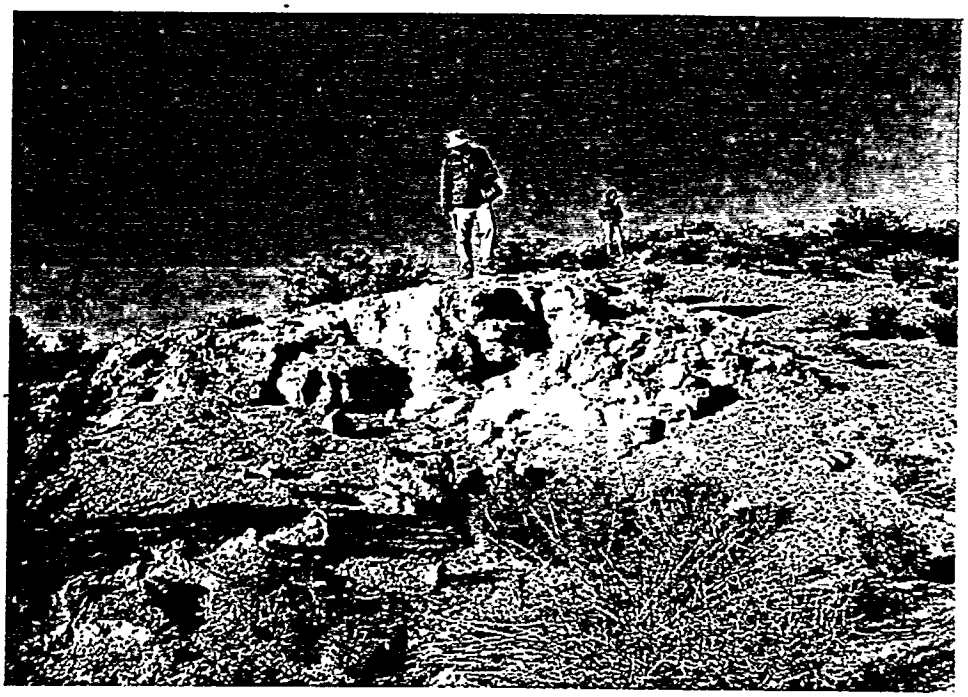

Figure 12. Wahmonie travertine/gypsite mound. The mound occurs along the same N30°E-trending fault zone as the Wahmonie Mining District. Photo: Carol A. Hill.

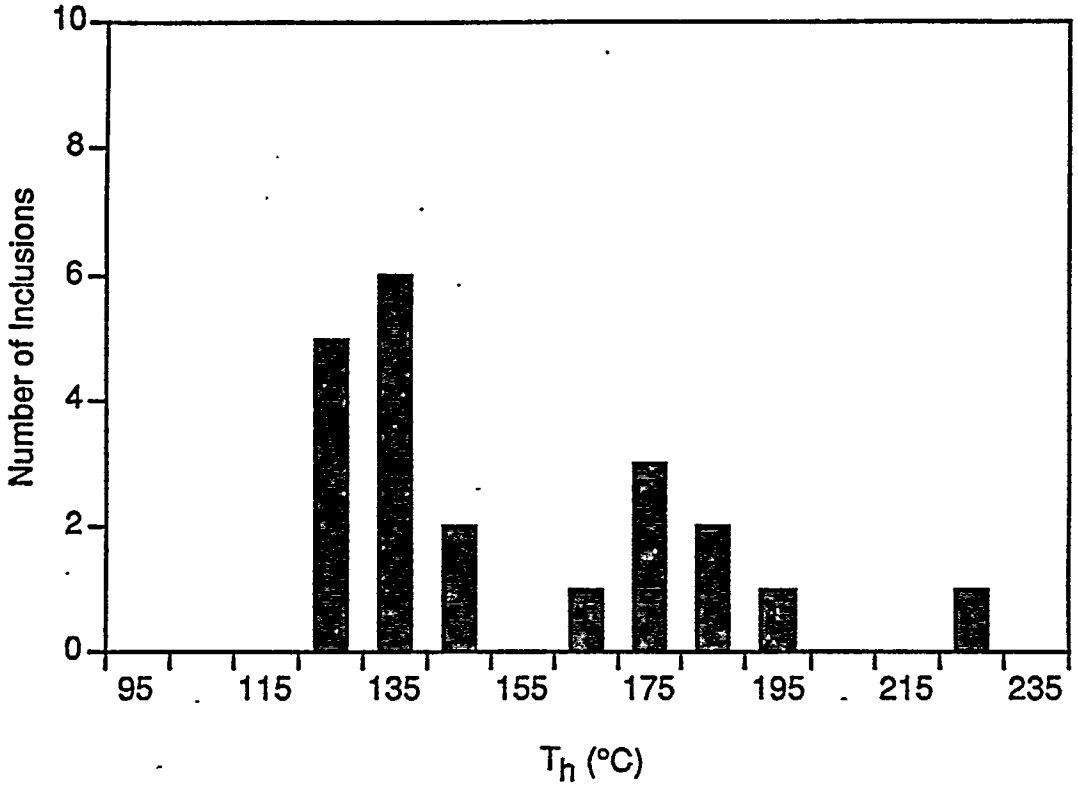

Figure 13. Distribution of fluid inclusion temperatures of homogenization (T_h), quartz, Pull Apart fault. From Harmon (1993).

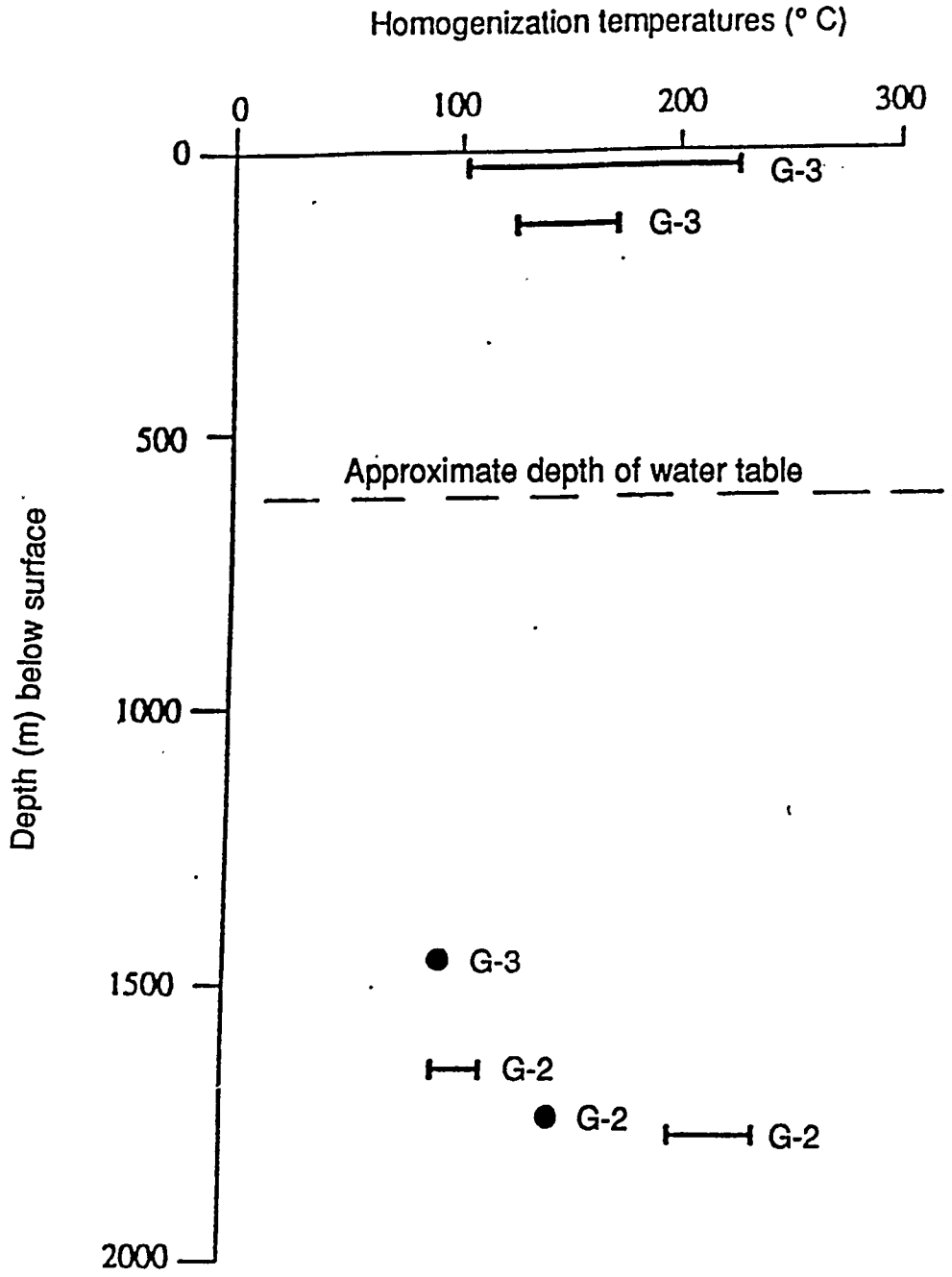

Figure 14. Fluid inclusion homogenization temperatures of calcite in boreholes USW G-2 and G–3/ GU-3. From Bish (1989) and Syzmanski et al. (1993).

(A)

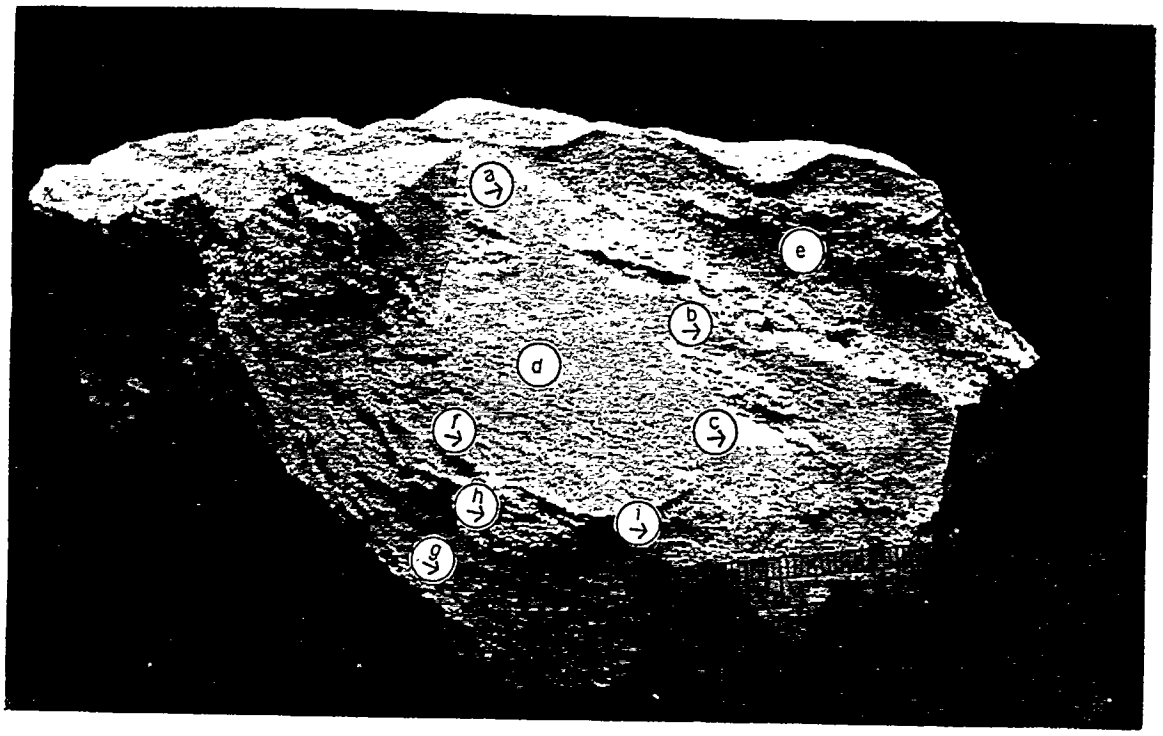

(B)

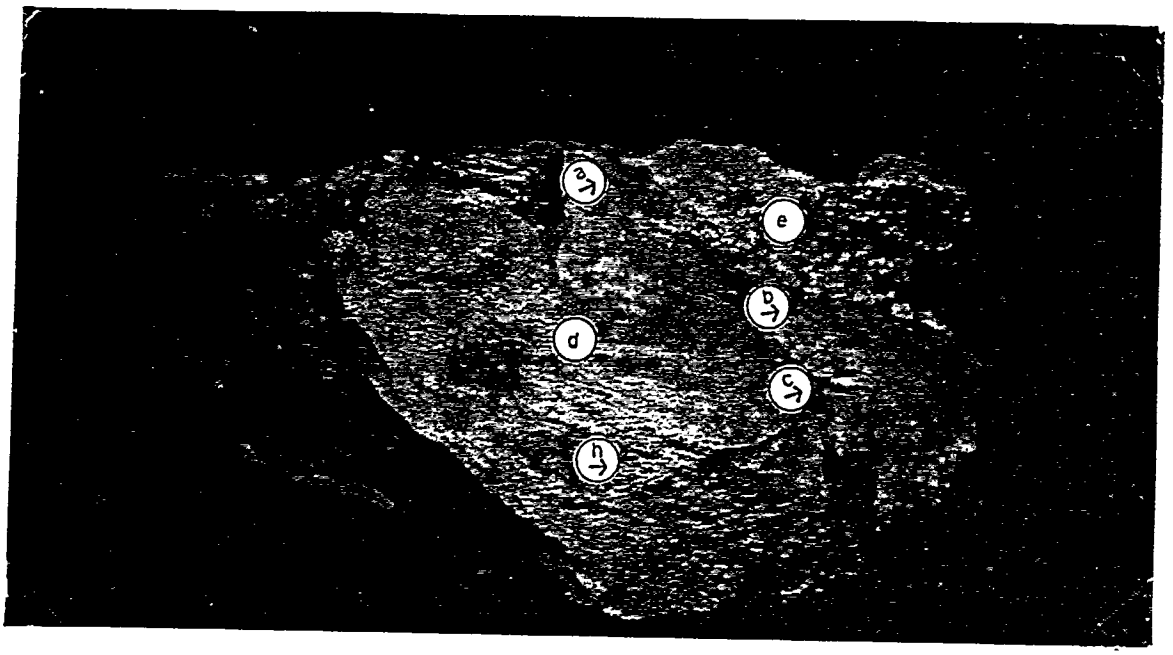

Figure 15. (A) Pods and seams of pure-texture, pearly opal (a,b,c) in a matrix of dense, buff-colored, mixed-textured calcite/opal (d). Lighter-colored sections are very soft and porous (easily scratched), massive-textured calcite/opal (e). Note the holes (vesicular/phenocrystic texture) throughout the mass, especially in the dense, buff colored calcite/opal (f,g), but also in the massive-textured calcite/opal (h). Also note how the vesicles seem to line up in bands (i and elsewhere). (B) Using a UVG-54 Mineralight, this photo (same position as A) illustrates bands of pure opal fluorescing a brilliant green (a,b,c) in a mixed-textured calcite/opal matrix which does not fluoresce (d,e,h). Sample is from Trench 14. Photos: Christine M. Schluter.

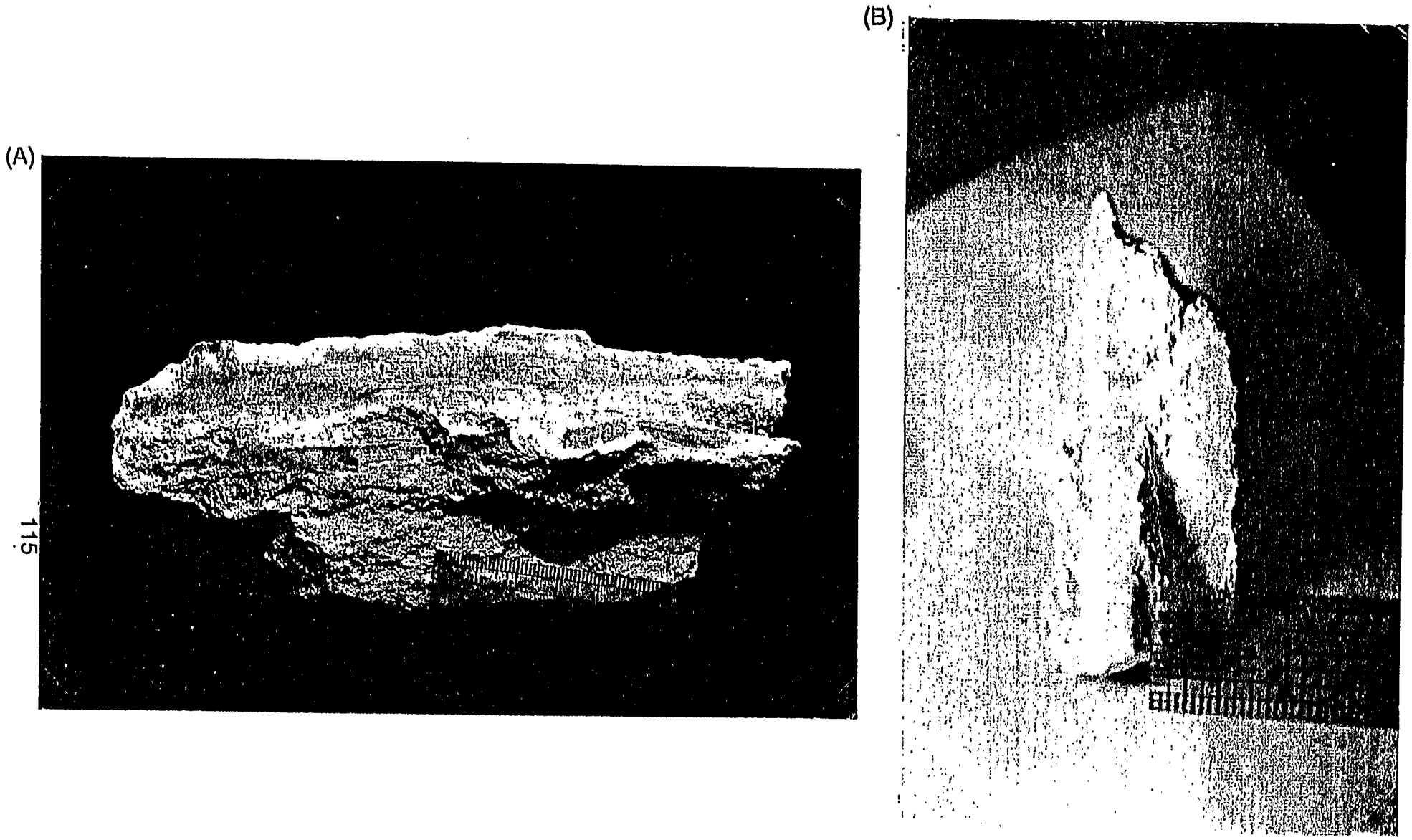

Figure 16. Banding in a mixed-textured calcite/opal matrix. Banding represents different mixtures of calcite and opal. (A) Horizontal banding, WT-7, and (B) vertical banding, east Busted Butte. Photos: Christine M. Schluter.

(A)

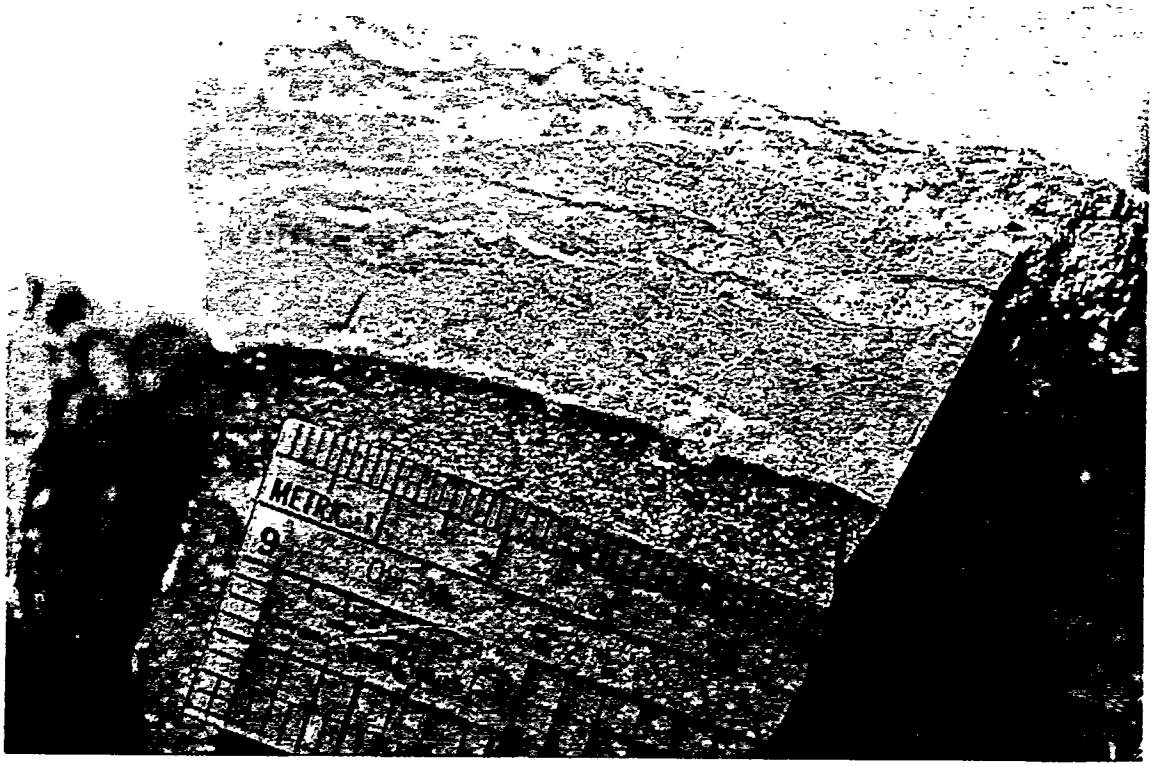

(B)

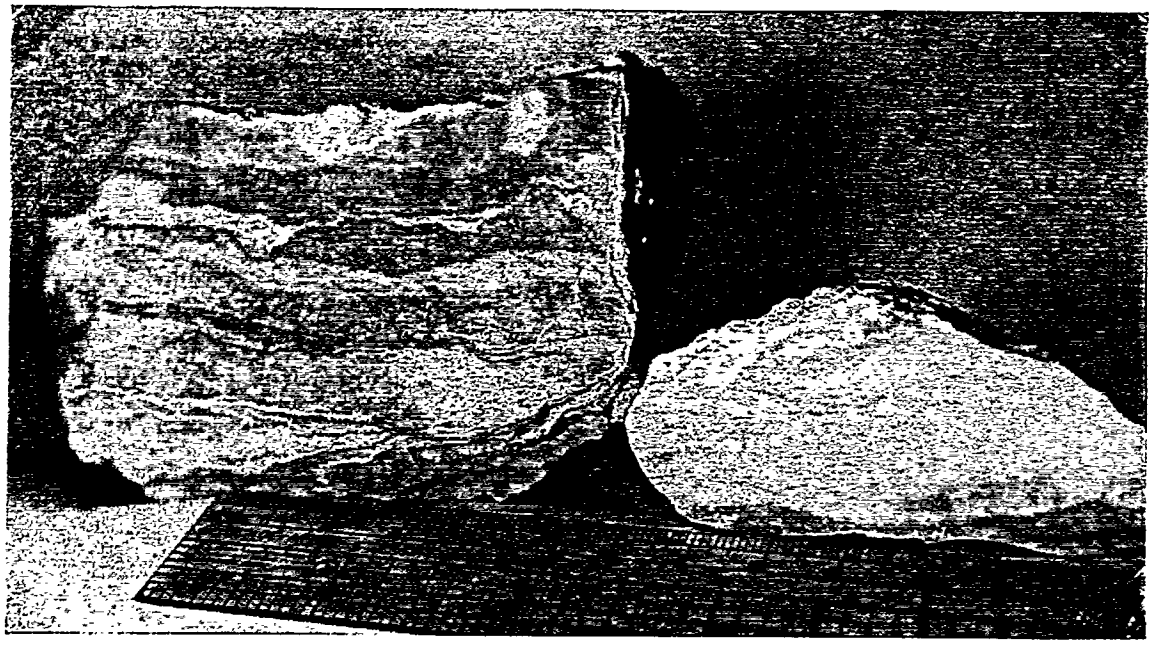

Figure 17. Two more examples of banded/laminated texture. (A) Laminated texture where the individual layers are narrow (a few millimeters). This sample also displays flow texture, where darker and lighter bands exhibit a marbly or wavy pattern. Note the dark reaction rim at the edge of the Tiva Canyon tuff where it comes in contact with the calcite/opal matrix. Under thin section this rim does not appear to have been altered or invaded by calcite/opal; rather, it appears to be a "baked" rim possibly caused by hot calcite/opal solutions. (B) Two banded textures from the Wailing Wall. Photos: Christine M. Schluter.

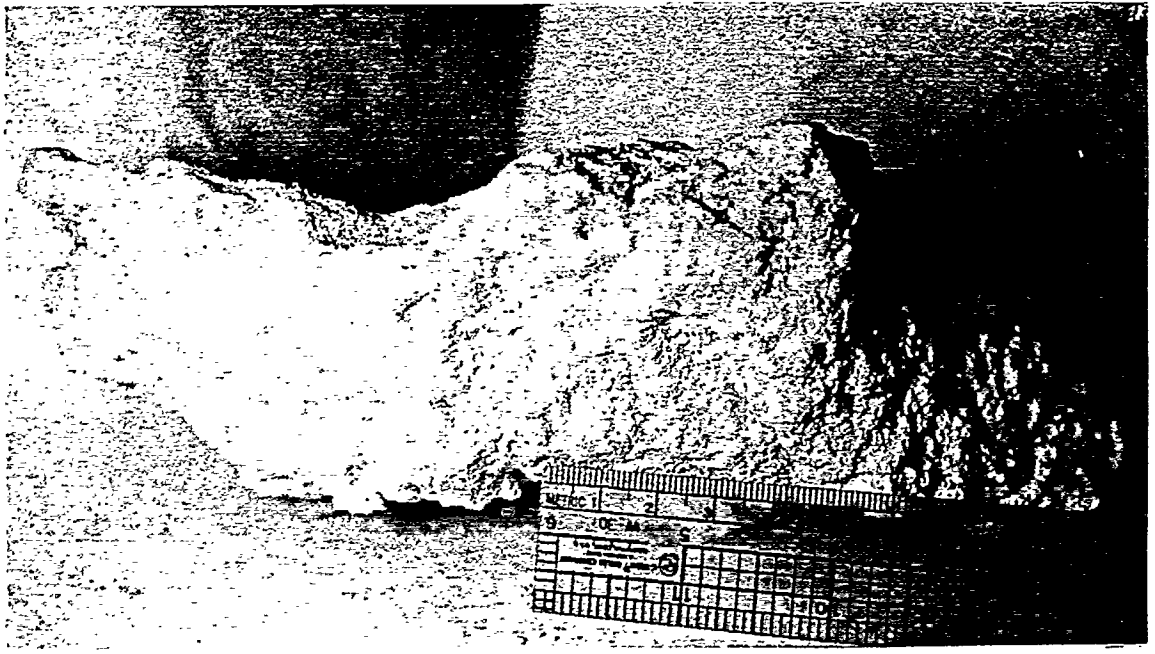

Figure 18. Massive texture showing porous, unlayered to roughly-layered, calcite/gypsum. This sample was collected from the Wahmonie travertine/gypsite mound and consists of about 70–80% calcite and 20–30% gypsum. Photo: Christine M. Schluter.

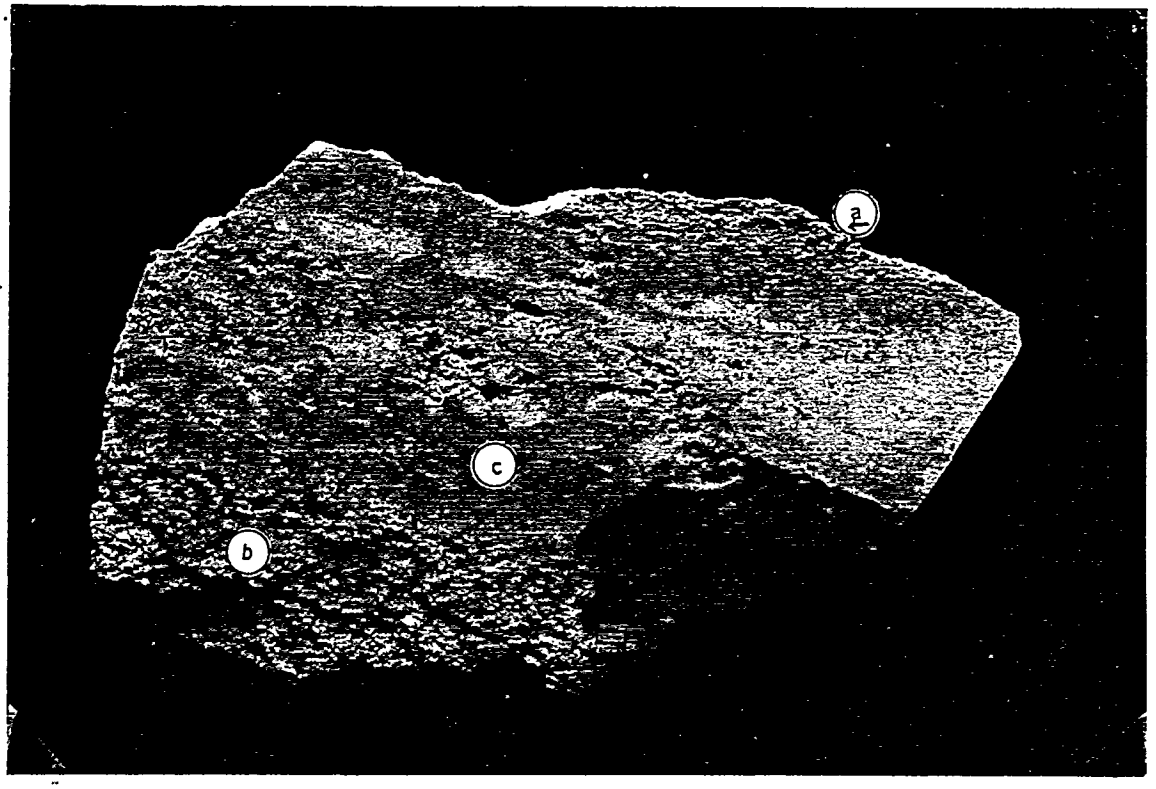

Figure 19. Powdery-texture calcitic layers (a,b) interbedded with dense, buff-colored, mixed-textured calcite/opal (c). This sample was collected from the Bare Mountain Mining District west of Yucca Mountain, yet it displays textures identical to samples collected from Yucca Mountain. Photo: Christine M. Schluter.

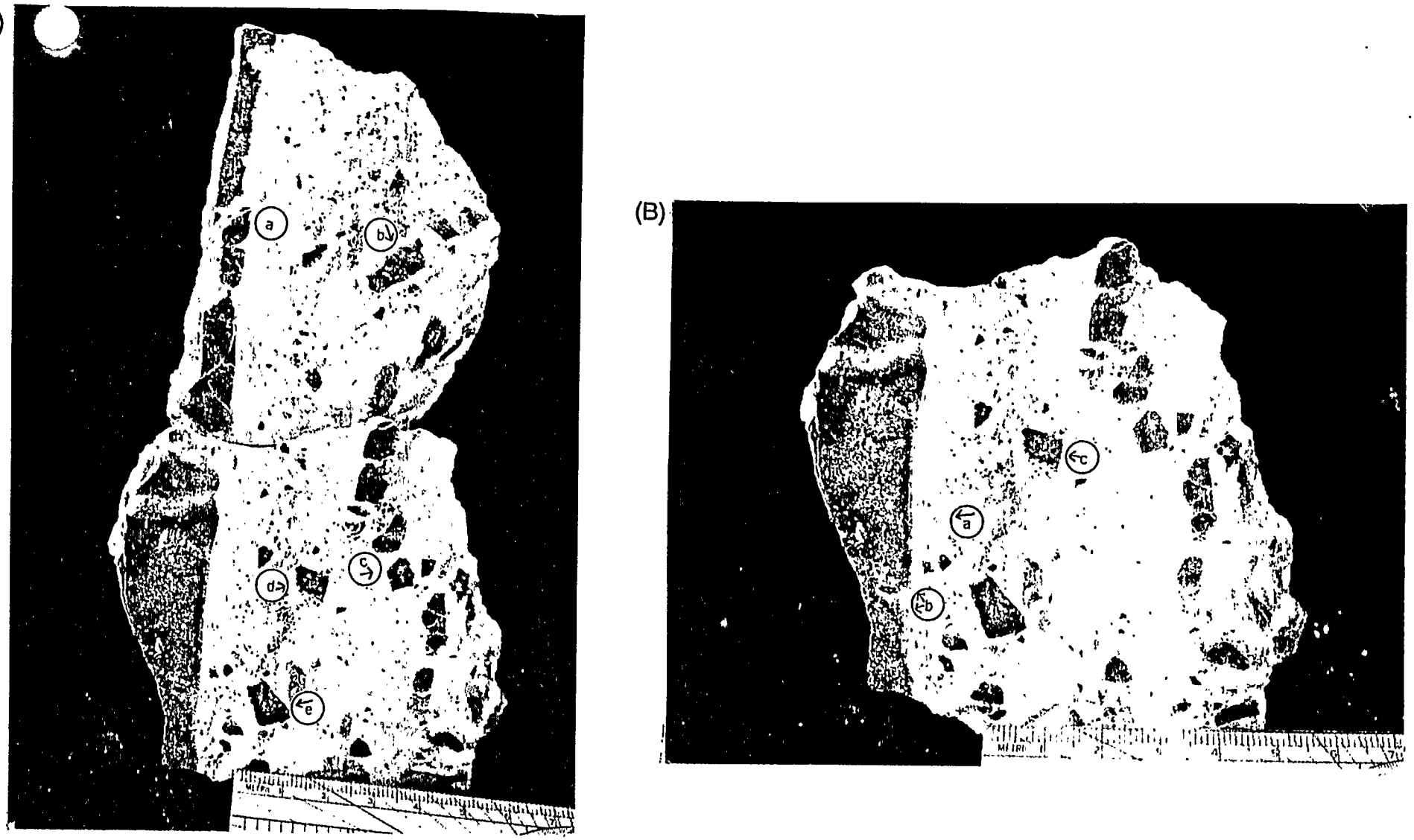

Figure 20. Mosaic- and floating-brecciated texture, Trench 14. (A) Note the mosaic-brecciated texture on the left and how the clasts at (a) have been cross-cut by calcite/opal material and offset slightly to the right. Note also the mosaic- to floating-brecciated textures on the right; how the clast at (b) has been turned about 30° to the vertical and how the "line of clasts" veers to the right at (c). Clasts (d) and (e) may have been part of the "line" but were swept to the left. (B) Close-up of bottom part of (A) which shows the marbly flow-texture of the calcite/opal matrix (e.g., at a). Note the possible reaction (baked?) rims surrounding clasts (b) and (c). Photos: Christine M. Schluter.

(A)

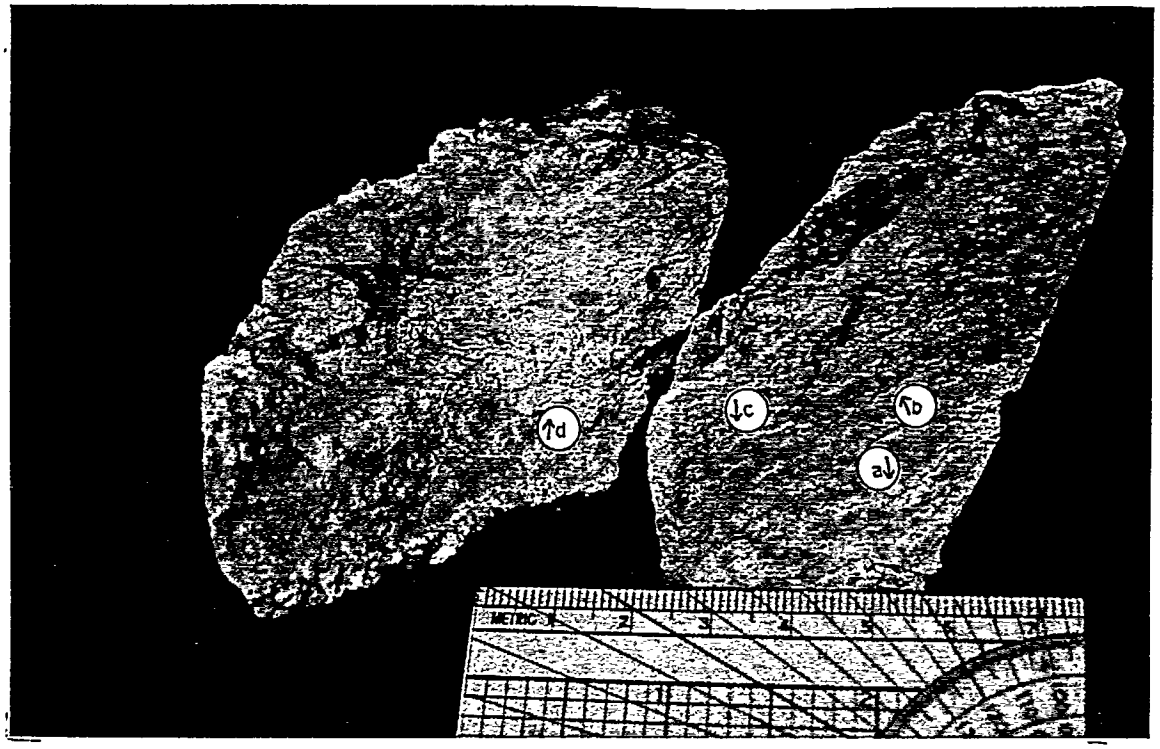

(B)

Figure 21. Vesicular/phenocrystic texture: (A) Note how the vesicles are aligned in rows along roughly-layered banded sequences; lighter bands (a), darker bands (b), or along wavy flow texture (c,d). This sample was collected from the Bare Mountain Mining District west of Yucca Mountain. (B) Note how the vesicles occur in both the mixed-texture, buff-colored calcite/opal (a) and also across the boundary into the powdery-texture matrix (b). This sample was collected at Trench 14 and possibly indicates that the mixed and powdery textures formed penecontemporaneously, with degassing of solutions creating the vesicular texture. Photos: Christine M. Schluter.

(A)

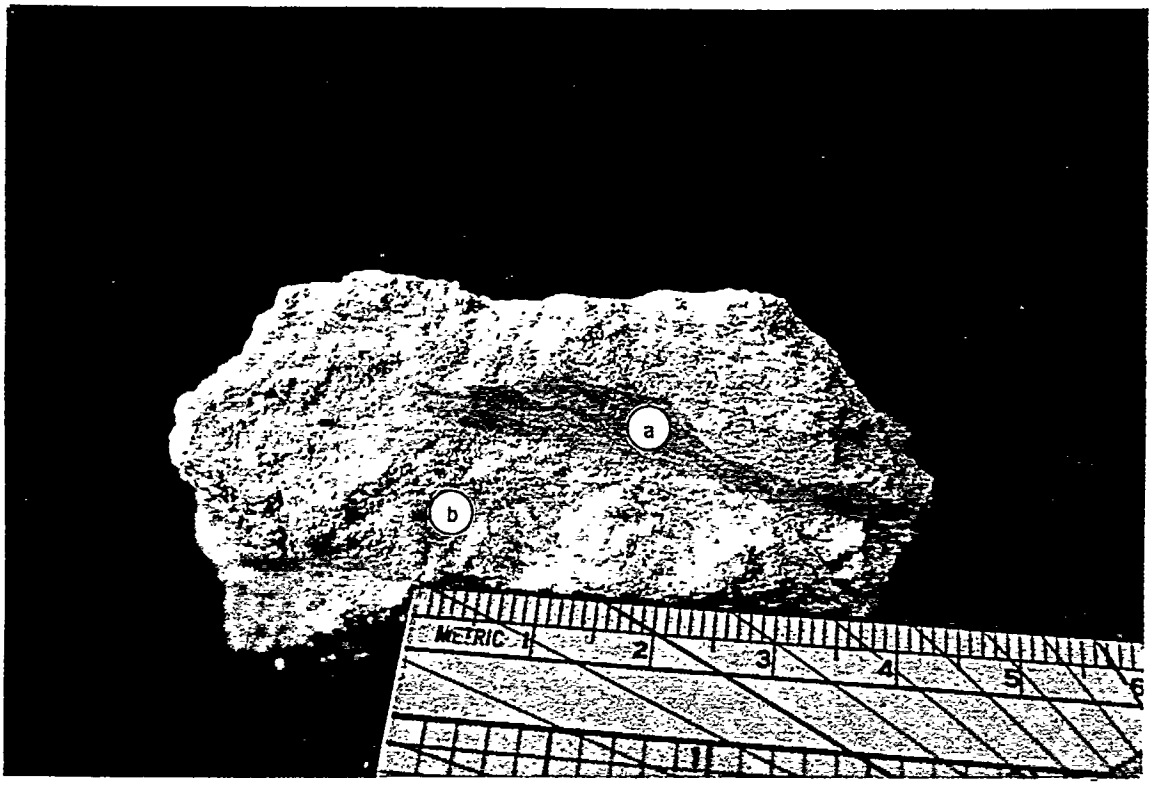

(B)

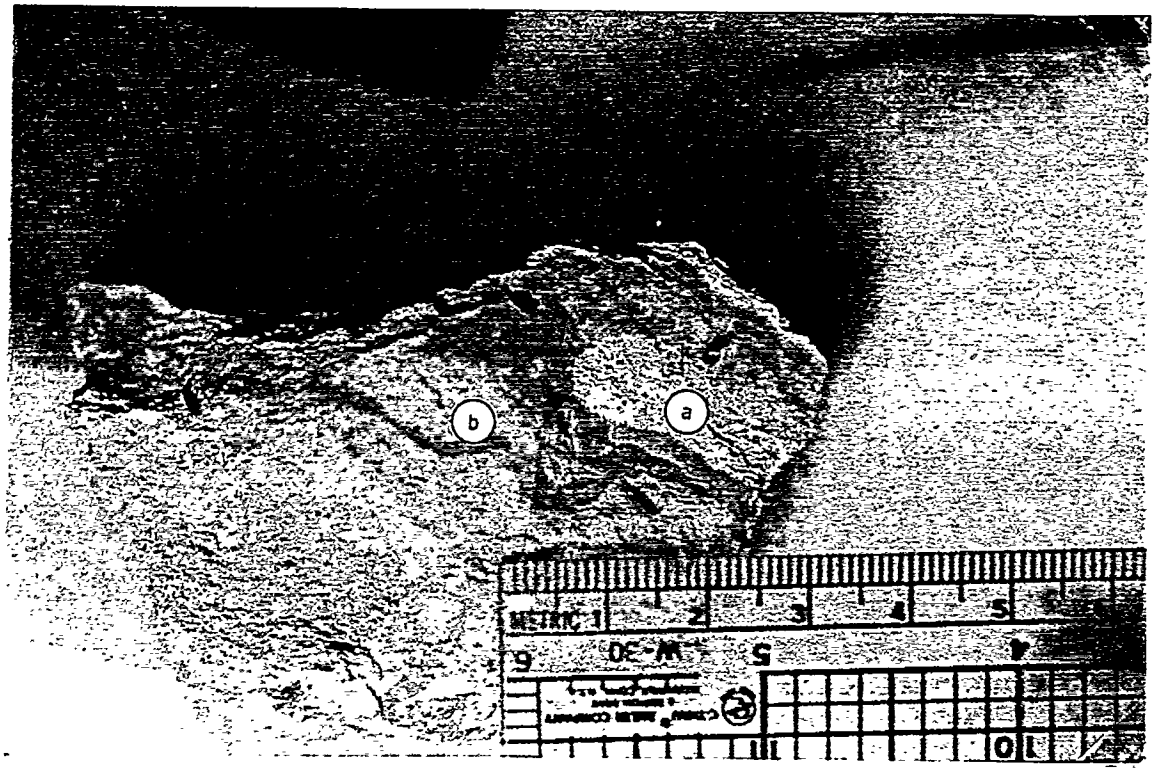

Figure 22. Two examples of invasive texture: (A) where dense, buff-colored, calcite/opal of mixed texture (a) has invaded a powdery-textured mass composed primarily of calcite (b), Wailing Wall; (B) where a "blob" displaying powdery texture (a) has invaded a calcite/opal banded mass of mixed texture, WT-7 (b). Photos: Christine M. Schluter.

Figure 23. Root cast texture, west Busted Butte. Photo: Carol A. Hill.

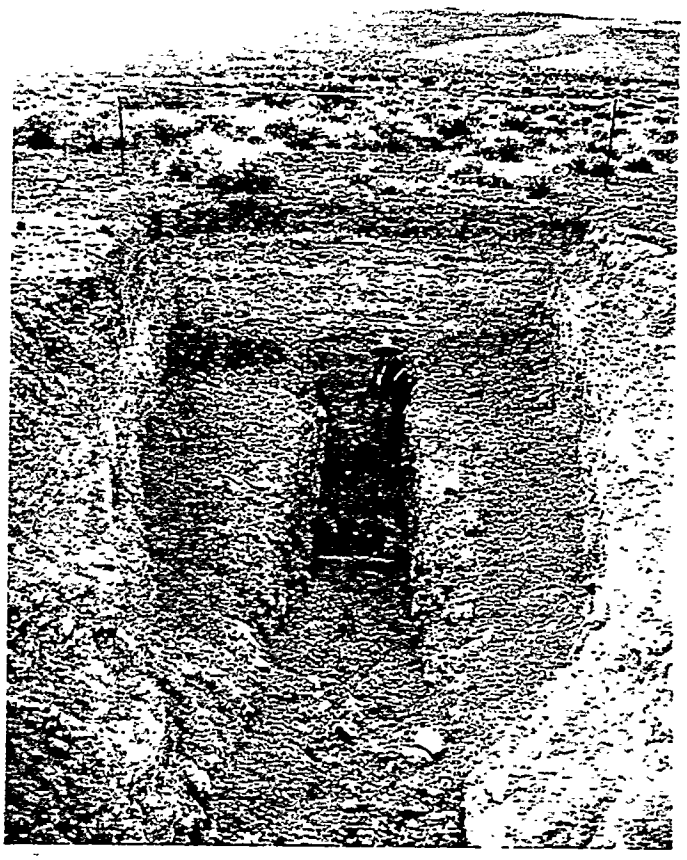

Figure 24. A petrocalcic horizon approximately 1 m thick, Fortymile Wash-Midway Valley. A pedogenic calcrete horizon this thick would have taken hundreds of thousands (or more) years to have formed. This "true" pedogenic calcrete horizon is not located directly along a fault nor does it contain any layers of opal (see description of sample FMW-3 collected from this site; Table 1).

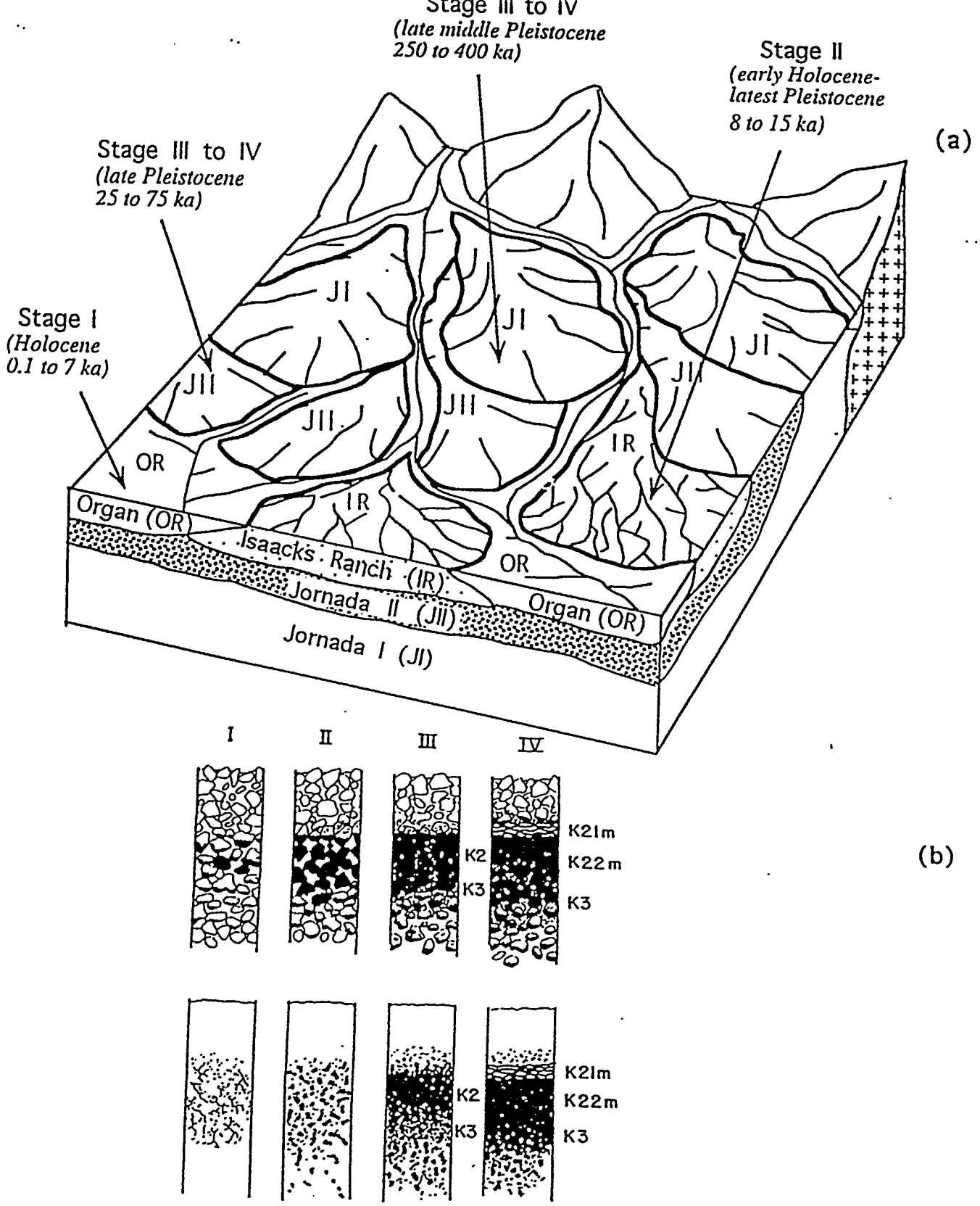

Figure 25. (a) Illustration of the geomorphic surfaces and associated soils on the fan-piedmont of the Organ Mountains in southern New Mexico (modified from Monger, 1993; names of geomorphic surfaces, their ages, and morphogenic stages are from Gile et al., 1981). Similar soil patterns were observed on and near the Nevada Test Site. (b) Illustration of the morphogenetic carbonate stages of Gile et al. (1966). Carbonate is represented by black shading.

Figure 26. Pedogenic calcrete horizon, Red Cone, Crater Flat. The upper, surface layer is a desert pavement composed of volcanic shards and pieces of calcrete which moved up to the surface from below. A vesicular A horizon approximately 15 cm thick occurs below the desert pavement, and a pedogenic calcrete horizon (the white carbonate center of the dug-out trench) occurs below the vesicular A horizon. Pedogenic calcrete horizons such as this are common throughout Yucca Mountain on older geomorphic surfaces. Photo: Carol A. Hill.

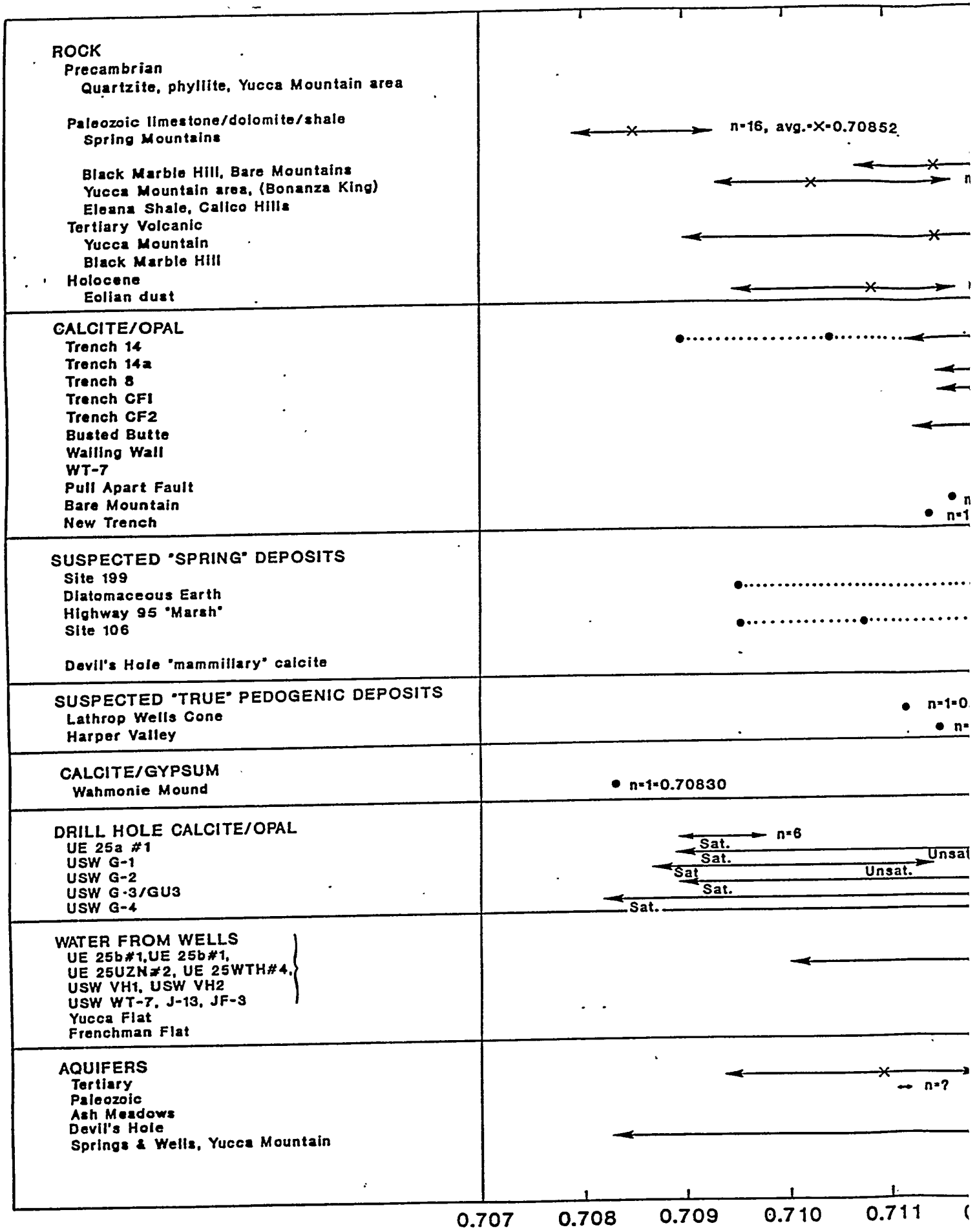

Figure 27. $^{87}Sr/^{86}Sr$ isotopic data, Yucca Mountain and vicinity.

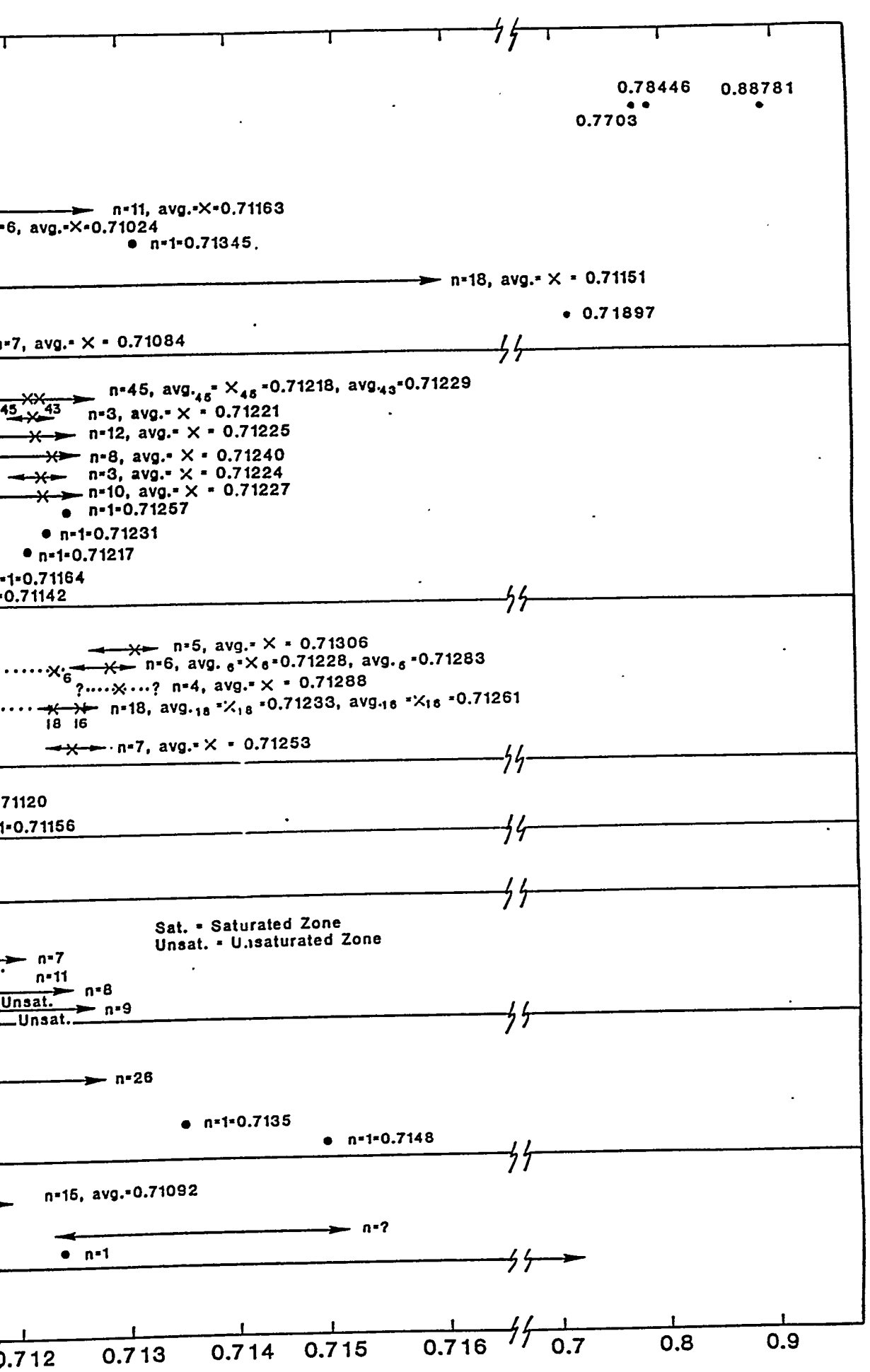
0.78446
0.88781
0.7703
n=11, avg.=X=0.71163
=6, avg.=X=0.71024
n=1=0.71345.
n=18, avg.= X = 0.71151
0.71897
=7, avg.= X = 0.71084
n=45, avg.45= X45 =0.71218, avg.43=0.71229
45 43
n=3, avg.= X = 0.71221
n=12, avg.= X = 0.71225
n=8, avg.= X = 0.71240
n=3, avg.= X = 0.71224
n=10, avg.= X = 0.71227
n=1=0.71257
n=1=0.71231
n=1=0.71217
=1=0.71164
=0.71142
n=5, avg.= X = 0.71306
6
n=6, avg.6=X6=0.71228, avg.6=0.71283
?....X...? n=4, avg.= X = 0.71288
18 16
n=18, avg.18 =X18 =0.71233, avg.16 =X16 =0.71261
n=7, avg.= X = 0.71253
71120
1=0.71156
Sat. = Saturated Zone
Unsat. = Unsaturated Zone
n=7
n=11
n=8
Unsat.
n=9
Unsat.
n=26
n=1=0.7135
n=1=0.7148
n=15, avg.=0.71092
n=?
n=1
0.712
0.713
0.714
0.715
0.716
0.7
0.8
0.9

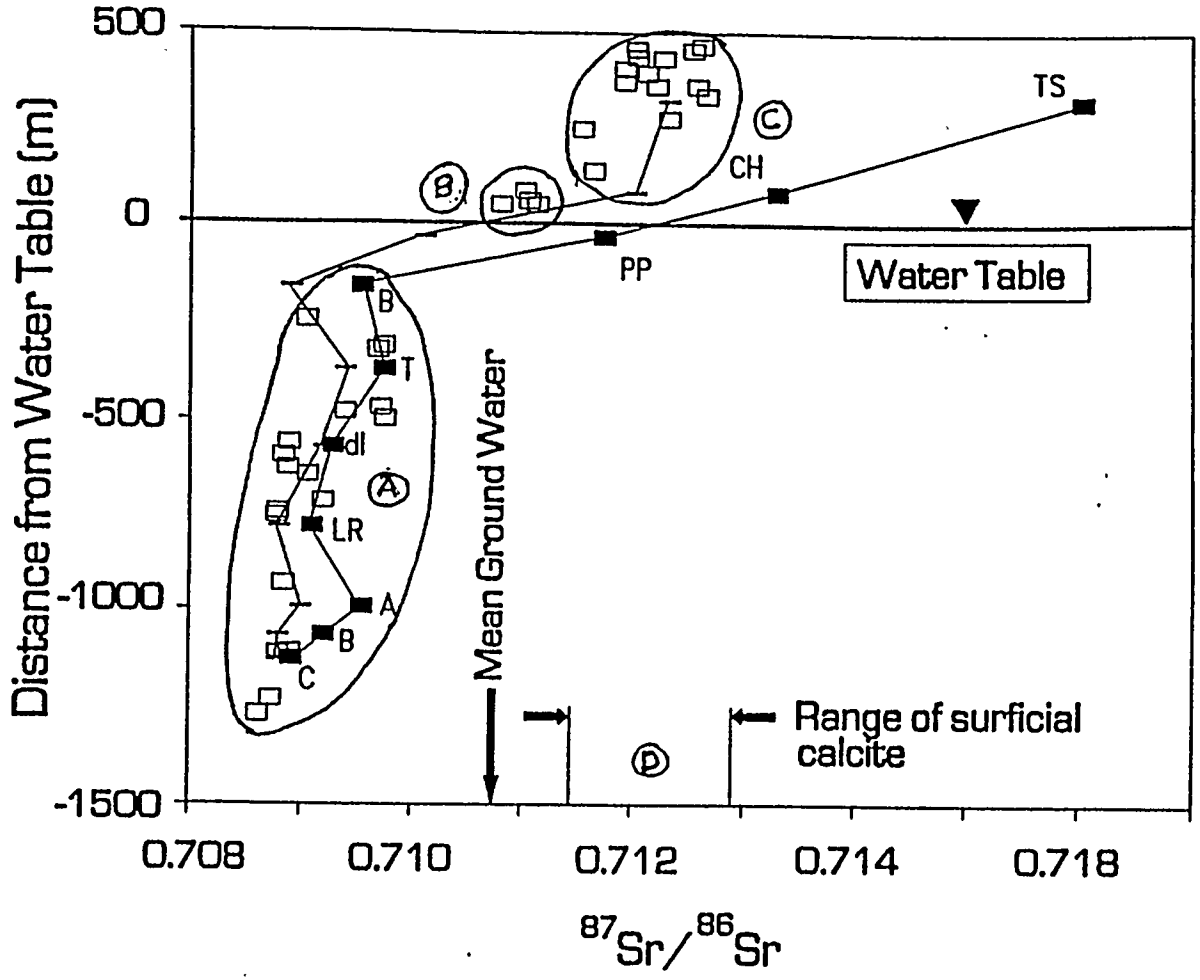

Figure 28. $^{87}Sr/^{86}Sr$ values (open rectangles) for calcite fracture fillings plotted as a function of distance from the modern water table. The range of $^{87}Sr/^{86}Sr$ values for surficial calcites from the Yucca Mountain area is shown in the lower part of the figure. The vertical arrow marks the average $^{87}Sr/^{86}Sr$ value for ground water from the Cenozoic volcanic aquifer. Present-day $^{87}Sr/^{86}Sr$ values for the volcanic rocks are shown by filled rectangles. The short horizontal lines are calculated initial values that the rocks would have had when they were deposited assuming closed-system evolution to the present-day. The rock units are: TS - Topopah Spring; CH - rhyolite of Calico Hills; PP - Prow Pass; B - Bullfrog; T - Tram; dl - dacite lava; LR - Lithic Ridge; A,B, and C - unnamed units. From Peterman et al. (1992).

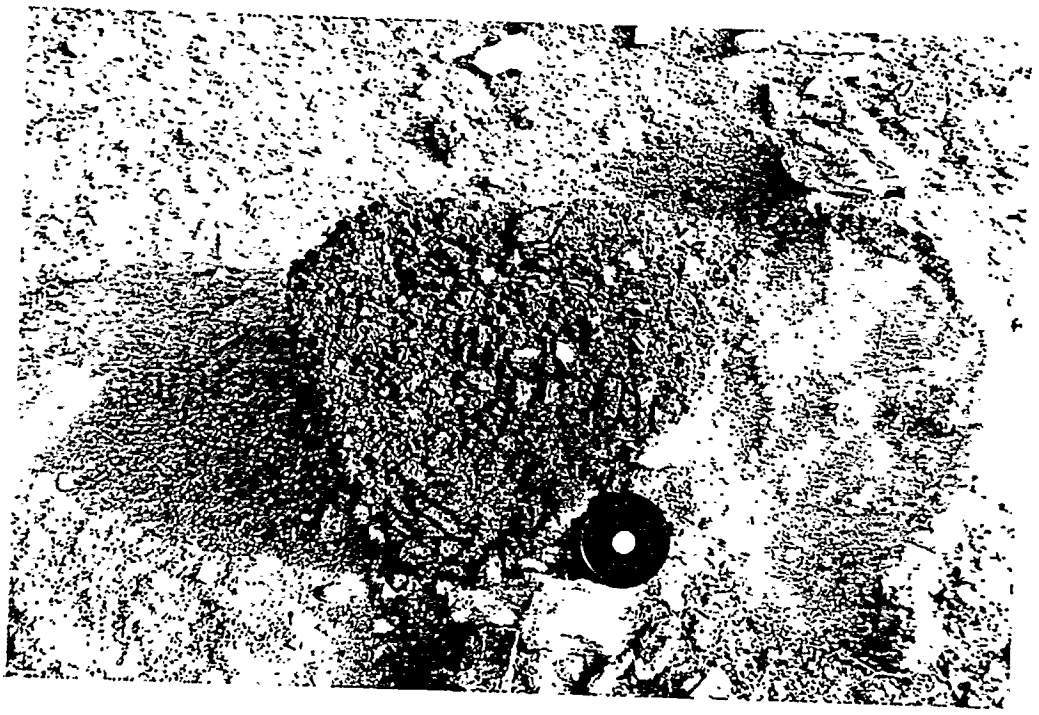

Figure 29. Piece of brecciated limestone from the Bonanza King Formation, Diatomaceous Earth site. Such limestone has been highly altered with respect to its strontium and carbon-oxygen isotopic composition. This brecciation and alteration is most likely due to thrust faulting where the Paleozoic Bonanza King limestone has been thrust over Tertiary volcanic rock. Photo: Carol A. Hill.

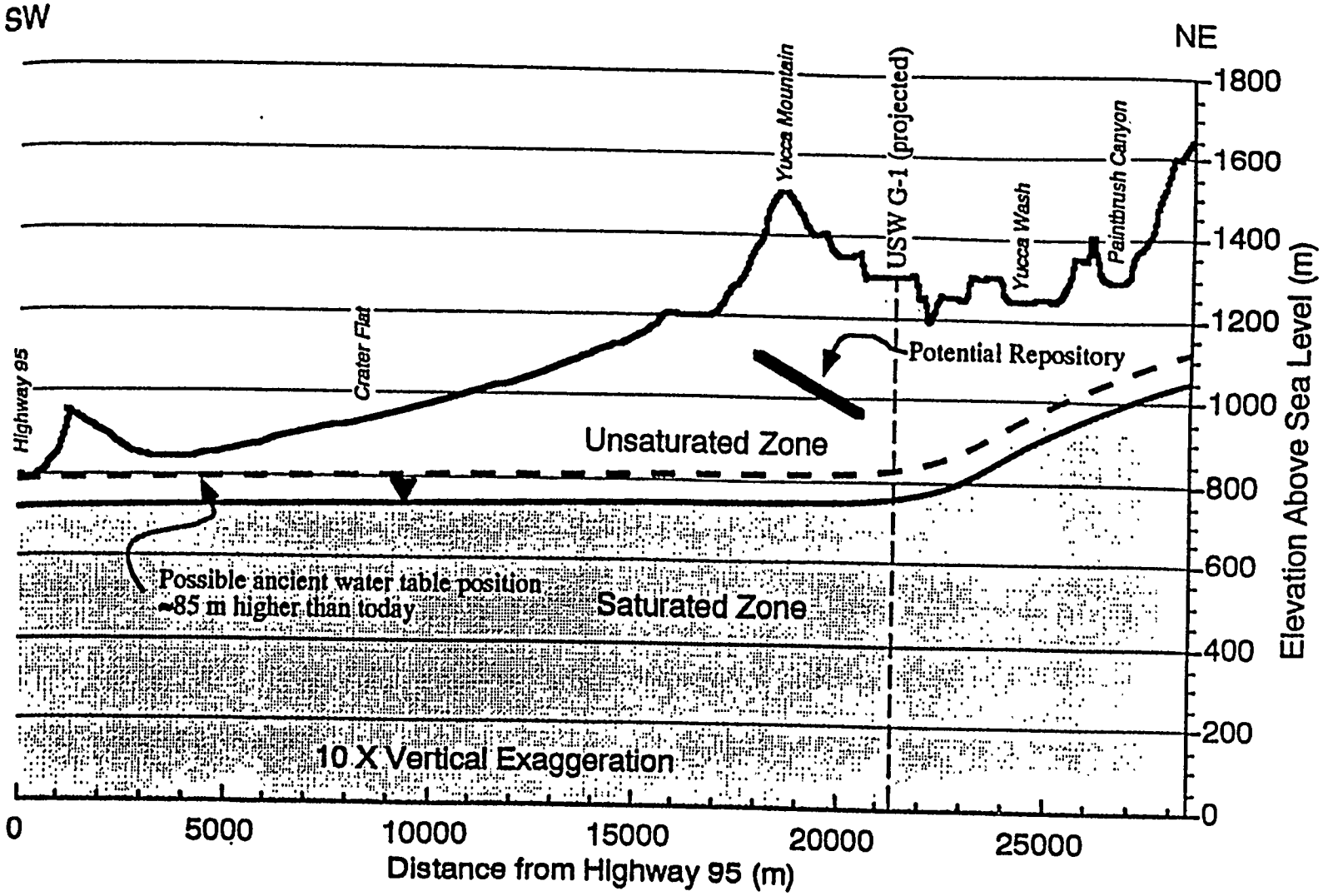

Figure 30. Cross section drawn N30E from the discharge site along highway 95 through Crater Flat and Yucca Mountain showing a possible ~85 m rise in the water table. Section is drawn at 10 X vertical exaggeration. From Marshall et al. (1993).

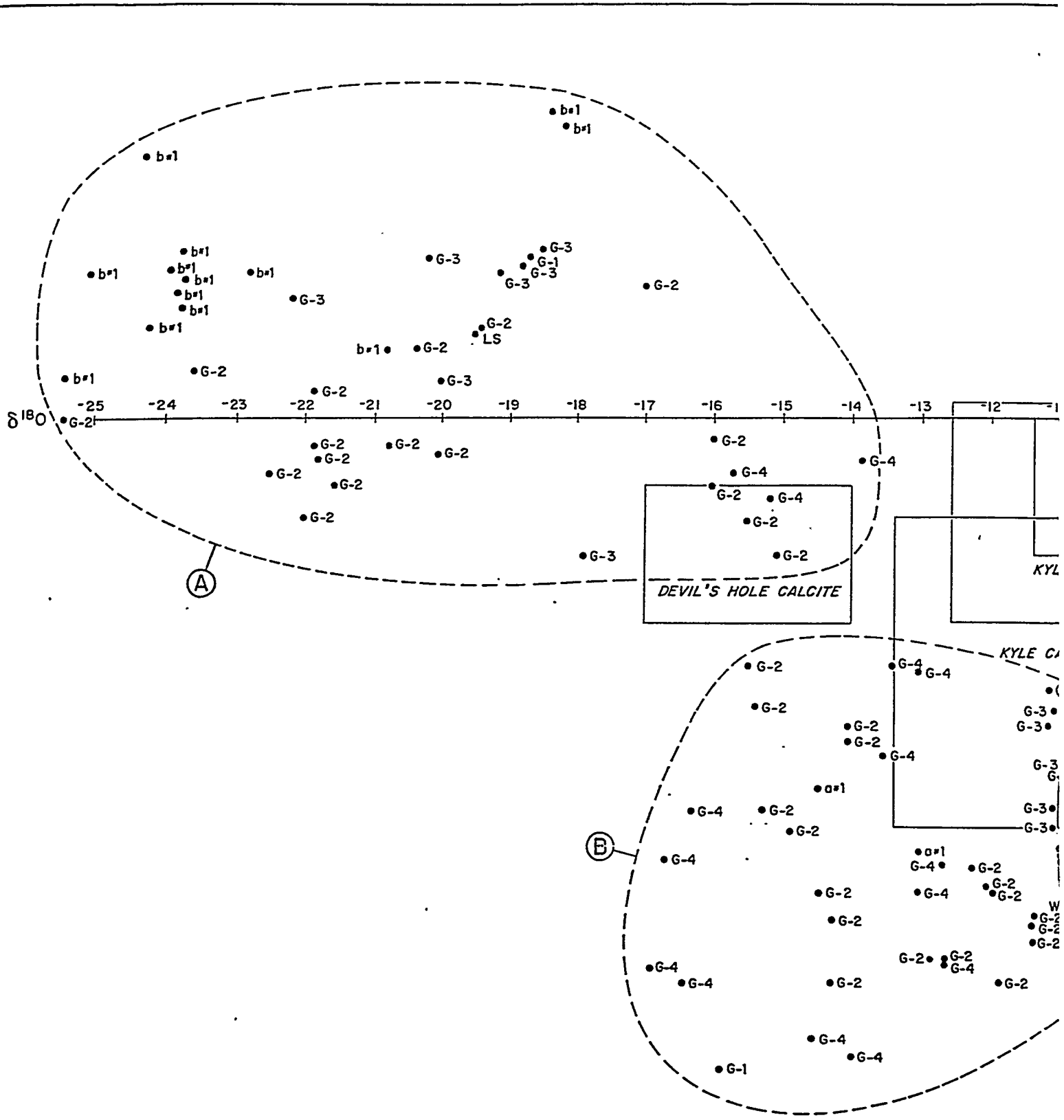

Figure 31. Carbon-oxygen isotopes, carbonate deposits, Yucca Mountain and vicinity.

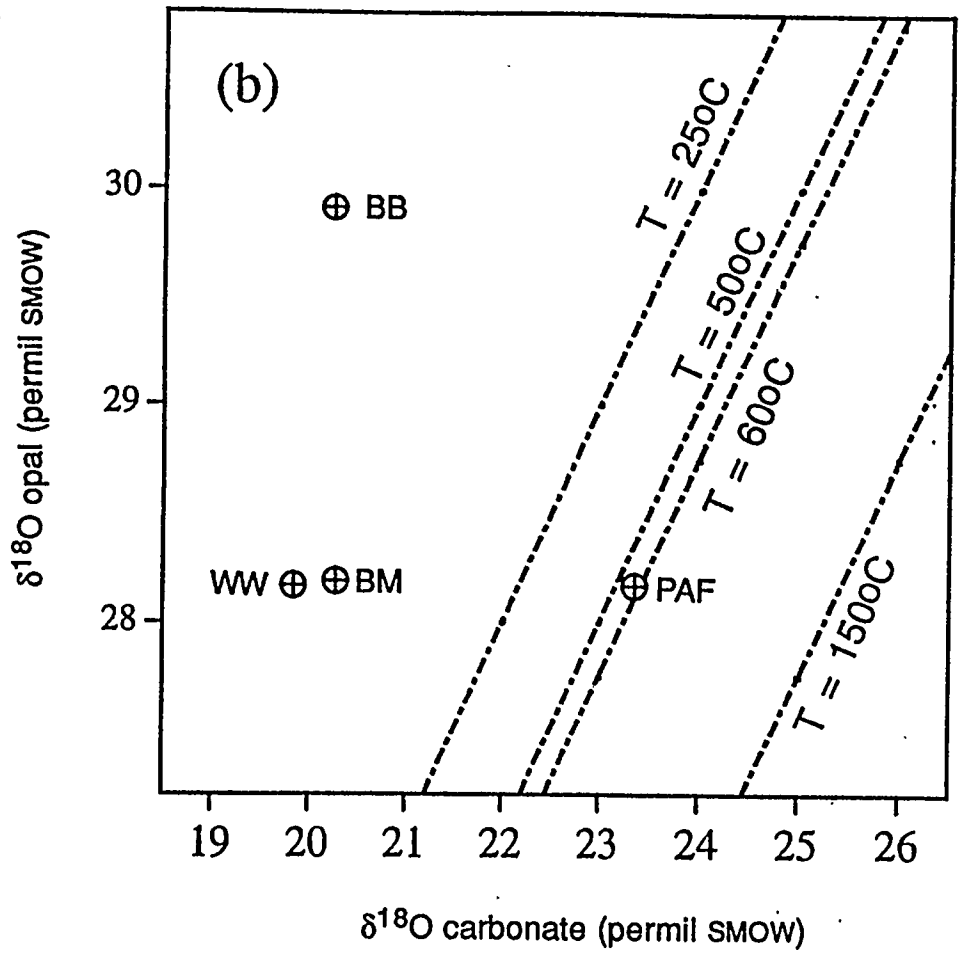

Figure 32. Carbonate/opal pairs and isotherms. PAF = Pull Apart fault, BB = Busted Butte, WW = Wailing Wall, BM = Bare Mountain. Values taken from Table 2. From Harmon (1993).

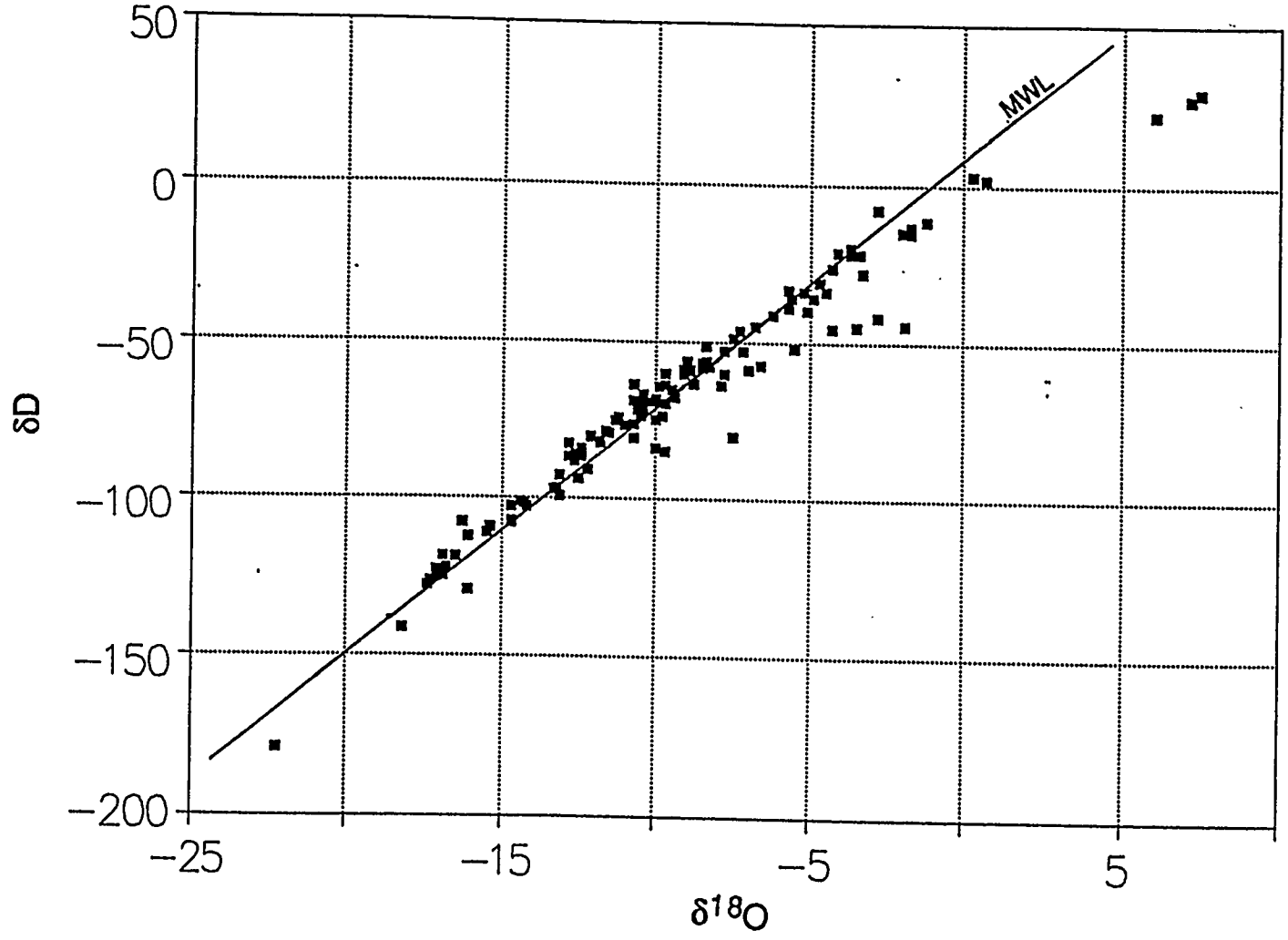

Figure 33. Deuterium-oxygen diagram for precipitation, Yucca Mountain. Mean of deuterium values is -67, that for oxygen is -9.3. From data of Milne et al. (1987). Data of Ingraham et al. (1990) fall within this range of values.

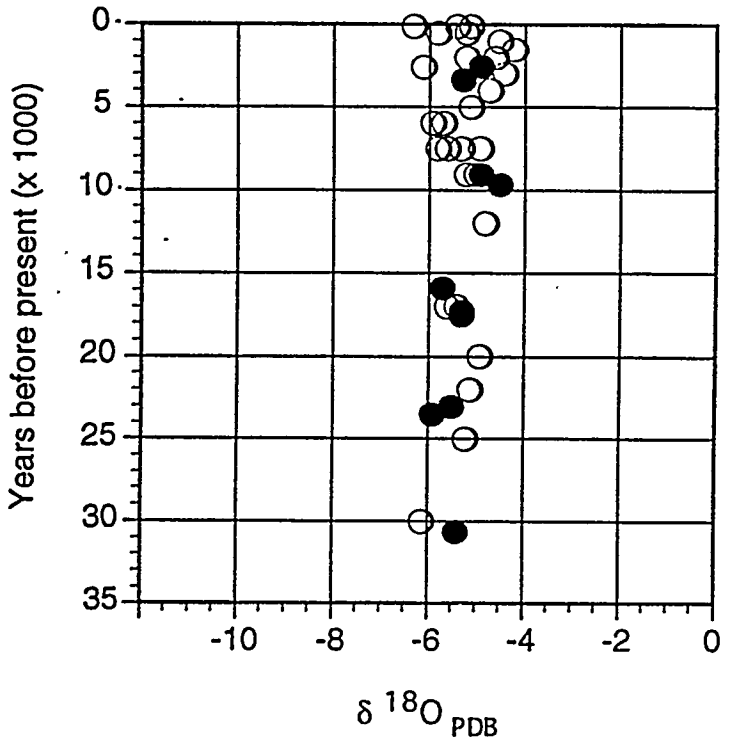

Figure 34. $\delta^{18}O$ values of pedogenic carbonates from southern New Mexico plotted against time. Solid circles represent radiocarbon-dated samples. After Monger (1993).

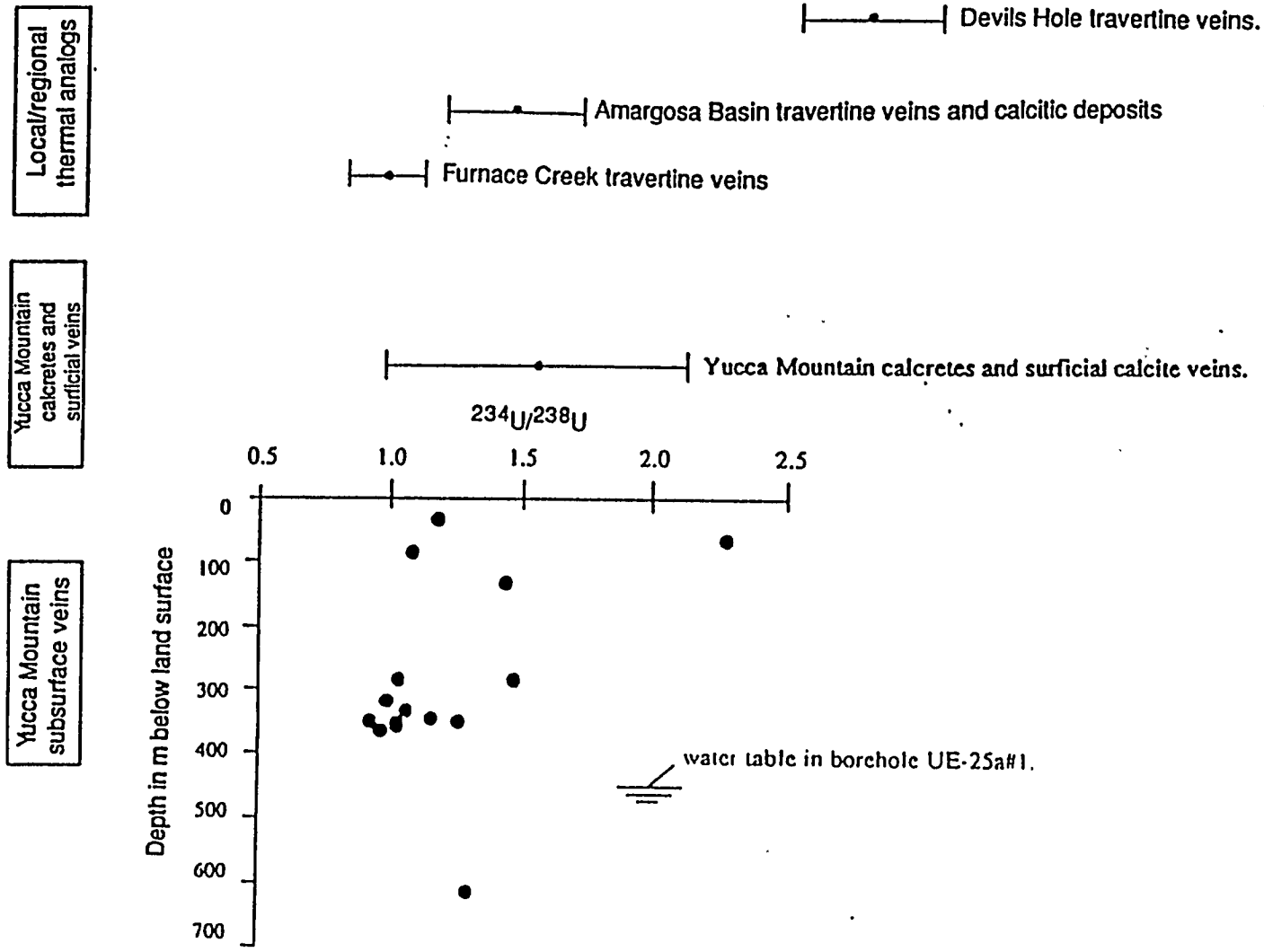

Figure 35. Isotopic character of uranium incorporated in the Yucca Mountain veins and calcretes and the local travertine veins and associated surficial deposits. Isotopic data from Szabo et al. (1981); Szabo and O'Malley (1985); and Szabo and Kyser (1985).

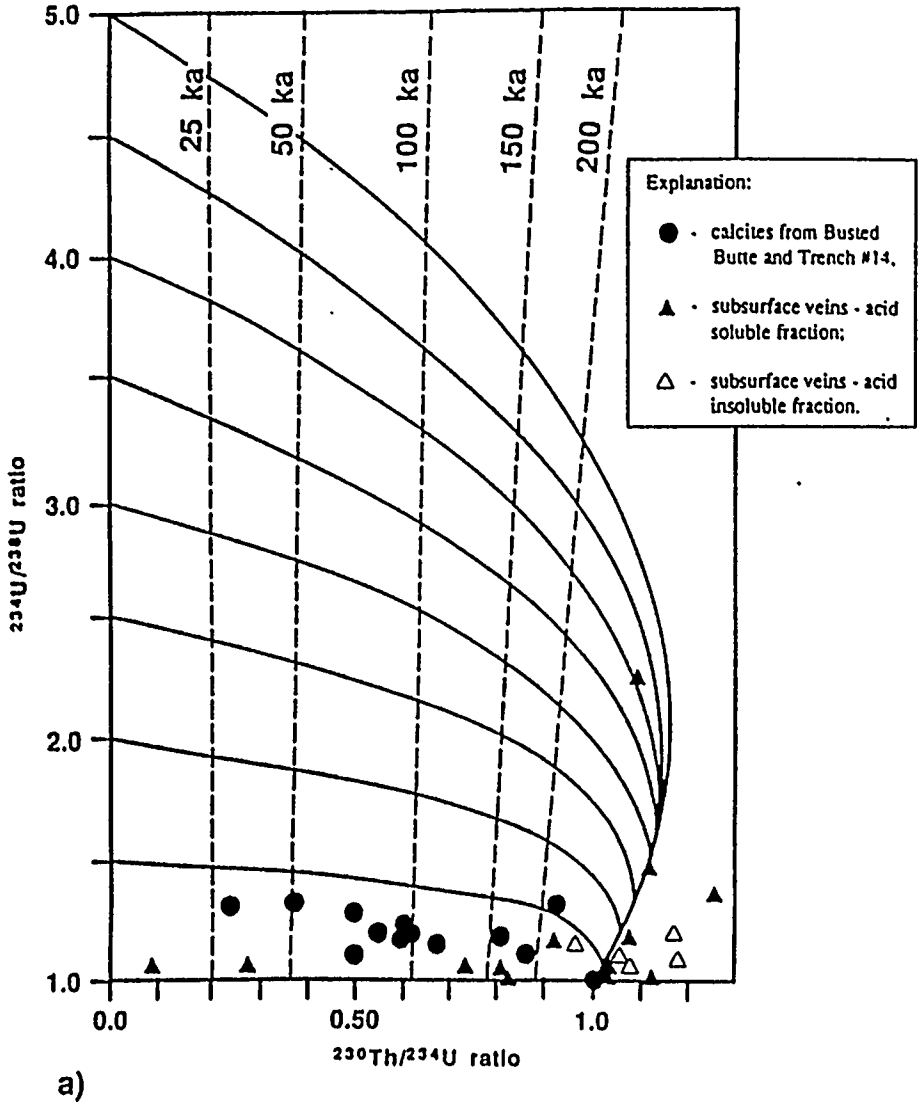

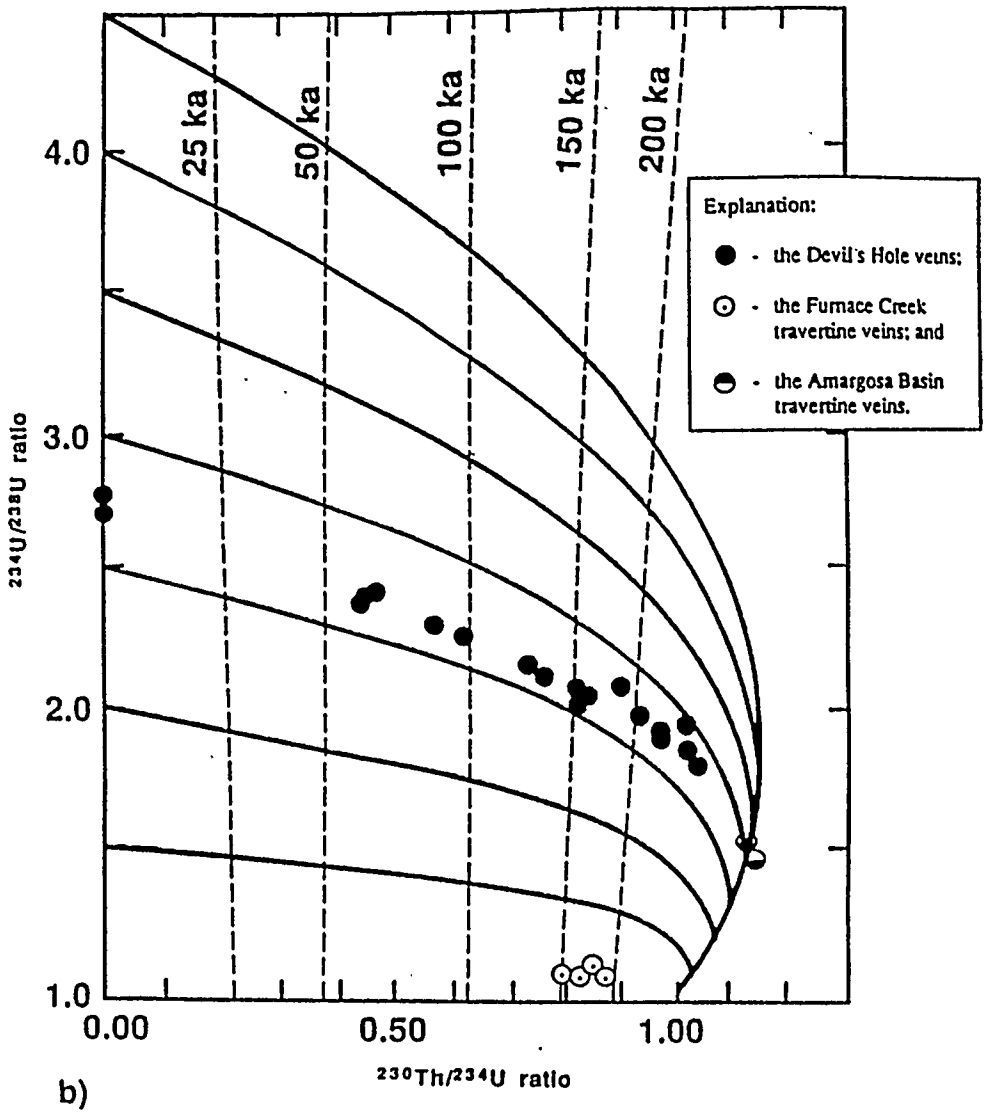

Figure 36a and 36b. $^{234}U/^{238}U$ vs. $^{230}Th/^{234}U$ ratios from samples of: a) Yucca Mountain calcretes, surficial veins, and subsurface veins, and b) travertine veins from Devils Hole, Amargosa Basin, and Furnace Creek. Data from Szabo et al. (1981); Szabo and Kyser (1985); Szabo and O'Malley (1985); and Stuckless (1991).

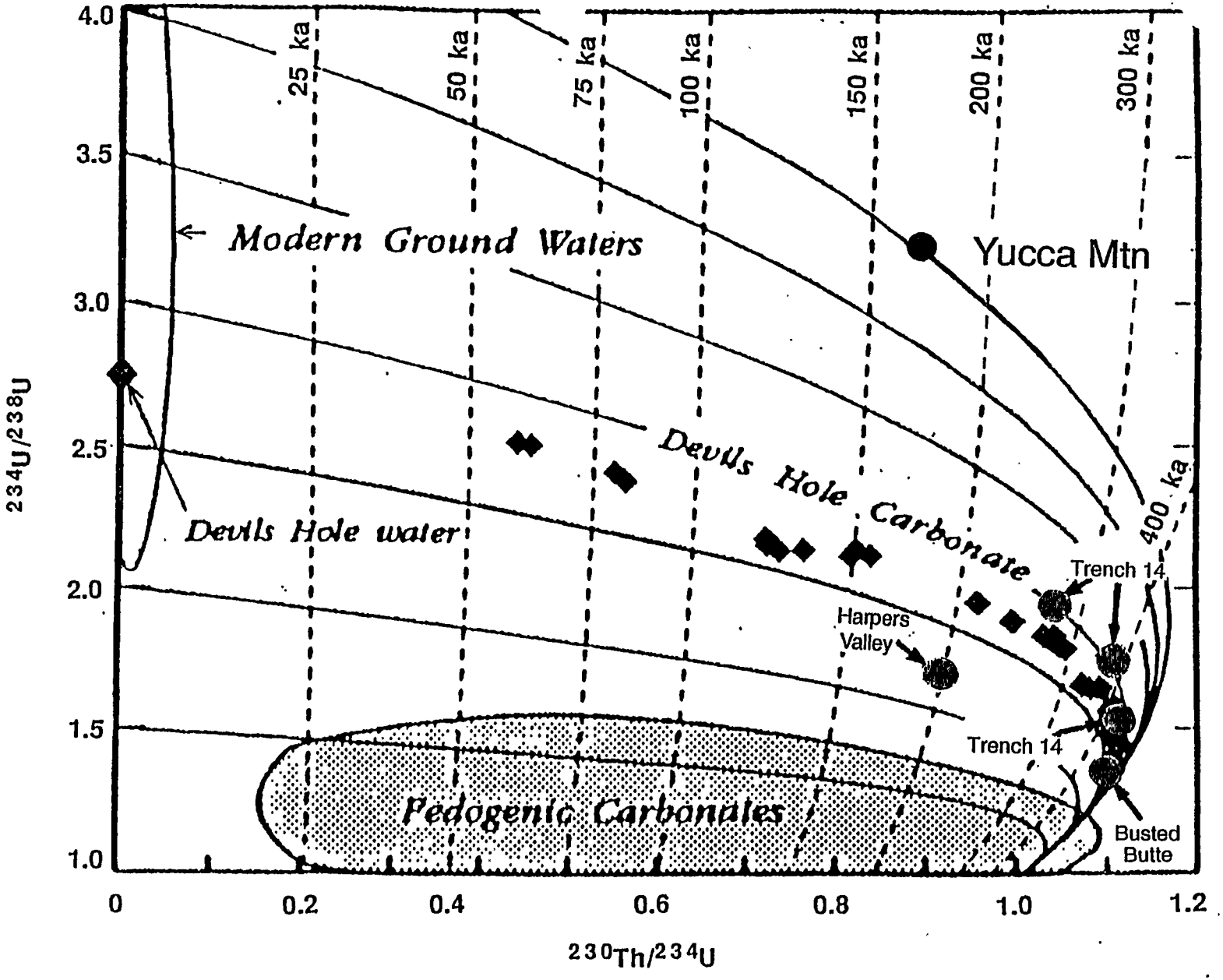

Figure 37. U-series isochron diagram modified from Paces et al. (1993). The "pedogenic carbonates" category of Paces et al. (1993) is presumed "pedogenic," not "true" pedogenic, and reflects calcite/opal deposits which have been leached of uranium. Red dots represent "pristine" (unleached) samples from Trench 14, west Busted Butte, and Harper Valley analyzed by Harmon (1993).

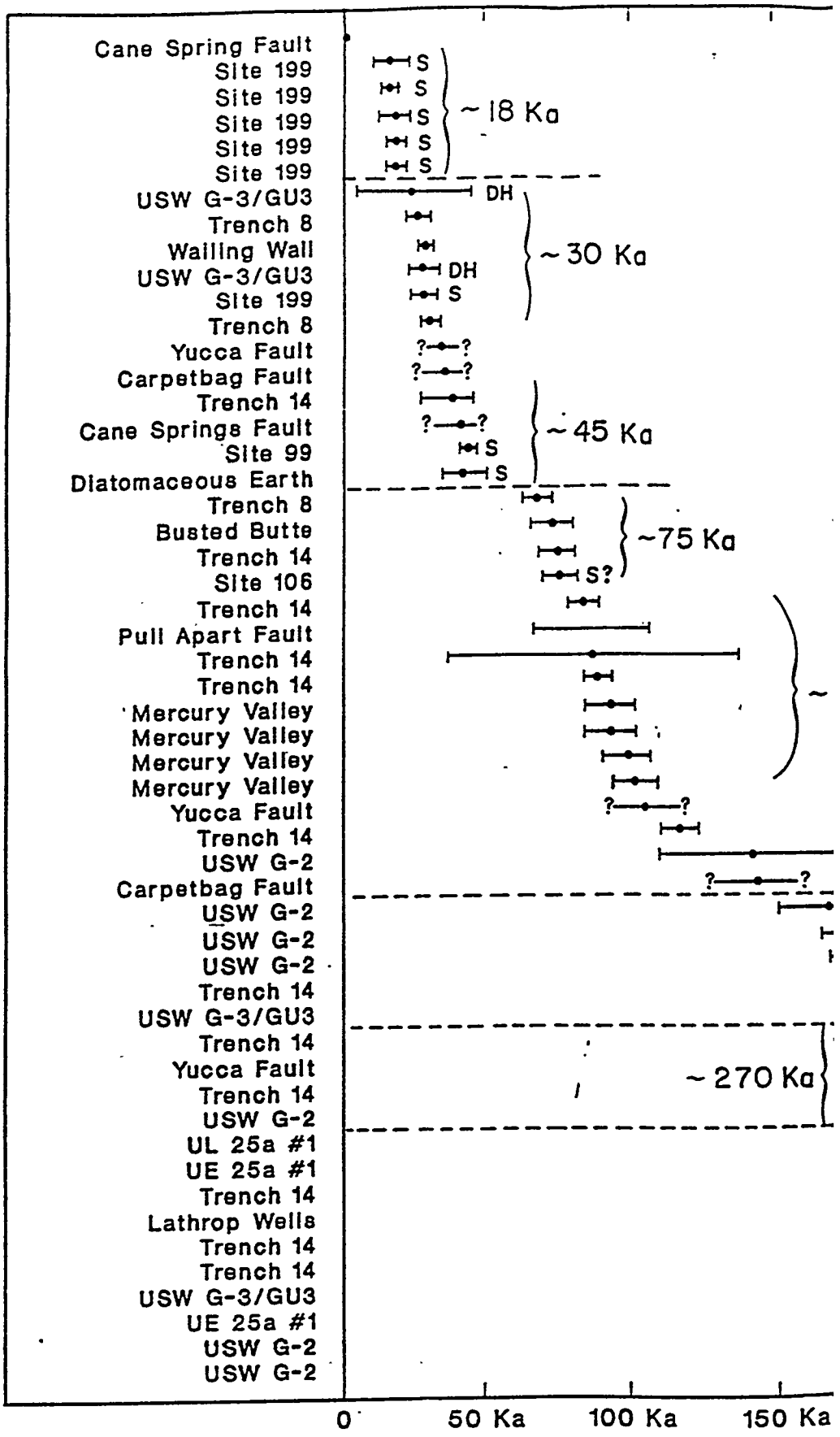

Figure 38. Age, carbonate deposits, Yucca Mountain and vicinity.

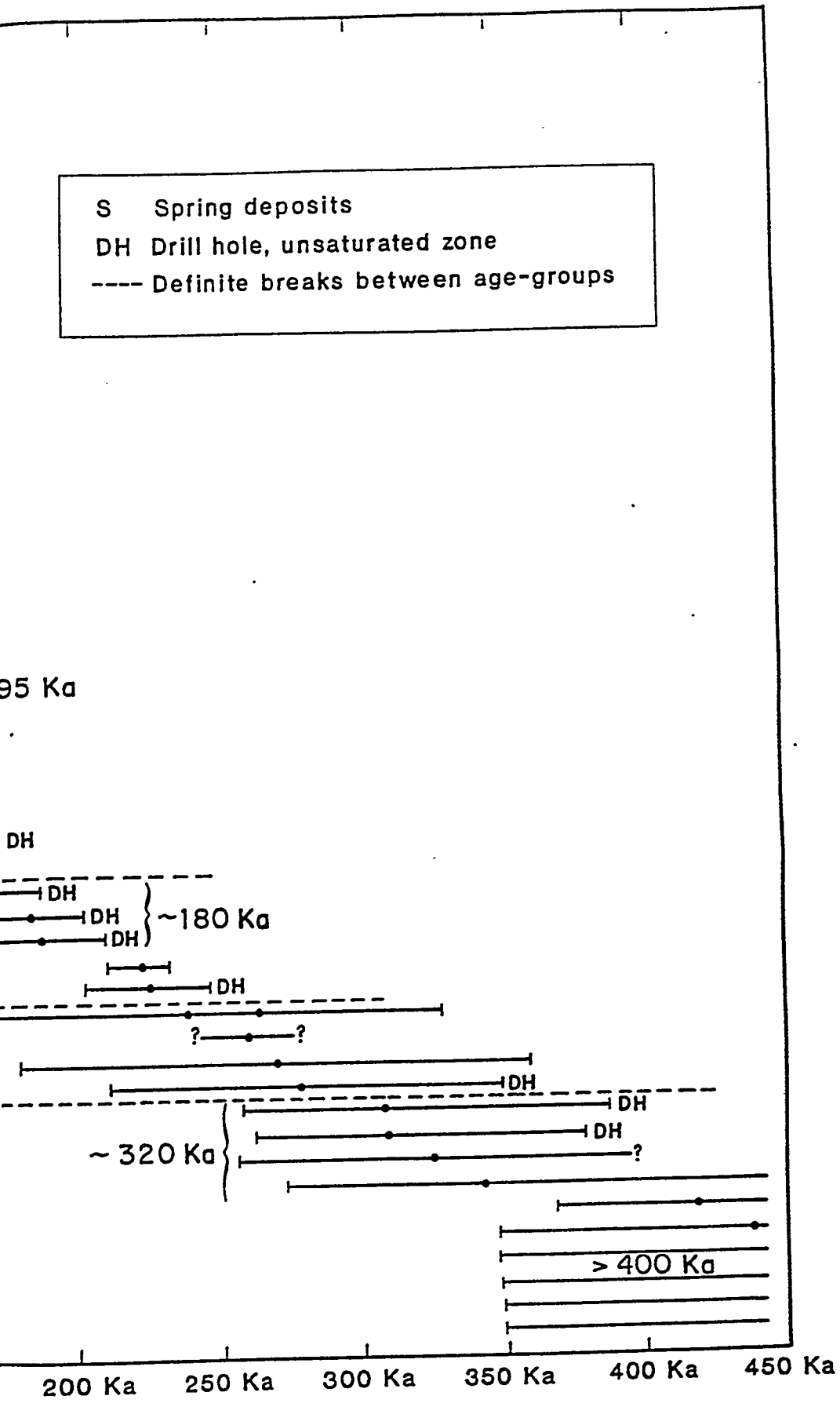
S Spring deposits
DH Drill hole, unsaturated zone
---- Definite breaks between age-groups
95 Ka
DH
DH
DH
DH
~180 Ka
DH
?
?
DH
DH
DH
?
~ 320 Ka
> 400 Ka
200 Ka
250 Ka
300 Ka
350 Ka
400 Ka
450 Ka

APPENDIX

Table 1. Trench 14 Samples

Element	36a Carbonate	36b Opaline	36c Carbonate vein	36e Silica vein	36f Carbonate vein	36h Silica vein
Na %	0.237	0.0170	0.301	0.0303	0.217	0.033
K %	0.28	0.010	0.19	0.012	0.124	–
Rb ppm	11.5	–	9.5	0.60	3.35	–
Cs ppm	0.54	0.014	0.55	0.038	0.20	–
Ca %	21.1	11.8	15.1	16.4	23.4	15.6
Sr ppm	815	431	520	575	797	680
Ba ppm	211	171	217	238	138	187
Sc ppm	0.576	0.0150	0.524	0.037	0.213	0.017
Cr ppm	2.4	0.32	2.2	0.30	1.02	0.29
Mn ppm	50.8	3.93	46.2	5.6	25.1	3.4
Fe %	0.178	0.0047	0.163	0.0124	0.067	0.0046
Co ppm	2.32	0.27	3.00	0.33	1.58	0.09
Ni ppm	–	–	–	–	5.450	3.140
Zn ppm	–	–	–	–	–	–
Cu ppm	–	–	–	–	–	–
Br ppm	4.62	2.39	5.20	5.62	4.12	3.89
As ppm	5.4	2.7	5.0	6.8	9.7	5.1
Sb ppm	0.89	0.07	1.50	0.95	0.75	1.84
La ppm	7.2	0.43	7.1	0.77	1.64	0.59
Ce ppm	10.3	–	10.3	–	3.10	–
Nd ppm	3.5	–	4.6	–	–	–
Sm ppm	0.89	–	1.20	–	0.26	–
Eu ppm	0.127	–	0.159	–	0.040	–
Tb ppm	0.13	–	0.22	–	0.045	–
Dy ppm	0.76	–	1.20	–	–	–
Yb ppm	0.46	0.027	0.74	0.045	0.29	–
Lu ppm	0.052	0.0047	0.089	0.0088	0.039	0.010
Zr ppm	–	–	–	–	–	–
Hf ppm	0.76	0.016	0.52	0.023	0.182	0.022
Ta ppm	0.16	–	0.12	0.015	0.042	–
W ppm	0.42	0.19	0.34	0.34	0.46	0.29
Au ppb	6.5	1.1	31.9	0.92	8.2	6.3
Th ppm	2.02	0.056	2.18	0.100	0.54	0.091
U ppm	8.2	13.6	13.7	19.3	7.1	14.7

Element	36i Carbonate vein	36j Opal vein	36k Opal-breccia -carbonate	36m Calcite vein	36o Carbonate vein	36p Calcite -opal vein
Na %	0.077	0.047	0.683	0.0269	0.198	0.150
K %	0.065	-	0.87	0.016	0.11	0.18
Rb ppm	3.9	-	36.0	0.69	4.3	8.6
Cs ppm	0.25	0.026	1.48	0.030	0.22	0.42
Ca %	24.7	18.2	17.0	15.1	24.0	25.3
Sr ppm	1040	714	663	377	879	662
Ba ppm	115	131	256	214	134	136
Sc ppm	0.217	0.037	1.40	0.035	0.198	0.404
Cr ppm	1.6	0.3	4.7	0.25	1.05	1.57
Mn ppm	18.8	6.3	107.6	5.2	13.2	36.5
Fe %	0.062	0.0092	0.414	0.011	0.061	0.124
Co ppm	2.63	0.64	3.23	0.28	0.86	1.00
Ni ppm	-	-	10.200	-	-	-
Zn ppm	-	-	-	-	-	-
Cl ppm	-	-	-	-	-	-
Br ppm	9.12	4.29	3.96	4.21	9.54	7.57
As ppm	9.8	5.8	5.2	5.0	10.2	9.5
Sb ppm	-	-	0.59	2.24	1.56	0.84
La ppm	1.83	0.40	22.1	0.67	1.53	3.24
Ce ppm	4.30	0.80	34.1	-	3.00	6.10
Nd ppm	0.97	-	17.0	-	0.82	2.25
Sm ppm	-		3.80	-	0.26	0.50
Eu ppm	0.039	-	0.425	-	0.034	0.069
Tb ppm	0.041	0.013	0.46	0.009	0.038	0.053
Dy ppm	0.28	-	2.41	-	-	0.35
Yb ppm	0.17	0.059	1.46	0.043	0.15	0.19
Lu ppm	0.031	0.014	0.32	-	0.022	0.027
Zr ppm	-	-	55	-	-	-
Hf ppm	0.227	0.046	1.91	0.029	0.212	0.388
Ta ppm	0.044	0.015	0.45	-	0.051	0.084
W ppm	0.73	0.42	0.55	0.34	0.55	0.68
Au ppb	8.6	5.1	-	2.0	8.6	6.2
Th ppm	0.84	0.145	5.53	0.097	0.61	1.03
U ppm	9.4	14.0	6.5	24.9	7.3	6.1

Element	36p2 Calcite -opal vein	36r Carbonate vein	36s Opal vein	36t Carbonate vein	36v Carbonate vein	36w Opal vein
Na %	1.150	0.077	0.049	0.177	0.132	0.056
K %	0.24	0.09	0.033	0.24	0.14	0.077
Rb ppm	9.7	3.7	1.4	5.0	4.6	4.0
Cs ppm	0.47	0.18	0.064	0.33	0.20	0.17
Ca %	26.9	26.5	27.1	28.2	22.7	19.3
Sr ppm	817	888	1210	1450	1120	1160
Ba ppm	141	109	137	161	113	35
Sc ppm	0.399	0.183	0.066	0.381	0.210	0.256
Cr ppm	1.5	0.94	0.50	0.90	0.68	1.2
Mn ppm	33.7	23.3	12.3	73.9	38.2	18.8
Fe %	0.120	0.060	0.0200	0.111	0.057	0.077
Co ppm	0.92	0.73	0.56	2.03	2.15	0.32
Ni ppm	-	-	-	18.400	-	-
Zn ppm	-	-	-	-	-	-
Cl ppm	-	-	-	-	-	-
Br ppm	29.2	7.05	7.80	5.36	5.73	2.58
As ppm	11.8	9.0	11.0	8.8	7.2	1.5
Sb ppm	0.38	0.65	1.18	0.36	0.51	0.05
La ppm	2.98	2.18	0.85	9.4	3.79	1.09
Ce ppm	5.60	3.30	1.20	13.1	5.3	2.4
Nd ppm	1.78	1.15	-	6.0	2.2	-
Sm ppm	0.45	0.38	0.14	1.58	0.57	0.21
Eu ppm	0.062	0.040	0.012	0.138	0.041	0.033
Tb ppm	0.045	0.030	0.014	0.19	0.072	0.020
Dy ppm	-	0.31	-	0.94	0.39	-
Yb ppm	0.17	0.11	0.057	0.59	0.25	-
Lu ppm	0.020	0.015	0.010	0.064	0.032	0.013
Zr ppm	-	-	-	26	-	-
Hf ppm	0.331	0.210	0.103	0.92	0.34	0.218
Ta ppm	0.103	0.043	0.021	0.21	0.088	0.036
W ppm	0.84	0.60	0.80	0.62	0.64	-
Au ppb	14.5	3.3	2.1	10.2	22.7	1.2
Th ppm	1.03	0.53	0.194	2.89	1.15	0.38
U ppm	3.5	5.5	11.1	3.3	5.8	0.3

Element	36x	36y Breccia -calcite	36z Breccia	40a1 Carbonate vein	40a2 Carbonate? vein	40a3 Carbonate? vein
Na %	0.312	0.305	0.794	0.068	0.129	0.046
K %	0.56	0.48	1.39	0.06	0.043	0.031
Rb ppm	21.0	22.0	60.7	1.5	1.4	0.8
Cs ppm	0.87	0.47	1.13	0.056	0.058	0.041
Ca %	24.3	32.1	11.4	27.7	27.0	25.6
Sr ppm	1730	940	385	721	868	647
Ba ppm	198	31	93	137	161	164
Sc ppm	1.54	0.248	0.494	0.066	0.071	0.038
Cr ppm	6.7	0.57	0.70	0.4	0.51	0.28
Mn ppm	99.8	70.9	199.7	7.6	9.4	5.1
Fe %	0.472	0.085	0.197	0.0198	0.0256	0.0114
Co ppm	1.80	0.63	0.38	0.62	0.53	0.46
Ni ppm	-	-	-	-	-	-
Zn ppm	-	-	-	-	-	-
Cl ppm	-	-	-	-	-	-
Br ppm	2.89	4.10	1.86	9.17	10.2	7.57
As ppm	3.8	8.3	9.1	10.3	12.9	9.2
Sb ppm	0.28	0.12	0.60	0.62	0.65	0.60
La ppm	8.8	4.4	10.4	0.79	0.89	0.67
Ce ppm	18.0	9.8	24.3	1.30	1.20	0.70
Nd ppm	6.4	3.3	8.0	0.53	0.62	-
Sm ppm	1.43	1.23	2.78	0.16	0.15	0.12
Eu ppm	0.265	0.045	0.098	0.012	0.016	0.019
Tb ppm	0.19	0.21	0.55	0.014	0.014	-
Dy ppm	1.14	1.18	3.18	-	-	-
Yb ppm	0.53	0.63	1.73	-	-	0.051
Lu ppm	0.084	0.10	0.33	0.0060	-	-
Zr ppm	52	-	52	-	-	-
Hf ppm	1.24	0.96	2.46	0.085	0.103	0.084
Ta ppm	0.20	0.22	0.55	-	0.017	0.009
W ppm	-	0.37	0.28	1.07	1.18	1.07
Au ppb	-	2.7	-	9.0	6.2	4.3
Th ppm	2.81	3.27	8.10	0.188	0.230	0.099
U ppm	1.0	1.2	2.8	5.7	7.0	9.3

Element	40b Calcite vein	40c Calcite -subsurface	Uncertainty %
Na %	0.200	0.168	<2
K %	0.25	0.27	5-25
Rb ppm	10.5	10.9	5-15
Cs ppm	0.49	0.50	3-10
Ca %	20.0	26.3	3-5
Sr ppm	613	680	3-5
Ba ppm	185	177	3-10
Sc ppm	0.389	0.533	<2
Cr ppm	1.7	2.1	5
Mn ppm	25.1	45.1	<2
Fe %	0.120	0.172	<2
Co ppm	0.79	1.19	<2
Ni ppm	-	-	15-25
Zn ppm	-	-	-
Cl ppm	-	-	-
Br ppm	3.22	5.31	3-10
As ppm	10.3	12.0	3-5
Sb ppm	0.88	0.52	5-20
La ppm	4.44	4.63	3-5
Ce ppm	8.0	8.2	3-10
Nd ppm	2.5	3.0	3-10
Sm ppm	0.66	0.75	3-20
Eu ppm	0.073	0.090	3-5
Tb ppm	0.093	0.084	5-25
Dy ppm	-	-	5-25
Yb ppm	0.28	0.31	5-25
Lu ppm	0.032	0.036	5-25
Zr ppm	-	-	5-15
Hf ppm	0.46	0.53	3-5
Ta ppm	0.119	0.135	3-5
W ppm	0.59	1.05	5-15
Au ppb	4.7	10.3	10-15
Th ppm	1.49	1.50	3-5
U ppm	8.6	4.7	3-5

Table 2. Busted Butte Samples

Element	38b Travertines	38c Opal -calcite	38g Carbonate caps tuff	Uncertainty %
Na %	0.436	0.395	0.432	<2
K %	0.59	0.85	0.63	5
Rb ppm	25.7	39.3	23.1	5
Cs ppm	1.08	1.90	0.85	3
Ca %	22.6	29.0	26.0	3
Sr ppm	337	642	454	3
Ba ppm	233	70.2	375	3
Sc ppm	1.90	1.26	1.60	<2
Cr ppm	8.6	3.8	5.3	3
Mn ppm	191.2	102.2	151.7	<2
Fe %	0.777	0.342	0.538	<2
Co ppm	2.62	2.05	2.15	<2
Ni ppm	11.4	-	-	20
Zn ppm	-	-	-	-
Cl ppm	-	-	-	-
Br ppm	4.38	2.02	9.73	3
As ppm	14.0	13.8	9.0	3
Sb ppm	0.64	1.75	0.47	5
La ppm	31.9	16.3	37.3	2
Ce ppm	47.5	29.1	67.2	3
Nd ppm	20.6	9.6	23.2	3
Sm ppm	4.08	2.24	3.80	5
Eu ppm	0.439	0.175	0.513	2
Tb ppm	0.50	0.32	0.42	3
Dy ppm	2.57	1.94	1.86	10
Yb ppm	1.36	1.04	1.27	3
Lu ppm	0.29	0.15	0.23	5
Zr ppm	174	37	139	5-10
Hf ppm	4.54	1.39	3.60	3
Ta ppm	0.44	0.34	0.32	3
W ppm	0.74	0.52	0.85	15
Au ppb	2.41	7.6	-	10
Th ppm	5.90	5.65	5.23	3
U ppm	7.6	1.5	4.3	3

Table 3. Stagecoach Trench Samples

Element	22a Carbonate -root casts	22e Carbonate -surficial	23a Carbonate -root casts	Uncertainty %
Na %	0.883	0.406	1.091	<2
K %	1.10	0.51	1.36	5
Rb ppm	36.0	20.6	45.9	5
Cs ppm	1.02	0.90	1.55	3
Ca %	15.0	21.6	9.8	3
Sr ppm	755	575	694	3
Ba ppm	345	259	346	3
Sc ppm	1.18	1.80	1.68	<2
Cr ppm	4.2	9.1	5.7	3
Mn ppm	139.3	161.8	203.6	<2
Fe %	0.476	0.816	0.608	<2
Co ppm	1.32	3.02	1.88	<2
Ni ppm	-	-	9.8	20
Zn ppm	-	-	-	-
Cl ppm	-	-	-	-
Br ppm	9.39	7.70	6.44	3
As ppm	14.1	12.3	8.5	3
Sb ppm	0.62	0.64	0.47	5
La ppm	22.2	31.3	39.9	2
Ce ppm	36.2	47.6	53.0	3
Nd ppm	14.0	16.7	22.7	3
Sm ppm	2.47	2.77	3.87	5
Eu ppm	0.340	0.349	0.453	2
Tb ppm	0.37	0.36	0.54	3
Dy ppm	1.57	1.52	2.24	10
Yb ppm	1.07	1.10	1.56	5
Lu ppm	0.28	0.24	0.33	5
Zr ppm	-	141	52	5-15
Hf ppm	2.12	5.00	3.11	3
Ta ppm	0.42	0.43	0.61	3
W ppm	0.50	0.48	0.74	15
Au ppb	2.3	3.4	4.4	15-25
Th ppm	6.21	5.56	7.89	3
U ppm	9.0	6.0	8.4	3

Table 4. Site 199 Samples

Element	24a Silicious clasts	24b Breccia carrera	24c Breccia Bonanza King	24d Tufa	25a Carbonate root casts	25b Sediments marsh/lake	Uncertainty %
Na %	0.0193	0.0196	0.0229	0.214	0.779	1.51	<2
K %	0.032	0.22	0.050	0.27	0.94	1.88	5
Rb ppm	0.79	7.3	1.5	13.5	37.3	76.0	5
Cs ppm	0.22	0.67	0.08	3.70	1.60	3.83	3
Ca %	18.3	29.2	17.8	37.6	22.5	6.3	3
Sr ppm	52.7	186	44.3	375	1480	688	3
Ba ppm	15.3	47.2	22	409	237	446	5
Sc ppm	0.090	0.879	0.131	0.779	1.77	3.43	<2
Cr ppm	0.64	3.2	0.66	3.3	7.1	13.6	5
Mn ppm	148.6	71.1	100.6	113.8	204.3	221.4	<2
Fe %	0.0161	0.120	0.0542	0.256	0.575	1.01	<2
Co ppm	0.062	0.38	0.17	1.04	3.99	3.59	<2
Ni ppm	–	–	–	–	–	13.4	25
Zn ppm	–	–	–	–	–	–	–
Cl ppm	–	–	–	–	–	–	–
Br ppm	0.61	0.46	1.15	2.32	2.58	1.23	3–10
As ppm	0.40	6.41	1.05	2.83	7.6	4.5	3–5
Sb ppm	0.25	0.57	0.42	0.25	0.59	2.30	5–10
La ppm	0.67	3.85	0.62	6.04	26.8	32.0	2–5
Ce ppm	1.20	7.4	1.6	10.6	53.7	54.9	3–5
Nd ppm	0.60	2.9	0.6	4.2	17.0	20.2	3–5
Sm ppm	0.135	0.546	0.135	0.742	4.43	3.87	3–10
Eu ppm	0.021	0.101	0.023	0.124	0.643	0.593	2
Tb ppm	0.020	0.079	0.024	0.10	0.78	0.51	3–10
Dy ppm	–	0.33	–	0.71	4.19	3.41	10–15
Yb ppm	0.055	0.33	0.088	0.38	3.36	1.86	5–20
Lu ppm	–	0.082	0.021	0.084	0.453	0.28	5–20
Zr ppm	–	–	7.4	15	97	4	5–7
Hf ppm	0.031	0.43	0.235	0.75	2.17	3.51	3–5
Ta ppm	0.012	0.114	0.019	0.14	0.42	0.78	3–5
W ppm	–	0.17	0.04	0.18	0.57	–	15–25
Au ppb	0.95	1.56	0.58	0.92	–	13	15–20
Th ppm	0.170	1.12	0.214	1.83	20.8	10.6	3–5
U ppm	0.40	1.95	0.50	1.47	1.95	4.4	3–5

Table 5. Wahmonie Mounds

Element	32a Gypsum +calcite	32b Carbonate	32c Calcite -gypsum	32d Calcite	32e Gypsum
Na %	0.149	0.071	0.051	1.99	0.058
K %	1.75	0.10	0.030	2.85	0.08
Rb ppm	50.0	4.8	-	100	4.1
Cs ppm	1.91	0.23	0.050	2.49	0.17
Ca %	12.5	24.4	19.9	0.0	22.6
Sr ppm	614	2420	1130	213	1950
Ba ppm	1060	52.5	230	1370	35.4
Sc ppm	5.56	0.412	0.045	5.41	0.291
Cr ppm	10.8	1.[illegible]	0.5	2.6	1.5
Mn ppm	56.7	28.4	10.2	463.6	18.6
Fe %	1.17	0.130	0.014	1.41	0.087
Co ppm	3.63	0.56	0.52	1.47	0.30
Ni ppm	-	-	-	15.3	-
Zn ppm	-	-	-	-	-
Cl ppm	-	-	-	-	-
Br ppm	2.04	1.13	4.16	-	1.87
As ppm	10.8	2.6	7.7	3.0	0.82
Sb ppm	0.93	0.15	0.84	0.32	0.08
La ppm	35.6	2.3	1.2	138	1.35
Ce ppm	57.0	4.2	1.4	241	2.8
Nd ppm	21.4	1.[illegible]	-	[illegible]9	-
Sm ppm	3.78	0.31	-	10.5	0.14
Eu ppm	0.664	0.058	0.020	2.2	0.041
Tb ppm	0.39	0.031	0.022	0.98	0.024
Dy ppm	1.77	0.29	-	4.25	-
Yb ppm	1.33	0.12	0.067	2.67	0.09
Lu ppm	0.19	0.027	0.011	0.37	0.010
Zr ppm	67	9	-	482	-
Hf ppm	2.99	0.30	0.069	11.70	0.21
Ta ppm	0.41	0.046	0.017	0.79	0.041
W ppm	0.69	0.10	0.35	1.03	-
Au ppb	2.8	0.79	6.1	-	0.72
Th ppm	7.88	0.73	0.26	15.3	0.40
U ppm	2.4	0.87	21.7	2.3	0.22

Element	33a Carbonate vein(mines)	33b Fluorite(?) +quartz	33c Calcite +quartz	Uncertainty %
Na %	2.37	0.0184	0.015?	<2
K %	4.49	0.085	0.060	5
Rb ppm	138.0	2.7	3.3	5
Cs ppm	1.26	0.27	0.39	3
Ca %	-	-	-	3
Sr ppm	182	-	-	3
Ba ppm	1250	17.3	36.3	3
Sc ppm	6.59	0.115	0.262	<2
Cr ppm	10.1	0.82	0.71	5
Mn ppm	1889	10.7	155.6	<2
Fe %	1.95	0.097	0.430	<2
Co ppm	9.24	0.25	0.38	<2
Ni ppm	11.?	-	-	20
Zn ppm	-	-	-	-
Cl ppm	-	-	-	-
Br ppm	-	0.064	0.061	3-10
As ppm	14.3	3.3	15.5	3
Sb ppm	2.02	7.05	15.40	5-15
La ppm	49.3	0.93	2.26	2-5
Ce ppm	88.9	1.69	2.58	3-5
Nd ppm	29.9	1.12	1.65	3-5
Sm ppm	5.11	0.12	0.32	3-20
Eu ppm	1.08	0.036	0.106	2-5
Tb ppm	0.57	-	-	3-10
Dy ppm	8.88	-	-	10-20
Yb ppm	2.27	-	0.084	5-15
Lu ppm	0.33	-	-	5-15
Zr ppm	185	-	-	5-15
Hf ppm	5.63	0.093	0.094	3
Ta ppm	0.68	-	-	3
W ppm	0.84	0.052	-	15-25
Au ppb	5.09	1080	483	15-25
Th ppm	13.1	0.166	0.30	3
U ppm	3.3	-	-	5-10

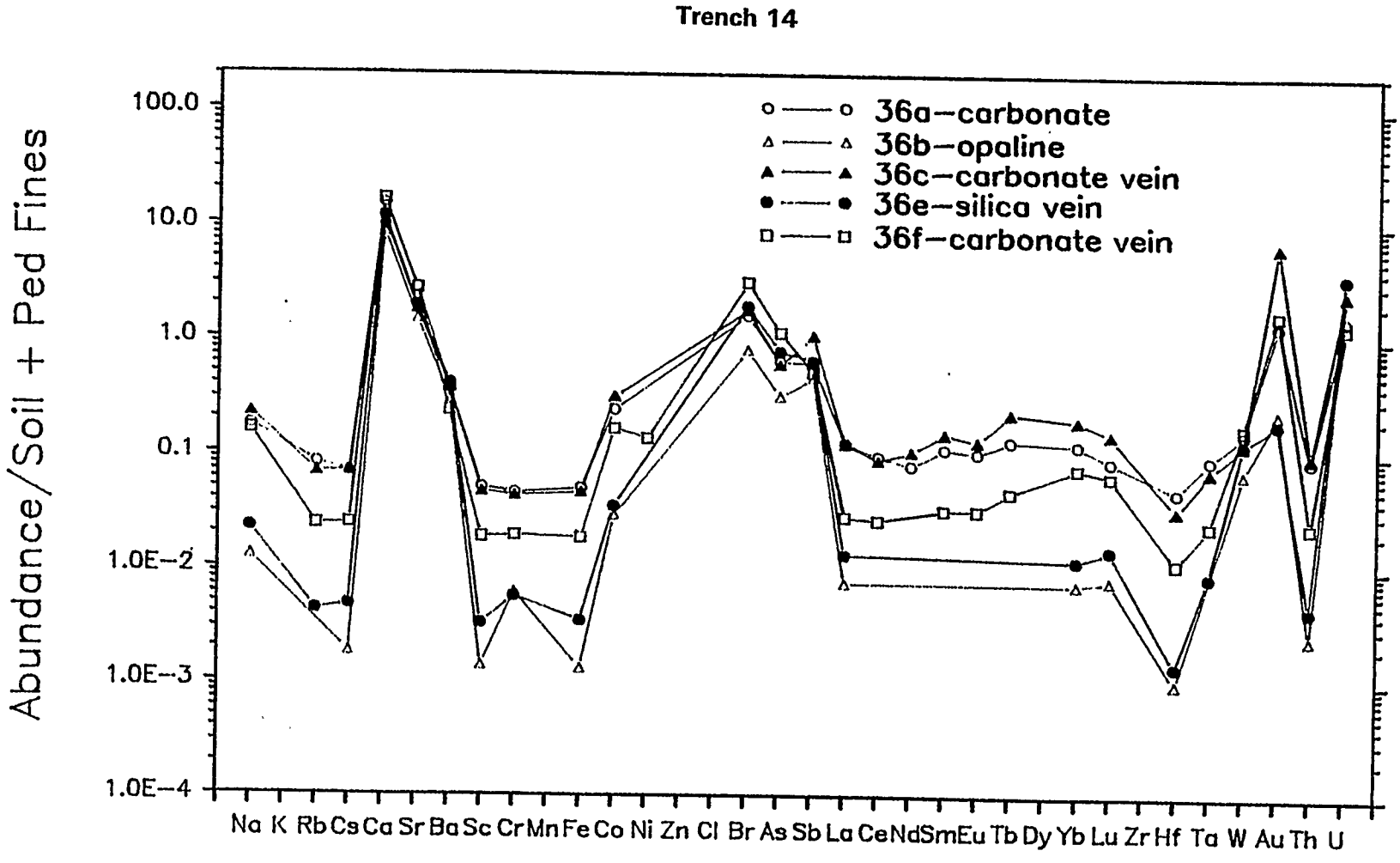
Trench 14
Abundance/Soil + Ped Fines
100.0
10.0
1.0
0.1
1.0E-2
1.0E-3
1.0E-4
36a-carbonate
36b-opaline
36c-carbonate vein
36e-silica vein
36f-carbonate vein
Na K Rb Cs Ca Sr Ba Sc Cr Mn Fe Co Ni Zn Cl Br As Sb La Ce Nd Sm Eu Tb Dy Yb Lu Zr Hf Ta W Au Th U

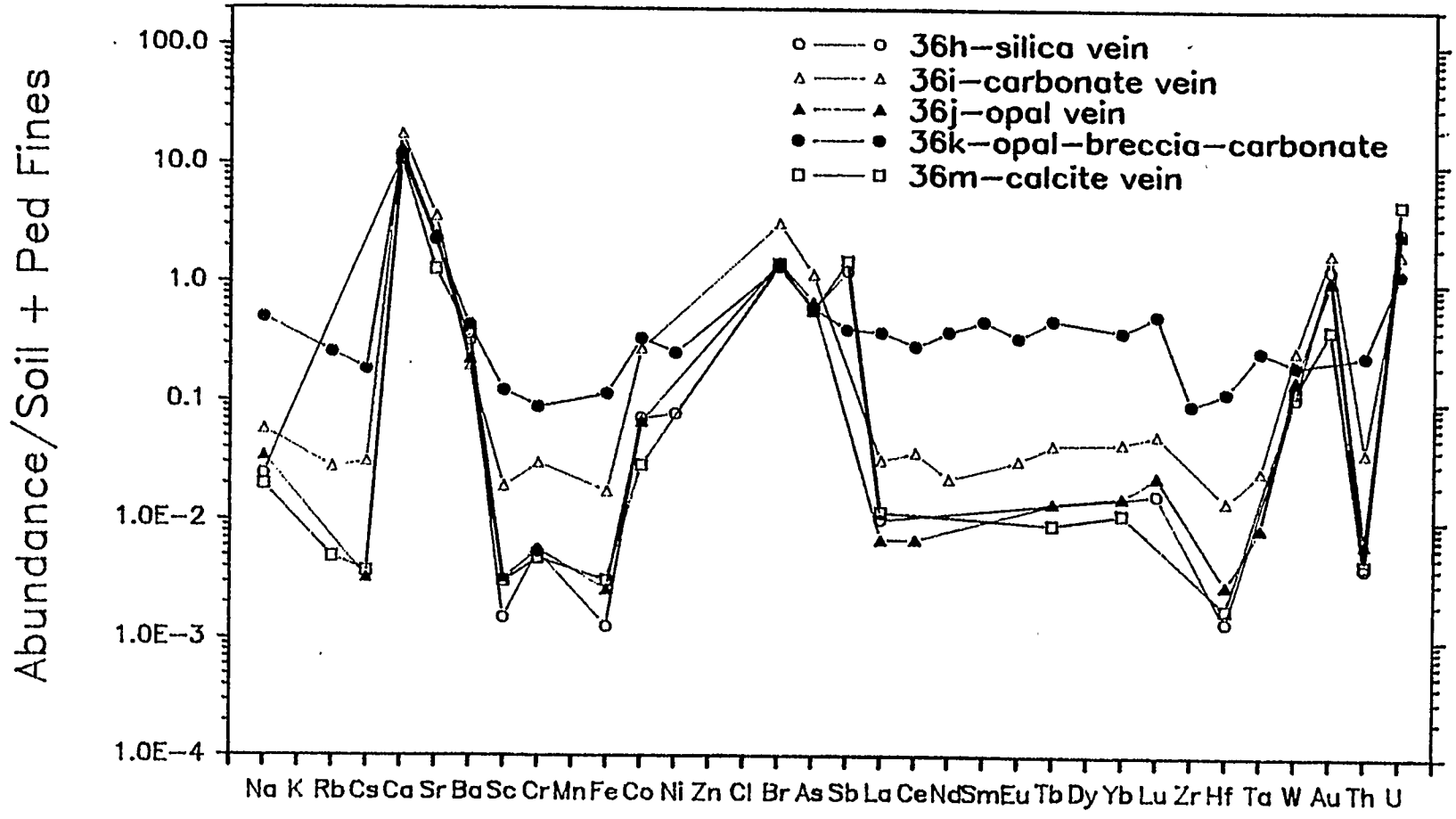
Abundance/Soil + Ped Fines
100.0
10.0
1.0
0.1
1.0E-2
1.0E-3
1.0E-4
36h-silica vein
36i-carbonate vein
36j-opal vein
36k-opal-breccia-carbonate
36m-calcite vein
Na K Rb Cs Ca Sr Ba Sc Cr Mn Fe Co Ni Zn Cl Br As Sb La Ce Nd Sm Eu Tb Dy Yb Lu Zr Hf Ta W Au Th U

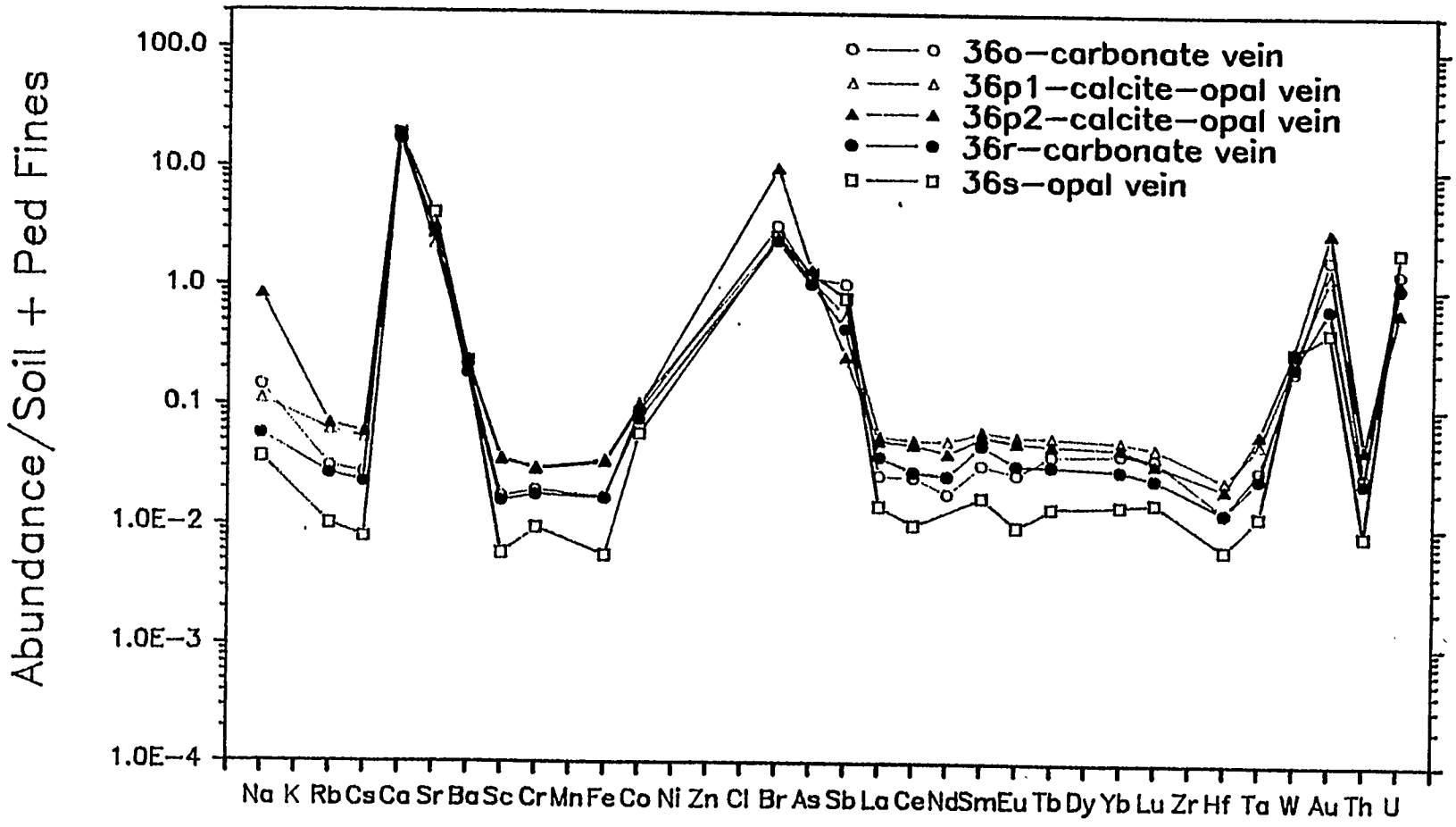
Abundance/Soil + Ped Fines
100.0
10.0
1.0
0.1
1.0E-2
1.0E-3
1.0E-4
Na K Rb Cs Ca Sr Ba Sc Cr Mn Fe Co Ni Zn Cl Br As Sb La Ce Nd Sm Eu Tb Dy Yb Lu Zr Hf Ta W Au Th U
36o—carbonate vein
36p1—calcite—opal vein
36p2—calcite—opal vein
36r—carbonate vein
36s—opal vein

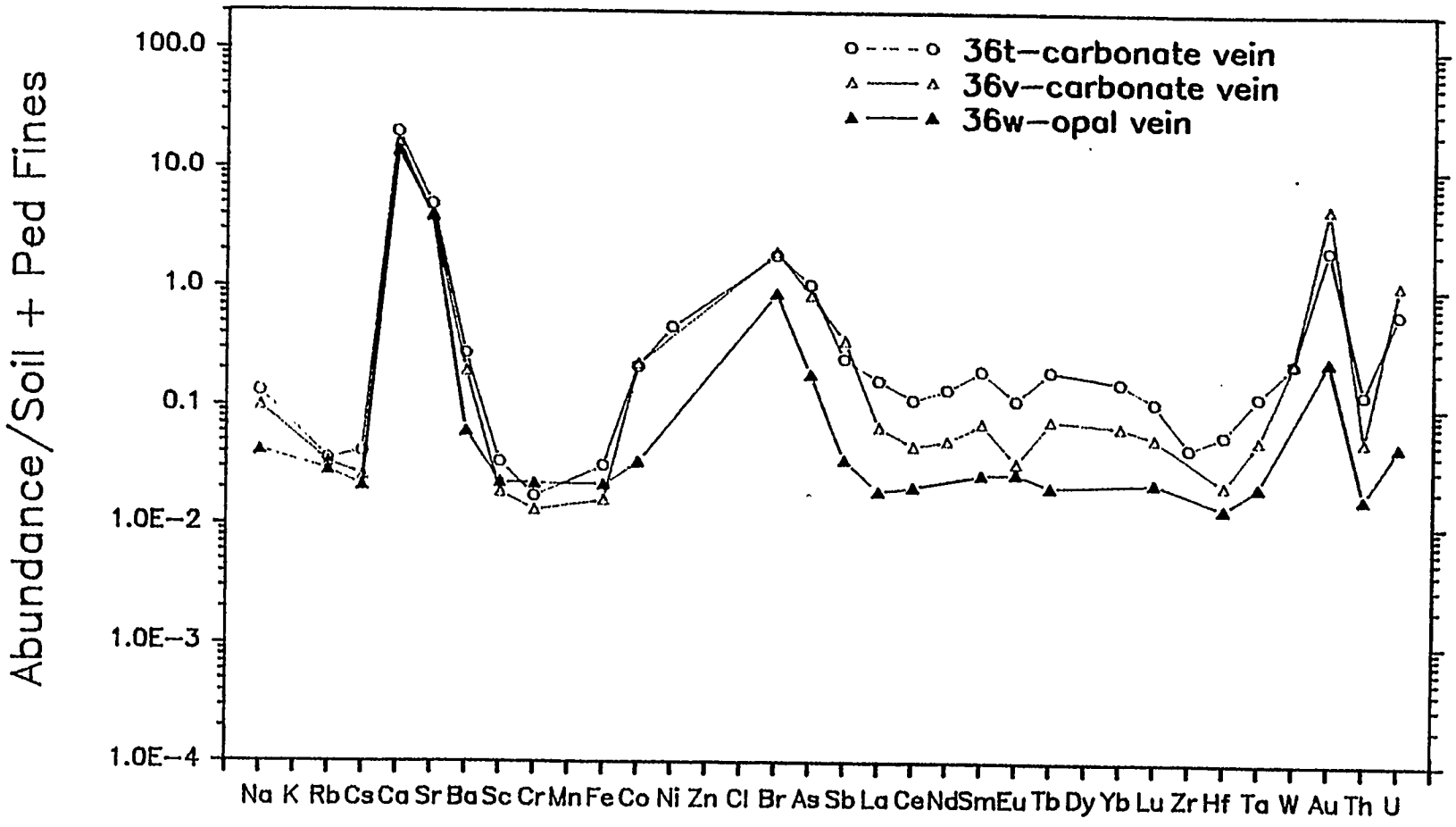
Abundance/Soil + Ped Fines
100.0
10.0
1.0
0.1
1.0E−2
1.0E−3
1.0E−4
36t—carbonate vein
36v—carbonate vein
36w—opal vein
Na K Rb Cs Ca Sr Ba Sc Cr Mn Fe Co Ni Zn Cl Br As Sb La Ce Nd Sm Eu Tb Dy Yb Lu Zr Hf Ta W Au Th U

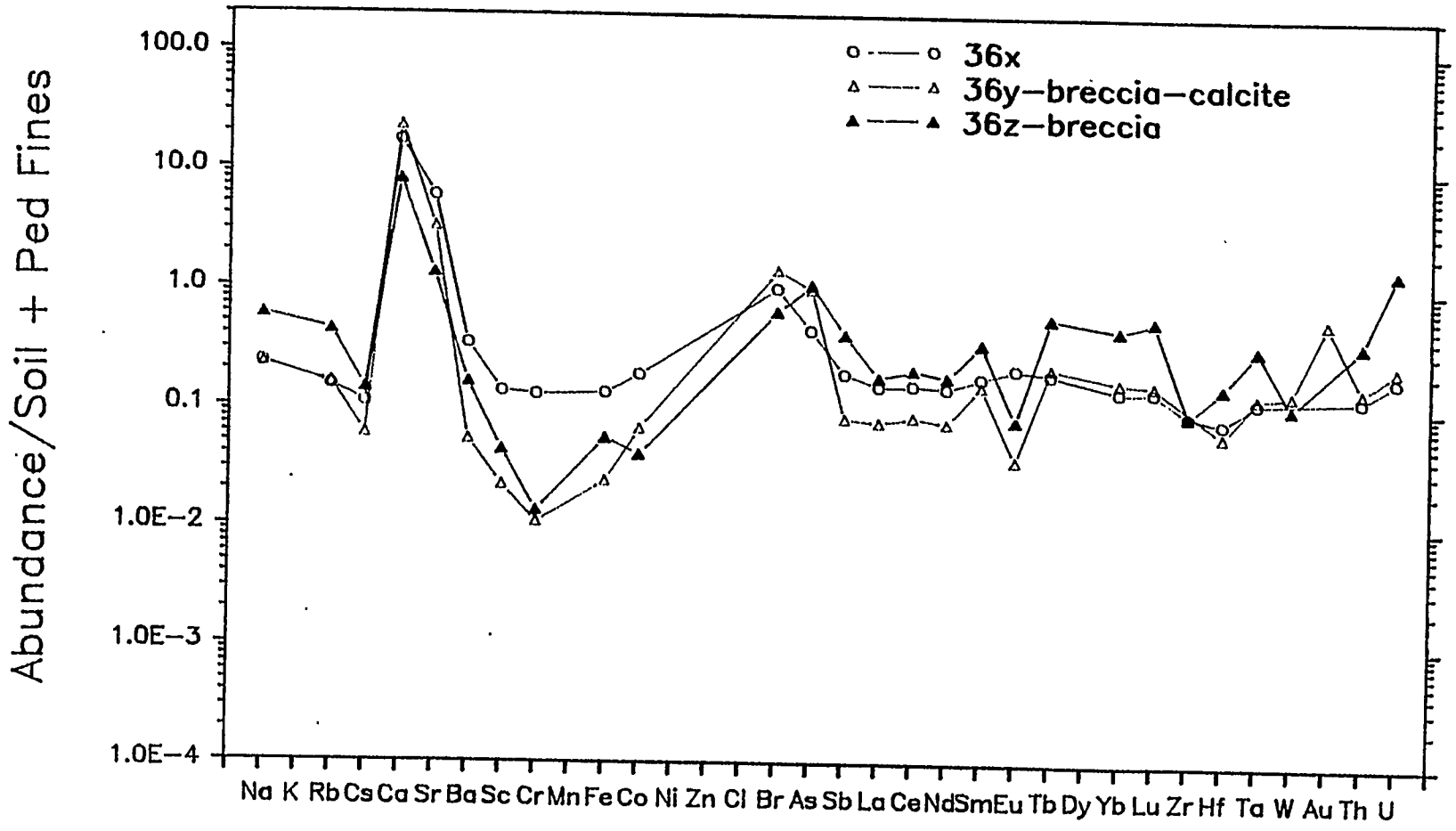
Abundance/Soil + Ped Fines
100.0
10.0
1.0
0.1
1.0E-2
1.0E-3
1.0E-4
36x
36y-breccia-calcite
36z-breccia
Na K Rb Cs Ca Sr Ba Sc Cr Mn Fe Co Ni Zn Cl Br As Sb La Ce Nd Sm Eu Tb Dy Yb Lu Zr Hf Ta W Au Th U

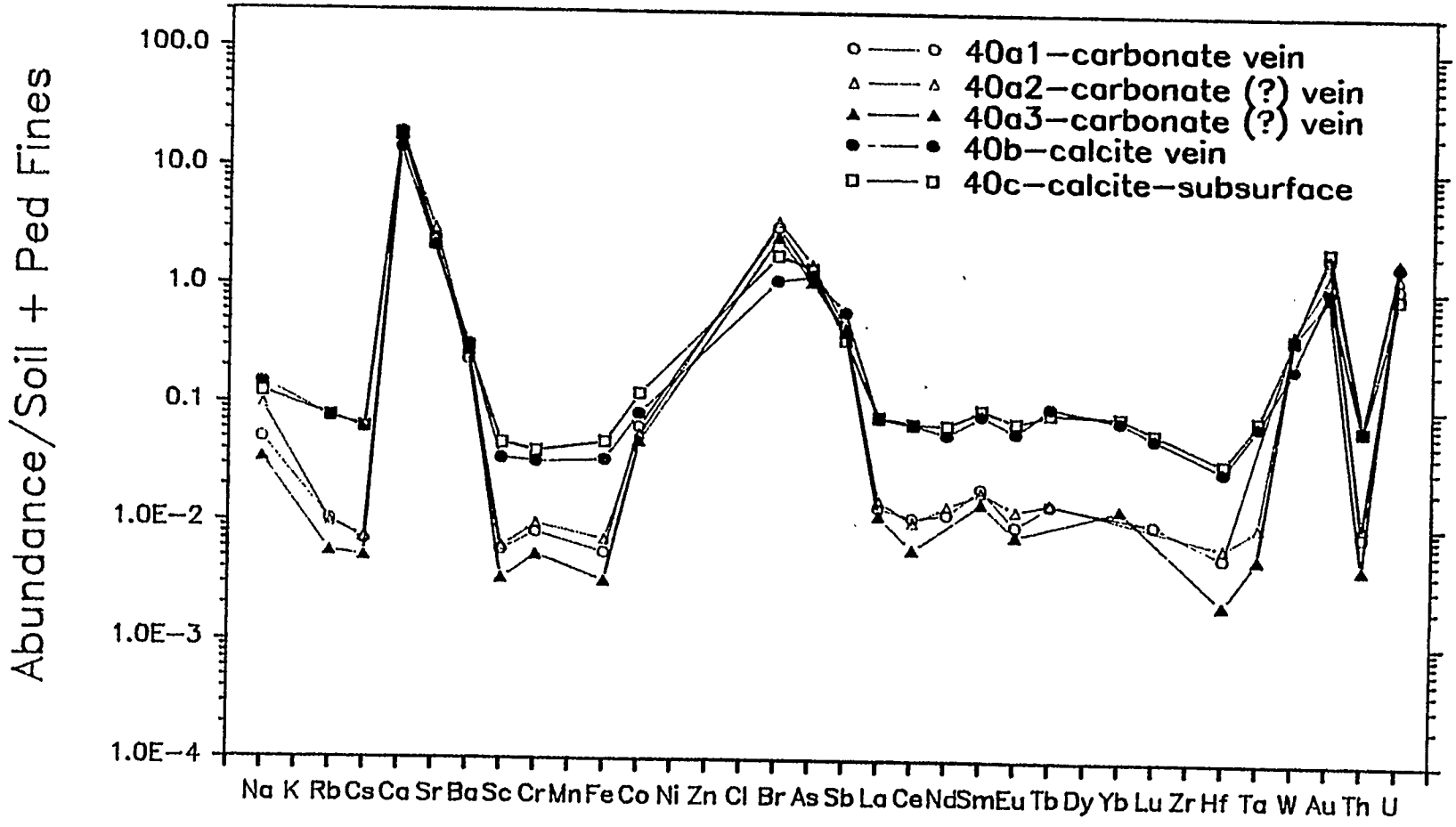
Abundance/Soil + Ped Fines
100.0
10.0
1.0
0.1
1.0E−2
1.0E−3
1.0E−4
40a1−carbonate vein
40a2−carbonate (?) vein
40a3−carbonate (?) vein
40b−calcite vein
40c−calcite−subsurface
Na K Rb Cs Ca Sr Ba Sc Cr Mn Fe Co Ni Zn Cl Br As Sb La Ce Nd Sm Eu Tb Dy Yb Lu Zr Hf Ta W Au Th U

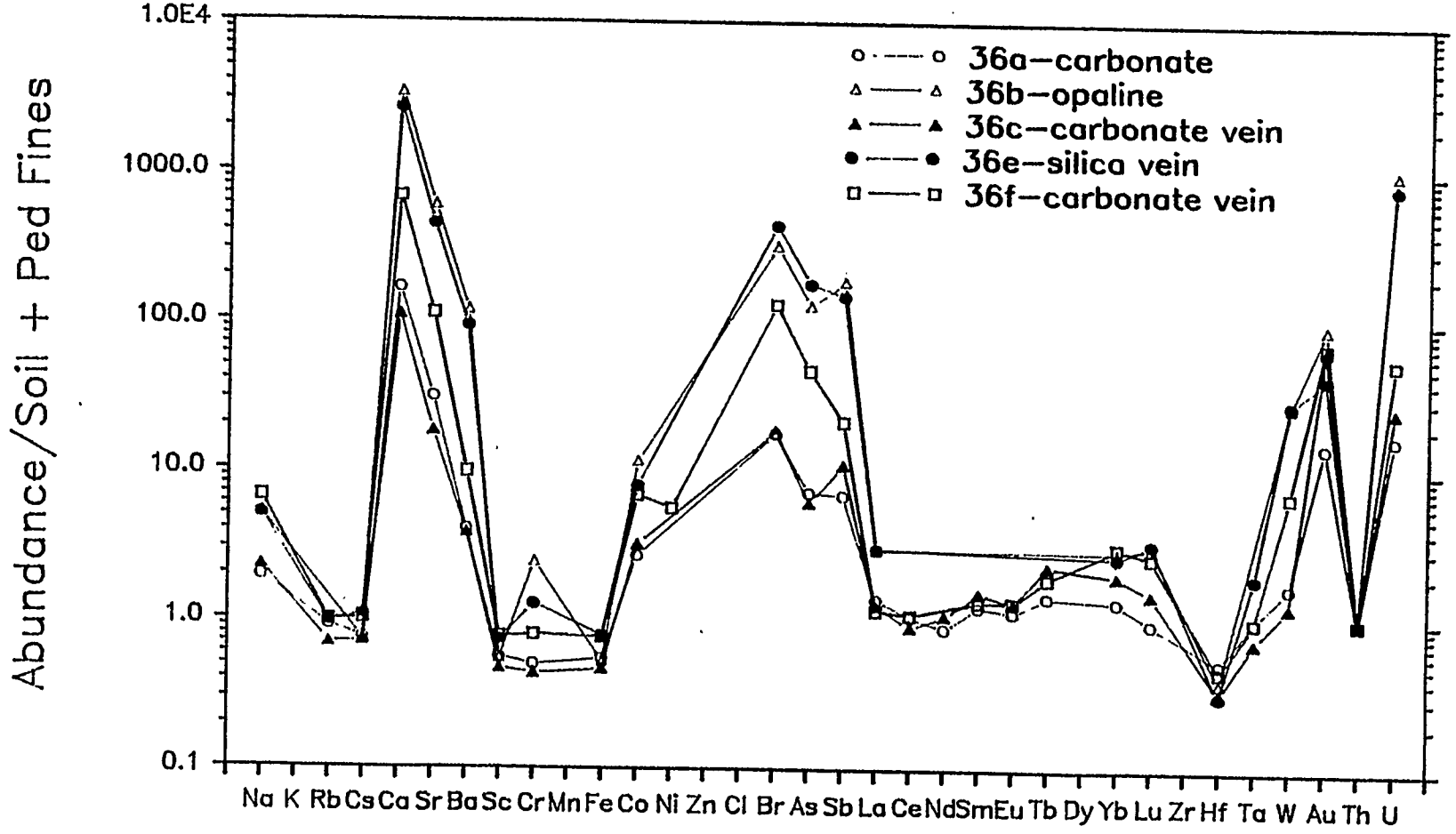
Abundance/Soil + Ped Fines
1.0E4
1000.0
100.0
10.0
1.0
0.1
36a—carbonate
36b—opaline
36c—carbonate vein
36e—silica vein
36f—carbonate vein
Na K Rb Cs Ca Sr Ba Sc Cr Mn Fe Co Ni Zn Cl Br As Sb La Ce Nd Sm Eu Tb Dy Yb Lu Zr Hf Ta W Au Th U

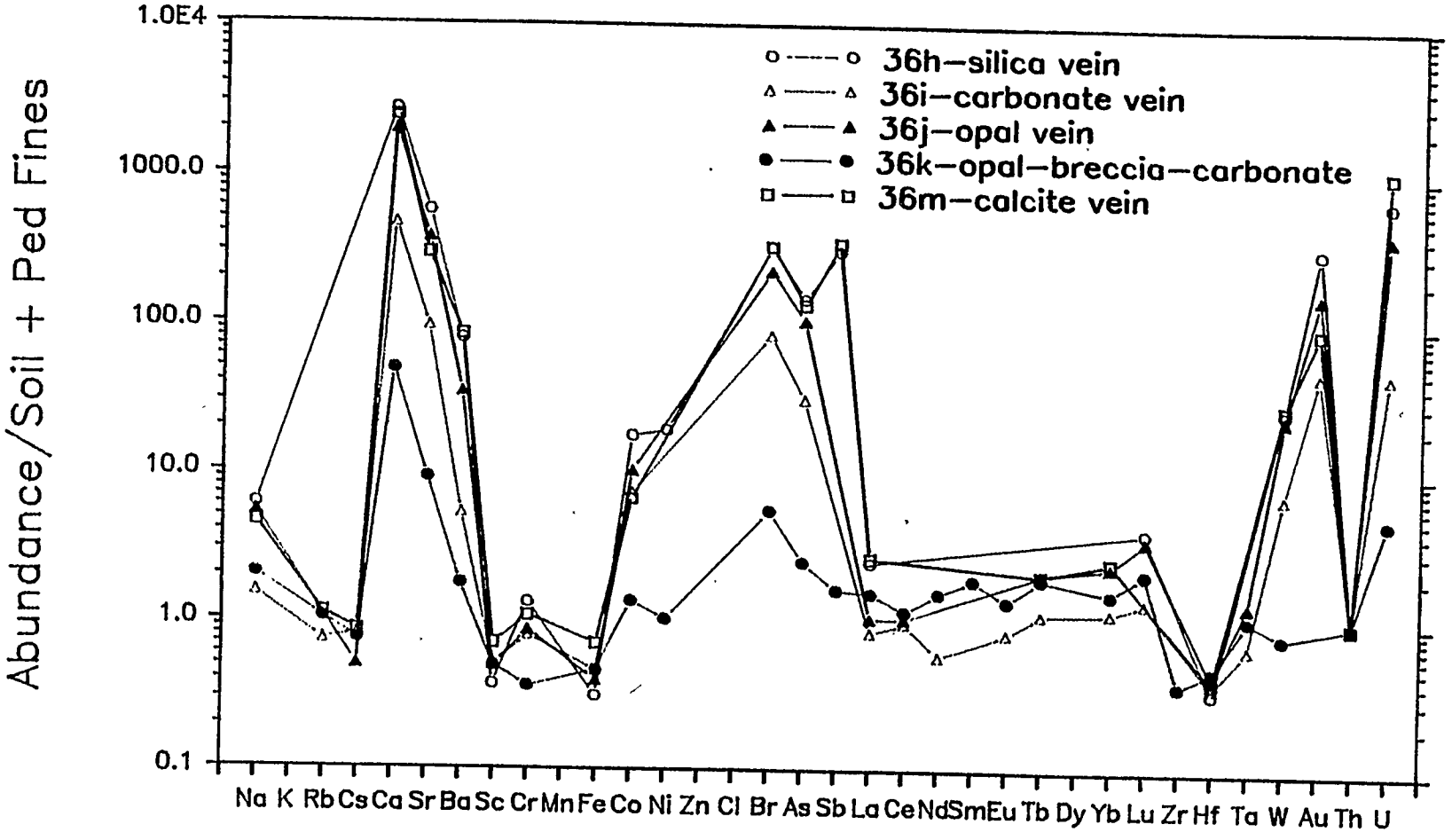
Abundance/Soil + Ped Fines
1.0E4
1000.0
100.0
10.0
1.0
0.1
36h–silica vein
36i–carbonate vein
36j–opal vein
36k–opal–breccia–carbonate
36m–calcite vein
Na K Rb Cs Ca Sr Ba Sc Cr Mn Fe Co Ni Zn Cl Br As Sb La Ce Nd Sm Eu Tb Dy Yb Lu Zr Hf Ta W Au Th U

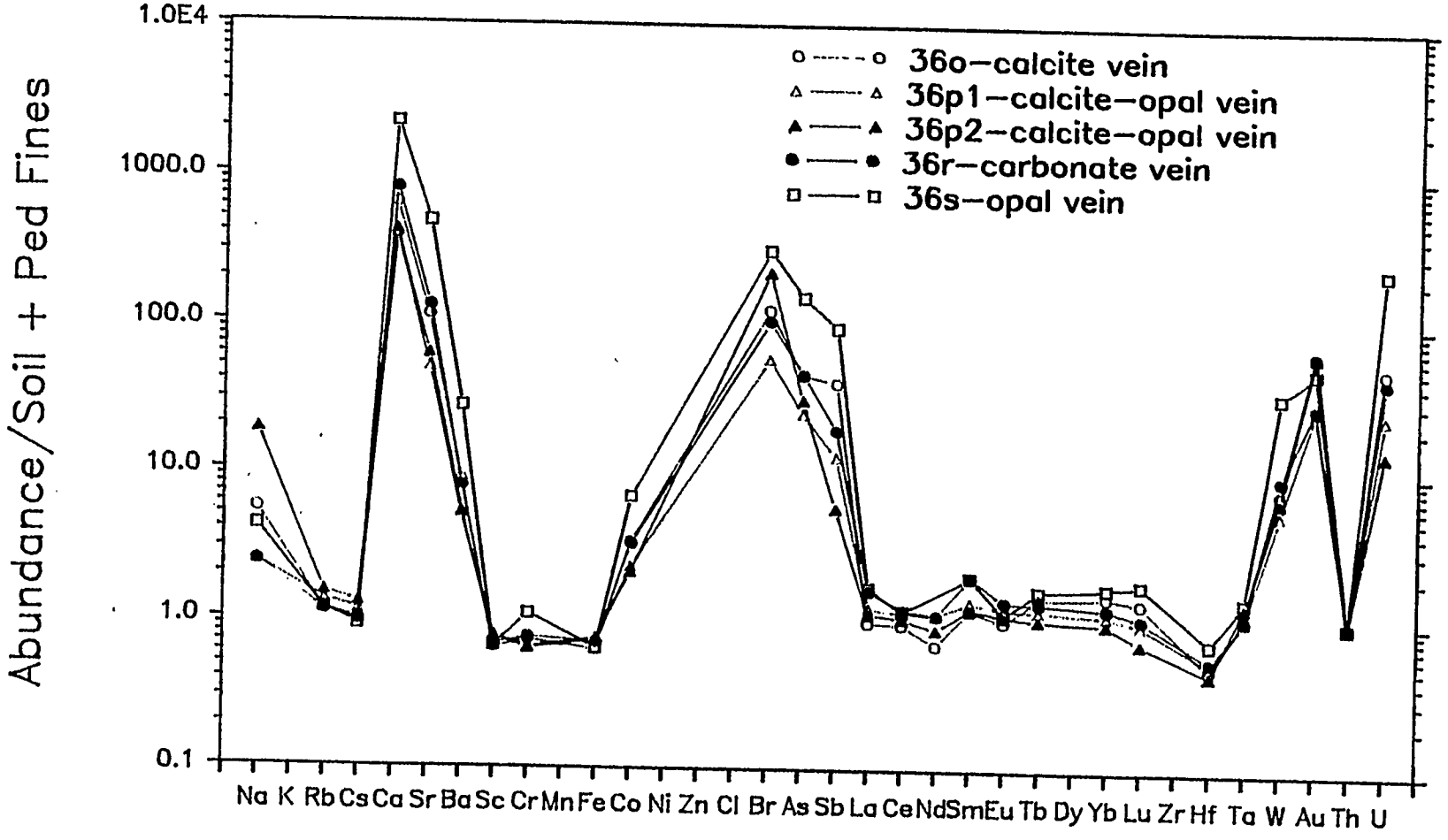
Abundance/Soil + Ped Fines
1.0E4
1000.0
100.0
10.0
1.0
0.1
36o—calcite vein
36p1—calcite—opal vein
36p2—calcite—opal vein
36r—carbonate vein
36s—opal vein
Na K Rb Cs Ca Sr Ba Sc Cr Mn Fe Co Ni Zn Cl Br As Sb La Ce Nd Sm Eu Tb Dy Yb Lu Zr Hf Ta W Au Th U

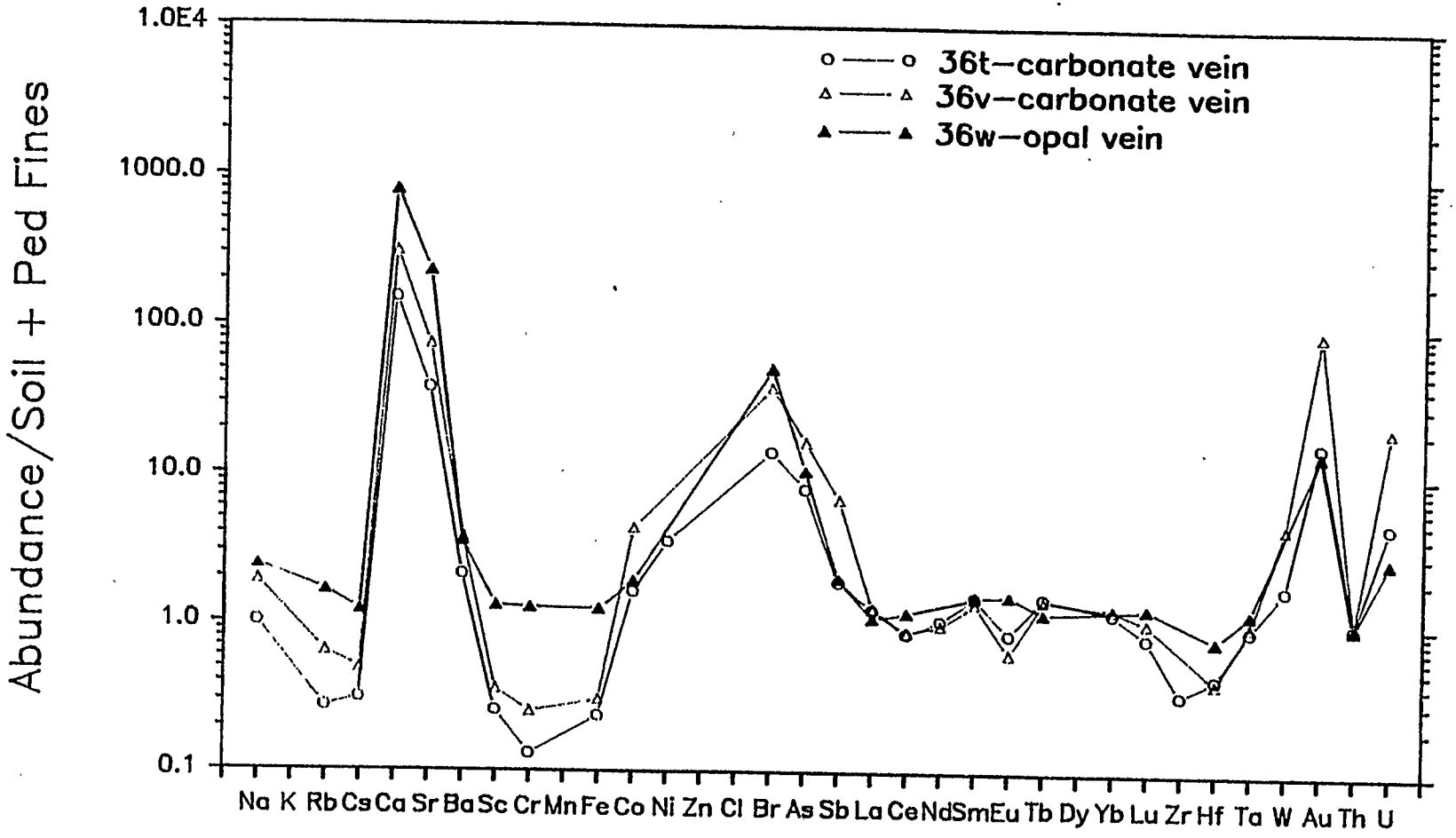
Abundance/Soil + Ped Fines
1.0E4
1000.0
100.0
10.0
1.0
0.1
36t–carbonate vein
36v–carbonate vein
36w–opal vein
Na K Rb Cs Ca Sr Ba Sc Cr Mn Fe Co Ni Zn Cl Br As Sb La Ce Nd Sm Eu Tb Dy Yb Lu Zr Hf Ta W Au Th U

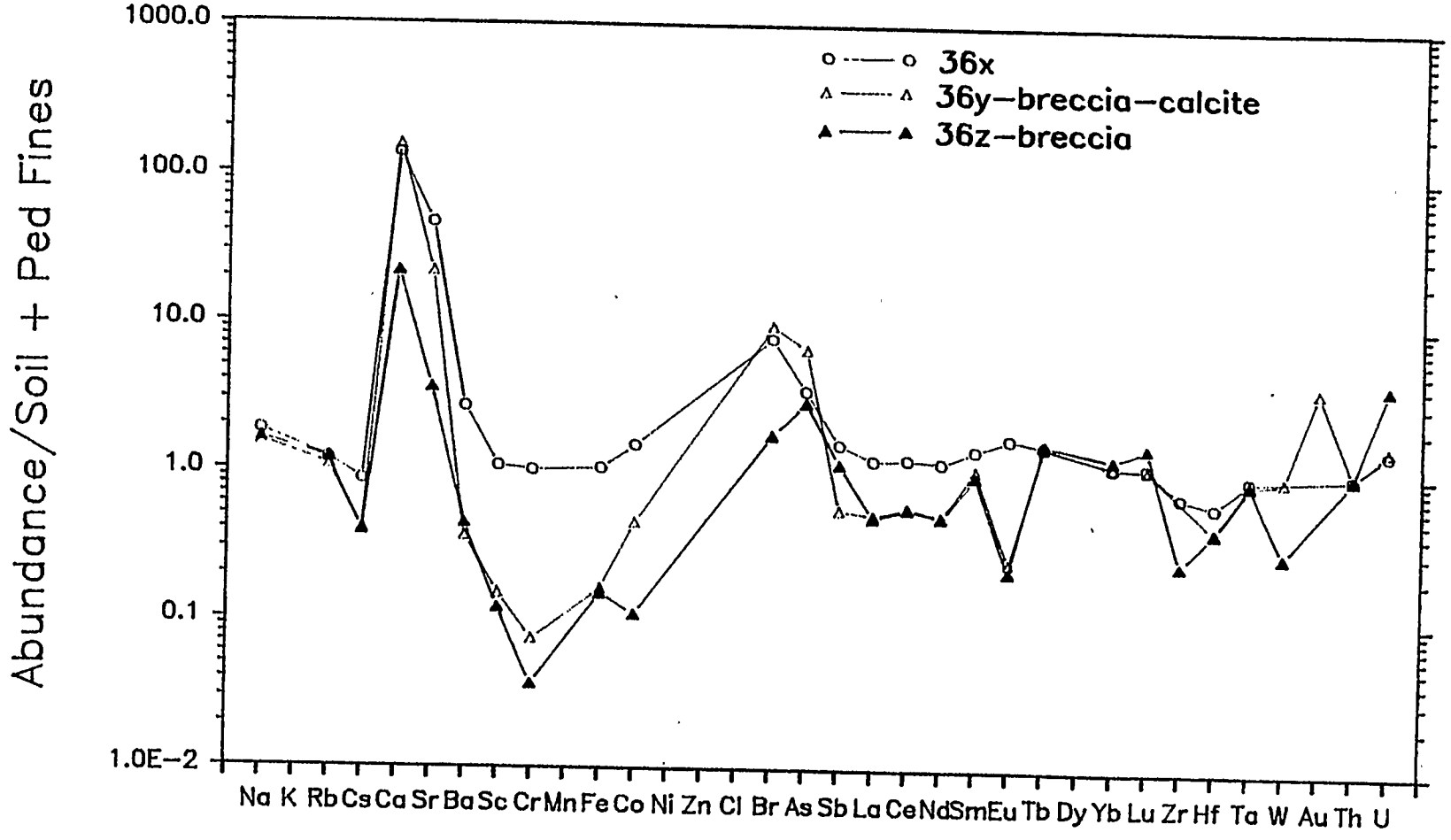
Abundance/Soil + Ped Fines
1000.0
100.0
10.0
1.0
0.1
1.0E-2
36x
36y-breccia-calcite
36z-breccia
Na K Rb Cs Ca Sr Ba Sc Cr Mn Fe Co Ni Zn Cl Br As Sb La Ce Nd Sm Eu Tb Dy Yb Lu Zr Hf Ta W Au Th U

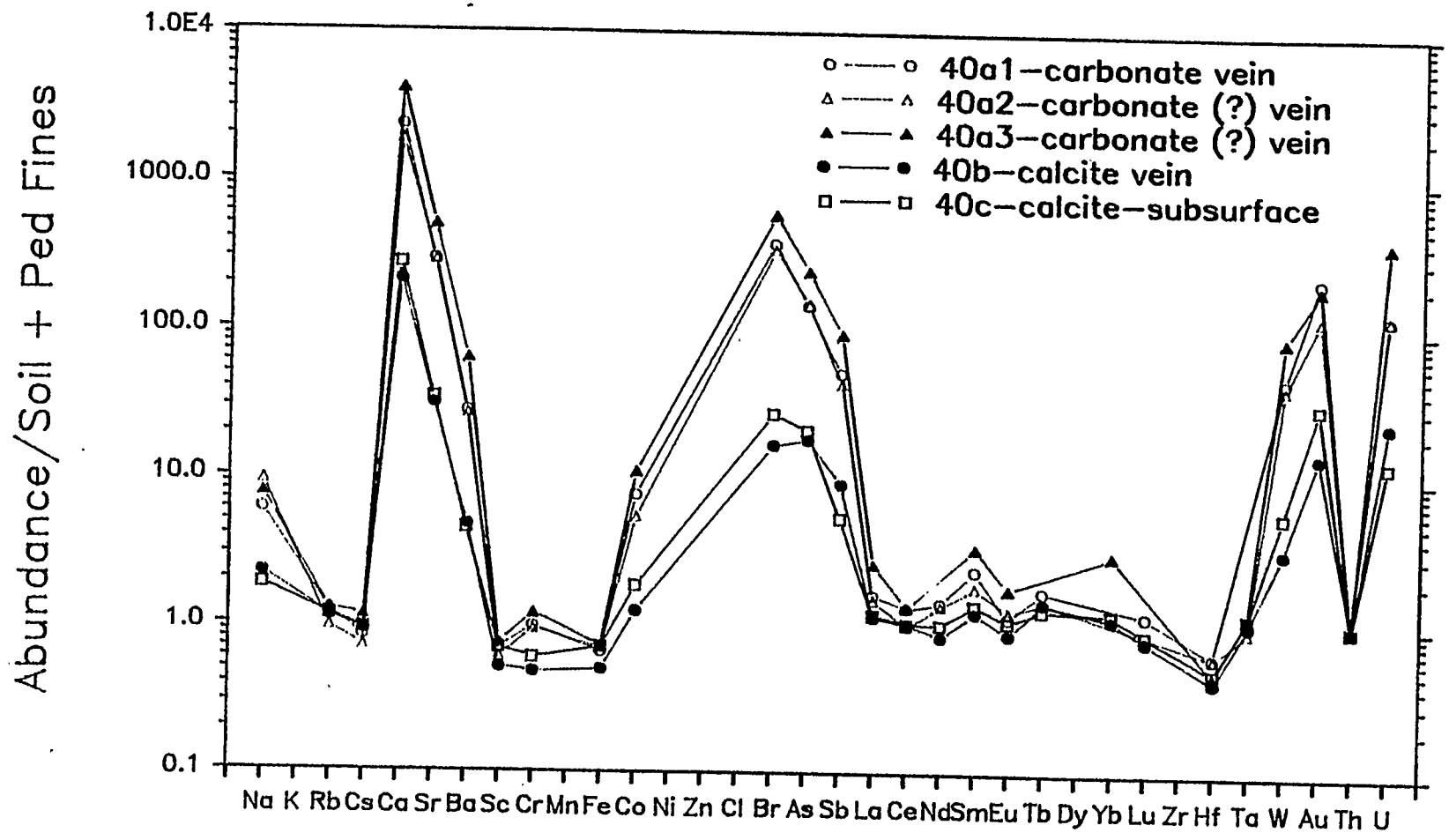
Abundance/Soil + Ped Fines
1.0E4
1000.0
100.0
10.0
1.0
0.1
40a1—carbonate vein
40a2—carbonate (?) vein
40a3—carbonate (?) vein
40b—calcite vein
40c—calcite—subsurface
Na K Rb Cs Ca Sr Ba Sc Cr Mn Fe Co Ni Zn Cl Br As Sb La Ce Nd Sm Eu Tb Dy Yb Lu Zr Hf Ta W Au Th U

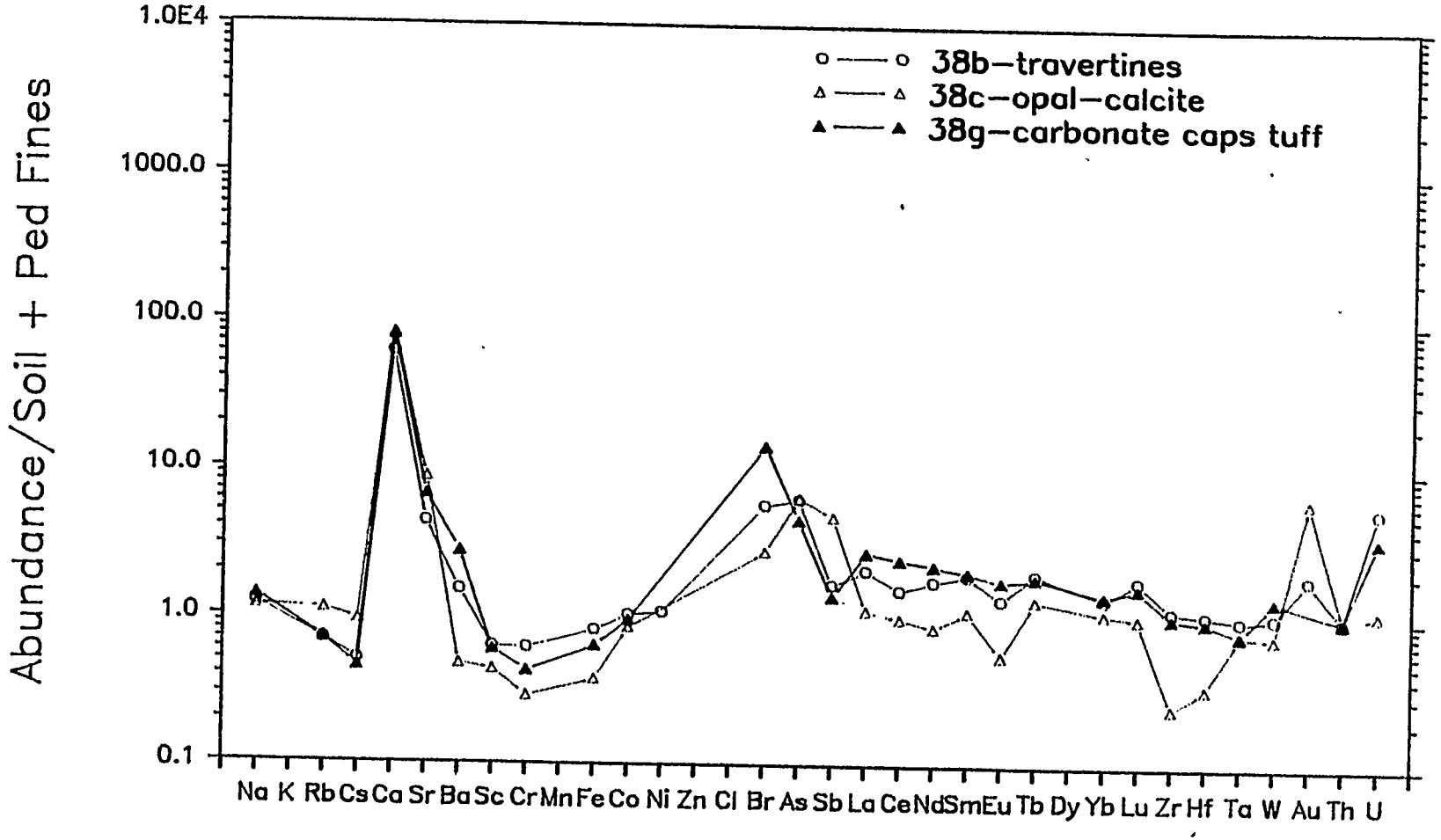
Abundance/Soil + Ped Fines
1.0E4
1000.0
100.0
10.0
1.0
0.1
38b—travertines
38c—opal—calcite
38g—carbonate caps tuff
Na K Rb Cs Ca Sr Ba Sc Cr Mn Fe Co Ni Zn Cl Br As Sb La Ce Nd Sm Eu Tb Dy Yb Lu Zr Hf Ta W Au Th U

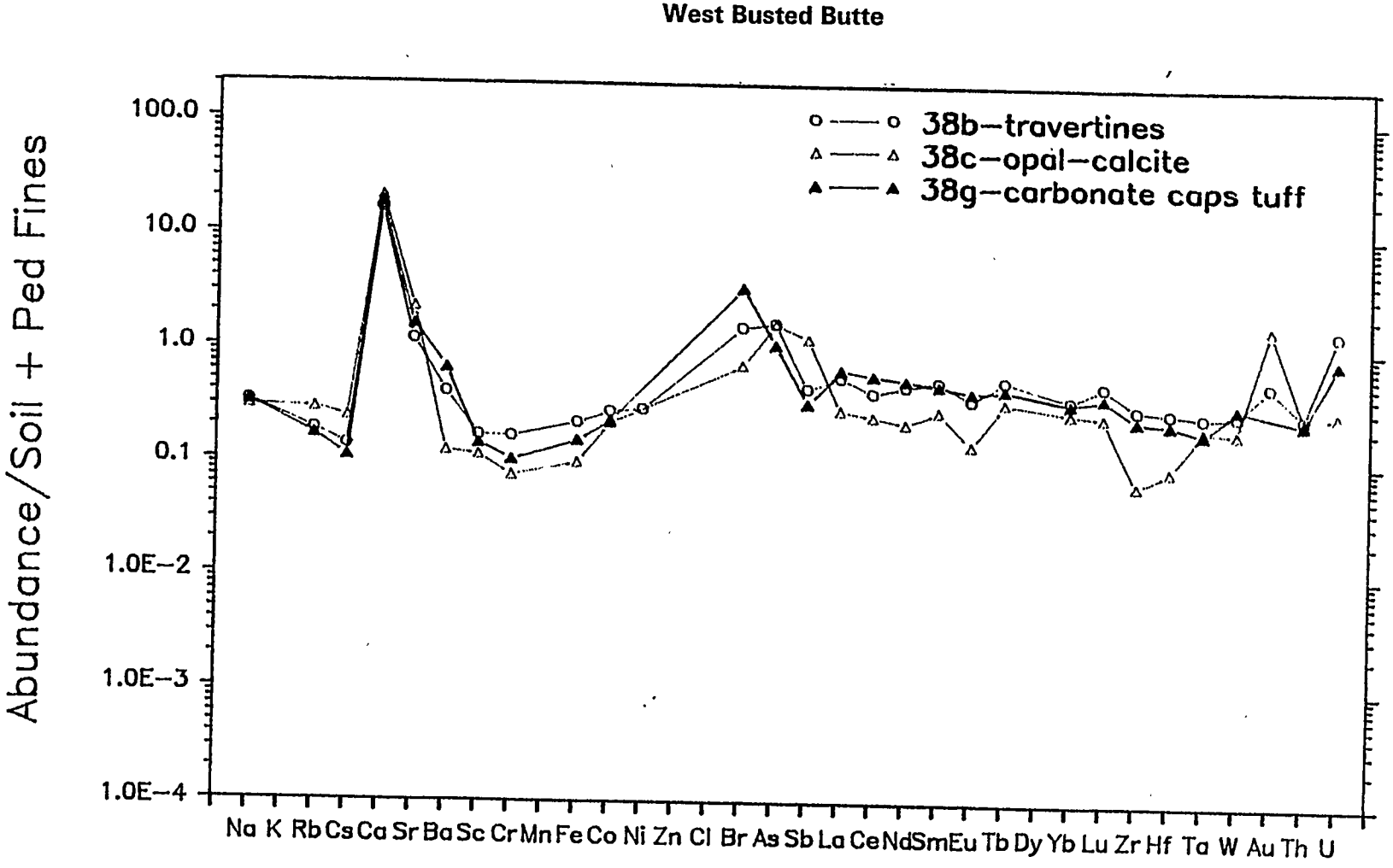
West Busted Butte
Abundance/Soil + Ped Fines
100.0
10.0
1.0
0.1
1.0E−2
1.0E−3
1.0E−4
38b−travertines
38c−opal−calcite
38g−carbonate caps tuff
Na K Rb Cs Ca Sr Ba Sc Cr Mn Fe Co Ni Zn Cl Br As Sb La Ce Nd Sm Eu Tb Dy Yb Lu Zr Hf Ta W Au Th U

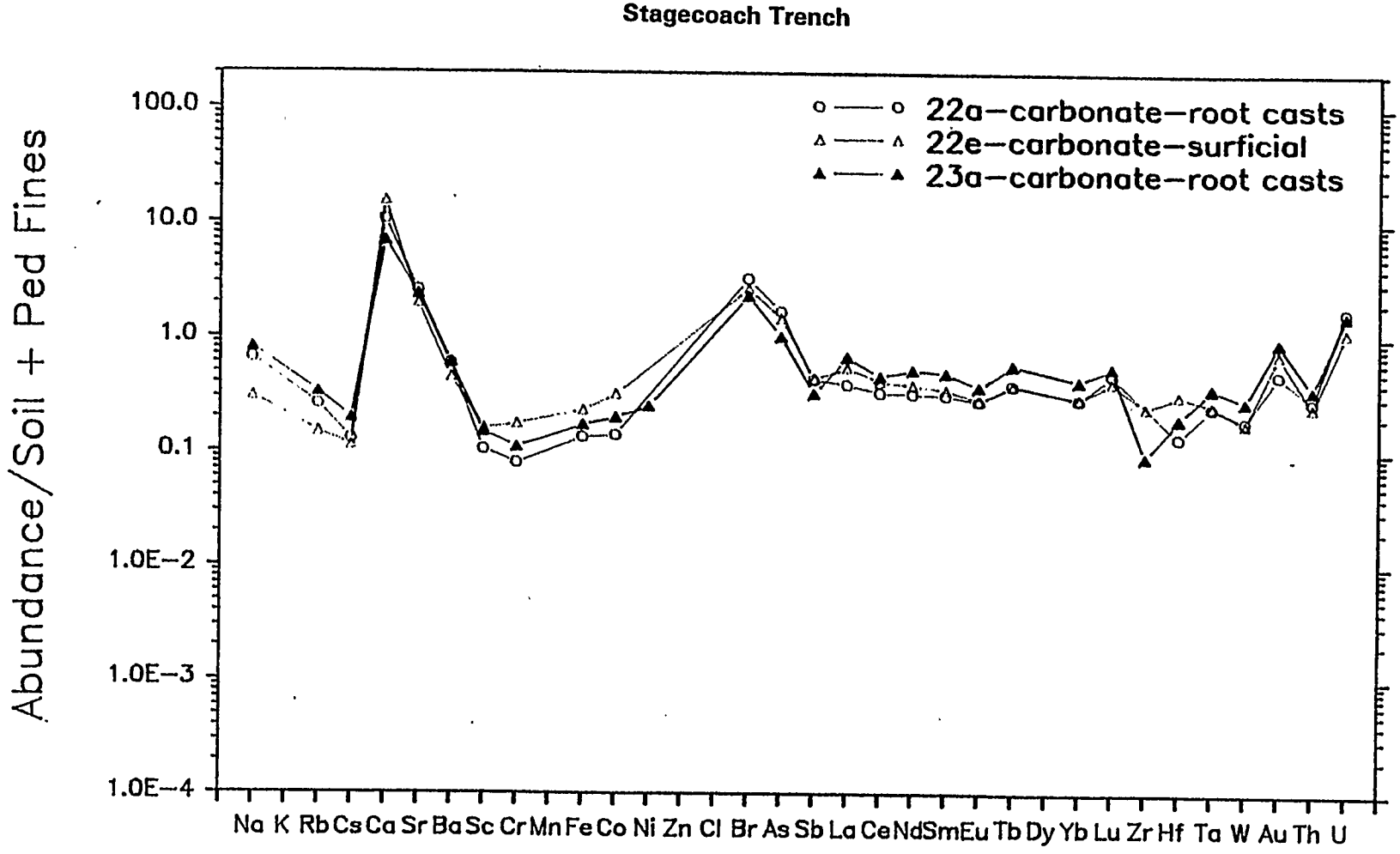
Stagecoach Trench
Abundance/Soil + Ped Fines
100.0
10.0
1.0
0.1
1.0E-2
1.0E-3
1.0E-4
22a-carbonate-root casts
22e-carbonate-surficial
23a-carbonate-root casts
Na K Rb Cs Ca Sr Ba Sc Cr Mn Fe Co Ni Zn Cl Br As Sb La Ce Nd Sm Eu Tb Dy Yb Lu Zr Hf Ta W Au Th U

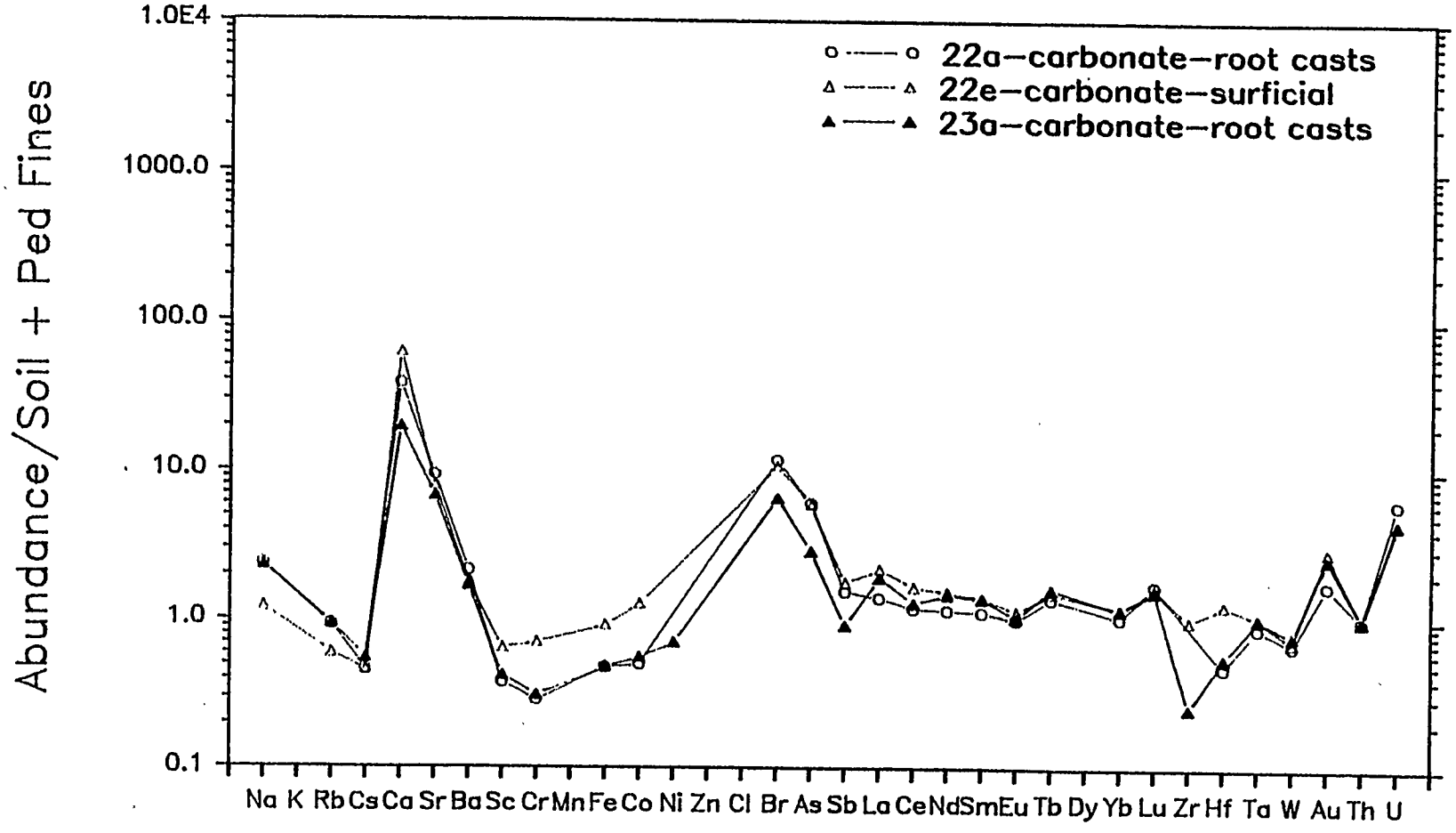
Abundance/Soil + Ped Fines
1.0E4
1000.0
100.0
10.0
1.0
0.1
22a–carbonate–root casts
22e–carbonate–surficial
23a–carbonate–root casts
Na K Rb Cs Ca Sr Ba Sc Cr Mn Fe Co Ni Zn Cl Br As Sb La Ce Nd Sm Eu Tb Dy Yb Lu Zr Hf Ta W Au Th U

Site 199

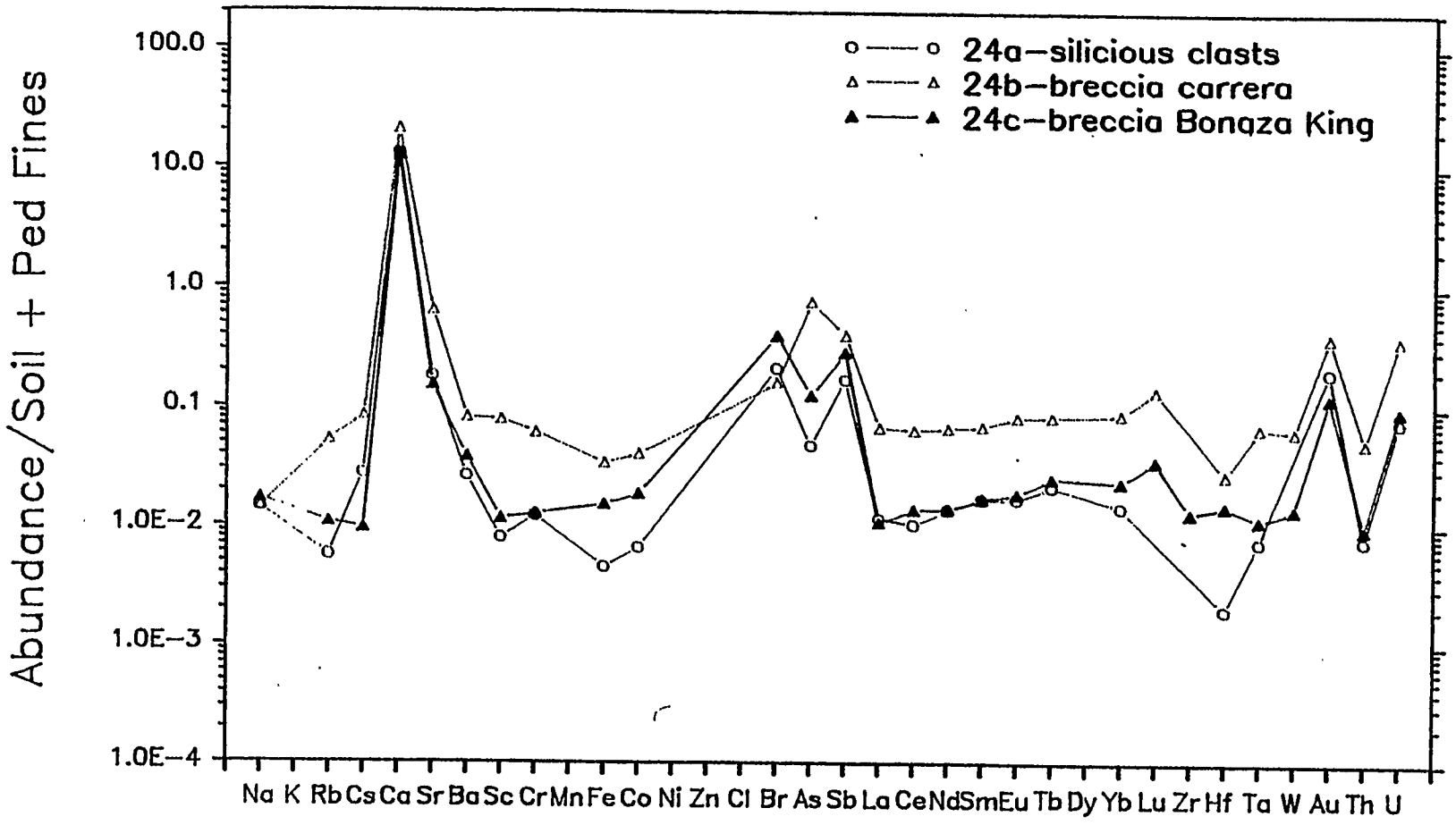
Abundance/Soil + Ped Fines
100.0
10.0
1.0
0.1
1.0E-2
1.0E-3
1.0E-4
24a—silicious clasts
24b—breccia carrera
24c—breccia Bonaza King
Na K Rb Cs Ca Sr Ba Sc Cr Mn Fe Co Ni Zn Cl Br As Sb La Ce Nd Sm Eu Tb Dy Yb Lu Zr Hf Ta W Au Th U

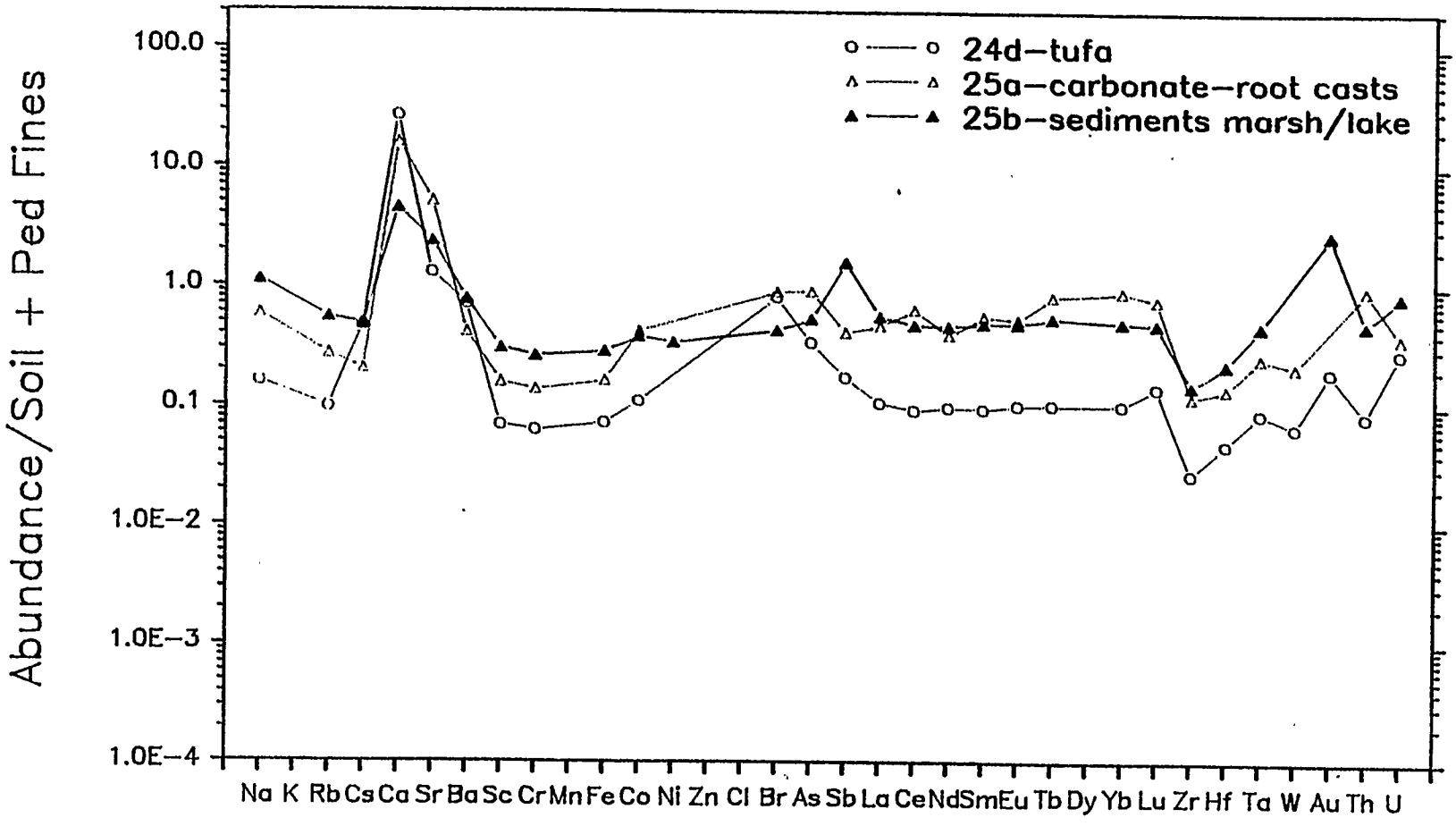
Abundance/Soil + Ped Fines
100.0
10.0
1.0
0.1
1.0E-2
1.0E-3
1.0E-4
24d-tufa
25a-carbonate-root casts
25b-sediments marsh/lake
Na K Rb Cs Ca Sr Ba Sc Cr Mn Fe Co Ni Zn Cl Br As Sb La Ce Nd Sm Eu Tb Dy Yb Lu Zr Hf Ta W Au Th U

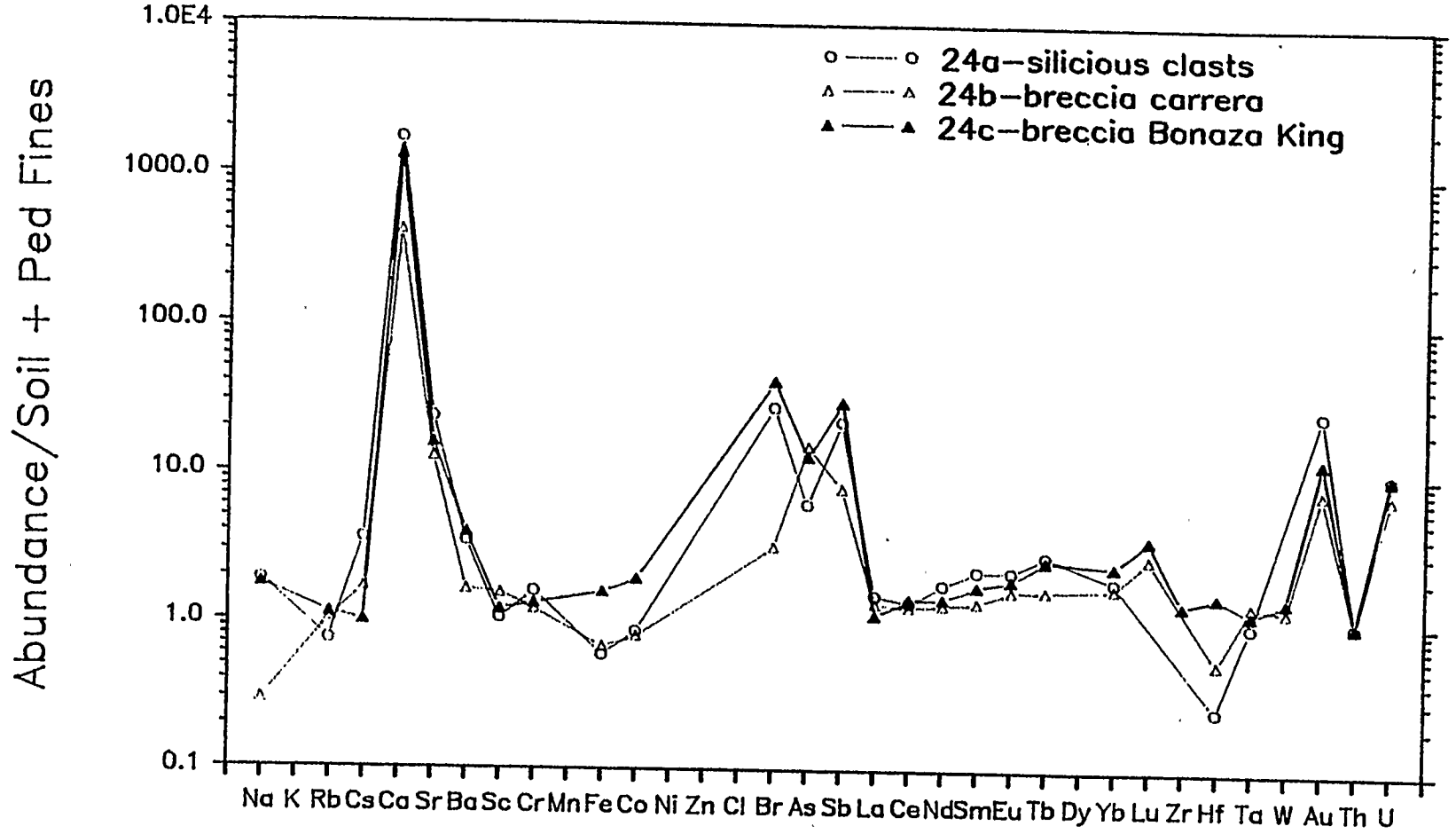
Abundance/Soil + Ped Fines
1.0E4
1000.0
100.0
10.0
1.0
0.1
24a–silicious clasts
24b–breccia carrera
24c–breccia Bonaza King
Na K Rb Cs Ca Sr Ba Sc Cr Mn Fe Co Ni Zn Cl Br As Sb La Ce Nd Sm Eu Tb Dy Yb Lu Zr Hf Ta W Au Th U

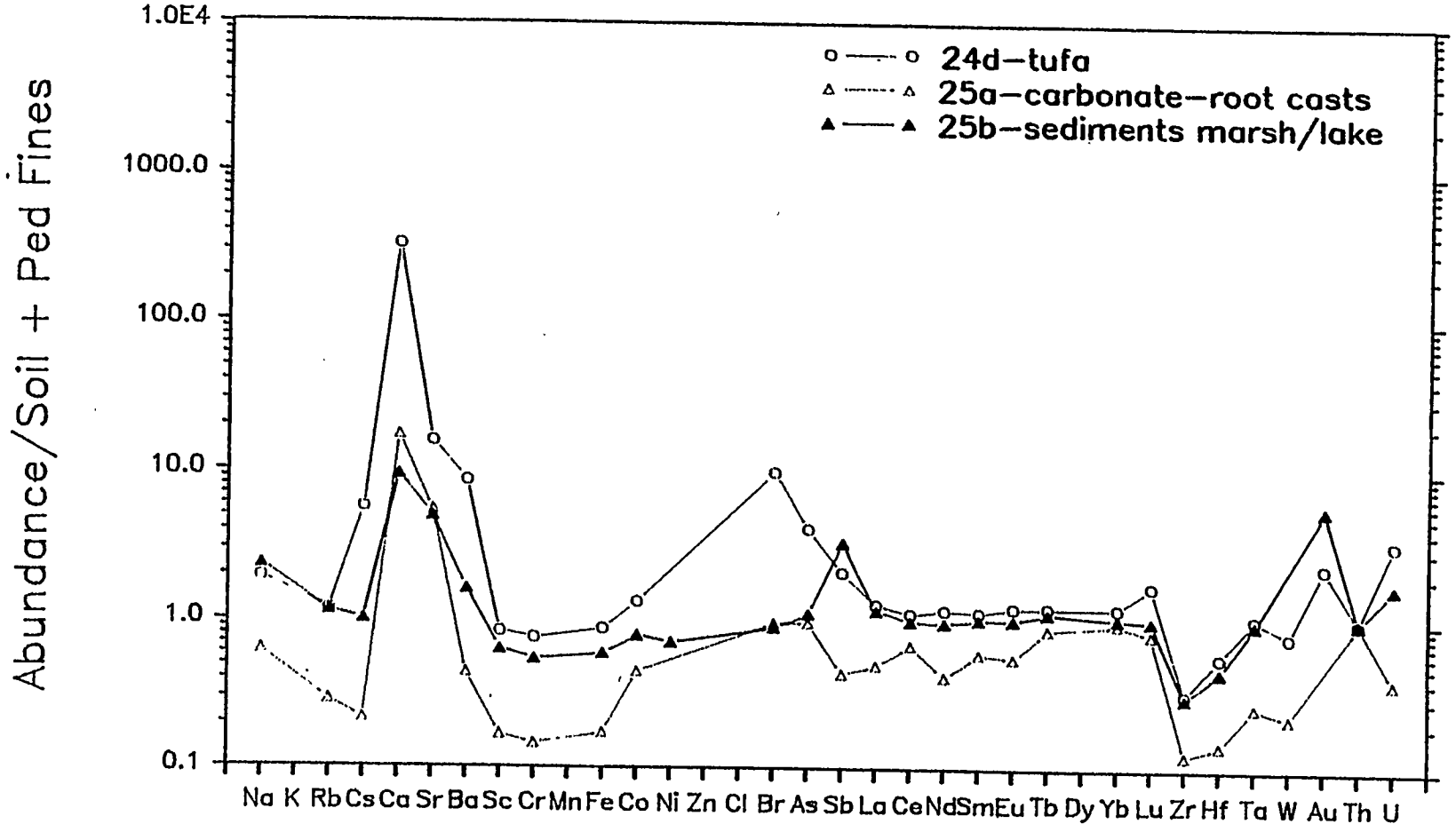
Abundance/Soil + Ped Fines
1.0E4
1000.0
100.0
10.0
1.0
0.1
24d–tufa
25a–carbonate–root casts
25b–sediments marsh/lake
Na K Rb Cs Ca Sr Ba Sc Cr Mn Fe Co Ni Zn Cl Br As Sb La Ce Nd Sm Eu Tb Dy Yb Lu Zr Hf Ta W Au Th U

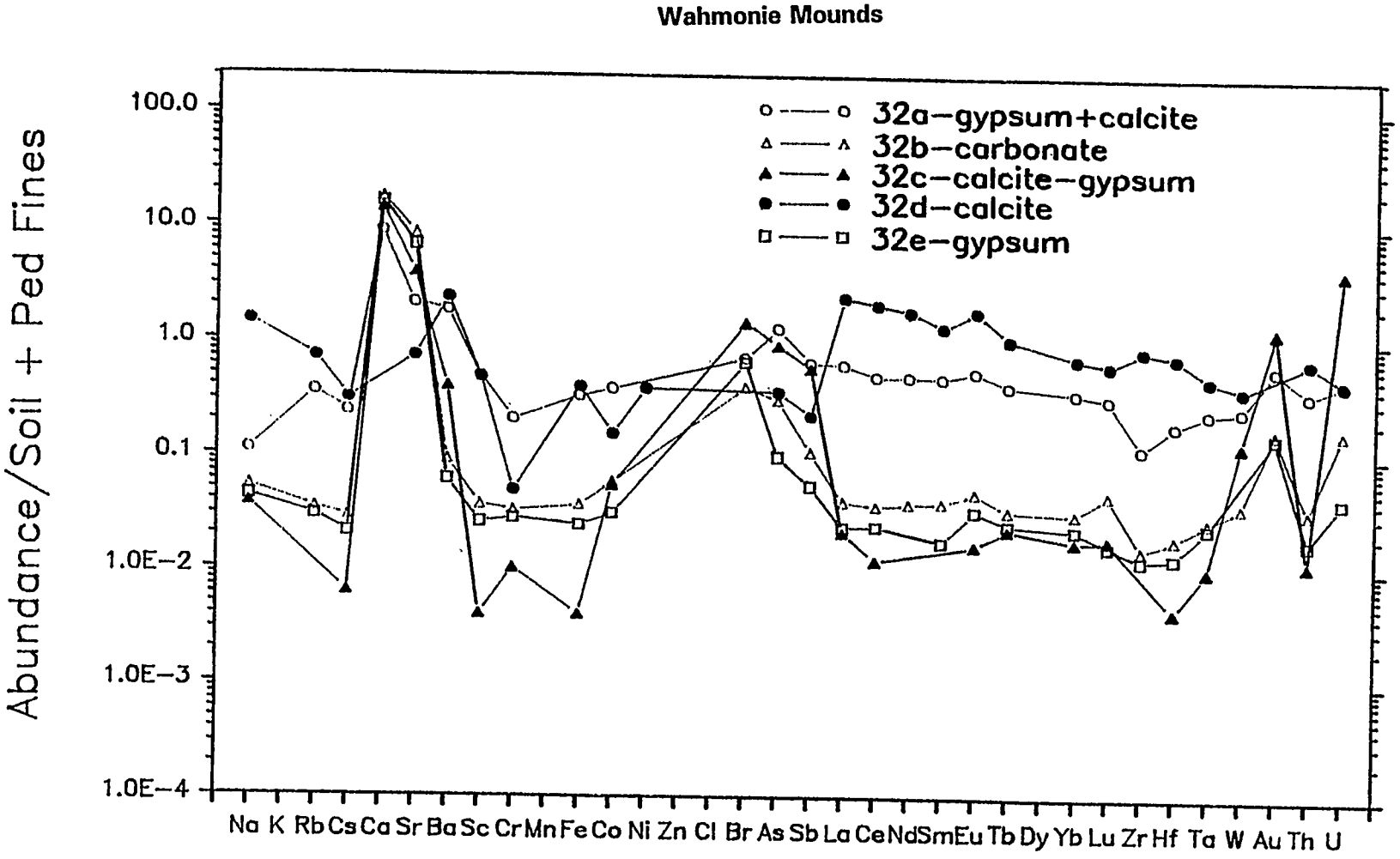
Wahmonie Mounds
Abundance/Soil + Ped Fines
100.0
10.0
1.0
0.1
1.0E−2
1.0E−3
1.0E−4
32a−gypsum+calcite
32b−carbonate
32c−calcite−gypsum
32d−calcite
32e−gypsum
Na K Rb Cs Ca Sr Ba Sc Cr Mn Fe Co Ni Zn Cl Br As Sb La Ce Nd Sm Eu Tb Dy Yb Lu Zr Hf Ta W Au Th U

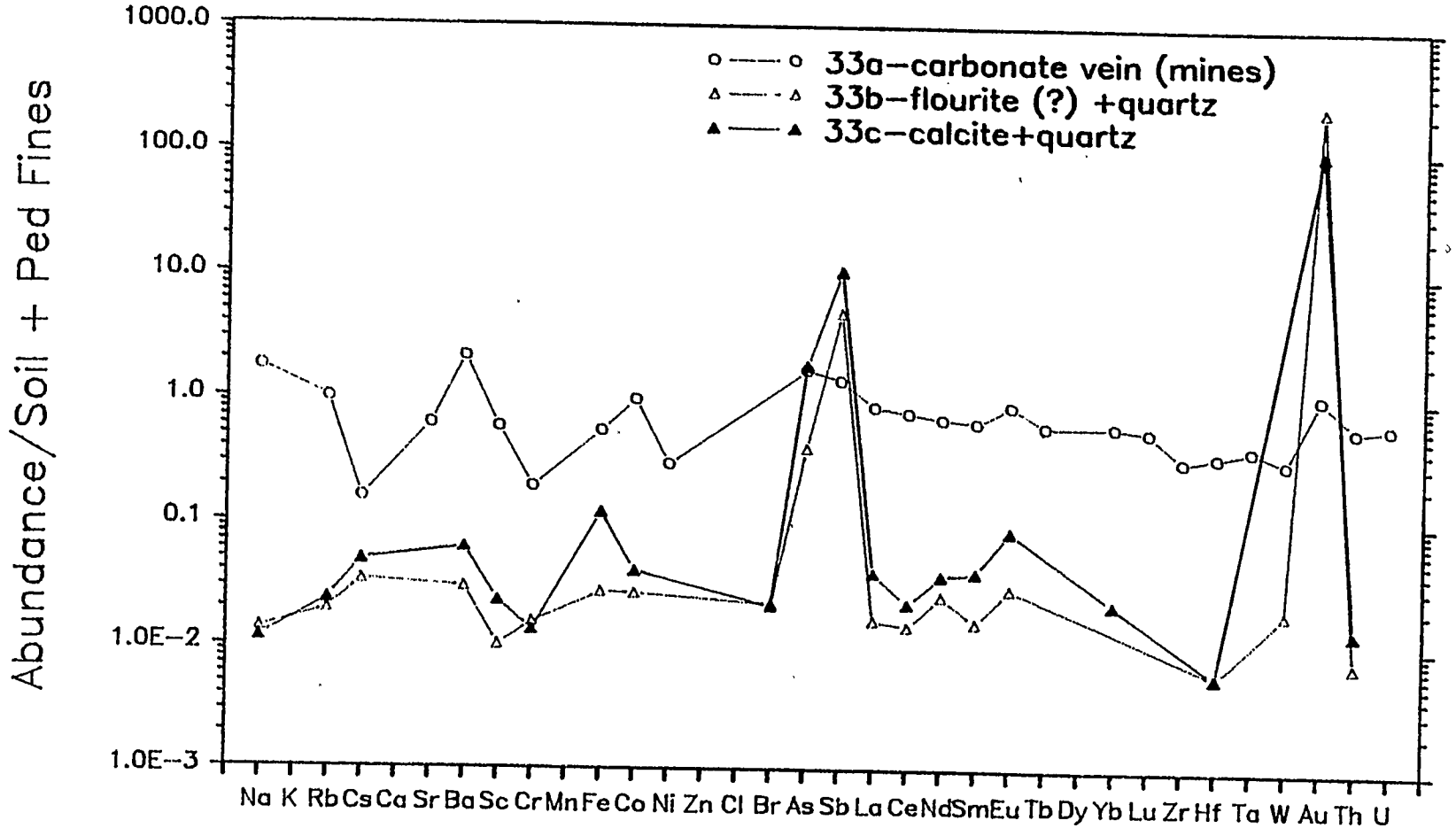
Abundance/Soil + Ped Fines
1000.0
100.0
10.0
1.0
0.1
1.0E-2
1.0E-3
33a-carbonate vein (mines)
33b-flourite (?) +quartz
33c-calcite+quartz
Na K Rb Cs Ca Sr Ba Sc Cr Mn Fe Co Ni Zn Cl Br As Sb La Ce Nd Sm Eu Tb Dy Yb Lu Zr Hf Ta W Au Th U

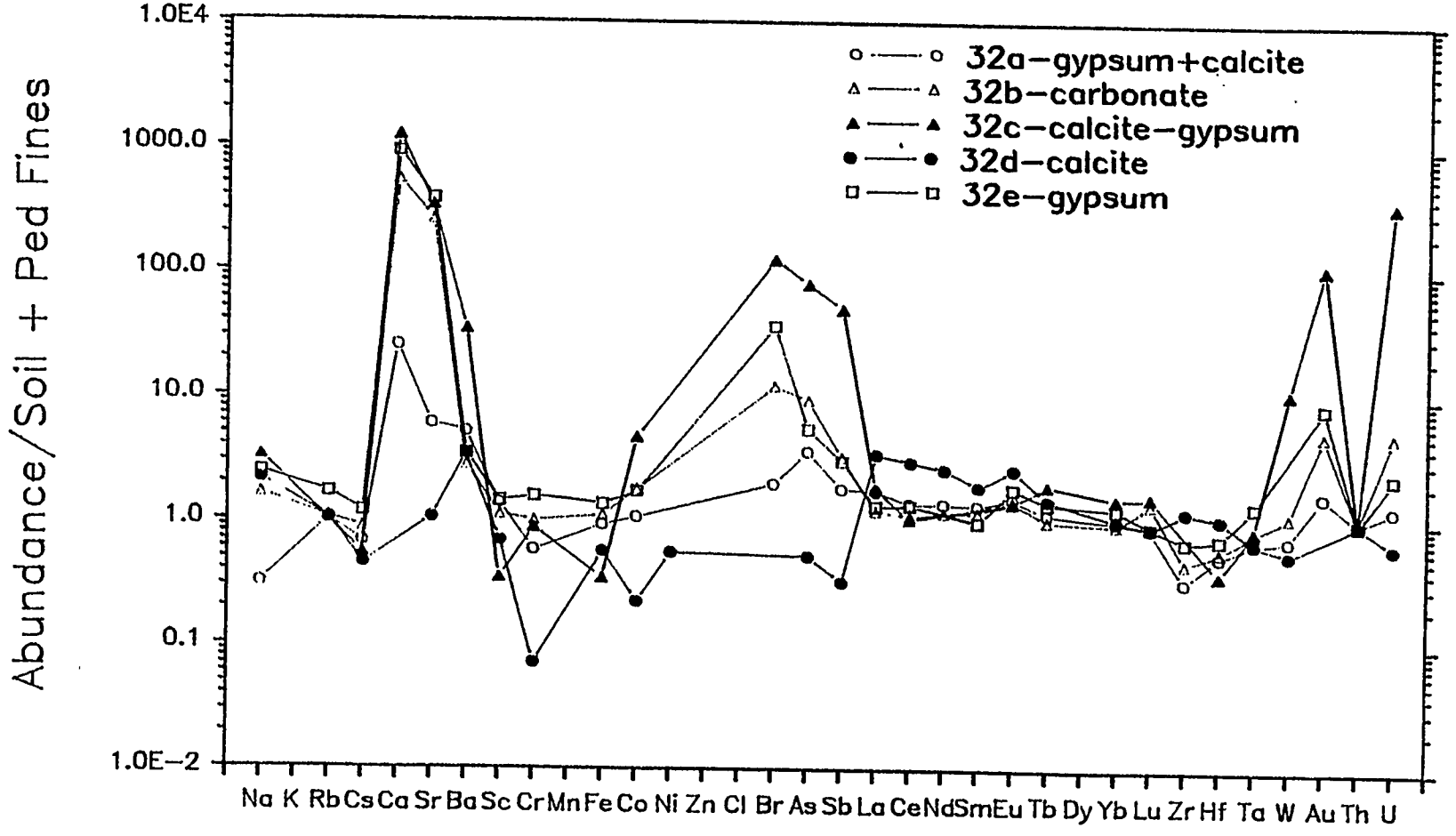
Abundance/Soil + Ped Fines
1.0E4
1000.0
100.0
10.0
1.0
0.1
1.0E-2
32a-gypsum+calcite
32b-carbonate
32c-calcite-gypsum
32d-calcite
32e-gypsum
Na K Rb Cs Ca Sr Ba Sc Cr Mn Fe Co Ni Zn Cl Br As Sb La Ce Nd Sm Eu Tb Dy Yb Lu Zr Hf Ta W Au Th U

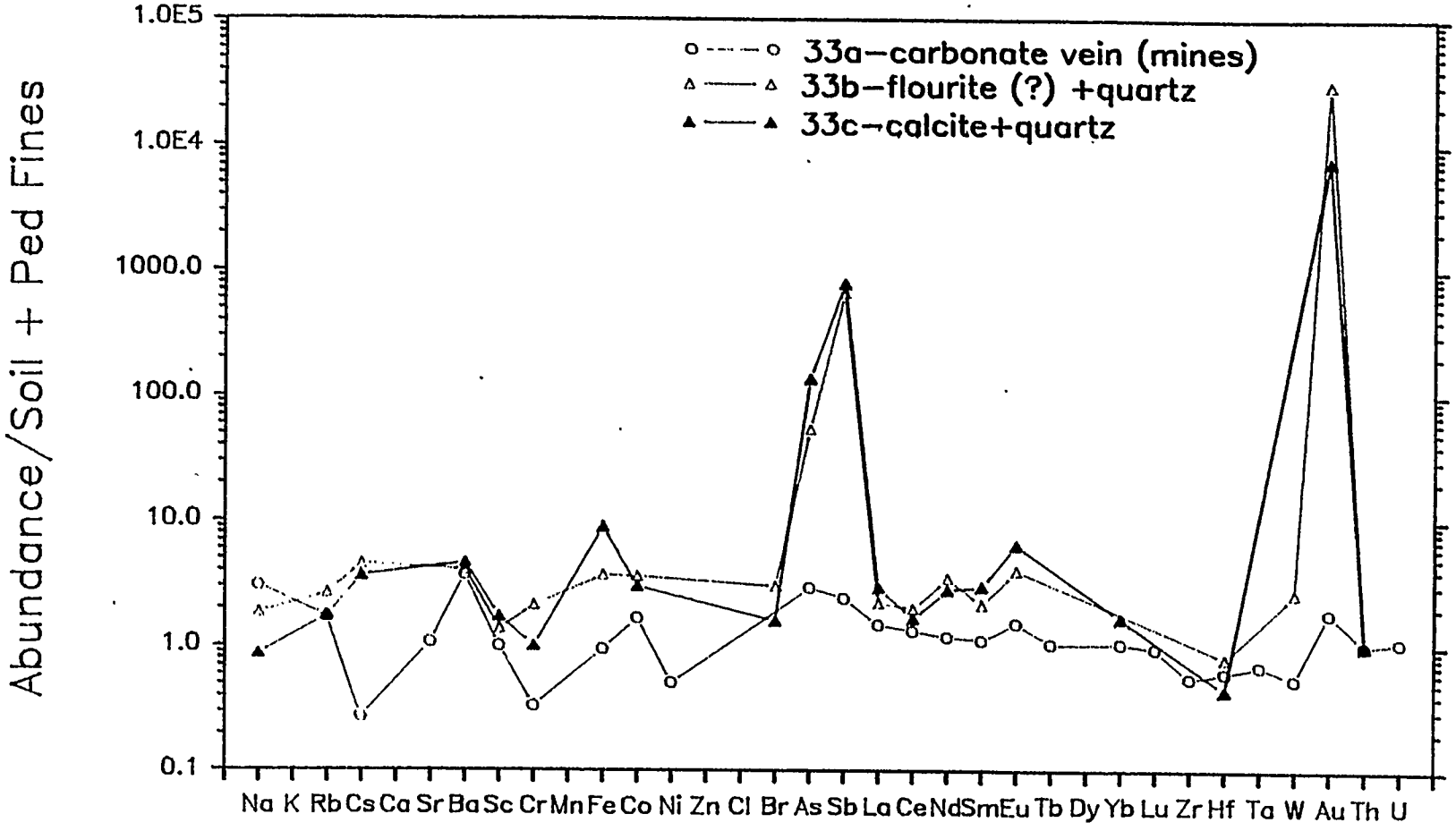
Abundance/Soil + Ped Fines
1.0E5
1.0E4
1000.0
100.0
10.0
1.0
0.1
33a–carbonate vein (mines)
33b–flourite (?) +quartz
33c–calcite+quartz
Na K Rb Cs Ca Sr Ba Sc Cr Mn Fe Co Ni Zn Cl Br As Sb La Ce Nd Sm Eu Tb Dy Yb Lu Zr Hf Ta W Au Th U

PART III: MODELING HYDROTECTONIC PHENOMENA AT YUCCA MOUNTAIN

Section A: Extension of In-Situ Stress Test Analysis to Rapid Hole Evacuation at Yucca Mountain Due to a Network of Open Conduits

By J. B. Davies

Extension of In-situ Stress Test Analysis to Rapid Hole Evacuation at Yucca Mountain due to a Network of Open Conduits

Dr. John Bruce Davies

Abstract

Yucca Mountain is underlain by tuffaceous rocks that are highly fractured and jointed. During drilling of bore-holes at Yucca Mountain there were numerous occurrences of lost circulation when whole mud was taken by the formation. This evidence suggests that parts of Yucca Mountain are controlled hydrologicaly by a network of open conduits along the existing joints and fractures. Also at Yucca Mountain, stress tests have been performed in-situ by charging a small section along the bore-holes with an excess pressure head of water. For many of these tests, the initial drop in water head was so rapid that within seconds up to hundreds of meters of fall had occurred. The opening of fractures as the excess head increases has previously been proposed as an important factor in explaining the shape of the stress test curves at lower pressures. We propose that such induced hydraulic fractures, under increasing water heads, can grow to a length sufficient to intersect the existing network of open joints and fractures. We extend our previous model to incorporate flow out along these open conduits and examine the initial rapid drop in terms of these extended models. We show that this rapid evacuation model fits the observed data from many slug tests in wells in the vicinity of Yucca Mountain. This result is confirmation of the drilling evidence that a network of open conduits exists at various depths below the water table and over a large geographic region around Yucca Mountain.

Introduction

The water table below Yucca Mountain is abnormally low compared to its surrounding hydrological environment. No general consensus has developed for an explanation of this abnormal depth of the water table which is of the order of 500 meters. One explanation is that the subsurface is a deforming fractured medium where dilatation of fractures has increased the storativity and hydraulic conductivity in this region and thereby depressed the water table. In order to investigate the state of stress above and below this abnormal water table, both hydrofracture and slug tests have been performed by injecting water into boreholes on and near Yucca Mountain. For many of these tests, the initial evacuation was so rapid that the first measurement after a few seconds showed the head had dropped by up to hundreds of meters.

In order to understand this phenomenon, we extend our simple but comprehensive model of these borehole and fracture flows. This flow model incorporates pre-existing fractures that readily dilate with increasing water head. New cracks can open above the critical pressure producing new crack surfaces. As these fractures grow with increasing head, they can intersect any existing network of open conduits and thereby affect the rate of flow. As well as the usual drainage into the surrounding rock matrix, the model incorporates loss of water out of the system through fractures that act as conduits to the external environment.

This situation is mathematically modeled by developing a formulation using conservation of water mass in the borehole-fracture system. We adopt constitutive laws which specify exiting fluxes and fracture properties as a function of the existing excess pressure head. Only the mass conservation law need be applied on assuming a func-

tional dependence of the area and aperture of the crack systems on the excess pressure head. These model solutions are used to determine discriminative graphs, "type curves", that are typical of different fracture systems and behaviour. Type curves and analyses, based on this modeling, are applied to Yucca Mountain data from slug tests performed by other investigators. The limited data has allowed initial analyses categorizing the observed curves in terms of the synthetic curves for different fracture systems. Closure pressures were previously determined, whenever possible, from inspection and non-linear curve fitting. In the present study, initial rapid evacuations are analysed in terms of flow through open conduits until the head drops to below the pressure needed to keep the hydrofracture connected to the open conduit.

Measurements of the early-time data are obtained from slug tests performed at wells in the vicinity of Yucca Mountain. This data is analysed and shown to be consistent with the rapid evacuation model. Values of time decay parameters obtained from the Yucca Mountain data imply that the flows to these open conduits are along narrow channels.

Drilling Evidence

A number of boreholes have been drilled in and near Yucca Mountain, Nevada, the proposed site for a nuclear waste depository. The site is shown in Figure 1. Healy (1988) has discussed the problems of drilling boreholes in and near Yucca Mountain. He comments : "At Yucca Mountain, drill crews talked about 'underground rivers', a description that attempts to explain the large amount of drilling fluids that were lost in the hole during drilling. Drilling conditions on Yucca Mountain are very unusual. The natural water table is about 1700 ft. below the surface and when the hole is drilled

with standard methods with circulating fluid, no fluid or drill cuttings return to the surface." Lost circulation occurs when whole mud is taken by the formation. The rate at which mud is lost is dependent on the type of formation and the mud density.

Whitaker (1985, p.137) has detailed the two major causes for rapid and continual mud loss during circulation: (1) fracturing of the formation due to mud pressure, and (2) loss through interconnected vugs or preexisting open fractures. We shall use these mechanisms in our modeling of in-situ water injection tests by incorporating the concepts of induced fractures growing under the increasing water head with the possible subsequent interconnection of this hydraulic fracture with an open conduit. The rapid loss of drilling fluids, together with the field evidence of a fracture-dominated geohydrology, is thus indicative of a pre-existing network of open conduits along joints and fractures.

Conservation Laws

Any fluid-rock system obeys the conservation laws for mass, momentum and energy. We shall develop the general equations of conservation for the simplest system which is composed of a borehole, the hydrofracture and its intersection at a few places with the network of open conduits in a fractured rock system of variable geometry. A stylized representation of such a system is illustrated in Figure 2 and is similar to that used by Hayashi and Haimson (1991). It is assumed that water can exit the borehole-fracture system either by percolation into the surrounding rock or by flow out along conduits. The walls of the borehole and fractures are assumed to transmit the fluid into the porous rock matrix. The water is considered to be incompressible, so the density will be removed from all equations.

The conservation of mass under these conditions is given by:

$$\frac{d}{dt}(V_c + V_p) = Q \tag{1}$$

where V_c is the volume of water in the cracks at time t and V_p is the volume of water in the borehole. Q is the rate at which water exits the system either along conduits or by percolation into the rock face from the fractures and borehole. This relation assumes no water is injected into the system after the head is allowed to free-fall. The volume of water in the borehole is given by the product of the cross-sectional area, $A_p = \pi R_p^2$, where R_p is the radius of the borehole pipe, times the height of the column of water. This height is equal to the sum of the excess head, h(t), and the depth of the borehole below the water table above the test region, which is a constant. Thus, conservation of mass can be written as:

$$A_p \frac{dh(t)}{dt} + \frac{d}{dt} V_c(t) = Q(t) \tag{2}$$

In order to examine the effect of the changing excess head, certain simple constitutive relations must be formulated for the storativity volume and the exiting flux. These will be inserted into the mass conservation law in the equation (2). In particular, the crack volume is an important property of the system whose value is the crack area times the aperture. The surface area of pre-existing cracks is assumed constant when the excess water head is below the critical pressure, though their aperture will be a function of the applied head. When the head is greater than the critical pressure, we assume a constitutive relation wherein the volume and surface area of newly opened cracks is a function of the difference between the excess head and the critical pressure.

The volume of the pre-existing cracked region can be approximated by the product of the cracked area and an effective displacement normal to the surface. We shall

assume that any cracks present below the closure pressure have initial values of crack surface area A_e and crack volume V_e. Thus, for $h(t) < P_c$ we assume A_e is a constant, and $V_e = A_e * D_e$, where the crack aperture D_e varies with changing head. As the imposed head increases, we expect the aperture of these pre-existing cracks to increase functionally with the applied head, i.e.

$$D_e = D_o + F(h) \tag{3}$$

where D_o is the aperture at ambient pressures, F(h) is assumed to be a power-law or logarithmic function of head h. Here F(h) measures how readily the existing open cracks dilate under external head. Thus, for $h(t) < P_c$ we obtain the time derivative of crack volume as :

$$\frac{d}{dt}V_e(t) = A_e \cdot \frac{dF}{dh} \cdot \frac{dh}{dt} \tag{4}$$

When the external head is greater than the fracture closure pressure, new cracks will open which have new surface area and a finite volume. It will be assumed, to the first order, that the area of the newly cracked region, A_c, is a function of the head above the critical pressure, P_c. Thus, for $h(t) > P_c$, we assume:

$$A_c = G(h-P_c) \tag{5}$$

where G is a measure of the change of area with excess head above the critical pressure $h-P_c$. We will not assume initial knowledge of these functions, but will advance the analysis as far as possible without a specific functional form assumed. We shall use a functional dependence of aperture on head, as in the case of pre-existing cracks, but with different parameters for these initially closed cracks. We take :

$$D_c = J(h,P_c) \tag{6}$$

where the aperture is zero when $h = P_c$. The function J can be power-law or loga-

rithmic depending on the constitutive relation assumed. Incorporating these constitutive assumptions, for $h>P_c$, the rate of change of crack volume is :

$$\frac{d}{dt}V_e = (A_e\frac{dF}{dh} + [G\frac{dJ}{dh} + J\frac{dG}{dh}])\cdot\frac{dh}{dt} \qquad (7)$$

Exiting Water Flows

Nature displays a wide range of flow phenomena in the subsurface where water can flow slowly through pores and rapidly along fractures. When water is pumped into a well for in-situ stress tests, it can display head rate drops ranging in time from slow, due to percolation into tight rocks, to the most rapid drop possible i.e. near free-fall. In near free-fall drops, values of the head at early times are difficult to determine, implying that the water is exiting the system rapidly through open fractures and/or is flushed out by subsurface flows along open conduits. We must incorporate these flow characteristics into the functional dependence of Q, the exiting flux. Consequently, we divide flow in this fractured system of porous and permeable rocks into two components.

1. Water flows into the rock matrix through fracture and borehole surfaces. A constitutive relation must be developed for Q_r, the rate at which water percolates into the rock matrix through the exposed surface area of the borehole and cracked region. From D'Arcy's Law, using the Dupuit approximation (Bear (1972), Harr (1991)) this flow rate is assumed to be proportional to the product of a some function, f(h), of the head, h(t), times the exposed area, which is the sum of the fracture area and the borehole area in the open zone. In this case, the percolation rate is given by :

$$Q_r = -f(h)\ (A_e + A_c + A_o) \qquad (8)$$

where A_o is the surface area of the open "packed-off interval" of the borehole, length d_o, where $A_o = 2\pi R_p d_o$.

In order to estimate the expected functional form of f(h), we apply Dupuit's approximation to flow out of a well surrounded by a finite thickness of permeable rock. We note, Harr (1991), that integration of the total flow out of the external boundary gives $f(h) = k \cdot h^q$ with $q = 1$ for cylindrical symmetry, but we can expect the observed functional dependence to vary when asymmetric cracks are present. Here k is a constant which can be determined from D'Arcy's law and represents the rock wall permeability and porosity.

2. Water flows along fractures that are open conduits to the external environment. Account must be taken of pre-existing conduits in order to model the functional form and magnitude of the appropriate exiting flux. For flow out along open conduits, which may dominate in the first few seconds of head drop, we must produce a relation for Q_c, the rate at which water exits the system through open conduits such as open fractures and joints. We advocate an extension of our previous successful model which, above the critical pressure, had cracks growing with increasing pressure. When the crack grows to a particular length, we argue that it may connect with the existing network of open joints and fractures. Then, the exiting flow will be dominated by conduits to the external network rather than by flow into the rock matrix through the borehole and fracture surfaces. Thus, this model argues that at a particular head the induced fracture will interconnect with the open existing external network. We shall call this pressure the interconnect pressure P_i.

The usual approach to flow along open conduits uses the model of flow between

parallel plates of a viscosity dominated fluid. Bear(1972,p.691), by ignoring the inertial terms in the Navier-Stokes equations, shows that the steady-state flux, Q_c, is given by :

$$Q_c = -\frac{D_c^3 H_c}{12\mu} \cdot \frac{dP}{dl} \tag{9}$$

where H_c is the length of the intersection between the induced fracture and the open network conduit, μ is the usual viscosity term, while the gradient term dP/dl is the pressure gradient along the induced fracture.

We assume that H_c stays constant as the pressure increases above P_i. The pressure gradient is taken to be the excess head h divided by the length of the crack between the borehole and the interconnect with the open network, L_c. Using these assumptions gives the flow into the open conduit as :

$$Q_c = -h \cdot \frac{\rho g D_c^3 H_c}{12\mu L_c} \tag{10}$$

where ρ is liquid density and g is the gravitational accelaration.

Equations Applicable to the Various Pressure Regimes

Inserting functional forms into the general mass conservation law gives the general equation :

$$\frac{dh}{dt}(A_p + A_e\frac{dF}{dh} + [G\frac{dJ}{dh} + J\frac{dG}{dh}]) = Q_r + Q_c \tag{11}$$

where we have assumed no specific constitutive relations. It is useful to examine the approximate solutions to the above equation for particular types of media and cracks under differing pressure regimes.

Let us first examine the simplest case where only existing fractures are considered. This complicated equation reduces in the lower pressure regime, $h < P_c$, to

the simpler equation :

$$\frac{dh}{dt}(A_p + A_e\frac{dF}{dh}) = -f(h)A_* \qquad (12)$$

where $A_* = A_o + A_e$ and is the total surface area through which the fluid percolates into the rock matrix when no head is applied. If we use $f(h) = h^q$, and a linear relation for F(h), then the solution is a simple exponential decay of head in time. Even with non-linear relations for f(h) and F(h), logarithmic plots of dh/dt versus h yields slopes which are indicative of this equation's form.

The next interesting pressure regime is where induced hydraulic fractures are opening and extending yet they have not connected with the open fracture network. For $P_i > h > P_c$ we obtain the general equation :

$$\frac{dh}{dt}(A_p + A_e\frac{dF}{dh} + [G\frac{dJ}{dh} + J\frac{dG}{dh}]) = -f(h)(A_* + G(h,P_c)) \qquad (13)$$

In previous analyses, we have used theoretical solutions of this equation with simple functional forms, to match observed test data.

When $h > P_i$, the hydraulic fracture has extended sufficiently to intersect the existing network of open conduits. Assuming the exiting flow is dominated by the conduit term, we obtain the simpler equation :

$$\frac{dh}{dt}(A_p + A_e\frac{dF}{dh} + G\frac{dJ}{dh}) = Q_c \qquad (14)$$

where we assume that the area of induced fracture, G(h), remains constant and equal to A_i during interconnection to the open network. Incorporating the relation (10) into this result gives :

$$\frac{dh}{dt}(A_p + A_e\frac{dF}{dh} + A_i\frac{dJ}{dh}) = -hJ^3\frac{H_c\rho g}{12\mu L_c} \qquad (15)$$

Rapid Evacuation Solutions

Consider the simplest example with F and J independent of pressure changes above P_i. This implies that the aperture and surface area of the induced hydrofracture do not change when the fracture is connected with the open conduit network. This also means that any water exiting the hydrofracture is equal to the drop in the head in the borehole as the amount of water in the hydrofractures stays constant. Thus equation (15) reduces in this case to :

$$\frac{dh}{dt} = -h \cdot D_c^3 \frac{\rho g H_c}{12 \mu L_c A_p} \tag{16}$$

Upon integration of (16) we get the solution of head exponentially decaying in time.

$$h = h_0 \cdot e^{-\kappa t} \tag{17}$$

where the decay constant κ is given by

$$\kappa = D_c^3 \frac{\rho g H_c}{12 \mu L_c A_p} \tag{18}$$

where the inverse of κ gives an estimate of the decay time.

It is instructive to determine the expected size of the decay constant in the equation. In this regard the borehole is usually of a diameter of the order of 0.1m; giving a value of its cross-sectional area $A_p \approx 10^{-2} m^2$. Minor changes in the experimental values of borehole radius and area occur if there is a skin effect i.e. fractures and/or pitting and/or mud effects on the borehole surface. The viscosity parameter μ has the value in the mks unit system of about $0.8 * 10^{-3}$ at 30^0 C. For water, the density ρ is 10^3 and $g = 9.8$.

The length of the hydrofracture, when it interconnects with the open network L_c, can be estimated from our previous analyses of typical decay curves when the head is

below the interconnect pressure. We found that these cracks were of lengths of about 1 to 10 metres long, which is of the same order as the distance between major joints and fractures observed in many rock systems. The highest order parameter is the aperture of the induced hydrofracture D_c. Our previous analyses of crack size from matching theoretical solutions to observed data gave aperture changes with head of the order 10^{-4} to 10^{-3} meters per bar. Thus, for an excess head of 10 bars we expect an aperture of between 10^{-3} to 10^{-2} meters. The decay constant is dependent on the ratio of the width of interconnection between hydrofracture and open conduit H_c to the hydrofracture length L_c. The value of H_c can vary from large, of the order of the height of the "packed-off interval" which is usually also about 10 meters, to small, of the order of 10^{-1} meters.

Putting this range of values into equation (18) gives a range of values of κ between 10^3 to 10^{-3}, which implies a half-life of head decay ranging from 10^{-3} to 10^3 seconds. The larger half-life value corresponds to the case of small H_c which means that the water flows through narrow channels to connect with the open conduit network. The largest half-life is of the same order as the length of time seen in many tests where the water exits solely through the walls of the hydrofracture. As H_c increases, the size of the flow channel increases and a much more rapid decay occurs. However, the fastest decay times we have observed are of the order of seconds implying that there is an upper limit to the speed at which water can evacuate to the open conduit..

Numerical Examples

Davies (1993) examined numerical solutions to the equations governing flow for pressures below the interconnect pressure. We solved these equations numerically in order to determine type curves that can illustrate the effects of the various parameters. We investigated solutions for different power law constitutive relations for the functions F and G. We assumed that $G = \alpha(h-P_c)^m$ with initial value of m=2 assumed for illustrative purposes and α is an arbitrary constant. We take $F = \gamma h^n$ and $J = \beta(h-P_c)^r$ with values of n and r equal to 1 or 2 assumed for numerical experiments and β and γ are arbitrary constants. Then, for pressures below the interconnect pressure, the applicable equation is given by :

$$\frac{dh}{dt} = -kh^q(A_* + \alpha(h-P_c)^m) \,/\, (A_p + nA_e\gamma h^{n-1} + \alpha\beta(m+r)(h-P_c)^{m+r-1}) \qquad (19)$$

where α=0 when $h<P_c$.

As in our previous numerical solutions, Davies (1993), we use the following typical area values : A_p=0.01m^2 , A_o=10m^2 , A_e=100m^2. We adopt the value q = 1 as this is the expected theoretical powerlaw. Examination of equation (19) shows that the slope of the head rate of change against head scales with k, the permeability parameter. We use the value $k = 10^{-4}$ as this gives a time to zero excess head similar to that observed in slug tests. Using m=2 and n=1, we take an initial example of $\alpha = 20$ and $\gamma=10^{-4}$. For the aperture function J, we take $\beta=10^{-4}$ and the power r=1. We assume a critical pressure P_c of 20 bars.

Above the critical pressure, both the functions G(h) and J(h) were important, as they govern the area and aperture of the newly opened crack region. We found that as G(h) increases, the area of opened new cracks will increase and therefore expedite the

exiting of the fluid. Consequently, an increase in the pressure gradient is to be expected above the critical pressure P_c . As J(h) increases, the aperture of these newly opened cracks increases thereby increasing the storativity of this cracked region. Thus, the head in the borehole will drop slower when J(h) is large as then the greatest fraction of the water is in the newly cracked region.

In this study we are primarily concerned with pressure regimes greater than the interconnect pressure P_i. We insert the relations for $D_c = \beta J(h=P_i)$ into Q_c in equation (16) and obtain :

$$\frac{dh}{dt} = - h\beta^3(P_i-P_c)^{3r}\frac{\rho g H_c}{12\mu L_c A_p} \qquad (20)$$

This equation is integrated numerically. By obtaining numerical solutions using these parameter values, we can investigate the effect of changing the initial head. Let us first examine the simplest cases when the interconnect pressure is higher than the initial head and there is no rapid evacuation to an open conduit. In Figure 3a, we take an initial head of 50 bars and plot head versus log time, measured in bars and minutes, as this is how the field data is presented in in-situ stress measurements. We see that at early times the head decays slowly in the log time coordinate with its value remaining near the 50 bar level for tens of seconds. In Figure 3b, we show a similar case where the initial head is 40 bars.

We now consider the effect of the interconnect pressure P_i being less than the initial head of 50 bars. In Figure 4 an interconnect pressure of 40 bars has been assumed along with crack length $L_c = 10$ meters and interconnect distance H_c of 0.3 meters. This theoretical curve has a much greater slope than the previous case above 40 bars, at which pressure we find a rapid change in slope corresponding to the ceasing of

interconnection with the network of open conduits. The time it takes for the head to drop to below the interconnection pressure is about 10 seconds.

In order to examine the effect of a smaller interconnect distance H_c we use a value of 0.2 meter and obtain the numerical solution shown in Figure 5a. We see that the slope above 40 bars is correspondingly less than the previous case. The time it takes for the head to drop to below the interconnection pressure for this case is about 14 seconds. In Figure 5b, we use an even smaller value of H_c of 0.1 meter which results in a time for the head to drop to below interconnect pressure of 27 seconds. Note that the change in slope of the decay curve at the interconnect pressure is difficult to observe in Figure 5b. Thus, for this narrow a channel, this "type curve" implies that, at the interconnect pressure, the flow rate out the conduit is of the order of the flow rate into the porous walls of the hydrofracture and drill-hole.

Yucca Mountain Data

A number of boreholes have been drilled in and near Yucca Mountain, Nevada, the proposed site for a nuclear waste depository. These holes have been subjected to in-situ stress tests utilizing both hydro-frac and slug tests. The repository site was mainly chosen for its very low anomalous water table which is of the order of 500 metres below the arid surface. Thus the slug tests performed were usually under high pressure, of the order of 50 bars, as the boreholes were usually filled to the top with water at the start of the test. The data used was from graphical information published in Szymanski (1989) which was obtained from USGS documentation on various well tests. Our interpretation will be preliminary and approximate until more detailed information becomes available.

In the following analysis of a select group of these tests, we examine sections from various boreholes. Because of inherent errors in the digitization process and the lack of accurate data at the highest pressures there is often much scatter in the values. We shall compare field data from tests in hole USW G-4 with theoretical curves designed to match the data. This gives some understanding of the expected range of parameter values and shows that rapid evacuation through an open conduit is necessary to match the data at the highest pressures and earliest times.

Figure 6 shows the raw data of hole USW G-4, test G-4.1, depth interval 792 to 838 meters, and with open interval of length 46 meters. Figure 7 shows a theoretical solution that matches the test data quite accurately below 43 bars of pressure. This solution uses only non-conduit exit flows and we cannot fit the data with an initial head of 54.6 bars. This implies that at high pressures the rapid evacuation effect must be taken into account and such a solution is shown in Figure 8a using an interconnect pressure of 43 bars. We have used values of H_c, the interconnect distance, of 0.3 meters with a value of 10 meters for L_c, the hydrofracture length at interconnection with the open conduit. Figure 8b shows the result using a larger value of 0.5 meters for H_c, with a shorter time to reach the interconnection pressure. We can allow these parameters to vary over a reasonable range in order to fit the data, as above 43 bars no head-time information is available.

Other slug tests from Yucca Mountain wells are inspected visually for similar rapid early evacuations. They are analysed by measuring the initial pressure drops and their times in order to determine model parameter values and derive fracture properties and media characteristics. On examination of the raw data, compiled by Szymanski

(1989), we conclude that the shape of the curve of head versus log time implies that, without a rapid evacuation effect, these curves would never approach the initial head.

Table 1 lists the raw data for the various interval tests for hole USW-G4 and also lists derived values of average speed, average accelaration, and the decay constant κ. Values of κ found are about 10^{-2} which is in the region of our theoretical values and implies that the interconnection distance H_c is much smaller than the hydrofracture length L_c.

Table 2 lists the raw data and derived evacuation parameter values for the various interval tests for hole USW-UE25p#1. Note the similar values of the decay parameters for both the usual 50 meter packed-off intervals and, in the last two cases, 250 and 150 meter intervals.

Table 3 lists the raw data for the various interval tests for hole USW-UE25b#1 and also lists derived values of average speed, average accelaration, and the decay constant κ. The usual interval length of 14 and 40 meters is increased to 428 and 214 meters in the last two tests. We see that the interval 792-1220 has decay values similar to the smaller interval values, while the interval 1006-1220 has decay values that are much smaller. We interpret this to imply that very few, if any, intersections occur between hydrofracture and open conduits below 1006 meters.

Table 4 lists the raw data for the various interval tests for hole USW-H4 and also lists derived values. Values of κ found are about $3*10^{-2}$ which is in the region of our theoretical values and implies that the interconnection distance H_c is much smaller than the hydrofracture length L_c. Note the similar values of the decay parameters for both the usual 20 to 50 meter packed-off intervals and, in the last case, 291 meter interval.

For holes UE25p#1 and USW-H4, the decay parameters for large lengths of the packed-off intervals were similar to the values found for the tests on the smaller packed-off intervals. This implies that the ratio of H_c to hydrofracture length L_c is the same for both small and large packed-off intervals. That this ratio stays approximately constant can be taken to imply that the flow alomg the hydrofracture to the open conduit is dominated by a single narrow channel for both large and small packed-off intervals.

Conclusions

Drilling of wells at and in the vicinity of Yucca Mountain experienced loss of mud in rapid evacuations. This implied that at certain depths and in certain geographical areas the drill intersected open conduits. Such conduits are usually found in jointed and fractured media. Certain in-situ slug tests in wells in the Yucca Mountain region experienced extremely rapid evacuation of the water in the first few seconds. These observations imply that hydrofractures created by the high pressure of the slug test must have interconnected with an open conduit.

In order to determine the properties of this fractured system, we have developed a simple but comprehensive model of these in-situ loading tests. This model has produced numerical solutions of head decay that match the experimental observations. Analysis of the rapid decay at the earliest times has yielded estimates of fracture properties and allowed a more accurate interpretation of the fracture behaviour and its intersection with the network of open conduits. We have shown that only flow out to these conduits can explain the data observed at the highest pressures in the slug tests. Our results imply that the hydrofractures intersect the open conduits through narrow

fingers whose interconnect lengths are much less than the hydrofracture lengths. That certain regions of the Yucca Mountain geohydrological system is dominated by a network of open conduits along joints and fractures is an important result of our analysis.

References

Archambeau, C.B. and N.J. Price, (1991); "*An Assessment of J.S. Szymanski's Conceptual Hydro-Tectonic Model and its Relevance to Hydrologic and Geologic Processes at the Proposed Yucca Mountain Nuclear Waste Repository*", Minority Report of the Special DOE Review Panel, U.S. Department of Energy, Las Vegas, Nevada.

Baumgartner, J. and M.D. Zoback, (1989); "*Interpretation of Hydraulic Fracturing Pressure-Time Records Using Interactive Analysis Methods*", Int. J. Rock Mech. Min. Sci. & Geomech. Abstr., v26, #6, 461-469.

Bear, J., (1972); "*Dynamics of Fluids in Porous Media*", Elsevier Press.

Davies, J.B., (1993); "*Extension of In-situ Stress Test Analysis to Fractured Media with Reference to Yucca Mountain Data*", TRAC Report to Nuclear Waste Project Office, State of Nevada.

Harr, M.E., (1991); "*Groundwater and Seepage*", Dover Press.

Hayashi, K. and B.C. Haimson, (1991); "*Characteristics of Shut-in Curves in Hydraulic Fracturing Stress Measurements and Determination of in Situ Minimum Compressive Stress*", Jnl. Geop. Res., v96, #B11, 18,311-18,321.

Healy, J.H., (1988); "*Stress Measurements at Yucca Mountain*", Draft to U.S.G.S., personal communication.

Slymanski, J.S., (1989); "*Conceptual Considerations of the Yucca Mountain Groundwater System with Special Emphasis on the Adequacy of the System to Accomodate a*

High-Level Nuclear Waste Repository", DOE Internal Report, U.S. Department of Energy, Las Vegas, Nevada.

Whitaker, A., (1985); "*Theory and Evaluation of Formation Pressures*", IHRDC Press.

Table 1 : Hole USW-G4

Interval	Start Hd	1st Hd	1st Tm	ave spd	ave accn	kappa
615-655	546	350	54	3.6	0.13	8.2e-03
655-701	546	399	15	9.8	1.31	2.1e-02
698-722	546	490	30	1.8	0.12	3.5e-03
702-747	546	360	15	12.4	1.65	2.7e-02
722-747	546	530	6	2.6	0.89	4.9e-03
747-792	546	426	15	8.0	1.07	1.7e-02
792-838	546	426	15	8.0	1.07	1.7e-02
802-826	546	415	15	8.7	1.16	1.8e-02
826-850	546	453	15	6.2	0.83	1.2e-02
850-875	546	355	15	12.7	1.70	2.9e-02
875-899	546	360	15	12.4	1.65	2.7e-02
899-915	546	371	15	11.7	1.56	2.6e-02

Table 2 : Hole USW-UE25p#1

Interval	Start Hd	1st Hd	1st Tm	ave spd	ave accn	kappa
550-600	389	354	12	2.9	0.48	7.9e-03
640-690	388	372	12	1.3	0.22	3.5e-03
764-834	386	371	12	1.3	0.22	3.5e-03
834-904	386	351	12	2.9	0.49	7.9e-03
974-1044	385	371	12	1.3	0.22	3.5e-03
1044-1114	386	317	12	5.7	0.96	1.6e-02
1341-1381	367	305	6	10.3	3.4	3.1e-02
1381-1421	367	312	6	9.2	3.1	2.7e-02
1423-1463	367	327	6	6.7	2.2	1.9e-02
1463-1509	367	301	10	6.6	1.3	2.0e-02
1509-1555	367	301	8	8.2	2.1	2.5e-02
1554-1600	367	301	9	7.3	1.6	2.2e-02
1597-1643	369	336	6	5.5	1.8	1.6e-02
1643-1689	368	324	8	5.5	1.4	1.6e-02
1689-1735	368	320	8	6.0	1.5	1.7e-02
1735-1781	368	320	8	6.0	1.5	1.7e-02
1558-1805	367	305	9	6.9	1.5	2.1e-02
1646-1805	369	325	8	5.5	1.4	1.6e-02

Table 3 : Hole USW-UE25b#1

Interval	Start Hd	1st Hd	1st Tm	ave spd	ave accn	kappa
477-491	477	301	66	2.7	0.08	7.0e-03
491-505	477	272	60	3.4	0.11	9.4e-03
504-544	477	176	60	5.0	0.17	1.6e-02
581-621	476	38	60	7.3	0.24	4.2e-02
621-661	477	191	60	4.8	0.16	1.5e-02
703-743	477	339	60	2.3	0.08	5.7e-03
743-783	477	191	60	4.8	0.16	1.5e-02
779-819	477	33	60	7.4	0.25	4.5e-02
820-860	477	200	60	4.6	0.15	1.4e-02
792-1220	477	19	60	7.6	0.26	5.4e-02
1006-1220	471	448	66	0.35	0.01	7.6e-04

Table 4 : Hole USW-H4

Interval	Start Hd	1st Hd	1st Tm	ave spd	ave accn	kappa
555-604	500	335	19	8.7	0.91	2.1e-02
652-701	500	285	15	14.3	1.9	3.7e-02
703-735	500	250	23	10.9	0.95	3.0e-02
735-767	500	380	8	15.0	3.7	3.4e-02
783-832	500	340	10	16.0	3.2	3.9e-02
832-850	500	330	12	14.2	2.4	3.5e-02
855-873	500	390	13	8.5	1.3	1.9e-02
873-892	500	370	14	9.3	1.3	2.2e-02
892-910	500	365	10	13.5	2.7	3.1e-02
910-926	500	360	20	7.0	0.7	1.6e-02
1173-1192	500	275	15	15.0	2.0	4.0e-02
1195-1219	500	395	15	7.0	0.9	1.6e-02
928-1219	500	310	18	10.6	1.2	2.7e-02

Figure Captions

Figure 1. Map of Yucca Mountain water table and location of wells.

Figure 2. Conceptual diagram of the borehole-hydrofracture-open conduit system subject to a head h(t) of water above the present water table.

Figure 3a. Synthetic graph of head versus log time. The initial pressure head of water in the borehole is 50 bars. The parameters used in the model synthesis are : P_c = 20bars, k = 0.01, A_o=0.01m^2 , A_p=10m^2 , A_e=100m^2, q =1, m=2, n=1, γ=1, α = 100, β = 0.

Figure 3b. Synthetic graph of head versus log time. The initial pressure head of water in the borehole is 40 bars. The parameters used in the model synthesis are the same as used in Figure 3a.

Figure 4. Synthetic graph of head versus log time. The initial pressure head of water in the borehole is 50 bars, the interconnect pressure is 40 bars, the crack length L_c = 10 meters and interconnect distance H_c = 0.3 meters. The parameters used in the model synthesis are the same as used in Figure 3a.

Figure 5a. Synthetic graph of head versus log time. The initial pressure head of water in the borehole is 50 bars, the interconnect pressure is 40 bars, the crack length L_c = 10 meters and a smaller interconnect distance H_c = 0.2 meters. The parameters used in the model synthesis are the same as used in Figure 3a.

Figure 5b. Synthetic graph of head versus log time. The initial pressure head of water

in the borehole is 50 bars, the interconnect pressure is 40 bars, the crack length $L_c = 10$ meters and a smaller interconnect distance $H_c = 0.1$ meters. The parameters used in the model synthesis are the same as used in Figure 3a.

Figure 6. Raw data of hole USW G-4, test G-4.1, depth interval 792 to 838 meters, and with open interval of length 46 meters.

Figure 7. Theoretical solution that matches the test data quite accurately below 43 bars of pressure. This solution uses only non-conduit exit flows and cannot fit the data with an initial head of 54.6 bars.

Figure 8a. Theoretical solution incorporating rapid initial flow out open conduits and using an interconnect pressure of 43 bars. Value of H_c, the interconnect distance, is 0.3 meters with a value of 10 meters for L_c, the hydrofracture length at interconnection with the open conduit.

Figure 8b. Theoretical solution with open conduit that shows the result using a larger value of 0.5 meters for H_c, with a shorter time to reach the interconnection pressure.

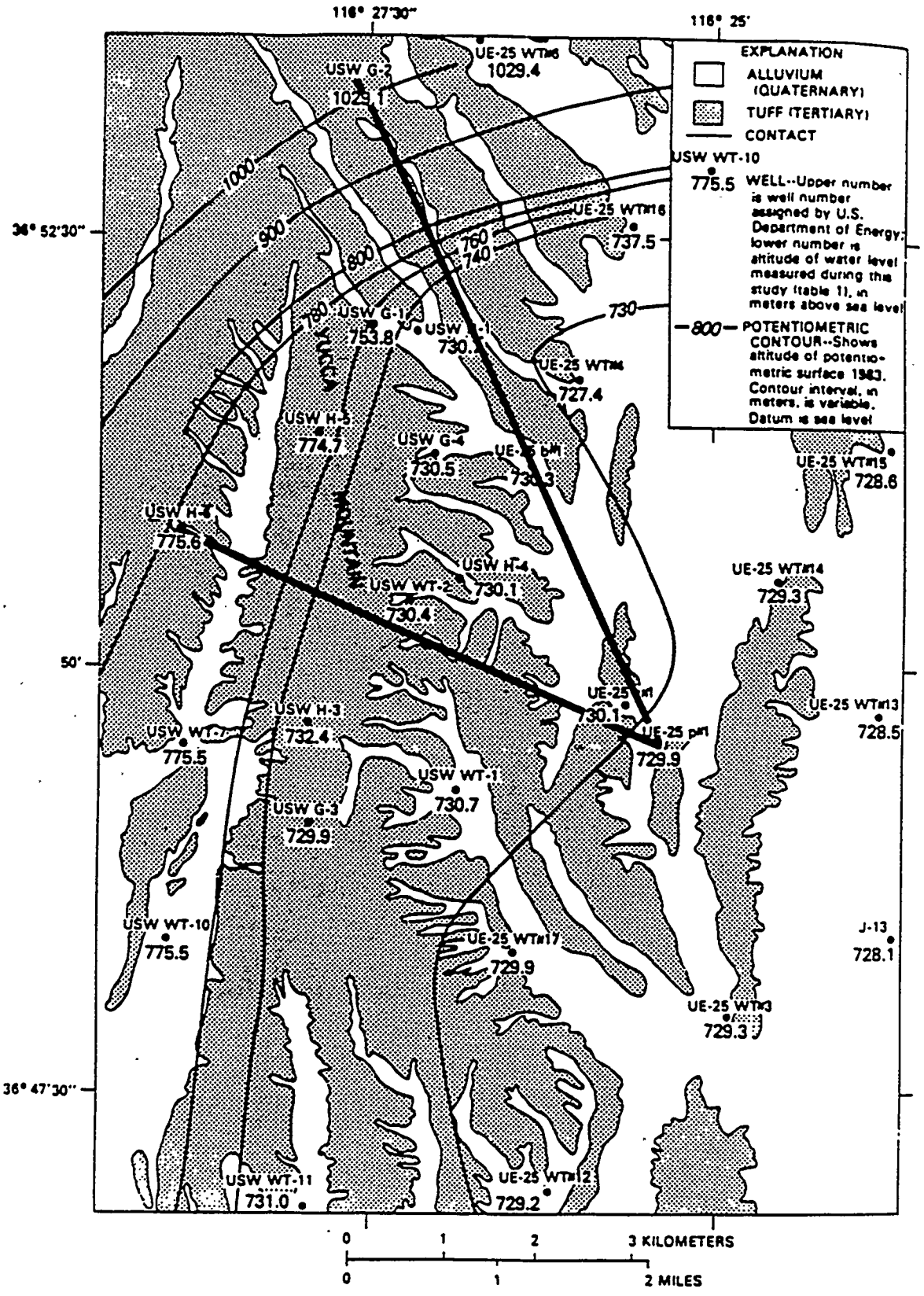

Location map for hydraulic conductivity cross-sections. Modified from Robison, 1984.

FIGURE 1.

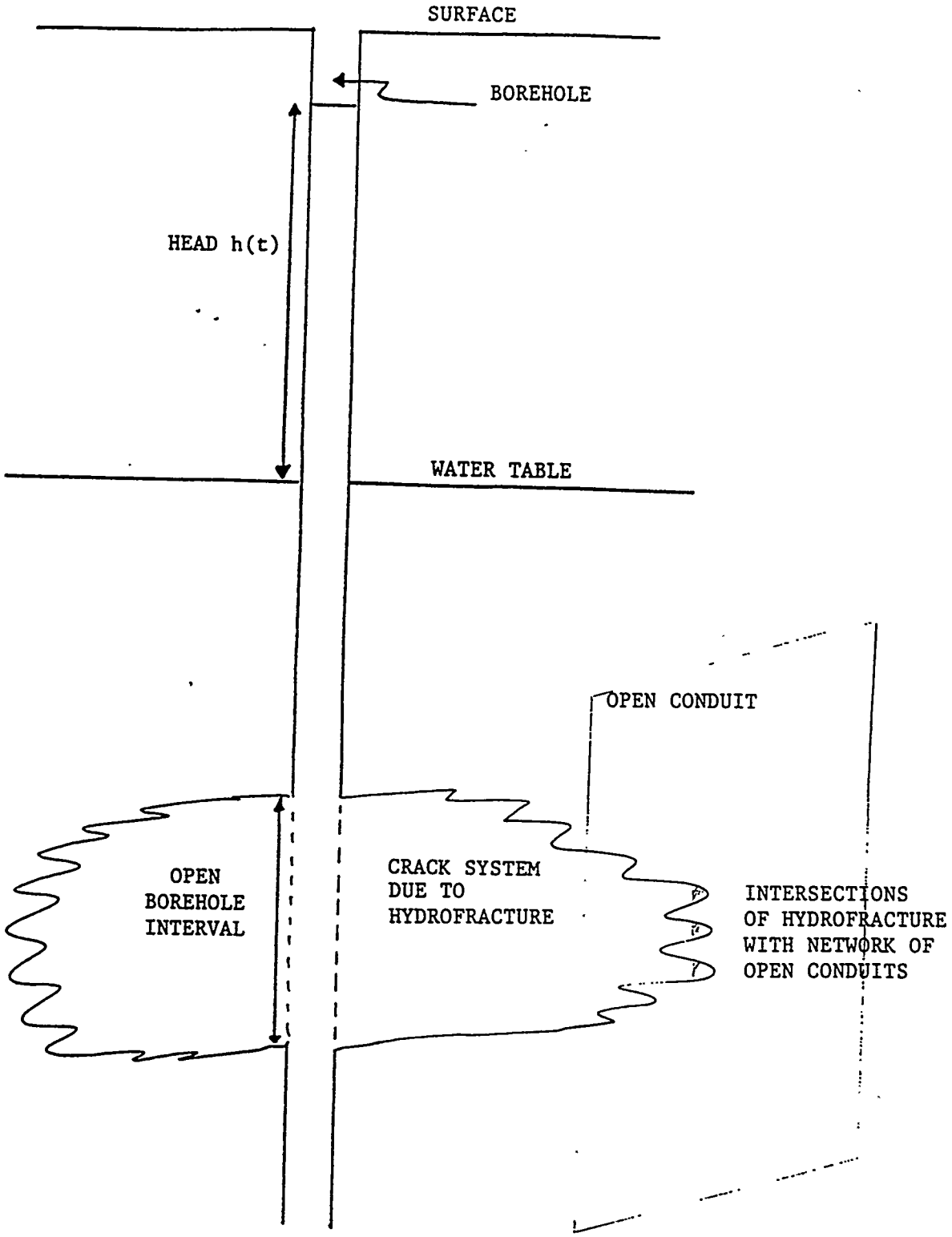
SURFACE
BOREHOLE
HEAD h(t)
WATER TABLE
OPEN CONDUIT
OPEN
BOREHOLE
INTERVAL
CRACK SYSTEM
DUE TO
HYDROFRACTURE
INTERSECTIONS
OF HYDROFRACTURE
WITH NETWORK OF
OPEN CONDUITS

FIGURE 2.

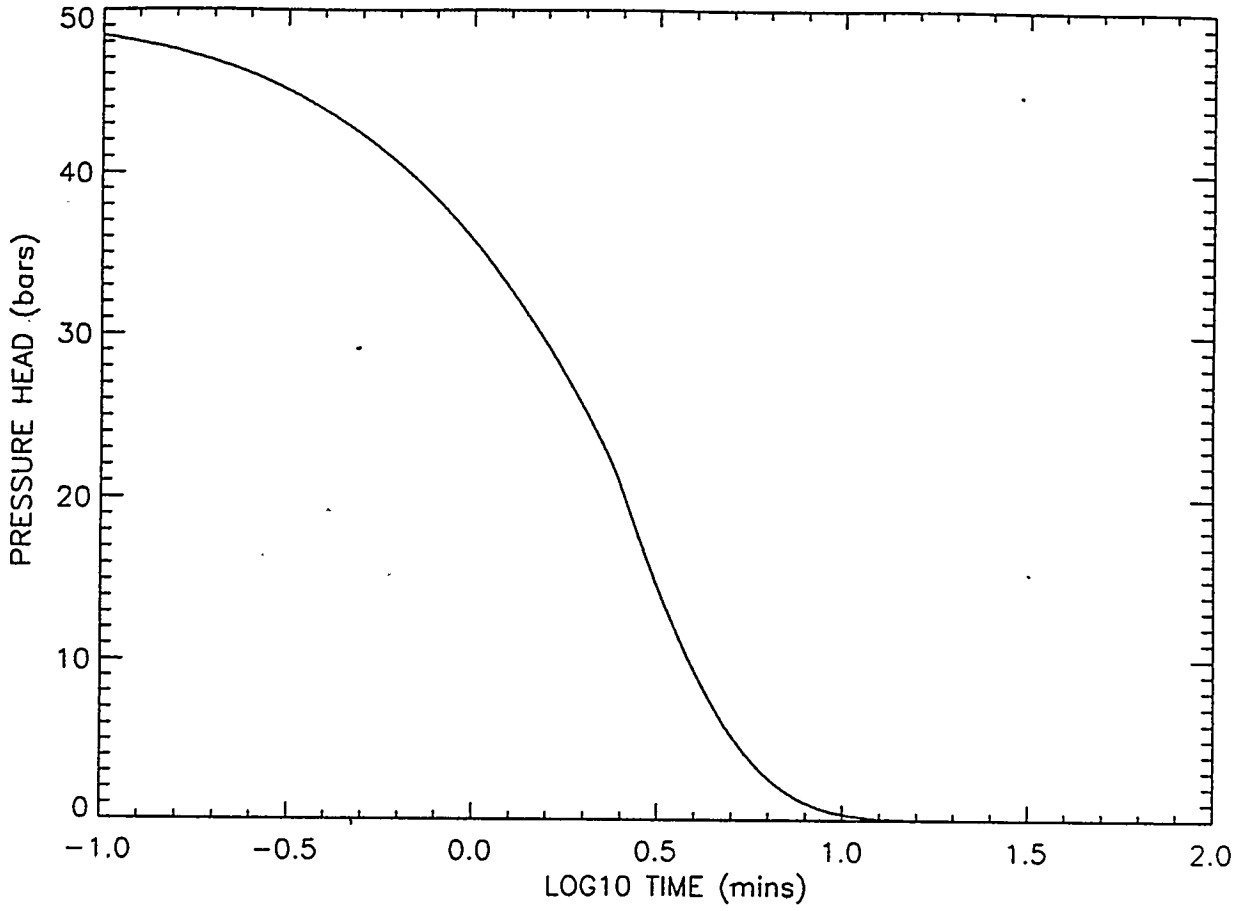

FIGURE 3a.

Typical Slug Test curve for initial head of 50 bars
but with no rapid evacuation effects at early times.

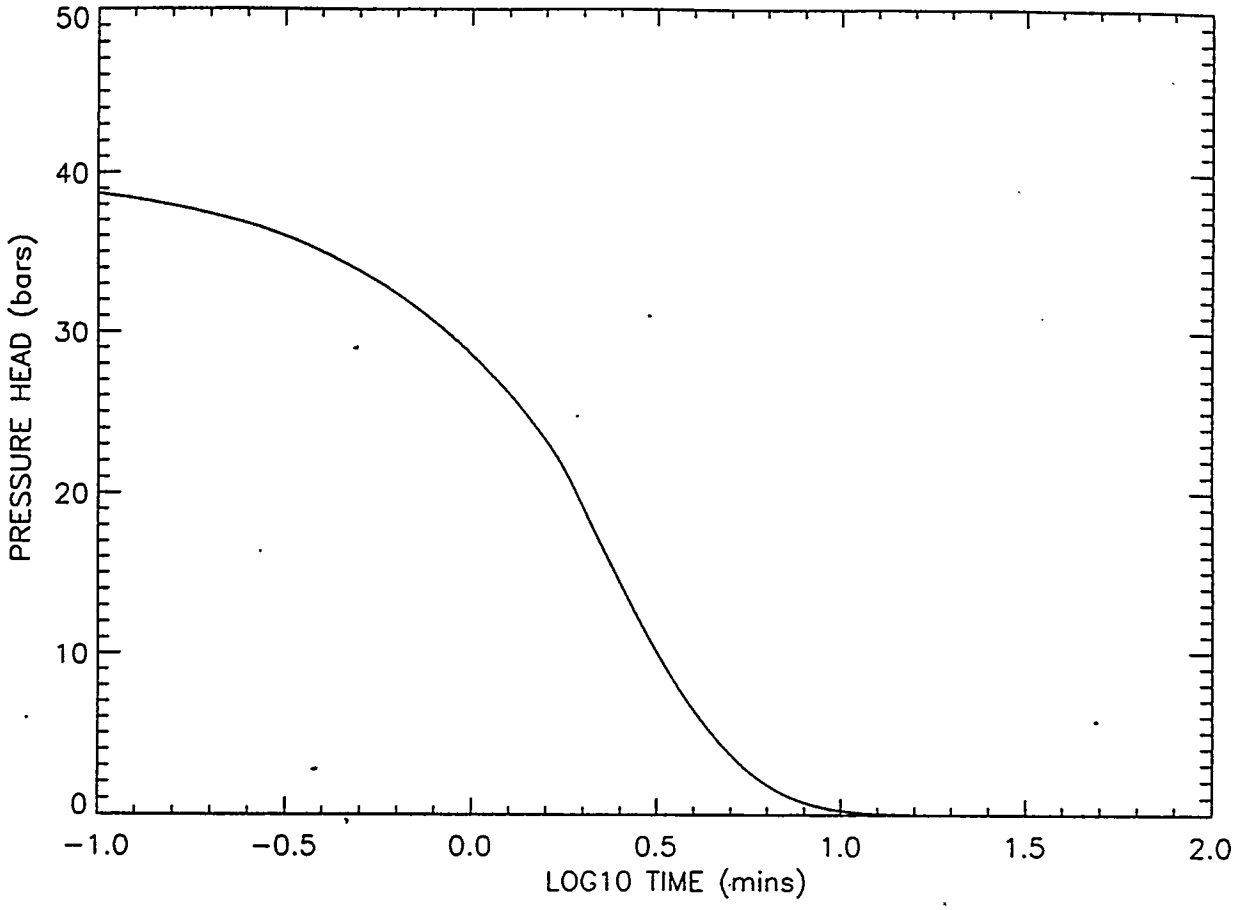

FIGURE 3b.

Typical Slug Test curve for initial head of 40 bars
but with no rapid evacuation effects at early times.

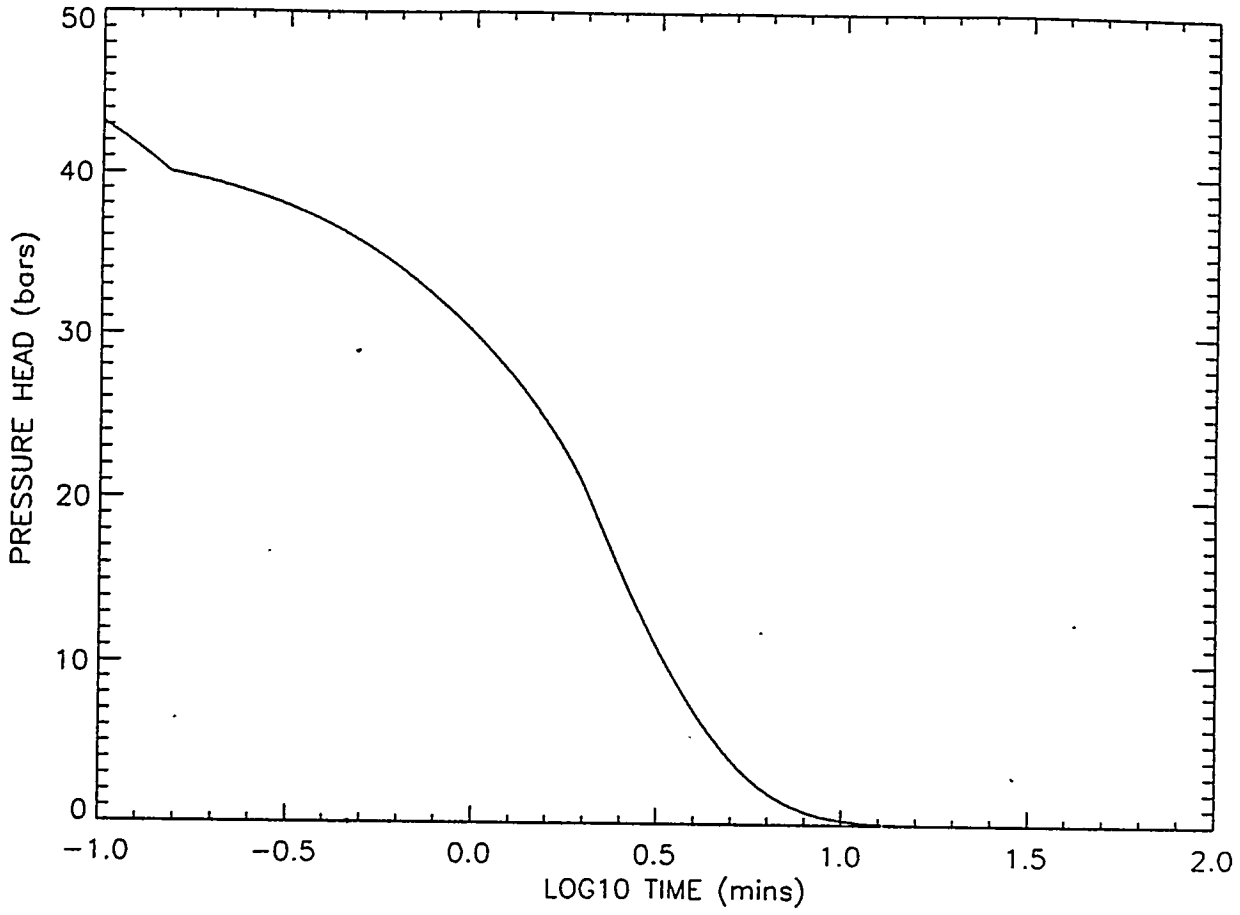

FIGURE 4.

Typical Slug Test curve with initial head of 50 bars and with rapid evacuation effects above 40 bars, the interconnect pressure when the hydrofracture intersects the network of open conduits.

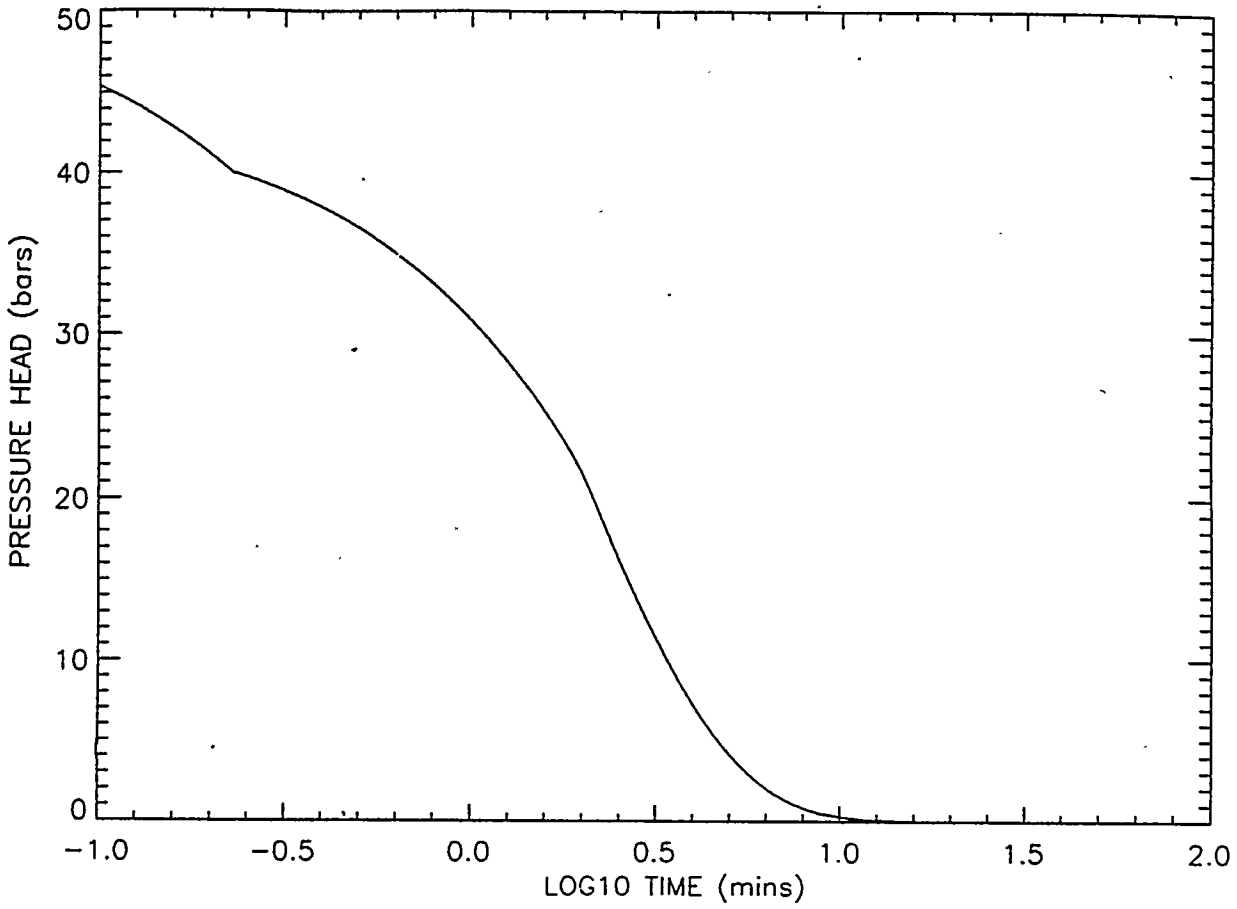

FIGURE 5a.

As in Figure 4, but with a smaller distance of interconnection between hydrofracture and open conduit resulting in a longer time in the rapid evacuation zone.

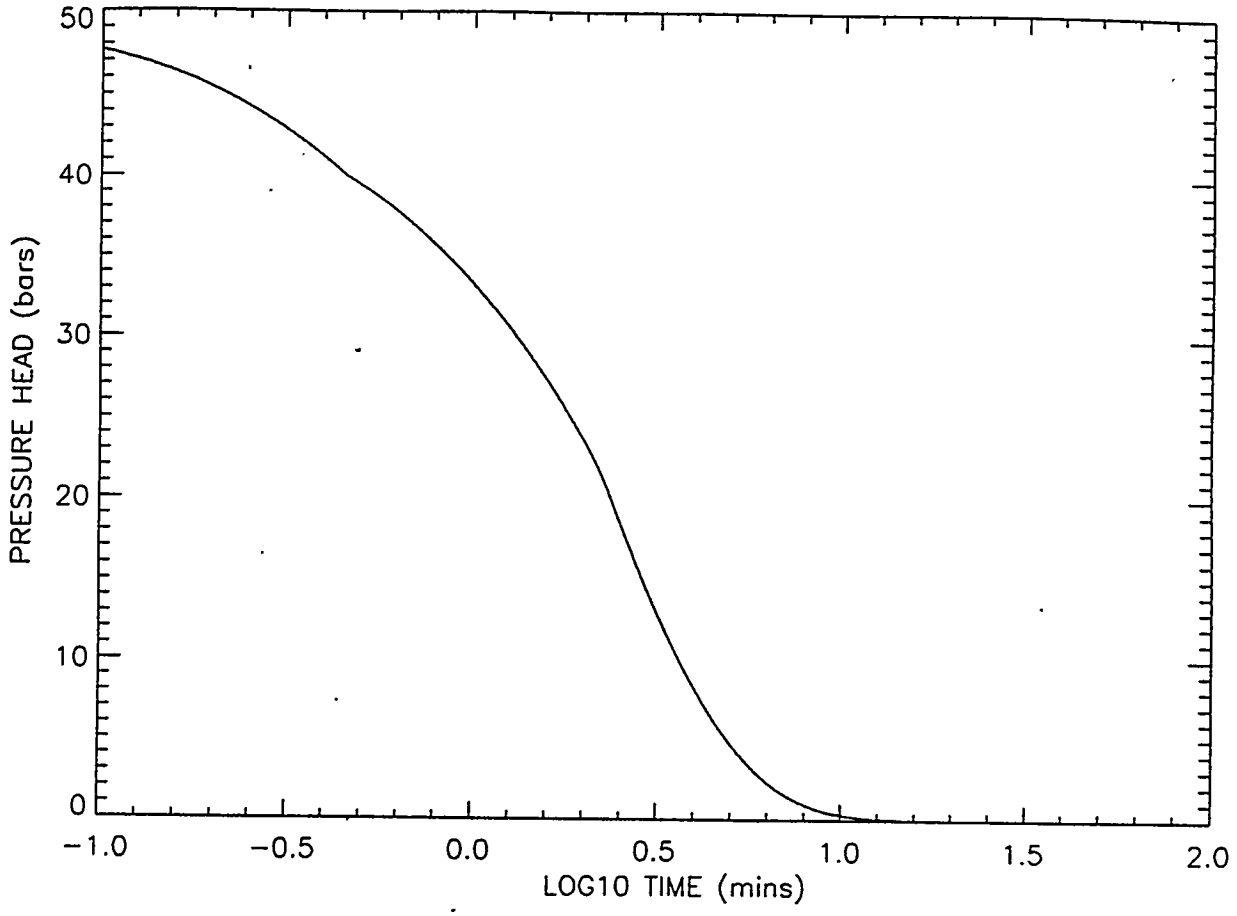

FIGURE 5b.

As in Figures 4 and 5a, but with such a small interconnection width that the slope change at 40 bars is barely observable implying that flow rates through open conduit and porous walls are similar.

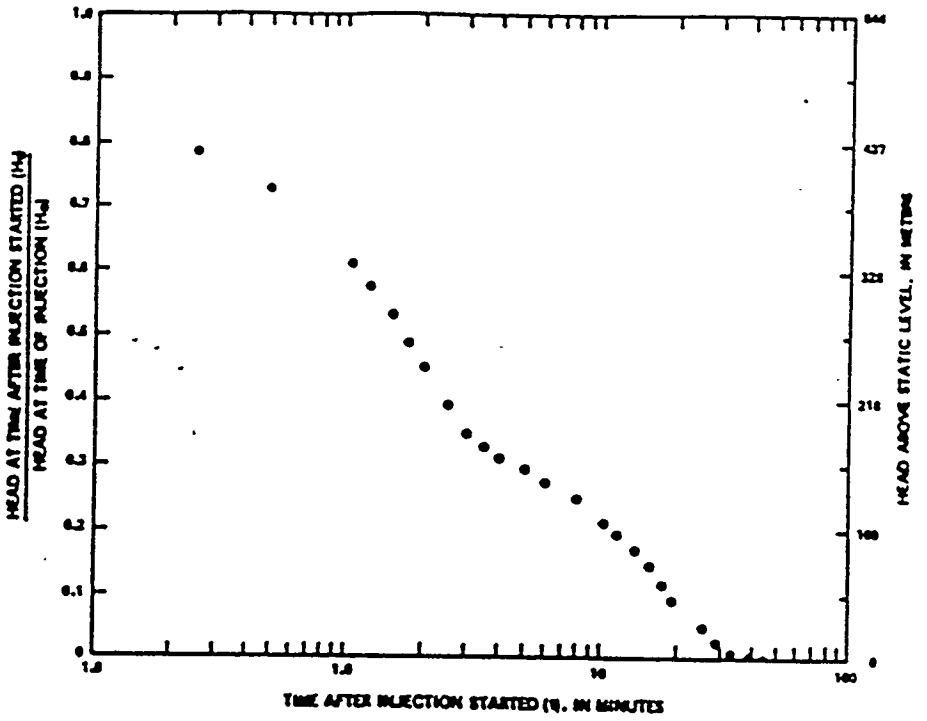

-Packer-injection test for depth interval from 792 to 838 meters.

Figure 6. Raw data of hole USW G-4, test G-4.1, depth interval 792 to 838 meters, and with open interval of length 46 meters.

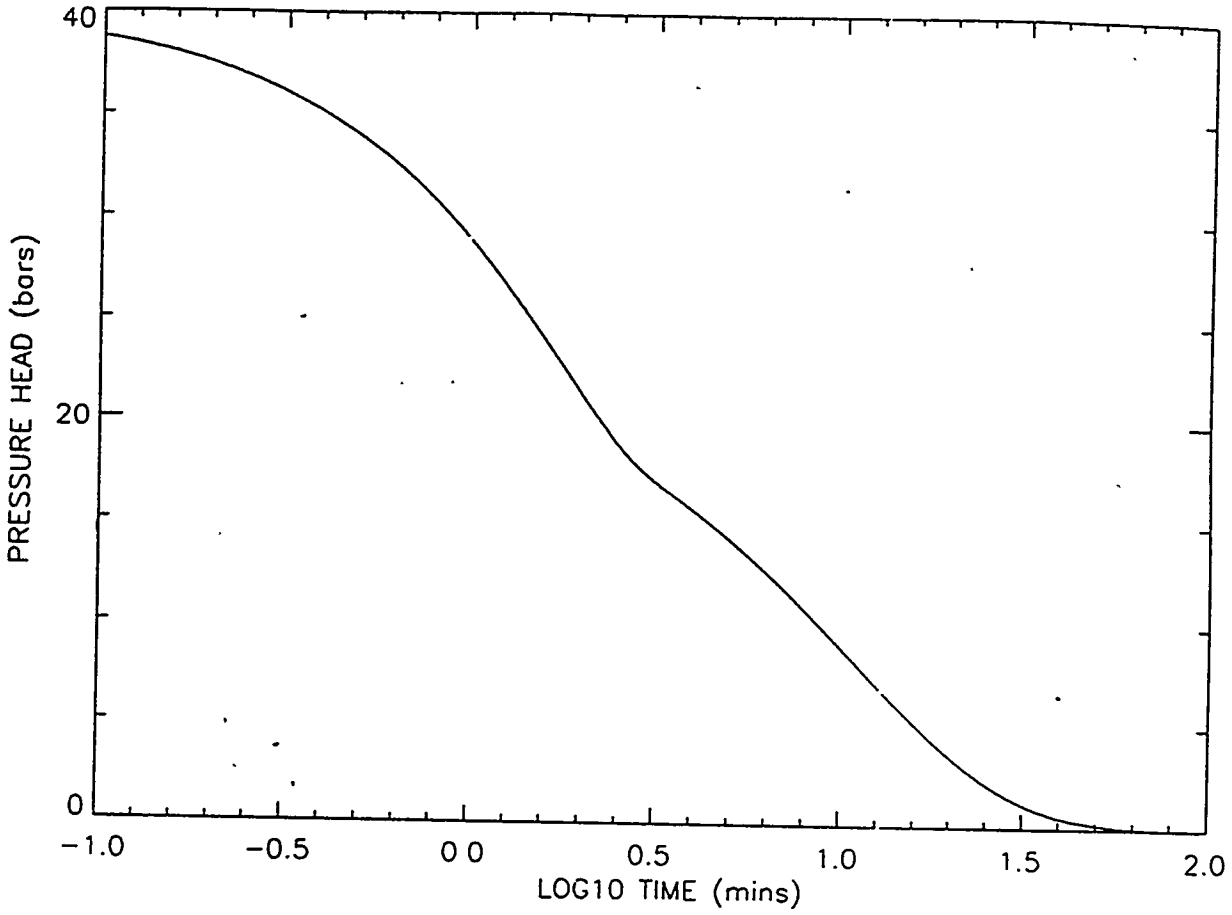

Figure 7.

Theoretical solution to match Figure 6 using no flows to open conduits and an initial head of 40 bars.

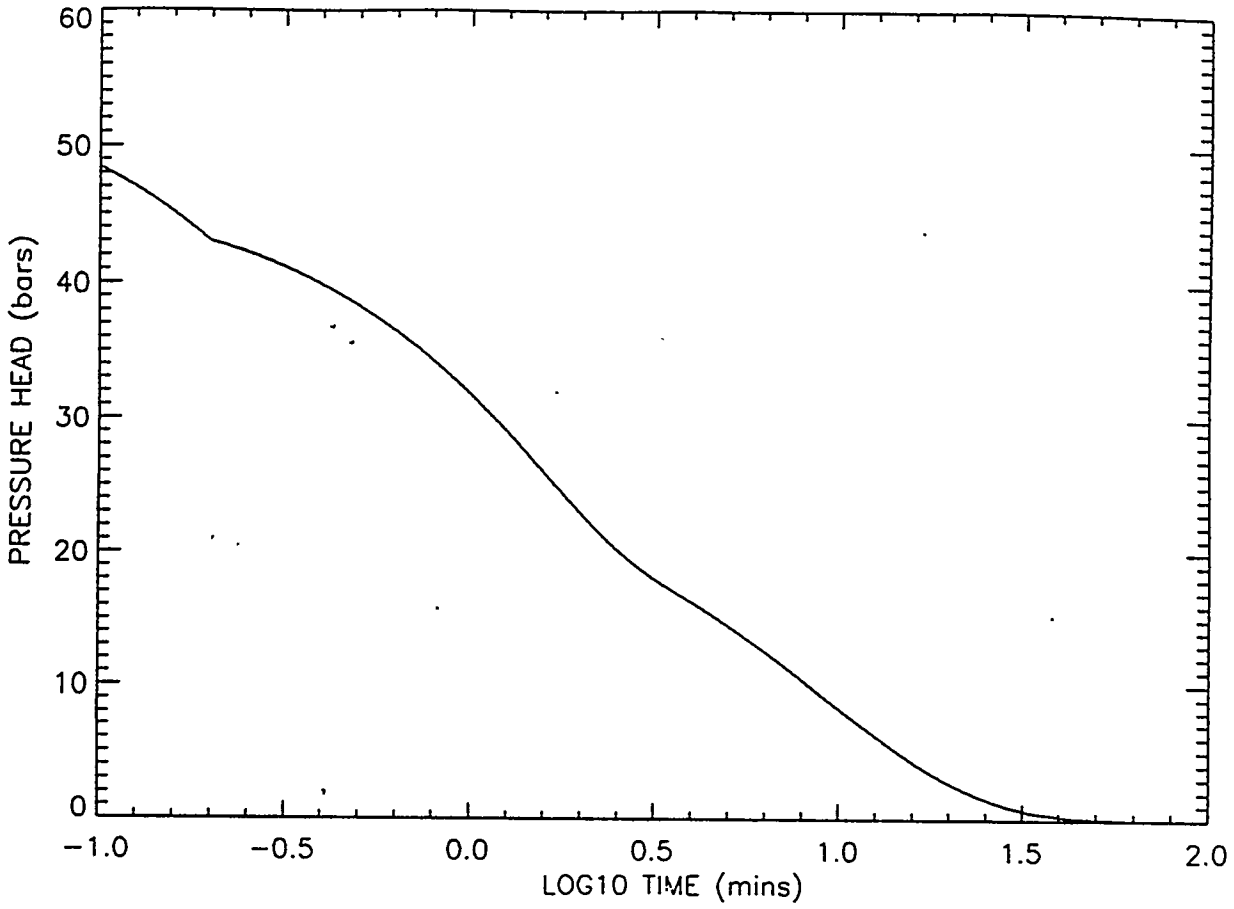

FIGURE 8a.

Theoretical solution to match Figure 6 using rapid evacuation flows to open conduits above 43 bars.

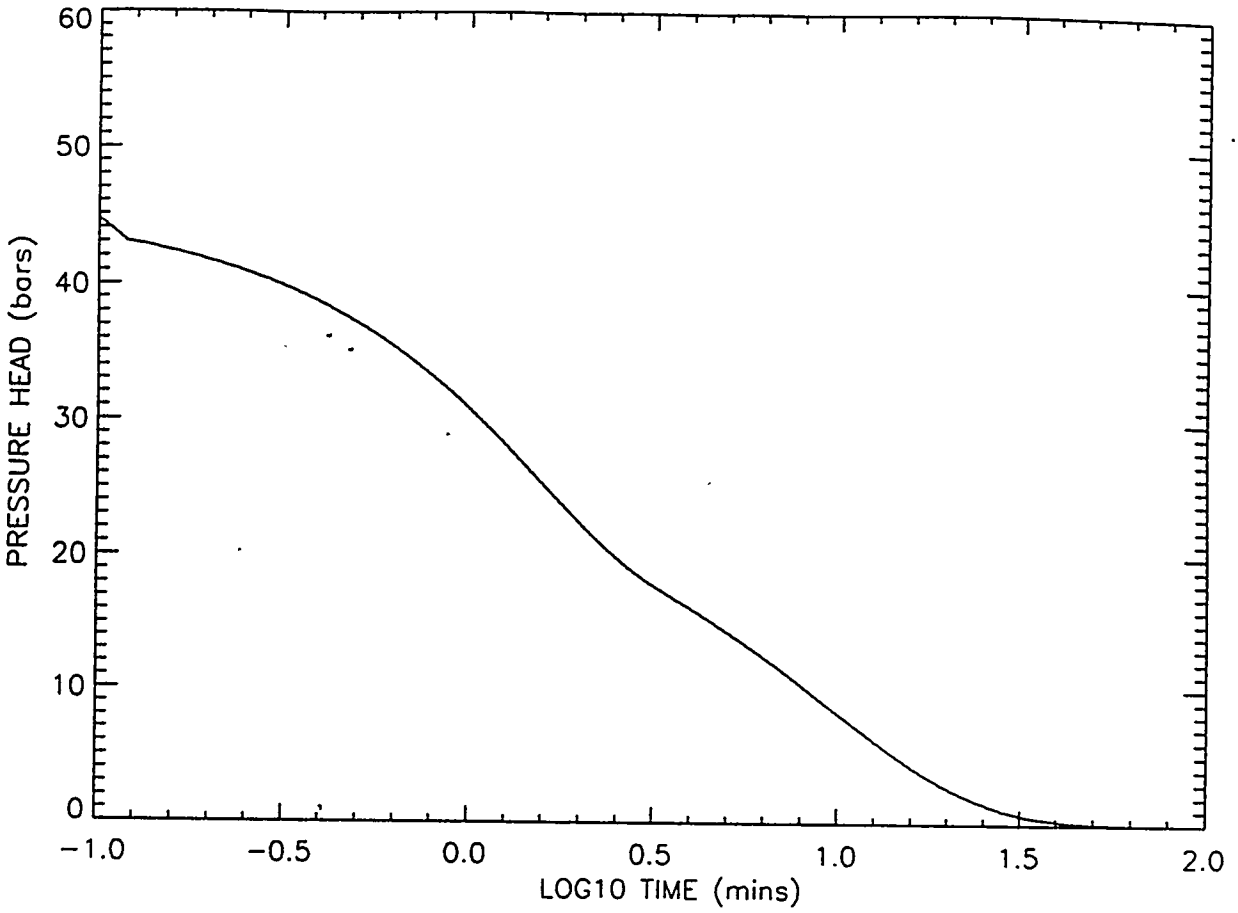

FIGURE 8b.

Theoretical solution to match Figure 6, using rapid evacution flows to open conduits above 43 bars but with a wider interconnect distance than as in Figure 8a.

PART III: MODELING HYDROTECTONIC PHENOMENA AT YUCCA MOUNTAIN

Section B: Non-Linear Hydrotectonic Phenomena: Part I - Fluid Flow in Open Fractures Under Dynamical Stress Loading

By C. B. Archambeau

Non-Linear Hydrotectonic Phenomena: Part I - Fluid Flow in Open Fractures Under Dynamical Stress Loading

Charles B. Archambeau

Theoretical and Applied Geophysics Group
Department of Physics
University of Colorado, Boulder

Introduction

A fractured solid under stress loading (or unloading) can be viewed as behaving macroscopically as a medium with internal, hidden, degrees of freedom, wherein changes in fracture geometry (*i.e.* opening, closing and extension) and flow of fluid and gas within fractures will produce major changes in stresses and strains within the solid. Likewise, the flow process within fractures will be strongly coupled to deformation within the solid through boundary conditions on the fracture surfaces. The effects in the solid can, in part, be phenomenologically represented as inelastic or plastic processes in the macroscopic view. However, there are clearly phenomena associated with fracture growth and open fracture fluid flows that produce effects that can not be described using ordinary inelastic phenomenology. This is evident from the fact that a variety of energy release phenomena can occur, including seismic emissions of previously stored strain energy due to fracture growth, release of dissolved gas from fluids in the fractures resulting in enhanced buoyancy and subsequent energetic flows of gas and fluids through the fracture system which can produce rapid extension of old fractures and the creation of new ones. Additionally, the flows will be modulated by the opening and closing of fractures due to deformation in the solid, so that the flow process is strongly coupled to dynamical processes in the surrounding solid matrix, some of which are induced by the flow itself.

In studying such highly interactive, non-linear fluid-gas-solid systems, and attempting to quantitatively describe them with some degree of generality and accuracy, one approach is to first break down this complicated non-linear problem into its basic elemental parts. Here the idea would be to solve component problems in sufficient generality so that they can be combined together in a way that allows

the complete interactive phenomena to be represented, at least in some well defined degree of approximation.

Clearly in the case of interest here, one elemental phenomena is flow of a fluid or gas (or a fluid-gas mixture) in a fracture. In order that this flow problem be of relevance in the present context however, the boundaries of the fracture must be assumed to move, since in the fractured solid the fracture geometry responds to changes of strain in the solid matrix as well as to changes of fluid pressure due to the flow. This coupling of the fluid flow in a fracture with deformation in the solid is through boundary conditions of continuity of traction and continuity of the normal component of the particle velocity on the fracture surfaces. In the usual case the fracture boundaries move at a rate equal to the normal component of the particle velocity of the solid at the fracture surface. Thus, by considering fluid flow in a narrow fracture with arbitrarily moving boundaries, we can focus on basic flow solutions in a "simple" variable aperture fracture where the movement of a boundary is considered an unknown function of time.

Elementary Considerations of the Dynamics of Fluid-Solid Interactions

To link the flow in fractures, or along connected pores, to the deformation of the surrounding solid matrix one would equate the normal particle velocity in the solid to the rate of boundary movement and also equate fluid-solid tractions across the interface. As a first approximation the dynamical response of the solid could be computed using macroscopically averaged material properties for the composite. Then, as an approximation, the amount (and sense) of boundary movement in fractures would be computed from the dilatation in the composite; that is from the divergence of the particle displacement field at fracture locations.

In this regard, if we let $\mathbf{u}$ represent the displacement in the solid, then the dilatation is $\nabla \cdot \mathbf{u}$ and the change in volume ∇V of the composite within a small volume V_0 is

$$\frac{\nabla V}{V} = \nabla \cdot \mathbf{u}$$

If the entire volume change in the composite is taken up by changes in the aperture, δ, of fractures (or connected pores), then with N_f representing the fixed number of fractures in V_0 , with fixed average surface area $\overline{A}_f$ and average aperture $\overline{\delta}$ at any time t, we have:

$$\frac{\nabla V}{V_0} = \frac{V - V_0}{V_0} = \frac{N_f (\overline{\delta} - \overline{\delta}_0) \overline{A}_f}{V_0}$$

where $\overline{\delta}_0$ is the initial average aperture of the fractures (at t = o) in V_0 , while V is the volume at time t after imposition of the displacement in the solid at time t = 0. Here the fractures are assumed not to grow, so that N_f and A_f are constant in time and only the aperture changes with time due to the volume dilatation in the solid. Since the average initial fracture volume in V_0 is $\overline{V}_f = N_f \, \delta_0 \, \overline{A}_f$, then the previous expression can be written as

$$\frac{\nabla V}{V_0} = \frac{\overline{V}_f}{V_0} (\overline{\delta} - \overline{\delta}_0) / \delta_0 = \varepsilon_f (\overline{\delta} - \overline{\delta}_0) / \overline{\delta}_0$$

where ε_f represents the ratio of fracture volume to the total composite volume. Consequently, in terms of the dilatation we have

$$\overline{\delta} = \overline{\delta}_0 \left[1 + \frac{\nabla \cdot \mathbf{u}}{\varepsilon_f} \right]$$

where, of course, it is presummed that $\varepsilon_f > 0$ and $\overline{\delta} > 0$. (Note that $\nabla \cdot \mathbf{u}$ will be negative for compression in the composite and that if all the volume change is to be taken up by changes in fracture apertures, then $|\nabla \cdot \mathbf{u}|$ must be less than ε_f. When these quantities are equal it simply means that all fractures close and that no further volume change can be accommodated by fracture closing.) It is evident from this result that large aperture changes can take place when fractures are open and the fluid within them is free to flow, as is assumed here.

A compatible approximation for fluid-solid traction continuity at fracture boundaries would be to equate the change in the fluid pressure ($p^{(1)}$) from its equilibrium value to the product of the bulk modulus of the composite (k_c) times the dilatation ($\nabla \cdot \mathbf{u}$) at the fracture boundary. Note, in this regard, that if we consider changes in stresses in the solid to occur much more rapidly than the flow in

fractures can change pressure, then the initial value of $p^{(1)}$ is given by the equilibrium value of the dilatation in the solid composite following an earthquake or some other tectonic event.

If the relation $p^{(1)} \approx k_c \nabla \cdot \mathbf{u}$ is used and combined with the previous expression for the aperture function, $\bar{\delta}$, then the continuity conditions can be satisfied to first order by requiring

$$\bar{\delta}(t) = \delta_0 [\, 1 + p^{(1)} / \varepsilon_f k_c \,]$$

where $p^{(1)} < 0$ for compression in the fluid. Boundary movement specified in this way will satisfy boundary conditions and cause the fracture to open or close as the pressure in the fluid increases or decreases from the ambient value during the flow.

Thus, for the fluid the entire effect of the surrounding solid, and the deformational changes within it, can be approximated by the movement of the fracture boundary surface in the manner described. On the other hand the changes of pressure in the fluid and boundary movement associated with the flow will also manifest themselves in the surrounding solid matrix through the boundary conditions at the fracture surfaces. As a higher order approximation for the estimate of secondary deformation in the solid due to fluid flow and changes of pressure in the fracture, one could employ dislocation equivalents in the solid, where imposed displacement offsets and stress discontinuities could be used to represent the effect of fluid pressure changes and fracture boundary movement due to the flow. Thus, a second order approximation for the composite response could involve imposing dislocation equivalents at the fracture locations to produce the effects of coupling between flow of fluids in the fracture and induced, secondary, deformation in the solid. In this study we will focus on the fluid flow problems and defer detailed consideration of the higher order approximations of the composite behavior for subsequent studies.

Beyond anticipating the solid-fluid interactive features inherent in this physical system, and accounting for them in the elemental flow solutions, it is also necessary to account for the fact that fractures in a solid would ordinarily occur as an intersecting network, where orientations of fractures are widely distributed and where intersections occur at essentially all scale lengths. Thus, individual

fracture lengths will be distributed and intersections will result in bifurcations in flow patterns that must be taken into account. The approach that can be taken is to use integral mass, momentum and energy balance methods (*e.g.* Brodkey, 1967) at the intersections to obtain a balance of conserved quantities entering and leaving the intersection zones. In this case elemental solutions in fracture regions removed from the intersection zones would be linked across the zone using the integral balance method, much in the way two asymptotic solutions are joined. In this approach the elemental solution for flow in a fracture would be taken to be a solution in a fracture with no specified end conditions, that is in a fracture of unbounded length. Such a solution would be a good approximation at distances removed from intersection zones. Solutions for flow in elemental fractures could then be linked by choosing free parameters in the solutions to satisfy equations arising from mass, momentum and energy balance across fracture intersections. In this way linkages could be developed through an ensemble of intersecting fractures.

The analysis to follow addresses the most fundamental problem in the program of development of a quantitative model for hydrotectonic phenomena, that is flow in a dynamically deforming fracture. The approach that will be taken is to consider a class of flow behavior that is non-turbulent and has properties of a time dependent laminar flow but includes effects of a time and spatially varying fracture aperture. The essential simplifications that will allow this problem to be successfully attacked and solved analytically involve making use of the knowledge that this type of flow will be characterized by particle velocity derivatives in the direction normal to the fracture boundaries that are much larger than in the other directions and also that the functional dependence of field variables (*e.g.* pressure and particle velocity) can be accurately expressed, within the narrow fracture, as a power series in the direction along the normal to the fracture boundaries. These restrictions and approximations result in closed form solutions that can be used with the integral balance method described earlier to obtain a representation of flows in networks of fractures. Therefore, while restricted to transient laminar flows, this elemental solution will allow us to formulate a general representation for relatively uniform "late-time"

flow in a fractured system that accounts for nonlinear fluid-solid interactions.

Basic Flow Relations and Constraints

We consider the fluid (or fluid and gas mixture in some cases) to be isotropic. The general equation expressing the conservation of momentum is:†

$$\rho\left[\frac{\partial v_i}{\partial t} + v_j\frac{\partial v_i}{\partial x_j}\right] = \frac{\partial T_{ij}}{\partial x_j} + \rho f_i$$

where T_{ij} is the stress tensor and f_i the body force density. Here (*eg.* Landau and Lifshitz, 1959):

$$T_{ij} = -p\delta_{ij} + V_{ij}$$

Where p is the pressure and V_{ij} the viscosity tensor. The viscosity tensor must depend on the spatial derivatives of the velocity field and must vanish under rigid rotation and translation of the fluid. The most general second order tensor with such properties is:

$$V_{ij} = a\left[\frac{\partial v_i}{\partial x_j} + \frac{\partial v_j}{\partial x_i}\right] + b\,\frac{\partial v_k}{\partial x_k}\,\delta_{ij}$$

where a and b are independent of the fluid velocity. (Also, isotropy of the fluid is assumed.) The equation for V_{ij} may be rewritten and the constants a and b can be redefined in terms of the usual viscosity coefficients, that is the relation can be rewritten as:

$$V_{ij} = \eta\left[\frac{\partial v_i}{\partial x_j} + \frac{\partial v_j}{\partial x_i} - \frac{2}{3}\,\delta_{ij}\frac{\partial v_k}{\partial x_k}\right] + \zeta\delta_{ij}\,\frac{\partial v_k}{\partial x_k}$$

where the term in brackets vanishes when contracted on i and j. Here η is the shear viscosity and ζ the bulk viscosity. It can be shown that:

$$\eta > 0 \text{ and } \zeta > 0.$$

Now, the equation of motion becomes

$$\rho\left[\frac{\partial v_i}{\partial t} + v_j\frac{\partial v_i}{\partial x_j}\right] = -\frac{\partial p}{\partial x_i} + \frac{\partial}{\partial x_j}\left\{\eta\left[\frac{\partial v_i}{\partial x_j} + \frac{\partial v_j}{\partial x_i} - \frac{2}{3}\delta_{ij}\frac{\partial v_k}{\partial x_k}\right]\right\} + \frac{\partial}{\partial x_i}\left[\zeta\,\frac{\partial v_k}{\partial x_k}\right] + \rho f_i$$

† The summation convention on repeated indices is used throughout.

In general η and ζ are functions of temperature and pressure, so their spatial derivatives are non-zero. However, to a good approximation they can be taken to be nearly constant in the fluid over a reasonably extended spatial region. In this case we get:

$$\rho\left[\frac{\partial v_i}{\partial t} + v_j\frac{\partial v_i}{\partial x_j}\right] = -\frac{\partial p}{\partial x_i} + \eta\left\{\frac{\partial^2 v_i}{\partial x_j \partial x_j} + \frac{\partial}{\partial x_i}\left[\frac{\partial v_j}{\partial x_j}\right] - \frac{2}{3}\frac{\partial}{\partial x_i}\left[\frac{\partial v_k}{\partial x_k}\right]\right\} + \zeta\frac{\partial}{\partial x_i}\left[\frac{\partial v_k}{\partial x_k}\right] + \rho f_i$$

Therefore:

$$\rho\left[\frac{\partial v_i}{\partial t} + v_j\frac{\partial v_i}{\partial x_j}\right] = -\frac{\partial p}{\partial x_i} + \eta\frac{\partial^2 v_i}{\partial x_j \partial x_j} + (\zeta + \eta/3)\frac{\partial}{\partial x_i}\left[\frac{\partial v_k}{\partial x_k}\right] + \rho f_i$$

Since:

$$\nabla^2 v_i \equiv \frac{\partial^2 v_i}{\partial x_j \partial x_j} \; ; \; \nabla\cdot v \equiv \frac{\partial v_k}{\partial x_k}$$

then, in vector form:

$$\rho\left[\frac{\partial v}{\partial t} + (v\cdot\nabla)v\right] = -\nabla p + \eta\nabla^2 v + (\zeta + \eta/3)\,\nabla\,(\nabla\cdot v) + \rho f \qquad (1a.)$$

If the fluid has a bulk viscosity, ζ, that is small relative to the shear viscosity, η, then

$$\rho\left[\frac{\partial v}{\partial t} + (v\cdot\nabla)v\right] = -\nabla p + \eta\left[\nabla^2 v + \frac{1}{3}\nabla\,(\nabla\cdot v)\right] + \rho f \qquad (1b.)$$

If the fluid is incompressible, so $\nabla\cdot v = 0$ (and $\frac{\partial\rho}{\partial t} + \rho\,\nabla\cdot v = \frac{d\rho}{dt} = 0$), then

$$\rho\left[\frac{\partial v}{\partial t} + (v\cdot\nabla)v\right] = -\nabla p + \eta\,\nabla^2 v + \rho f \qquad (1c.)$$

which is usually called the Navier-Stokes equation.

Laminar Flow in a Fracture

The geometry for the flow to be considered is in Cartesian coordinates. The flow of interest will be quasi-laminar in that the velocity gradients in the x_2 direction dominate over those in the x_1 , x_3 directions. Therefore:

$$\left| \frac{\partial v_i}{\partial x_2} \right| \gg \left[\left| \frac{\partial v_i}{\partial x_1} \right| , \left| \frac{\partial v_i}{\partial x_3} \right| \right] ; \; i = 1, 2, 3 \qquad (2.)$$

and, as well, the change in gradient in the x_2 direction dominates, so:

$$\left| \frac{\partial^2 v_i}{\partial x_2^2} \right| \gg \left[\left| \frac{\partial^2 v_i}{\partial x_1^2} \right| , \left| \frac{\partial^2 v_i}{\partial x_3^2} \right| \right] ; \; i = 1, 2, 3 \; \ldots (3) \qquad (3.)$$

In component form, the equation (1.a) becomes, for i = 1 and setting $b_i = \rho f_i$:

$$\frac{\partial p}{\partial x_i} = \eta \left[\frac{\partial^2 v_1}{\partial x_1^2} + \frac{\partial^2 v_1}{\partial x_2^2} + \frac{\partial^2 v_1}{\partial x_3^2} \right] + \left(\zeta + \frac{\eta}{3} \right) \frac{\partial}{\partial x_1} \left[\frac{\partial v_1}{\partial x_1} + \frac{\partial v_2}{\partial x_2} + \frac{\partial v_3}{\partial x_3} \right]$$
$$- \rho \left[v_1 \frac{\partial v_1}{\partial x_1} + v_2 \frac{\partial v_1}{\partial x_2} + v_3 \frac{\partial v_1}{\partial x_3} \right] - \rho \frac{\partial v_1}{\partial t} + b_1$$

Or, after neglecting the smaller terms, according to equations (2) and (3):

$$\frac{\partial p}{\partial x_1} = \eta \frac{\partial^2 v_1}{\partial x_2^2} - \rho v_2 \frac{\partial v_1}{\partial x_2} - \rho \frac{\partial v_1}{\partial t} + b_1 \qquad (4.)$$

The x_2 component equation becomes:

$$\frac{\partial p}{\partial x_2} = \eta \frac{\partial^2 v_1}{\partial x_2^2} + (\zeta + \eta/3) \frac{\partial^2 v_2}{\partial x_2^2} - \rho v_2 \frac{\partial v_2}{\partial x_2} - \rho \frac{\partial v_2}{\partial t} + b_2$$

or,

$$\frac{\partial p}{\partial x_2} = (4/3\eta + \zeta) \frac{\partial^2 v_2}{\partial x_2^2} - \rho v_2 \frac{\partial^2 v}{\partial x_2} - \rho \frac{\partial v_2}{\partial t} + b_2 \qquad (5.)$$

The x_3 component equation becomes:

$$\frac{\partial p}{\partial x_3} = \eta \frac{\partial^2 v_3}{\partial x_2^2} - \rho v_2 \frac{\partial v_3}{\partial x_2} - \rho \frac{\partial v_3}{\partial t} + b_3 \qquad (6.)$$

For the case when ζ is negligible, as in (1-b.) we have:

$$\frac{\partial p}{\partial x_1} = \eta \frac{\partial^2 v_1}{\partial x_2^2} - \rho v_2 \frac{\partial v_1}{\partial x_2} - \rho \frac{\partial v_1}{\partial t} + b_1$$

$$\frac{\partial p}{\partial x_2} = 4/3 \; \eta \frac{\partial^2 v_2}{\partial x_2^2} - \rho v_2 \frac{\partial v_2}{\partial x_2} - \rho \frac{\partial v_2}{\partial t} + b_2$$

$$\frac{\partial p}{\partial x_3} = \eta \frac{\partial^2 v_3}{\partial x_2^2} - \rho v_2 \frac{\partial v_3}{\partial x_2} - \rho \frac{\partial v_3}{\partial t} + b_3$$

When the fluid is incompressible, as in (1-c.), then:

$$\frac{\partial p}{\partial x_i} = \eta \frac{\partial^2 v_i}{\partial x_2^2} - \rho v_2 \frac{\partial v_i}{\partial x_2} - \rho \frac{\partial v_i}{\partial t} + b_i, \quad i = 1, 2, 3$$

The general form of all these equations is the same. That is we can write them all in the form:

$$\frac{\partial p}{\partial x_k} = \mu^{(k)} \frac{\partial^2 v_k}{\partial x_2^2} - \rho v_2 \frac{\partial v_k}{\partial x_2} - \rho \frac{\partial v_k}{\partial t} + b_k \; ; \quad k = 1, 2, 3$$

where

$\mu^{(1)} = \mu^{(3)} = \eta$ in all cases, and

$\mu^{(2)} = 4/3\ \eta + \zeta$ (in the general case)

$\mu^{(2)} = 4/3\ \eta$ (when $\zeta \ll \eta$)

$\mu^{(2)} = \eta$ (when $\nabla \cdot v = 0$)

Zeroth and first order approximations.

The "zeroth order" approximation corresponds to the equilibrium situation where $v \equiv 0$. In the first order approximation we take:

$$\left|v_2^{(1)}\right| \ll \left|v_1^{(1)}\right| , \quad \left|v_2^{(1)}\right| \ll \left|v_3^{(1)}\right| \tag{8.}$$

and the flow under consideration becomes strictly laminar when v_2 is neglected in (7.). For a steady state laminar flow, then $\partial v_i/\partial t \equiv 0$ also, and this will constitute the first order approximation.

In order to develop zeroth order, first order and higher order approximations for the flow, we consider the fluid variables (v and p) to be expandable in the forms:

$$\begin{aligned} v &= v^{(0)} + v^{(1)} + v^{(2)} + \ \ldots \\ p &= p^{(0)} + p^{(1)} + p^{(2)} + \ \ldots \end{aligned} \tag{9.}$$

Where $v^{(0)}$ and $p^{(0)}$ refer to the equilibrium values and $v^{(1)}$ and $p^{(1)}$ to the steady state laminar flow values of velocity and pressure. As indicated above, $v^{(0)} \equiv 0$ (by definition of an equilibrium state) and for laminar flow there is negligible flow in the x_2 direction ($v_2^{(1)} = 0$). Further, when the flow is steady state, then $\partial v_i/\partial t = 0$. Under these definitions for the zeroth and first order fields, the equations

(7.) give, with b_i representing gravity forces only:

$$\frac{\partial p^{(0)}}{\partial x_i} = b_i^{(0)} = \rho^{(0)} g^{(0)} \cdot \hat{e}_i \qquad i = 1, 2, 3 \tag{10.}$$

since $v \equiv o$ by definition.

For the first order steady state laminar flow approximation:

$$\left[\frac{\partial p^{(0)}}{\partial x_i} + \frac{\partial p^{(1)}}{\partial x_i}\right] = \mu^{(i)}\frac{\partial^2 v_i}{\partial x_2^2} - \rho v_2 \frac{\partial v_i}{\partial x_2} + \rho g \cdot \hat{e}$$

where, $\rho = \rho^{(0)} + \rho^{(1)}$, $g = g^{(0)} + g^{(1)}$ $v_i = v_i^{(0)} + v_i^{(1)} = v_i^{(1)}$, $i = 1, 2, 3$; to first order. In view of equation (8.), we have:

$$\frac{\partial p^{(1)}}{\partial x_i} = \eta^i \frac{\partial^2 v_i^{(1)}}{\partial x_2^2} - \rho^{(0)} v_2^{(1)} \frac{\partial v_i^{(1)}}{\partial x_2} + \rho^{(1)} g^{(0)} \cdot \hat{e}_i$$

Finally if $v_2^{(1)} = 0$ for the laminar first order case, then the component equations are:

$$\frac{\partial p^{(1)}}{\partial x_1} = \eta \frac{\partial^2 v_i^{(1)}}{\partial x_2^2} + \rho^{(1)} g^{(0)} \cdot \hat{e}_1$$

$$\frac{\partial p^{(1)}}{\partial x_2} = \rho^{(1)} g^{(0)} \cdot \hat{e}_2$$

$$\frac{\partial p^{(1)}}{\partial x_3} = \eta \frac{\partial^2 v_3^{(1)}}{\partial x_2^2} + \rho^{(1)} g^{(0)} \cdot \hat{e}_3$$

or setting

$$g_i^{(0)} \equiv g^{(0)} \cdot \hat{e}_i$$

then:

$$\left.\begin{aligned} \frac{\partial p^{(1)}}{\partial x_j} &= \eta \frac{\partial^2 v_j}{\partial x_2^2} + \rho^{(1)} g_j^{(0)} : \quad j = 1, 3 \\ \frac{\partial p^{(1)}}{\partial x_j} &= \rho^{(1)} g_2^{(0)} \end{aligned}\right\} \tag{11.}$$

Solutions for the First Order Approximation in the Steady State

To the first order consider both pressure driven (pumped) flows and thermally driven (convected) flows

in a gravity field. Thus, the terms $\rho^{(1)}b_i^{(0)}$, with j = 1, 2, 3, will not be neglected in (9.), except as special cases. (*e.g.* $g_2^{(0)} = 0$ for fractures aligned with the gravity field or if, for narrow fractures, the approximation $g_2^{(0)} \approx 0$ is used.)

Consequently, take v_i to be of the form:

$$v_i = f(x_2)\,\frac{\partial p^{(1)}}{\partial x_i} + h(x_2)\,\frac{\partial T^{(1)}}{\partial x_i} + k_i(x_1, x_2, x_3)\;; \quad i = 1, 3 \tag{12.}$$

where we also take the temperature change across the aperture of the fracture to be small and uniform, so:

$$\frac{\partial T^{(1)}}{\partial x_2} \approx 0 \ldots \tag{13.}$$

Now using (12.) in the first relation in (11.) gives for i = 1, 3:

$$\frac{\partial p^{(1)}}{\partial x_i} = \eta \frac{\partial}{\partial x_2}\left\{\frac{\partial f}{\partial x_2}\,\frac{\partial p^{(1)}}{\partial x_i} + f\,\frac{\partial^2 p^{(1)}}{\partial x_2 \partial x_i}\right\} + \eta\,\frac{\partial T^{(1)}}{\partial x_i}\left[\frac{\partial^2 h}{\partial x_2^2}\right] + \eta\frac{\partial^2 k_i}{\partial x_2^2} + \rho^{(1)} g_i^{(0)} \tag{14.}$$

From the second equation in (11.) however, note that:

$$\frac{\partial^2 p^{(1)}}{\partial x_2 \partial x_i} = \frac{\partial}{\partial x_i}\left[\frac{\partial p^{(1)}}{\partial x_2}\right] = \frac{\partial}{\partial x_i}\left[\rho^{(1)} g_2^{(0)}\right]$$

Taking $g^{(0)}$ to be nearly constant (over the extent of the fracture segment under consideration), then

$$\frac{\partial^2 p^{(1)}}{\partial x_2 \partial x_i} = g_2^{(0)}\,\frac{\partial \rho^{(1)}}{\partial x_i} + \rho^{(1)}\frac{\partial g_2^{(0)}}{\partial x_i} \approx g_2^{(0)}\,\frac{\partial \rho^{(1)}}{\partial x_i}$$

when

$$\left|\frac{1}{\rho^{(1)}}\,\frac{\partial \rho^{(1)}}{\partial x_i}\right| \gg \left|\frac{1}{g_2^{(0)}}\,\frac{\partial g_2^{(0)}}{\partial x_i}\right|$$

provided $\rho^{(1)} \neq 0$ and $g_2^{(0)} \neq 0$. (Note that if either $\rho^{(1)}$ or $g_2^{(0)}$ are zero, then $\partial^2 p^{(1)}/\partial x_2\,\partial x_i = 0$.) Under these conditions:

$$\frac{\partial^2 p^{(1)}}{\partial x_2 \partial x_i} = g_2^{(0)}\,\frac{\partial p^{(1)}}{\partial x_i}$$

and equation (14.) becomes:

$$\frac{\partial p^{(1)}}{\partial x_i} = \eta \left[\frac{\partial^2 f}{\partial x_2^2} \frac{\partial p^{(1)}}{\partial x_i} + 2 \frac{\partial f}{\partial x_2} \frac{\partial \rho^{(1)}}{\partial x_i} g_2^{(0)} + f \frac{\partial^2 \rho^{(1)}}{\partial x_i \partial x_2} g_2^{(0)} \right]$$
$$+ \eta \frac{\partial^2 h}{\partial x_2^2} \left[\frac{\partial T^{(1)}}{\partial x_i} \right] + \eta \frac{\partial^2 k_i}{\partial x_2^2} + \rho^{(1)} g_i^{(0)} \qquad (15.)$$

Consider, however, that because of the existence of an equation of state, we can write:

$$\rho = \rho(p, T) \qquad (16.)$$

Consequently we have:

$$\delta\rho = \left[\frac{\partial \rho}{\partial p} \right]_T \delta p + \left[\frac{\partial \rho}{\partial T} \right]_p \delta T \qquad (17a.)$$

Since $\rho = \rho^{(0)} + \delta\rho$, $p = p^{(0)} + \delta p$ and $T = T^{(0)} + \delta T$, where $\delta\rho$, etc. are small qualities and $\rho^{(0)}$, etc. are equilibrium values, then to a good approximation $\rho^{(1)} = \delta\rho$, $p^{(1)} = \delta p$ and $T^{(1)} = \delta T$ and (17a.) can be rewritten as

$$\rho^{(1)} = \left[\frac{\partial \rho}{\partial p} \right]_T p^{(1)} + \left[\frac{\partial \rho}{\partial T} \right]_p T^{(1)} \equiv a_1 p^{(1)} + a_2 T^{(1)} \qquad (17b.)$$

Here a_1 and a_2 are constants of the material (isothermal coefficient of compressibility and isobaric coefficient of thermal expansion) where

$$a_1 \equiv \left[\frac{\partial \rho}{\partial p} \right]_T \; ; \; a_2 \equiv \left[\frac{\partial \rho}{\partial T} \right]_p$$

and are both evaluated at $T^{(0)}$ and $p^{(0)}$.

Now, noting that by use of (17b.) we have that:

$$\frac{\partial \rho^{(1)}}{\partial x_i \partial x_2} = \frac{\partial}{\partial x_i} \left[\frac{\partial}{\partial x_2} \left[a_1 p_{(1)} + a_2 T^{(1)} \right] \right] \approx \frac{\partial}{\partial x_i} \left[a_1 \frac{\partial p^{(1)}}{\partial x_2} \right]$$

since $\partial T^{(1)}/\partial x_2 \approx 0$ from equation (13.). Therefore, using the second equation in (11) again,

$$\frac{\partial^2 \rho^{(1)}}{\partial x_i \partial x_2} \approx a_1 \frac{\partial}{\partial x_i} \left[\rho^{(1)} g_2^{(0)} \right] \approx a_1 g_2^{(0)} \frac{\partial \rho^{(1)}}{\partial x_i}$$

Thus equation (15.) becomes:

$$\frac{\partial p^{(1)}}{\partial x_i} = \eta \left[\frac{\partial^2 f}{\partial x_2^2} \frac{\partial p^{(1)}}{\partial x_i} + \left\{ 2 \frac{\partial f}{\partial x_2} + a_1 f \right\} \frac{\partial \rho^{(1)}}{\partial x_i} g_2^{(0)} \right] + \eta \frac{\partial^2 h}{\partial x_2^2} \left[\frac{\partial T^{(1)}}{\partial x_i} \right] + \eta \frac{\partial^2 k_i}{\partial x_2^2} + \rho^{(1)} g_i^{(0)} \; ; \; i = i, 3$$

Again expressing $\rho^{(1)}$ in terms of $T^{(1)}$ and $p^{(1)}$, this becomes,

$$\frac{\partial p^{(1)}}{\partial x_i} = \eta \left[\frac{\partial^2 f}{\partial x_2^2} + \left\{ 2\,\frac{\partial f}{\partial x_2} + a_1 g_2^{(0)} f \right\} a_1 g_2^{(0)}\right]\left[\frac{\partial p^{(1)}}{\partial x_i}\right] + \eta\left[\frac{\partial^2 h}{\partial x_2^2} + \left\{2\frac{\partial f}{\partial x_2} + a_1 g_2^{(0)} f\right\} a_2 g_2^{(0)}\right]\left[\frac{\partial T^{(1)}}{\partial x_i}\right]$$
$$+ \eta\,\frac{\partial^2 k_i}{\partial x_2^2} + \rho^{(1)} g_i^{(0)} \qquad (18.)$$

or

$$\left[\frac{\partial^2 f}{\partial x_2^2} + 2a_1\, g_2^{(0)}\,\frac{\partial f}{\partial x_2} + (a_1\, g_2^{(0)})^2\, f - \frac{1}{\eta}\right]\frac{\partial p^{(1)}}{\partial x_i} + \left[\frac{\partial^2 h}{\partial x_2^2} + 2a_2\, g_2^{(0)}\,\frac{\partial f}{\partial x_2} + a_1\, a_2\, (g_2^{(0)})^2\, f\right]\frac{\partial T^{(1)}}{\partial x_i}$$
$$+ \left[\frac{\partial^2 k_i}{\partial x_2^2} + \frac{\rho^{(1)} g_i^{(0)}}{\eta}\right] = 0 \qquad (19.)$$

Now we must chose the functions f, h and k_i so as to satisfy this equation for i = 1, 3. Consider first the final bracketed term involving k_i. We can choose $k_i\,(x_1, x_2, x_3)$ to cause this quantity to vanish, that is take k_i such that:

$$\frac{\partial^2 k_i}{\partial x_2^2} + \frac{\rho^{(1)} g_i^{(0)}}{\eta} = 0 \qquad (20.)$$

Let:

$$k_i\,(x_1, x_2, x_3) = w_i\,(x_1, x_3)\left[\gamma_2 x_2^2 + \gamma_1\, x_2 + \gamma_0\right] \qquad (21.)$$

Then:

$$\frac{\partial^2 k_i}{\partial x_2^2} = 2\gamma_2 w_i = -\,\frac{\rho^{(1)} g_i^{(0)}}{\eta}$$

Consequently

$$k_i\,(x_1, x_2, x_3) = -\,\frac{\rho^{(1)} g_i^{(0)}}{2\eta}\left[x_2^2 + \left[\frac{\gamma_1}{\gamma_2}\right] x_2 + \left[\frac{\gamma_0}{\gamma_2}\right]\right] \qquad (22.)$$

Next it is necessary to find the functions f and h such that both the first and second bracketed relations in (19.) also vanish. That is, we require:

$$\left.\begin{aligned} &\frac{\partial^2 f}{\partial x_2^2} + 2\, a_1\, g_2^{(0)}\frac{\partial f}{\partial x_2} + (\,a_1\, g_2^{(0)}\,)^2\, f = \frac{1}{\eta} \\ &\frac{\partial^2 h}{\partial x_2^2} + 2\, a_1\, g_2^{(0)}\frac{\partial f}{\partial x_2} + a_1\, a_2 (g_2^{(0)})^2\, f = 0 \end{aligned}\right\} \qquad (23.)$$

Or, letting

$$c \equiv a_1\, g_2^{(0)} \text{ and } b \equiv a_2\, g_2^{(0)} \tag{24.}$$

then we need to have

$$\left.\begin{aligned} \frac{\partial^2 f}{\partial x_2^2} + 2c\frac{\partial f}{\partial x_2} + c^2 f &= \frac{1}{\eta} \\ \frac{\partial^2 h}{\partial x_2^2} + 2b\frac{\partial f}{\partial x_2} + b\,c\,f &= 0 \end{aligned}\right\} \tag{25.}$$

Multiplying the second equation by c/b and subtracting from the first gives:

$$\frac{\partial^2 f}{\partial x_2^2} - \left[\frac{c}{b}\right]\frac{\partial^2 h}{\partial x_2^2} = \frac{\partial^2}{\partial x_2^2}\left[f - \left[\frac{a_1}{a_2}\right]h\right] = \frac{1}{\eta}$$

where $c/b = a_1/a_2$ from (24.). Taking

$$F(x_2) \equiv f(x_2) - \left[\frac{a_1}{a_2}\right] h(x_2)$$

then we have:

$$\frac{\partial^2 F}{\partial x_2^2} = \frac{1}{\eta}$$

now taking

$$F(x_2) = \alpha_2\, x_2^2 + \alpha_1 x_2 + \alpha_0$$

then

$$\frac{\partial^2 F}{\partial x_2^2} = 2\alpha_2 = \frac{1}{\eta}\ ;\ \ \alpha_2 = \frac{1}{2\eta}$$

Consequently

$$F(x_2) = \frac{1}{2\eta}\, x_2^2 + \alpha_1\, x_2 + \alpha_0 = f - \left[\frac{a_1}{a_2}\right] h$$

and, for $a_1 \neq 0$,

$$h(x_2) = \left[\frac{a_2}{a_1}\right]\left[f(x_2) - \frac{1}{2\eta}x_2^2 - \alpha_1\, x_2 - \alpha_0\right] \tag{26.}$$

For $h(x_2)$ of this form, the second equation in (25.) becomes the same as the first equation. Therefore, we must find $f(x_2)$ such that

$$\frac{\partial^2 f}{\partial x_2^2} + 2c\frac{\partial f}{\partial x_2} + c^2 f = \frac{1}{\eta}$$

Taking:

$$f(x_2) = \beta_2 x_2^2 + \beta_1 x_2 + \beta_0$$

produces

$$2\beta_2 + 2c(2\beta_2 x_2 + \beta_1) + c^2(\beta_2 x_2^2 + \beta_1 x_2 + \beta_0) = \frac{1}{\eta}$$

Here η is regarded as constant, so we must have:

$$\beta_2 = 0 \quad \text{and} \quad \beta_1 = 0$$

while

$$\beta_0 = \frac{1}{c^2\eta}$$

is required. Thus

$$\left.\begin{aligned} f(x_2) &= \frac{1}{c^2\eta} \\ h(x_2) &= -\left[\frac{a_2}{a_1}\right]\left[\frac{1}{2\eta}x_2^2 + \alpha_1 x_2 + \left[\alpha_0 - \frac{1}{c^2\eta}\right]\right] \end{aligned}\right\} \qquad (27.)$$

The velocity components are therefore, assuming $c \neq 0$:

$$\begin{aligned} v_i = \left[\frac{1}{c^2\eta}\right]\frac{\partial p^{(1)}}{\partial x_i} - \left[\frac{a_2}{a_1}\right]\left[\frac{x_2^2}{2\eta} + \alpha_1 x_2 + \left[\alpha_0 - \frac{1}{c^2\eta}\right]\right]\frac{\partial T^{(1)}}{\partial x_i} \\ - \frac{\rho^{(1)} g_i^{(0)}}{2\eta}\left[x_2^2 + \left[\frac{\gamma_1}{\gamma_2}\right]x_2 + \left[\frac{\gamma_0}{\gamma_2}\right]\right] \end{aligned} \qquad (28.)$$

for $i = 1, 3$; and where $v_2 = 0$.

Alternate Solution Forms and Special Cases for Steady State Flows

The solution in (28.) can be put in alternate form by making use of the equation of state relationships between $\rho^{(1)}$, $p^{(1)}$ and $T^{(1)}$. That is, from (17b.)

$$\rho^{(1)} = a_1\, p^{(1)} + a_2\, T^{(1)}$$

then

$$\frac{\partial \rho^{(1)}}{\partial x_i} = a_1\, \frac{\partial p^{(1)}}{\partial x_i} + a_2 \frac{\partial T^{(1)}}{\partial x_i}$$

Using this in (28.) to eliminate $\dfrac{\partial p^{(1)}}{\partial x_i}$ gives:

$$v_i = \left[\frac{1}{\eta a_1 c^2}\right] \frac{\partial \rho^{(1)}}{\partial x_i} - \left[\frac{a_2}{a_1}\right] \left[\frac{x_2^2}{2\eta} + \alpha_1\, x_2 + \alpha_0\right] \frac{\partial T^{(1)}}{\partial x_i} - \rho^1 g_i^{(0)} \left[x_2^2 + \left[\frac{\gamma_1}{\gamma_2}\right] x_2 + \left[\frac{\gamma_0}{\gamma_2}\right]\right] \quad (29a.)$$

Further, eliminating $\dfrac{\partial T^{(1)}}{\partial x_i}$ gives:

$$v_i = \left[\frac{x_2^2}{2\eta} + \alpha_1 x_2 + \alpha_0\right] \frac{\partial p^{(1)}}{\partial x_i} - \left[\frac{1}{a_1}\right] \left[\frac{x_2^2}{2\eta} + \alpha_1 x_2 + \left[\alpha_0 - \frac{1}{\eta c^2}\right]\right] \frac{\partial \rho^{(1)}}{\partial x_i} - \frac{\rho^{(1)} g_i^{(0)}}{2\eta} \left[x_2^2 + \frac{\gamma_1}{\gamma_2} x_2 + \frac{\gamma_0}{\gamma_2}\right] \quad (29b.)$$

The special cases of importance involve the cases in which the gravity force component in the x_2 direction can be neglected. Consider the case when $g_2^{(0)}$ is small and so $\rho^{(1)} g_2^{(0)}$ can be neglected in the first order approximation. (This occurs, for example, when the fractures are aligned, or nearly aligned, with the gravity field, so that $\hat{e}_2$ is normal to $g^{(0)}$ or when the derivatives $\partial \rho^{(1)} / \partial x_i$ are small.) In this case the equation (11.) becomes:

$$\left.\begin{aligned} \frac{\partial p^{(1)}}{\partial x_j} &= \eta\, \frac{\partial^2 v_j}{\partial x_2^2} + \rho^{(1)}\, g_j^{(0)}\,, \quad j = 1, 3 \\ \frac{\partial p^{(1)}}{\partial x_2} &= 0 \end{aligned}\right\} \quad (30.)$$

Here again taking the solution for v_i to have the form as in (12.), that is:

$$v_i = f(x_2)\,\frac{\partial p^{(1)}}{\partial x_i} + hx_2\,\frac{\partial T^{(1)}}{\partial x_i} + k_i\,(x_1, x_2, x_3)$$

we get for (30.):

$$\frac{\partial p^{(1)}}{\partial x_i} = \eta\left[\frac{\partial^2 f}{\partial x_2^2}\right]\frac{\partial p^{(1)}}{\partial x_i} + \eta\left[\frac{\partial^2 h}{\partial x_2^2}\right]\frac{\partial T^{(1)}}{\partial x_i} + \eta\,\frac{\partial^2 k_i}{\partial x_2^2} + \rho^{(1)}\,g_i^{(0)} \qquad (31.)$$

This same result is produced from eqn. (15.) when the spatial derivatives of $\rho^{(1)}$ are neglected relative to $p^{(1)}$ pressure derivatives. Again we can take k_i to be such that:

$$\eta\,\frac{\partial^2 k_i}{\partial x_2^2} = -\rho^{(1)} g_i^{(0)}\,;\; i = 1, 3$$

Thus, with

$$k_i = w_i(x_1, x_3)\,[\,\gamma_2 x_2^2 + \gamma_1 x_2 + \gamma_0\,]$$

as in equation (21.) under similar circumstances, we get:

$$k_i = -\frac{\rho^{(1)} g_i^{(0)}}{2\eta}\left[x_2^2 + \left[\frac{\gamma_0}{\gamma_2}\right] x_2 + \left[\frac{\gamma_0}{\gamma_2}\right]\right] \qquad (32.)$$

Likewise, as before we require the coefficient factors multiplying the temperature and pressure gradients to vanish. That is:

$$\left.\begin{aligned}\left[\frac{\partial^2 f}{\partial x_2^2} - \frac{1}{\eta}\right]\frac{\partial p^{(1)}}{\partial x_i} = 0 \\ \left[\frac{\partial^2 h}{\partial x_2^2}\right]\frac{\partial T^{(1)}}{\partial x_i} = 0\end{aligned}\right\} \qquad (33.)$$

These conditions are satisfied by:

$$f(x_2) = \frac{x_2^2}{2\eta} + \alpha'_1\,x_2 + \alpha'_0$$

$$h(x_2) = \beta'_1\,x_2 + \beta'_0$$

Consequently the solution in this case is, from (12.):

$$v_i^{(1)} = \left[\frac{x_2^2}{2\eta} + \alpha'_1\,x_2 + \alpha'_0\right]\frac{\partial p^{(1)}}{\partial x_i} + \left[\beta'_1\,x_2 + \beta'_0\right]\frac{\partial T^{(1)}}{\partial x_i} - \frac{\rho^{(1)} g_i^{(0)}}{2\eta}\left[x_2^2 + \left[\frac{\gamma_1}{\gamma_2}\right] x_2 + \left[\frac{\gamma_0}{\gamma_2}\right]\right] \qquad (34.)$$

Here again the relation $\rho^{(1)} = a_1 p^{(1)} + a_2 T^{(1)}$ can be used to generate alternate expressions of this result.

Boundary Conditions: Application to Steady State Laminar Flows

There are only two required conditions at the boundaries of a fracture in a solid; these are that the tractions are continuous (conservation of momentum across the boundary) and that the normal component of the particle velocity is continuous (conservation of mass across the boundary). The assumption here is that the boundary moves with the particles. These conditions require:

$$[[\, T_{ij}\, n_j]]_B = 0 \quad \text{and} \quad [[\, v_i\, n_i]]_B = 0 \tag{35.}$$

where n_j denotes the jth component of the normal vector at the boundary surface and the double bracket $[[\phi]]_B$ denotes the difference in the quantity ϕ across the boundary B; that is:

$$[[\phi]]_B = \phi\,(B^+) - \phi\,(B^-)$$

In the steady state approximation the boundary is considered fixed and in the first order approximation $v_2 = 0$, so that the second equation in (35.) is automatically satisfied. (The normal particle velocity at the boundary is zero on both sides of B.)

Ordinarily, the velocities v_1 and v_3 are required to be zero at the boundary. (See for example Landau and Lifshtz, 1959). This is based on a physical premise, namely that if the fluid is viscous and the solid rigid (the particles on the solid boundary do not move) then the fluid adheres to the solid at the boundary and all velocities vanish there. This seems to give good agreement with flow tests but is, in fact, not required by the conservation relations (boundary conditions) in (35.).

If this condition ($v_1 = v_3 = 0$ at $x_2 = \pm\delta$) is nevertheless applied to the results of the previous sections, then only the special case in which $\rho^{(1)} g_2^{(0)}$ is neglected in the equations, as expressed in equation (30), can satisfy these conditions in the first order steady state approximation. In this case (34) is the solution and we have:

At $x_2 = \delta$; for i = 1, 3

$$\left[\frac{(\delta)^2}{2\eta} + \alpha'_1\,\delta + \alpha'_0\right]\frac{\partial p^{(1)}}{\partial x_i} + \left[\beta'_1\delta + \beta'_0\right]\frac{\partial T_1}{\partial x_i} - \frac{\rho^{(1)}g_i^{(0)}}{2\eta}\left[(\delta)^2 + \left[\frac{\gamma_1}{\gamma_2}\right]\delta + \frac{\gamma_0}{\gamma_2}\right] = 0$$

At $x_2 = -\delta$, for i = 1, 3 :

$$\left[\frac{(-\delta)^2}{2\eta} + \alpha'_1\,(-\delta) + \alpha'_0\right]\frac{\partial p^{(1)}}{\partial x_i} + \left[-\beta'_1\,\delta + \beta'_0\right]\frac{\partial T^{(1)}}{\partial x_i} - \frac{\rho^{(1)}g_i^{(0)}}{2\eta}\left[(-\delta)^2 - \left[\frac{\gamma_1}{\gamma_2}\right]\delta + \frac{\gamma_0}{\gamma_2}\right] = 0$$

These equations can only be satisfied if:

$$\alpha'_1 = 0,\ \beta'_1 = 0,\ \beta'_0 = 0,\ \gamma_1 = 0$$

$$\alpha'_0 = -\frac{\delta^2}{2\eta},\ \frac{\gamma_0}{\gamma_2} = -\delta^2$$

The solution is , in this case:

$$v_i = \frac{1}{2\eta}\left[x_2^2 - \delta^2\right]\left\{\frac{\partial p^{(1)}}{\partial x_i} - \rho^{(1)}g_i^{(0)}\right\} \qquad (36.)$$

with i = 1, 3 and $v_2 = 0$. Here the term involving the density perturbation $\rho^{(1)}$ can correspond to a buoyancy effect ($\rho^{(1)} < 0$), or since $\rho^{(1)} = a_2T^{(1)}$, it can correspond to a thermal convection effect.

On the other hand, it is reasonable to also consider flows that involve slip at the boundaries of the fracture and a non-rigid solid boundary. In this case the solid is coupled to the fluid through the boundary condition $[[\ T_{ij}n_j\ ]]_B = 0$ and the solution forms in (28.) and (29a,b) are all possible, so long as $a_1 \neq 0$. If, however, density gradients are small compared to pressure and gravitational (buoyancy) effects, then the solution has the same general form as that in (37.), that is:

$$v_i = \left[\frac{x_2^2}{2\eta} + \alpha_1\,x_2 + \alpha_0\right]\frac{\partial p^{(1)}}{\partial x_i} - \frac{\rho^{(1)}g_i^{(0)}}{2\eta}\left[x_2^2 + \left[\frac{\gamma_1}{\gamma_2}\right]x_2 + \frac{\gamma_0}{\gamma_2}\right] \qquad (37.)$$

but now with the constants α_1, α_0, γ_1/γ_2, γ_0/γ_2 constrained by the condition of traction continuity at $x_2 = \pm\delta$.

Finally, it is worth noting that neither (36) nor (37) depends on the temperature gradients, although they can be alternatively expressed in terms of both temperature and density gradients, using

the equation of state.

Time dependent Flows with Moving Fracture Boundaries

If we consider the case in which flow in a fracture is driven by the movement of the fracture boundary, in response to a changing stress state in the solid, then we cannot take $v_2 = 0$. Further, in order to calculate the response of the fluid to movement of the boundary it is necessary to consider the time dependent problem. However, we can still approximate the flow as quasi-laminar, that is we can still assume that the gradients in the x_2 direction are much larger than those in the x_1 or x_3 directions. In this case equations (2.) and (3.) still apply and we therefore consider the equations (7.), which are:

$$\frac{\partial p}{\partial x_k} = \mu^{(k)} \frac{\partial^2 v_k}{\partial x_2^2} - \rho v_k \frac{\partial v_k}{\partial x_2} - \rho \frac{\partial v_k}{\partial t} + b_k \; ; \; k = 1, 2, 3 \qquad (38.)$$

Where $\mu^{(1)} = \mu^{(3)} \equiv \eta$ and $\mu^{(2)} = 4/3\eta + \zeta$ in general, and in special cases, $\mu^{(2)} = 4/3\eta$ when $\zeta \ll \eta$, or $\mu^{(2)} = \eta$ when $\nabla \cdot v = 0$.

We can again use an approximation for the $k = 2$ equation by noting that if the boundaries at $x_2 = \pm \delta$ move with the particles then, with $x_2 = \delta(x_1, x_3, t)$ as the fracture boundary equation, $v_2 = (\partial\delta/\partial t)$ at $x_2 = \delta$ and similarly for v_2 at $x_2 = -\delta$. Further, since only an expansion or contraction of the fracture aperture affects the flow (local rigid translations or rotations of the fracture produce no deformation) then we can require:

$$v_2|_{x_2 = \delta} = - v_2|_{x_2 = -\delta}$$

Thus v_2 will be an odd function of x_2. Using a power law expansion in x_2 for v_2 gives:

$$v_2 = a_0 + a_1 x_2 + a_2 x_2^2 + a_3 x_2^3$$

The requirement of an odd function gives $a_0 = a_2 = 0$, so $v_2 = a_1 x_2 + a_3 x_2^3$ to third order. Since we require

$$v_2|_{x_2 = \delta} = \frac{\partial \delta}{\partial t} \equiv \delta_t$$

then

$$v_2|_{x_2=\delta} = a_1\delta + a_3\delta^3 = \delta_t$$

or

$$a_1 = \left[\frac{\delta_t}{\delta}\right] - a_3\delta^2 \; ; \; \delta \equiv \delta(x_1, x_3, t)$$

Therefore:

$$v_2 = \left[\frac{\delta_t}{\delta}\right] x_2 + a_3 (x_2^2 - \delta^2) x_2 \; ; \; -\delta \le x_2 \le +\delta \qquad (39a.)$$

as a third order approximation that should be quite accurate over the small width of fractures.

Now, if the fracture surface function given by $x_2 = \delta(x_1, x_3, t)$ is expressed as a separable function in time and space; so:

$$\delta (x_1, x_3, t) = \Delta(x_1, x_3)\, s(t)$$

then

$$(\delta_t / \delta) = s_t(t) / s(t)$$

so that the ratio δ_t / δ is a function of time only. Now, if we use

$$v_2 = \left[\frac{\delta_t}{\delta}\right] x_2 \; ; \; -\delta \le x_2 \le +\delta \qquad (39b.)$$

corresponding to the second order approximation for v_2, then the quasi-laminar flow inequalities for v_2, in equations (2.), are met. That is, the inequality

$$\left|\frac{\partial v_2}{\partial x_2}\right| \gg \left[\left|\frac{\partial v_2}{\partial x_1}\right| , \left|\frac{\partial v_2}{\partial x_3}\right|\right]$$

becomes equivalent to

$$\left|s_t(t)/s(t)\right| \gg 0$$

Indeed, these inequalities are too strong as conditions since $\partial v_2^{(1)}/\partial x_1 = \partial v_2^{(1)}/\partial x_3 \equiv 0$ are obviously sufficient (but not necessary) to reduce the equations of motion in the manner required. Further, in this

case the conditions in (3) are replaced by

$$\frac{\partial^2 v_2}{\partial x_i^2} = 0 \; ; \; i = 1, 2, 3$$

which is sufficient, but not necessary, to give the quasi-laminar approximation to the equations of motion. Therefore with

$$v_2(x_1, x_2, x_3, t) = \left[\frac{\delta_t}{\delta}\right] x_2 = \left[\frac{s_t(t)}{s(t)}\right] x_2 \qquad (39c.)$$

$$\delta\,(x_1, x_3, t) = \Delta\,(x_1, x_3)\; s(t)$$

then the equations in (38.) are still appropriate. For v_2 as in (39c.), we get

$$\frac{\partial v_2}{\partial x_2} = \left[\frac{\delta_t}{\delta}\right], \quad \frac{\partial^2 v_2}{\partial x_2^2} = 0$$

and

$$\frac{\partial v_2}{\partial t} = \left[\frac{\delta_{tt}}{\delta} - \left[\frac{\delta_t}{\delta}\right]^2\right] x_2$$

Now the equation for v_2 is, from (38.):

$$\frac{\partial p^{(1)}}{\partial x_2} = -\rho\left[v_2^{(1)}\,\frac{\partial v_2^{(1)}}{\partial x_2} + \frac{\partial v_2^{(1)}}{\partial t}\right] + \rho^{(1)} g_2^{(0)} \qquad (40.)$$

Where the zeroth order (equilibrium) equation

$$\frac{\partial p^{(0)}}{\partial x_2} = \rho^{(0)} g_2^{(0)}$$

has been used and where $p^{(1)} = p - p^{(0)}$, $\rho^{(1)} = \rho - \rho^{(0)}$ and $v_2 = v_2^{(0)} + v_2^{(1)}$, with $v_2^{(0)} = 0$. (Consequently, v_2 in equations (38) and (39.) is the same as $v_2^{(1)}$ in (40.).)

Using the relations between the boundary surface movement in (39.) and v_2 gives, from (40.):

$$\frac{\partial p^{(1)}}{\partial x_2} = \rho^{(1)} g_2^{(0)} - \rho\left[\left[\frac{\delta_t}{\delta} x_2\right]\left[\frac{\delta_t}{\delta}\right] + \frac{\delta_{tt}}{\delta} x_2 - \left[\frac{\delta_t}{\delta}\right]^2 x_2\right]$$

or

$$\frac{\partial p^{(1)}}{\partial x_2} = \rho^{(1)} g_2^{(0)} - \rho \left[\frac{\delta_{tt}}{\delta} \right] x_2$$

Now using the approximation for v_2 from (39.) in all the momentum component equations and using the relations from (39c.), that is:

$$v_2 = \left[\frac{s_t}{s} \right] x_2, \quad \delta(x_1, x_3, t) = \Delta(x_1, x_3)\, s(t)$$

$$\frac{\delta_t}{\delta} = \frac{s_t(t)}{s(t)}; \quad \frac{\delta_{tt}}{\delta} = \frac{s_{tt}(t)}{s(t)}$$

then we have

$$\frac{\partial p^{(1)}}{\partial x_2} = \rho^{(1)} g_2^{(0)} - \rho \left[\frac{s_{tt}}{s} \right] x_2 \tag{41.}$$

$$\frac{\partial p^{(1)}}{\partial x_i} = \rho^{(1)} g_i^{(0)} - \rho \left[\left[\frac{s_t}{s} \right] \frac{\partial v_i}{\partial x_2} x_2 + \frac{\partial v_i}{\partial t} \right] + \eta \frac{\partial^2 v_i}{\partial x_2^2} \tag{42.}$$

with $i = 1, 3$.

In addition to these equations, conservation of mass requires;

$$\frac{d\rho}{dt} + \rho \, \nabla \cdot v = 0, \quad \text{or} \quad \frac{\partial \rho}{\partial t} + \nabla \cdot (\rho v) = 0 \tag{43.}$$

where

$$\nabla \cdot v \equiv \frac{\partial v_i}{\partial x_i} \equiv \frac{\partial v_1}{\partial x_1} + \frac{\partial v_2}{\partial x_2} + \frac{\partial v_3}{\partial x_3}$$

Using the order relations in (2.), that is

$$\left| \frac{\partial v_i}{\partial x_2} \right| \gg \left[\left| \frac{\partial v_i}{\partial x_1} \right|, \left| \frac{\partial v_i}{\partial x_3} \right| \right] \quad i = 1, 2,3$$

then, consistent with previous approximations:

$$\nabla \cdot v \approx \frac{\partial v_2}{\partial x_2}$$

With this approximation and the result $v_2 = (s_t/s)\, x_2$, then $\nabla \cdot v \approx (s_t/s)$ and (43.) becomes

$$\frac{\partial \rho}{\partial t} + \rho\left[\frac{s_t}{s}\right] = 0$$

Integrating from 0 to t gives

$$\frac{\rho(t)}{\rho(0)} = \frac{s(0)}{s(t)}$$

Since $\rho(0)$ is the density at $t = 0$, it is equivalent to the equilibrium density $\rho^{(0)}$. Therefore:

$$\rho = \rho^{(0)}\left[\frac{s(0)}{s(t)}\right] \tag{44a.}$$

By definition $\rho = \rho^{(0)} + \rho^{(1)}$ and therefore

$$\rho^{(1)} = \rho^{(0)}\left\{\frac{s(0)}{s(t)} - 1\right\} \tag{44b.}$$

Using the results (44.) in the momentum equations of (41) - (42) gives

$$\left.\begin{aligned} \frac{1}{\rho}\frac{\partial p^{(1)}}{\partial x_2} &= g_2^{(0)}\left\{1 - \frac{s(t)}{s(0)}\right\} - \left[\frac{s_{tt}}{s}\right] x_2 \\ \frac{1}{\rho}\frac{\partial p^{(1)}}{\partial x_i} &= g_i^{(0)}\left\{1 - \frac{s(t)}{s(0)}\right\} + \frac{\eta}{\rho}\frac{\partial^2 v_i}{\partial x_2^2} - \left[\frac{\partial v_i}{\partial t} + \left[\frac{s_t}{s}\right]\frac{\partial v_i}{\partial x_2} x_2\right] \end{aligned}\right\} \tag{45.}$$

Since the interval in x_2 of the open fracture is small, then it is reasonable to expand $p^{(1)}$ in a power series in x_2 over the interval $-\delta \le x_2 \le \delta$, and use this series to approximate $p^{(1)}$. Thus, to second order, with $P_\alpha^{(1)} \equiv \left[\frac{\partial^\alpha p^{(1)}}{\partial x_2^\alpha}\right]_{x_2=0}$

$$p^{(1)}(x, t) = P_0^{(1)}(x_1, x_3, t) + P_1^{(1)}(x_1, x_3, t)x_2 + \frac{1}{2}P_2^{(1)}(x_1, x_3, t)x_2^2 \tag{46a.}$$

Using this expansion in (45.) now gives for the first equation (the x_2 component equation),

$$P_1^{(1)} + P_2^{(1)}x_2 = \rho^{(0)}g_2^{(0)}\left\{\frac{s(0)}{s(t)} - 1\right\} - \rho^{(0)}\left[\frac{s(0)}{s(t)}\right]\left[\frac{s_{tt}}{s}\right] x_2$$

Furthermore, we can expand $\rho^{(0)}(x)$ and $g_2^{(0)}(x)$ in similar series, so for example

$$\rho^{(0)}(x) = D_0^{(0)}(x_1, x_3) + D_1^{(0)}(x_1, x_3)\, x_2 + \frac{1}{2}D_2^{(0)}(x_1, x_3)\, x_2^2\ ;\ D_\alpha^{(0)} \equiv \left[\frac{\partial^\alpha \rho^{(0)}}{\partial x_2^\alpha}\right]_{s_2 = 0}.$$

Since $-\delta \le x_2 \le \delta$ is a small interval, a good approximation is obtained simply by using the first term of the series for both $\rho^{(0)}$ and $g_2^{(0)}$ in the momentum equations. Therefore, taking $g_2^{(0)}$ constant and $\rho^{(0)}$ independent of x_2, so:

$$\rho^{(0)}(x) \approx D_0^{(0)}(x_1,x_3) \tag{46b.}$$

then on has

$$P_1^{(1)}(x_1, x_3, t) + P_2^{(1)}(x_1, x_3, t)x_2 = D_0^{(0)}(x_1, x_3)\, g_2^{(0)}\left\{\frac{s(0)}{s(t)} - 1\right\} - D_0^{(0)}(x_1, x_3)\left[\frac{s(0)}{s(t)}\right]\left[\frac{s_{tt}}{s}\right]x_2$$

Now the coefficients multiplying the powers of x_2 in this expression are independent of x_2 and therefore this expression can only be satisfied if all the coefficients of powers of x_2 vanish independently. Therefore, to second order we must have:

$$P_1^{(0)} - D_0^{(0)}g_2^{(0)}\left\{\frac{s(0)}{s(t)} - 1\right\} = 0$$

$$P_2^{(1)} + D_0^{(0)}\left[\frac{s(0)}{s(t)}\right]\left[\frac{s_{tt}}{s}\right] = 0$$

Thus, re-introducing $\rho^{(0)}$ for $D_0^{(0)}$ with the understanding that this is the value of ρ^0 at $x_2 = 0$:

$$P_1^{(0)}(x_1, x_3, t) = \rho^{(0)}g_2^{(0)}\left\{\frac{s(0)}{s(t)} - 1\right\} \tag{47.}$$

$$P_2^{(1)}(x_1, x_3, t) = -\rho^{(0)}\left[\frac{s(0)}{s(t)}\right]\left[\frac{s_{tt}}{s}\right]$$

Therefore; from (46a.) and (47.):

$$p^{(1)}(x,t) = P_0^{(1)}(x_1, x_3, t) + \rho^{(0)}g_2^{(0)}\left\{\frac{s(0)}{s(t)} - 1\right\}x_2 - \rho^{(0)}\left[\frac{s(0)}{s(t)}\right]\left[\frac{s_{tt}}{s}\right]\frac{x_2^2}{2} \tag{48.}$$

The second set of component equations in (45.) become, using (48.) and $\rho^{(0)} \approx D_0^{(0)}$ and $g_i^{(0}$ constant:

$$\frac{1}{\rho}\left[\frac{\partial P_0^{(1)}}{\partial x_i} + \frac{\partial \rho^{(0)}}{\partial x_i}\, g_2^{(0)}\left\{\frac{s(0)}{s(t)} - 1\right\}x_2 - \frac{\partial \rho^{(0)}}{\partial x_i}\left[\frac{s(0)}{s(t)}\right]\left[\frac{s_{tt}}{s}\right]\frac{x_2^2}{2}\right] =$$

$$g_i^{(0)}\left\{1 - \frac{s(t)}{s(0)}\right\} + \frac{\eta}{\rho}\frac{\partial^2 v_i^{(1)}}{\partial x_2^2} - \left[\frac{s_t}{s}\right]\frac{\partial v_i^{(1)}}{\partial x_2}x_2 - \frac{\partial v_i^{(1)}}{\partial t} \tag{49.}$$

where the index i takes on the values 1 and 3 for components in the x_1 and x_3 directions. Now, as with $p^{(1)}(x,t)$, the particle velocity components $v_i(x, t)$ can be expanded in x_2, to second order, as:

$$v_i^{(1)}(x, t) = {}_0V_i^{(1)}(x_1, x_3, t) + {}_1V_i^{(1)}(x_1, x_3, t)x_2 + \frac{1}{2}\,{}_2V_i^{(1)}(x_1, x_3, t)x_2^2 \qquad (50.)$$

where

$$ {}_\alpha V_i^{(1)}(x_1, x_3, t) \equiv \left[\frac{\partial^{(\alpha)}v_i}{\partial x_2^{(\alpha)}}\right]_{x_2=0}$$

Using the approximation of (50.) in (49.) gives

$$\frac{\partial P_0^{(1)}}{\partial x_i} + \frac{\partial \rho^{(0)}}{\partial x_i} g_2^{(0)}\left\{\frac{s(0)}{s(t)} - 1\right\}x_2 - \frac{1}{2}\frac{\partial \rho^{(0)}}{\partial x_i}\left[\frac{s(0)}{s(t)}\right]\left[\frac{s_{tt}}{s}\right]x_2^2 =$$

$$\rho^{(0)} g_i^{(0)}\left\{\frac{s(0)}{s(t)} - 1\right\} + \eta\,{}_2V_i^{(1)} - \rho\left[\left[\frac{s_t}{s}\right]{}_1V_i^{(1)}x_2 + \left[\frac{s_t}{s}\right]{}_2V_i^{(1)}x_2^2 + \frac{\partial_0 V_i^{(1)}}{\partial t} + \frac{\partial_1 V_i^{(1)}}{\partial t}x_2 + \frac{1}{2}\frac{\partial_2 V_i^{(1)}}{\partial t}x_2^2\right]$$

Here again the coefficient multipliers of the powers of x_2 are independent of x_2 and so these coefficients must vanish independently if the equation is to be satisfied for all x_2. Therefore we must have:

$$\frac{\partial P_0^{(1)}}{\partial x_i} = \eta\,{}_2V_i^{(1)} + \rho^{(0)} g_i^{(0)}\left\{\frac{s(0)}{s(t)} - 1\right\} - \rho^{(0)}\left[\frac{s(0)}{s(t)}\right]\frac{\partial_0 V_i^{(1)}}{\partial t} \qquad (51a.)$$

$$\frac{\partial \rho^{(0)}}{\partial x_i} g_2^{(0)}\left\{1 - \frac{s(t)}{s(0)}\right\} = -\rho^{(0)}\left[\left[\frac{s_t}{s}\right]{}_1V_i^{(1)} + \frac{\partial_1 V_i^{(1)}}{\partial t}\right] \qquad (51b.)$$

$$\frac{\partial \rho^{(0)}}{\partial x_i}\left[\frac{s_{tt}}{s}\right] = \rho^{(0)}\left[2\left[\frac{s_t}{s}\right]{}_2V_i^{(1)} + \frac{\partial_2 V_i^{(1)}}{\partial t}\right] \qquad (51c.)$$

where the result $\rho = \rho^{(0)}(s(0) / s(t))$, from the equation of continuity, has been used repeatedly.

Now, as in the steady state case, take:

$$ {}_\alpha V_i^{(1)}(x_1, x_3, t) \equiv \beta_p^\alpha \frac{\partial P_0^{(1)}}{\partial x_i} + k_i^\alpha(x_1, x_3, t) \qquad (52a.)$$

where

$$v_i^{(1)} = {}_0V_i^{(1)} + {}_1V_i^{(1)}x_2 + \frac{1}{2}{}_2V_i^{(1)}x_2^2$$

and with the functions taken as separable in time, so that:

$$P_0^{(1)} = P_0^{(1)}(x_1, x_3) f_p(t) \qquad (52b.)$$
$$k_i^{\alpha} = K_i^{\alpha}(x_1, x_3)\, h_{\alpha}^{(i)}(t)$$

(Here, there is no sum on repeated greek letter indices. Further, Latin indices enclosed in parentheses are excluded from the summation convention.) Using this representation of the velocity field, the component equations of motion in (51.) become:

$$\frac{\partial P_0^{(1)}}{\partial x_i}\left[f_p - \eta\beta_p^{(2)} f_p + \rho^{(0)}\left[\frac{s(0)}{s(t)}\right]\beta_p^{(0)}\frac{df_p}{dt}\right] + \rho^{(0)}\left[\frac{s(0)}{s(t)}\right]K_i^{(0)}\frac{dh_0^{(i)}(t)}{dt} - \rho^{(0)} g_i^{(0)}\left\{\frac{s(0)}{s(t)} - 1\right\}$$

$$- \eta K_i^{(2)} h_2^{(i)}(t) = 0 \qquad (53a.)$$

$$\beta_p^{(1)}\frac{\partial P_0^{(1)}}{\partial x_i}\left[\left[\frac{s_t}{s}\right]f_p + \frac{df_p}{dt}\right] + K_i^{(1)}\left[\left[\frac{s_t}{s}\right]h_1^{(i)} + \frac{dh_1^{(i)}}{dt}\right] + \left[\frac{1}{\rho^{(0)}}\right]\frac{\partial \rho^{(0)}}{\partial x_i} g_2^{(0)}\left\{1 - \frac{s(t)}{s(0)}\right\} = 0 \qquad (53b.)$$

$$\beta_p^{(2)}\frac{\partial P_0^{(1)}}{\partial x_i}\left[2\left[\frac{s_t}{s}\right]\dot{f}_p + \frac{df_p}{dt}\right] + K_i^{(2)}\left[2\left[\frac{s_t}{s}\right]h_2^{(i)} + \frac{dh_2^{(i)}}{dt}\right] - \left[\frac{1}{\rho^{(0)}}\right]\frac{\partial \rho^{(0)}}{\partial x_i}\left[\frac{s_{tt}}{s}\right] = 0 \qquad (52c.)$$

There are many possibilities for solutions of these equations since all the functions f_p, $h_{\alpha}^{(i)}$, $K_i^{(\alpha)}$ and constants $\beta_p^{(\alpha)}$, for $\alpha = 0, 1, 2$ and $i = 1, 3$ can be freely chosen to satisfy the relations. These multiple possibilities reflect the many flows that are possible. Only with additional constraining equations (*e.g.* involving boundary conditions) can a subset of solutions be isolated and, even then, many solutions may be possible reflecting different flow patterns in different ranges of physical parameters or for different initial conditions.

Type I Transient Laminar Flow

Inspection of the equations in (53.) suggests a class of solution having characteristics of non-steady near laminar flow in a open fracture and this class of elemental solution will be developed as a type of interest for use in constructing global solutions for flow in complex fracture systems.

To develop such solutions we can chose the constants $\beta_p^{(\alpha)}$ to be:

$$\beta_p^{(0)} = 0 \ , \ \beta_p^{(1)} = 0 \ , \ \beta_p^{(2)} = \frac{1}{\eta}$$

In this case the equations in (53.) reduce to:

$$\rho^{(0)}\left[\frac{s(0)}{s(t)}\right]\left[K_i^{(0)}\frac{\partial h_0^{(i)}}{\partial t} - g_i^{(0)}\left\{1 - \frac{s(t)}{s(0)}\right\} - \left[\frac{\eta}{\rho^{(0)}}\right]K_i^{(2)}\left[\frac{s(t)}{s(0)}\right]h_2^{(i)}\right] = 0 \qquad (54a.)$$

$$K_i^{(1)}\left[\left[\frac{s_t}{s}\right]h_i^{(i)} + \frac{dh_i^{(i)}}{dt}\right] + \frac{1}{\rho^{(0)}}\left[\frac{\partial \rho^{(0)}}{\partial x_i}\right]g_2^{(0)}\left\{1 - \frac{s(t)}{s(0)}\right\} = 0 \qquad (54b.)$$

$$\frac{1}{\eta}\frac{\partial P_0^{(1)}}{\partial x_i}\left[2\left[\frac{s_t}{s}\right]f_p + \frac{df_p}{dt}\right] + K_i^{(2)}\left[2\left[\frac{s_t}{s}\right]h_2^{(i)} + \frac{dh_2^{(i)}}{dt}\right] - \frac{1}{\rho^{(0)}}\left[\frac{\partial \rho^{(0)}}{\partial x_i}\right]\left[\frac{s_{tt}}{s}\right] = 0 \qquad (54c.)$$

These equations can now be satisfied in the following manner:

(i.) In (54c.) note that the only term involving a pressure gradient term can be eliminated if

$$\frac{df_p}{dt} + 2\left[\frac{s_t}{s}\right]f_p = 0$$

Therefore, upon integration over the range (o,t), we get:

$$f_p(t) = f_p(0)\left[\frac{s(0)}{s(t)}\right]^2 \qquad (55a.)$$

with f_p normalized to unity at t = 0, then

$$f_p(t) = \left[\frac{s(0)}{s(t)}\right]^2 \qquad (55b.)$$

(ii.) Inspection of the equations in (54.) shows that if:

$$K_i^{(0)} = K_i^{(1)} = K_i^{(2)} = \frac{1}{\rho^{(0)}}\left[\frac{\partial \rho^{(0)}}{\partial x_i}\right] \qquad (56.)$$

Then, also using (55.), the equations in (54) reduce to:

$$\left[\frac{\partial \rho^{(0)}}{\partial x_i}\right]\frac{\partial h_0^{(i)}}{\partial t} - \rho^{(0)}g_i^{(0)}\left\{1 - \frac{s(t)}{s(0)}\right\} - \left[\frac{\partial \rho^{(0)}}{\partial x_i}\right]\left[\frac{\eta}{\rho^{(0)}}\right]\left[\frac{s(t)}{s(0)}\right]h_2^{(i)} = 0 \qquad (57a.)$$

$$\frac{dh_i^{(i)}}{dt} + \left[\frac{s_t}{s}\right]h_i^{(i)} + g_2^{(0)}\left\{1 - \frac{s(t)}{s(0)}\right\} = 0 \qquad (57b.)$$

$$\frac{dh_2^{(i)}}{dt} + 2\left[\frac{s_t}{s}\right]h_2^{(i)} - \left[\frac{s_{tt}}{s}\right] = 0 \qquad (57c.)$$

(iii.) Noting that (*e.g.* Richards, Manual of Mathematical Physics, Pergamon, 1959; p 341):

$$\frac{dg(t)}{dt} + f_1(t)g(t) + f_2(t) = 0 \tag{58a.}$$

$$g(t) = \left[c_0 - \int_{\beta}^{t} f_2(t') \left[\exp \int_{\alpha}^{t'} f_1(t'')dt'' \right] dt' \right] \exp \int_{\alpha}^{t} f_1(t')dt' \tag{58b.}$$

where α and β are arbitrary constants, which upon changes in their values results, at most, in changes in the constant c_0. Applying this result to (57.) allows each of the first order differential equations to be solved in closed form. In particular, from (57c.) we get:

$$h_2^{(i)}(t) = \left\{ \gamma_2^{(i)} + \int_0^t \frac{s_{t't'}}{s} \left[\exp \int_0^{t'} \frac{2s_{t''}}{s} dt'' \right] dt' \right\} \exp \left[-2 \int_0^t \frac{s_t'}{s} dt' \right]$$

so that

$$h_2^{(i)}(t) = \left[\frac{s(0)}{s(t)} \right]^2 \left\{ \gamma_2^{(i)} + \left[\frac{1}{s(0)} \right]^2 \int_0^t s_{t't'}\, s\, dt' \right\} \tag{59a.}$$

or, after integrating by parts;

$$h_2^{(i)}(t) = \gamma_2^{(i)} \left[\frac{s(0)}{s(t)} \right]^2 + \left[\frac{1}{s} \right]^2 \left\{ s(t)s_t(t) - s(0)s_t(0) - \int_0^t s_t^2 dt' \right\} \tag{59b.}$$

where $\gamma_2^{(i)}$ are constants, which may be different for i = 1 and 3.

Similarly, equation (57b.) is

$$\frac{dh_1^{(i)}}{dt} + \left[\frac{s_t}{s} \right] h_1^{(i)} + g_2^{(0)} \left\{ 1 - \frac{s(t)}{s(0)} \right\} = 0$$

and has the general solution

$$h_1^{(i)}(t) = \left\{ \gamma_1^{(i)} - \int_0^t g_2^{(0)} \left\{ 1 - \frac{s(t)}{s(0)} \right\} \exp \left[\int_0^{t'} \frac{s_{t''}}{s} dt'' \right] dt' \right\} \exp \left[- \int_0^t \frac{s_{t'}}{s} dt' \right]$$

which integrates to:

$$h_1^{(i)} = \left[\frac{s(0)}{s(t)}\right]\left[\gamma_1^{(i)} + g_2^{(0)} \int_0^t \frac{s(t)}{s(0)}\left\{1 - \frac{s(t)}{s(0)}\right\} dt'\right] \tag{60.}$$

Here $\gamma_1^{(i)}$ represents constants for i = 1 and 3.

Finally, (57a.) now becomes, using (59.) in the equation:

$$\left[\frac{\partial \rho^{(0)}}{\partial x_i}\right]\frac{dh_0^{(i)}}{dt} = \left[\frac{\partial \rho^{(0)}}{\partial x_i}\right]\left[\frac{\eta}{\rho^{(0)}}\right]\left[\frac{s(0)}{s(t)}\right]\left\{\gamma_2^{(i)} + \left[\frac{1}{s(0)}\right]^2 \int_0^t s_{t't'}\, s\, dt'\right\} + \rho^{(0)} g_i^{(0)}\left\{1 - \frac{s(t)}{s(0)}\right\}$$

Integration over the interval (o,t) gives:

$$\left[\frac{\partial \rho^{(0)}}{\partial x_i}\right]\left[h_0^{(i)}(t) - h_0^{(i)}(0)\right] = \left[\frac{\partial \rho^{(0)}}{\partial x_i}\right]\left[\frac{\eta}{\rho^{(0)}}\right]\left\{\gamma_2^{(i)} \int_0^t \frac{s(0)}{s(t')}\, dt' + \left[\frac{1}{s(0)}\right] \int_0^t \frac{dt'}{s(t')} \int_0^{t'} s_{t''t''}\, s(t'')\, dt''\right\}$$

$$+ \rho^{(0)} g_i^{(0)} \int_0^t \left\{1 - \frac{s(t')}{s(0)}\right\} dt' \tag{61a.}$$

Now, collecting results we have:

$$v_i^{(1)}(x, t) = {}_0V_i^{(1)}(x_1, x_3, t) + {}_1V_i^{(1)}(x_1, x_3, t)\, x_2 + \frac{1}{2}\, {}_2V_i^{(1)}(x_1, x_3, t)\, x_2^2$$

$${}_\alpha V_i(x_1, x_3, t) = \beta_p^{(\alpha)} \frac{\partial P_0^{(1)}}{\partial x_i} + k_i^{(\alpha)} = \beta_p^{(\alpha)} \frac{\partial P_0^{(1)}}{\partial x_i} f_p(t) + K_i^{(\alpha)}(x_1, x_3) h_\alpha^{(i)}(t)$$

Therefore, with $\beta_p^{(0)} = \beta_p^{(1)} = 0$ and $\beta_p^{(2)} = 1/\eta$:

$$v_i^{(1)}(x, t) = K_i^{(0)}\, h_0^{(i)} + K_i^{(1)}\, h_1^{(i)}\, x_2 + K_i^{(2)}\, h_2^{(i)}\, \frac{x_2^2}{2} + \beta_p^{(2)}\left[\frac{\partial P_0^{(1)}}{\partial x_i}\right] f_p(t) \frac{x_2^2}{2}$$

where $-\delta \le x_2 \le \delta$ and $\delta(x_1, x_3, t) = \Delta(x_1, x_3)s(t)$ defines the fracture surfaces at $x_2 = \pm\, \delta$. Since

$$K_i^{(0)} = K_i^{(1)} = K_i^{(2)} = \left[\frac{1}{\rho^{(0)}}\right]\frac{\partial \rho^{(0)}}{\partial x_i}$$

then, with $\beta_p^{(2)} = 1/\eta$, $f_p(t) = \left[\frac{s(0)}{s(t)}\right]^2$ and taking $\gamma_2^{(i)} = (\eta/\rho^{(0)})^{-1}$ for i = 1,3:

$$v_i^{(1)}(x,\,t) = \left[\frac{1}{\rho^{(0)}}\right]\frac{\partial \rho^{(0)}}{\partial x_i}\left[h_0^{(i)}(0) + \int_0^t \frac{s(0)}{s(t')}dt' + \left[\frac{\eta}{\rho^{(0)}}\right]\int_0^t \frac{dt'}{s(t')}\int_0^{t'} s_{t''t''}\left[\frac{s(t'')}{s(0)}\right]dt'' + h_1^{(i)}x_2 + h_2^{(i)}\frac{x_2^2}{2}\right]$$

$$+ g_i^{(0)}\int_0^t \left\{1 - \frac{s(t')}{s(0)}\right\}dt' + \frac{1}{2\eta}\left[\frac{\partial P_0^{(1)}}{\partial x_i}\right]\left\{\frac{s(0)}{s(t)}\right\}^2 x_2^2 \qquad (62.)$$

where $i = 1, 3$ and where $h_1^{(i)}$ and $h_2^{(i)}$ are given by equations (59.) and (60.). Here also

$$v_2^{(1)}(x,\,t) = \left[\frac{s_t(t)}{s(t)}\right]x_2 \qquad (63.)$$

$$\rho(x,\,t) = \rho^{(0)} + \rho^{(1)} = \rho^{(0)}\left[\frac{s(0)}{s(t)}\right] \qquad (64.)$$

$$p^{(1)}(x,t) = P_0^{(1)}(x_1,\,x_3,\,t) + \rho^{(0)}g_2^{(0)}\left\{\frac{s(0)}{s(t)} - 1\right\}x_2 - \frac{\rho^{(0)}}{2}\left[\frac{s(0)}{s(t)}\right]\left[\frac{s_{tt}}{s}\right]x_2^2 \qquad (65.)$$

In all these expressions $\rho^{(0)}(x)$ is evaluated at $x_2 = 0$ in the fracture zone, defined by $-\delta \le x_2 \le \delta$, as an approximation. Therefore $\rho^{(0)}$ is, at most, a function of x_1 and x_3 only.

The velocity components $v_i^{(1)}$ given in (62.) can also be written in a different form by noting that from (64.):

$$\frac{\partial \rho^{(1)}}{\partial x_i} = \frac{\partial \rho^{(0)}}{\partial x_i}\left[\frac{s(0)}{s(t)} - 1\right] = \frac{\rho^{(1)}}{\rho^{(0)}}\left[\frac{\partial \rho^{(0)}}{\partial x_i}\right]$$

Therefore

$$\frac{1}{\rho^{(0)}}\frac{\partial \rho^{(0)}}{\partial x_i} = \frac{1}{\rho^{(1)}}\frac{\partial \rho^{(1)}}{\partial x_i} \qquad (66.)$$

and so the equilibrium density gradient can be replaced by the perturbed density gradient in (62.). Since an equation of state for the fluid relates the density to the pressure and temperature, that is:

$$\rho = \rho\,(p,\,T) \qquad (67.)$$

then for small changes in the fluid state variables, denoted by $\delta\rho$, δp, δT, we have:

$$\delta\rho = \left[\frac{\partial \rho}{\partial p}\right]_T \delta p + \left[\frac{\partial \rho}{\partial T}\right]_p \delta T \qquad (68a.)$$

Identifying these variations in the state variables with $\rho^{(1)}$, $p^{(1)}$ and $T^{(1)}$, the variations from equilibrium associated with flow of the fluid, gives

$$\rho^{(1)} = \left[\frac{\partial \rho}{\partial p}\right]_T^{(0)} p^{(1)} + \left[\frac{\partial \rho}{\partial T}\right]_p^{(0)} T^{(1)} \tag{68a.}$$

$$\frac{\partial \rho^{(1)}}{\partial x_i} = \left[\frac{\partial \rho}{\partial p}\right]_T^{(0)} \frac{\partial p^{(1)}}{\partial x_i} + \left[\frac{\partial \rho}{\partial T}\right]_p^{(0)} \frac{\partial T^{(1)}}{\partial x_i}$$

where the superscript (0) on the partial derivatives of the density denotes evaluation of the derivatives at the equilibrium state; that is at $\rho^{(0)}$, $p^{(0)}$ and $T^{(0)}$. (In the second relation in (68b.), involving gradients, the spatial variations of the coefficients $(\partial\rho/\partial p)_T$ and $(\partial\rho/\partial T)_p$ are assumed small enough that their gradients can be neglected.) Therefore, denoting the fluid moduli represented by the derivatives of density with respect to pressure and temperature by

$$\left.\begin{aligned} \alpha_p &= -\frac{1}{\rho^{(0)}}\left[\frac{\partial \rho}{\partial p}\right]_T^{(0)} \\ \alpha_T &= -\frac{1}{\rho^{(0)}}\left[\frac{\partial \rho}{\partial T}\right]_p^{(0)} \end{aligned}\right\} \tag{69.}$$

then

$$\left[\frac{1}{\rho^{(0)}}\right]\frac{\partial \rho^{(0)}}{\partial x_i} = -\left[\alpha_p \frac{\partial p^{(1)}}{\partial x_i} + \alpha_T \frac{\partial T^{(1)}}{\partial x_i}\right] \tag{70.}$$

Using the relations (66.) and (70.) in the equation (62.) for $v_i^{(1)}(x, t)$ allows the result to be expressed in alternate forms. These results have forms similar to the steady state solutions obtained earlier.

Type II Transient Laminar Flow

If the equilibrium density $\rho^{(0)}$ is taken to be approximately constant over the spatial domain of the elemental fracture, then a second type of solution to the basic "coefficient equations" in (52.) can be easily found. In particular, if we take:

$$\beta_p^{(0)} = \frac{1}{\rho^{(0)}}\,, \quad \beta_p^{(1)} = 0, \quad \beta_p^{(2)} = 0 \tag{71.}$$

then the equations in (52.) become

$$\frac{\partial P_0^{(1)}}{\partial x_i}\left\{f_0 + \left[\frac{s(0)}{s(t)}\right]\frac{df_p}{dt}\right\} + \rho^{(0)}\left[\frac{s(0)}{s(t)}\right]K_i^{(0)}\frac{dh_0^{(i)}}{dt} - \rho^{(0)}g_i^{(0)}\left\{\frac{s(0)}{s(t)} - 1\right\} - \eta K_i^{(2)}h_2^{(i)} = 0 \tag{72a.}$$

$$K_i^{(1)}\left[\left[\frac{s_t}{s}\right]h_i^{(i)} + \frac{dh_1^{(i)}}{dt}\right] + \frac{1}{\rho^{(0)}}\frac{\partial\rho^{(0)}}{\partial x_i}\,g_2^{(0)}\left\{1 - \frac{s(t)}{s(0)}\right\} = 0 \qquad (72b.)$$

$$K_i^{(2)}\left[2\left[\frac{s_t}{s}\right]h_2^{(i)} + \frac{dh_2^{(i)}}{dt}\right] - \frac{1}{\rho^{(0)}}\frac{\partial\rho^{(0)}}{\partial x_i}\left[\frac{s_{tt}}{s}\right] = 0 \qquad (72c.)$$

These equations can be satisfied in the same way as were those for Type I flow, that is:

(i.) The dependence on the terms involving the pressure derivatives are eliminated by requiring that f_p satisfy:

$$\frac{df_p}{dt} + \left[\frac{s(t)}{s(0)}\right]f_p = 0$$

so that

$$f_p(t) = f_p(0)\,\exp\left[\frac{-1}{s(0)}\int_0^t s(t')dt'\right];\quad f_p(0) \equiv 1$$

(ii.) Take the functions $K_i^{(\alpha)}(x_1, x_3)$, where $\alpha = 0, 1, 2$, to have the form

$$K_i^{(0)} = K_i^{(1)} = K_i^{(2)} = \frac{1}{\rho^{(0)}}\frac{\partial\rho^{(0)}}{\partial x_i} = \frac{1}{\rho^{(1)}}\frac{\partial\rho^{(1)}}{\partial x_i}$$

for i = 1 and 3.

In this case the equations in (72.) reduce to:

$$\frac{\partial\rho^{(0)}}{\partial x_i}\left[\frac{s(0)}{s(t)}\right]\frac{dh_0^{(i)}}{dt} - \rho^{(0)}g_i^{(0)}\left\{\frac{s(0)}{s(t)} - 1\right\} - \left[\frac{\eta}{\rho^{(0)}}\right]\frac{\partial\rho^{(0)}}{\partial x_i}h_2^{(i)} = 0 \qquad (73a.)$$

$$\frac{dh_1^{(i)}}{dt} + \left[\frac{s_t}{s}\right]h_1^{(i)} + g_2^{(0)}\left\{1 - \frac{s(t)}{s(0)}\right\} = 0 \qquad (73b.)$$

$$\frac{dh_2^{(i)}}{dt} + 2\left[\frac{s_t}{s}\right]h_2^{(i)} - \left[\frac{s_{tt}}{s}\right] = 0 \qquad (73c.)$$

These equations are identical to those in (57.), which apply to the Type I case, so that the solutions for the time dependent functions $h_\alpha^i(t)$ for this second case are the same as those obtained earlier. That is, with i = 1, 3:

$$h_2^{(i)}(t) = \left[\frac{s(0)}{s(t)}\right]^2\left\{\gamma_2^{(i)} + \left[\frac{1}{s(0)}\right]^2\int_0^t s_{t't'}\,s\,dt'\right\} \qquad (74a.)$$

$$h_2^{(i)}(t) = \left[\frac{s(0)}{s(t)}\right]\left\{\gamma_2^{(i)} + g_2^{(0)} \int_0^t \frac{s(t)}{s(0)}\left\{1 - \frac{s(t)}{s(0)}\right\}dt'\right\} \tag{74b.}$$

$$\left[\frac{\partial \rho^{(0)}}{\partial x_i}\right]\left[h_0^{(i)}(t) - h_0^{(i)}(0)\right] = \left[\frac{\partial \rho^{(0)}}{\partial x_i}\right]\left[\eta / \rho^{(0)}\right]\left\{\gamma_2^{(i)}\int_0^t \frac{s(0)}{s(t')}\,dt' + \left[\frac{1}{s(0)}\right]\int_0^t \frac{dt'}{s(t')}\int_0^{t''} s_{t''t''}\, s(t'')\,dt''\right\}$$

$$+ \rho_0 g_i^{(0)} \int_0^t \left\{1 - \frac{s(t')}{s(0)}\right\}dt' \tag{74c.}$$

where we can take $\gamma_2^{(i)} = (\eta / \rho^{(0)})^{-1}$, as in the type I case with $\rho^{(0)} \approx$ constant. The solution for the velocity components is now given by:

$$v_i^{(1)}(x, t) = K_i^{(0)} h_0^{(i)} + K_i^{(1)} h_1^{(i)} x_2 + K_i h_2^{(i)} \frac{x_2^2}{2} + \frac{1}{\rho^{(0)}}\left[\frac{\partial P_0^{(1)}}{\partial x_i}\right] f_p(t)$$

or, using the results in (i) and (ii) above:

$$v_i^{(1)}(x, t) = \left[\frac{1}{\rho^{(1)}}\right]\frac{\partial \rho^{(1)}}{\partial x_i}\left[\left\{h_0^{(i)}(0) + H_0^{(i)}(t)\right\} + h_1^{(i)} x_2 + h_2^{(i)} \frac{x_2^2}{2}\right] + g_i^{(0)} \int_0^t \left\{1 - \frac{s(t')}{s(0)}\right\} dt'$$

$$+ \frac{1}{\rho^{(0)}}\left[\frac{\partial P_0^{(1)}}{\partial x_i}\right] \exp\left[\frac{-1}{s(0)}\int_0^t s(t')\,dt'\right] \tag{75.}$$

where

$$H_0^{(i)} = \int_0^t \frac{s(0)}{s(t')}\,dt' + \frac{\eta}{\rho^{(0)}} \int_0^t \frac{dt'}{s(t')}\int_0^{t'} s_{t''t''}\left[\frac{s(t'')}{s(0)}\right] dt''$$

has been introduced and $\gamma_2^{(i)} = (\eta / \rho^{(0)})^{-1}$ has been used, as in the Type I solution. This solution has the same form as does the Type I solution, except the dependence in the pressure gradient term is different. Also we note that, as with the previous solution type:

$$\left[\frac{1}{\rho^{(0)}}\right]\frac{\partial \rho^{(0)}}{\partial x_i} = \left[\frac{1}{\rho^{(1)}}\right]\frac{\partial \rho^{(1)}}{\partial x_i}$$

and, from the existence of an equation of state,

$$\frac{\partial \rho^{(1)}}{\partial x_i} = -\left[\rho^{(0)}\alpha_p \frac{\partial p^{(1)}}{\partial x_i} + \rho^{(0)}\alpha_T \frac{\partial T^{(1)}}{\partial x_i}\right]$$

so that these relations can be used in (75.) to express the result in alternate forms.

The expressions for $v_2^{(1)}(x, t)$, $\rho(x, t)$ and $p^{(1)}(x, t)$ for this solution are the same as those given in equations (63.)-(65.) for the Type I solution.

Summary of Results

The solutions obtained apply only to cases in which fluid flows within a fracture is quasi-laminar, in that the spatial variations in particle velocities normal to the fracture boundaries are much more rapid than those in directions tangential to the boundaries. Both steady state solutions, where the fracture boundaries do not move and the particle velocity field is independent of time, and transient, time dependent solutions in which the fracture boundaries are allowed to move in an arbitrary, but well behaved manner, have been obtained. The latter class of solutions incorporate movement of the fracture boundaries in response to fluid pressure changes in the fracture as well as in response to stress changes in the solid medium, within which the fractures exist. In particular, they satisfy the condition that the normal component of the fluid particle velocity is equal to the particle velocity of the solid material at the fracture boundary, an expression of conservation of mass at the boundary.

All the solutions contain constant parameters that are fixed by boundary and initial conditions. The commonly applied boundary condition that the fluid particle velocity components tangent to the fracture boundary should vanish would imply, in the case of moving boundaries driven by relaxing stress fields or waves in the solid, an ideal fluid response at the boundary where no tangential tractions are transmitted to the fluid; that is perfect slip at the boundary. On the other hand, perfect slip of the fluid along the boundary of the fracture would also allow solutions in which the tangential components of the fluid particle velocity are unconstrained. Thus, no good physical argument justifying direct constraints on the tangential fluid velocities at the boundary is available in a moving boundary case. However, as noted earlier in the introduction, the condition that the tractions be continuous at the boundary, which expresses conservation of momentum at the boundary, can be used to specify the boundary

movement with time in terms of the dynamic pressure $p^{(1)}$ in the fluid. In addition, a viscous fluid, as treated here, would transmit tangential tractions from the solid into the fluid and this would produce a shear flow near the boundary. In this case fluid particle velocities tangent to the boundary would not necessarily be equal to tangential solid particle velocities at the boundary, but there would be a tendency for the fluid to be dragged, tangentially, along with the solid movement. The solutions obtained here, or variants of them, should have the generality and flexibility to incorporate fluid flows of this latter type and we shall consider such cases in subsequent studies through the application of shear traction continuity conditions at the fluid-solid fracture boundary using fundamental solutions of the type obtained in this study.

In addition to conditions along the fracture surface, it is necessary to consider end conditions other than those free-flow conditions implicitly used here. That is, elemental solutions satisfying conservation of mass and momentum in the fluid within a fracture with unconstrained end conditions have been obtained, but these solutions must be constrained by end conditions applied at the spatial intersections with other fractures. In this case the solutions obtained must be "joined" to other solutions of the same form by requiring conservation of mass and momentum between the solutions across the intersection zone. Thus, for a network of intersecting fractures, solutions of the form obtained here must be joined throughout by applying additional conservation relations so that each fracture flow solution will be constrained to match these conditions. This matching will have to be accomplished by proper choice of the remaining free paramenters in the solutions given here. This aspect of the problem will be considered in Part II of this study. The results given here are therefore the fundamental solutions required to complete the formulation for fluid flow in a intersecting network of fractures within a deformable and dynamically changing solid, as described in the introduction.

References

Brodkey, R.S., *The Phenomena of Fluid Motions*, Addison-Wesley, 1967.

Landau, L.D. and E.M. Lifshitz, *Course of Theoretical Physics, Volume 6 - Fluid Mechanics*, Pergamon Press, 1959.

Richards, P.I., *Manual of Mathematical Physics*, Pergamon Press, 1959.